UNIVERSITY OF GRANADA
FACULTY OF SCIENCES
Department of Mineralogy and Petrology

Doctoral Thesis

PETROLOGICAL AND GEOCHEMICAL STUDY OF A SUBDUCTION MÉLANGE (SIERRA DEL CONVENTO, EASTERN CUBA). A CASE OF PARTIALLY MELTED SLAB

Concepción Lázaro Calisalvo
November 16, 2007

UNIVERSIDAD DE GRANADA
FACULTAD DE CIENCIAS
Departmento de Mineralogía y Petrología

Tesis Doctoral

ESTUDIO PETROLÓGICO Y GEOQUÍMICO DE UNA MÉLANGE DE SUBDUCCIÓN (SIERRA DEL CONVENTO, CUBA ORIENTAL). UN CASO DE LÁMINA SUBDUCENTE PARCIALMENTE FUNDIDA.

Tesis que presenta
CONCEPCIÓN LÁZARO CALISALVO
para optar al Grado de Doctor
por la Universidad de Granada

El Director — La Doctoranda

Prof. Dr. Antonio García Casco — Concepción Lázaro Calisalvo

Granada, 16 de Noviembre de 2007

Editor: Editorial de la Universidad de Granada
Autor: Concepción Lázaro Calisalvo
D.L.: Gr. 2355 - 2007
ISBN: 978-84-338-4508-5

Table of Contents

Agradecimientos

Después de cuatro años de trabajo en la Universidad de Granada durante los cuales ha sido posible llevar a cabo esta investigación, quiero aprovechar estas líneas para agradecer a todas aquellas personas que de un modo u otro han contribuido a la realización de esta Tesis Doctoral.

En primer lugar, quiero agradecer a mi director de Tesis, Antonio García Casco, quien durante todo este tiempo me ha brindado su ayuda y su dedicación constante en este trabajo de investigación. Por brindarme la oportunidad de investigar en un tema tan apasionante como el que se aborda en este estudio, por confiar en mí y por la relación de amistad personal que se ha forjado entre nosotros a lo largo de este tiempo, muchas gracias.

Muchas gracias también a todo el personal del Departamento de Mineralogía y Petrología de la Universidad de Granada. Especialmente, tengo palabras de gratitud dirigidas al Director del Departamento, D. Miguel Ortega Huertas, por la disponibilidad y la colaboración que ha mostrado a lo largo de estos cuatro años. De igual modo, a todo el personal del Centro de Instrumentación Científica de la Universidad de Granada que trabajó y colaboró conmigo durante el desarrollo de este trabajo.

Vaya mi agradecimiento a todos aquellos investigadores y técnicos que han trabajado y me han ayudado durante mis estancias en el Laboratorio Argonaut de la Universidad de Salzburgo (Austria), especialmente los Dr. Franz Neubauer y Johann Genser, y en el Laboratorio de Alta Presión de la Universidad de Huelva, mi especial gratitud para los Dr. Antonio Castro y Jesús de la Rosa. No puedo, ni debo, olvidarme de los compañeros geólogos cubanos con quienes espero me une una amistad que va un poco mas allá de lo estrictamente profesional. Especialmente Manuel Iturralde-Vinent, Kenya Núñez Cambra y Antonio Rodríguez Vega, que hicieron posible la realización de las campañas de campo y muestreo desarrolladas y con quienes además viví experiencias inolvidables.

Por otro lado, quiero tener también unas palabras de gratitud para la Dra. María Dolores Ruiz Cruz, de la Universidad de Málaga, quien depositó toda su confianza y su apoyo en mí y que hizo posible mis comienzos en la investigación a la vez que encendió mi ilusión por esta actividad.

Un saludo y un recuerdo muy especial a mis amigos becarios o no de Huelva, Susana y Helena, y de Salzburgo, Maria. Un saludo y unos besis muy cariñosos a todos mis, mas que compañeros, amigos becarios o precarios de Granada que me ayudaron y animaron a seguir en los momentos mas duros, especialmente a mi compi Julia, mi compadre Jose María, mi italianini particular Claudio, David, Fermín, y a todos con los que he compartido algún que otro cafelito, Jose Alberto, Antonio, Ana, Rocío, Vicente,…. y todos los demás. Un recuerdo para mis otros amigos no vinculados actualmente con la Universidad, Patricia, Fini, Raquel, que también me animaron en momentos de dificultad.

También quiero tener un recuerdo muy especial para mi nueva familia, Diego, Lourdes, Rocío y Lour. Por ultimo, mi mas cariñoso agradecimiento es para mi familia, a mis padres, que confiaron en mi cuando tome la decisión de, en primer lugar, estudiar Geología y, posteriormente, de embarcarme en esta aventura que es la investigación, y a mis hermanos, María José y Fede, porque siempre estais a mi lado y habéis sabido apoyarme y hacerme reír cuando mas lo he necesitado. Y por supuesto, a mis niños, Diego y mi pequeñita, vosotros sois el motor que pone en marcha mi vida.

Y a ti, Diego.

Summary

The Sierra del Convento mélange, located in the province of Guantánamo (eastern Cuba), consists of a serpentinitic matrix and exotic metamorphic blocks of variable composition and metamorphic grade. This mélange represents a subduction channel developed in response to oceanic subduction in the northern margin of the Caribbean plate during the Cretaceous.

The most significant lithology among the exotic blocks is plagioclase-lacking pargasite + epidote ± quartz ± garnet amphibolite with variable grain size and degree of deformation. These blocks commonly contain cm- to m- size layers, pockets, and veins of low-K peraluminous leucocratic tonalite-trondhjemite. The magmatic assemblages of these rocks consist of plagioclase + quartz + epidote ± paragonite ± pargasite. The rocks show variable grain size and, in general, minor extent of deformation. Agmatitic and stromatic structures typical of migmatites are common. These leucocratic bodies appear associated with the amphibolites and do not crosscut other types of exotic block or the serpentinite matrix. Though the leucocratic material is trondhjemitic to tonalitic in composition, they are henceforth collectively named trondhjemites.

Field relationship, mineral assemblages, peak metamorphic conditions, theoretical phase relations, mass balance calculations, major and trace element geochemistry, Sr and Nd isotopic signatures, and geochemical models support that the trondhjemites formed by partial melting of the amphibolites under water-saturated conditions. This makes the Sierra del Convento mélange one of the few partially melted subducted oceanic complexes returned to the Earth's surface.

Thermobarometric estimates indicate that partial melting of the amphibolites took place at. 750ºC and 14-16 kbar, and that crystallization of the trondhjemites occurred at depth (ca. 700-750ºC and 12-15 kbar). Model mass-balance calculations and phase relations suggest that the melting process was characterized by large relative amounts of reactant plagioclase, which was eventually completely consumed upon melting, and that the melt fraction was small. Interestingly, melting of metaluminous mafic material formed peraluminous melts. This has important consequences for the interpretation of slab melts. Peraluminosity and crystallization at depth explain the presence of magmatic paragonite in the trondhjemites.

Major and trace element geochemistry of the amphibolites show normal-MORB geochemical signatures slightly modified by partial melting and melt extraction. The geochemistry of the trondhjemites compares to that of Cenozoic adakitic volcanic rocks, generally interpreted as partial melting products of subducted oceanic crust which react with the mantle wedge in the course of their ascend to the volcanic arc. The studied trondhjemites have SiO_2 >56 wt. %, 3.5< Na_2O< 7.5 wt. %, (K_2O/Na_2O) ~ 0.42, Mg# ~ 50, high La/Yb, and high Sr/Y. Their REE patterns are fractionated, with LREE enrichment and flat or slightly depleted HREE patterns. However, the trondhjemitic rocks from the Sierra del Convento mélange compare better to the acid rocks from the Catalina Schist complex (California), considered as primary slab melts that did not react with the mantle wedge. Geochemical models based on available melt-mineral partition coefficients indicate melt fractions in the range 1-30 % by weight. In agreement with major and trace element geochemistry, the Sr and Nd isotope geochemical signatures of amphibolites and trondhjemites suggest that MORB material underwent partial melting in the subduction environment. Interestingly, the Sr isotope ratios indicate that the external fluid fluxed into the amphibolites during melting did not have a sea-water and/or sedimentary component.

Metamorphic overprints made of combinations of omphacite, glaucophane, actinolite, tremolite, paragonite, lawsonite, albite, (clino)zoisite, chlorite, pumpellyite, and phengite formed during retrograde blueschist facies conditions both in the amphibolites and trondhjemites. Calculated P-T conditions indicate counterclockwise P-T paths (i.e., "Franciscan type" exhumation) consistent with syn-subduction exhumation in a subduction channel.

Formation of amphibolite-trondhjemite at high pressure and high temperature conditions documents high geothermal gradient during subduction of oceanic lithosphere. High geothermal gradient during subduction and counterclockwise P-T paths of blocks from the Sierra del Convento mélange contrast with the thermal evolution of blocks from other serpentinite mélanges in Cuba, where high-pressure

blocks record clockwise P-T evolutions typical of "Alpine-type" exhumation. This indicates distinct subduction environments of formation. Hot subduction in eastern Cuba is interpreted as the result of onset of subduction of young oceanic lithosphere.

Partial melting of subducted oceanic crust in eastern Cuba is unique in the Caribbean realm and has significant consequences for the plate tectonic interpretation of the region. U-Pb SHRIMP and Ar-Ar data constrain the evolution of the subduction zone. Zircon from a tonalitic rock from the complex provided a U-Pb crystallization age of 112.8 ± 1.1 Ma. Ar-Ar amphibole dating in several amphibolitic and trondhjemitic blocks yielded two groups of cooling ages, 106-97 Ma (interpreted as cooling of metamorphic/magmatic pargasite) and 87-83 Ma (interpreted as growth/cooling of retrograde overprints). These data, combined with the calculated counterclockwise P-T paths, allow establishing the following history of subduction and exhumation in the region: (a) a hot subduction stage during 120-115 Ma, developed shortly after the onset of subduction, (b) relatively fast near-isobaric cooling during 115-107 Ma, after accretion of the blocks to the upper mantle plate, (c) slow syn-subduction cooling and exhumation in the subduction channel during 107-70 Ma, and (d) fast syn-collision cooling and exhumation during 70-60 Ma, when subduction concluded in the region.

Resumen

La mélange de La Sierra del Convento se localiza en la provincia de Guantánamo (Cuba oriental) y consta de una matriz sepentinítica en la que se incluyen bloques exóticos de composición y grado metamórfico variable. Esta mélange representa un canal de subducción desarrollado como respuesta a una subducción oceánica en el margen norte de la placa del Caribe durante el Cretácico.

Las litologías más distintivas dentro de los bloques exóticos son anfibolitas cuya mineralogía esta constituida por pargasita +epidota ± cuarzo ± granate, sin plagioclasa. Estas anfibolitas tienen un tamaño de grano y un grado de deformación variable. Estos bloques exóticos comúnmente contienen capas, bolsas o venas de tamaño centimétrico a métrico de tonalita-trondhjemita peraluminosa de bajo K. Las asociaciones magmáticas de estas rocas están constituidas por plagioclasa + cuarzo +epidota ± paragonita ± pargasita. Además, tienen tamaño de grano variable y, en general, menor grado de deformación que las anfibolitas. Las estructuras agmatíticas y estromáticas típicas de las migmatitas son comunes. Estos cuerpos leucocráticos aparecen asociados exclusivamente a las anfibolitas y no cortan otros tipos de bloques exóticos ni a la propia matriz serpentinítica. Aunque el material leucocrático es de composición trondhjemítica a tonalítica, estas rocas son en conjunto denominadas trondhjemitas.

Tanto las relaciones de campo, como las asociaciones minerales, las condiciones de pico metamórfico, las relaciones de fase teóricas, los cálculos de balance de masas, la geoquímica de elementos mayores y traza, las características de isótopos de Sr y Nd, y los modelos geoquímicos llevados a cabo, apoyan la premisa de que las trondhjemitas se formaron por la fusión parcial de las anfibolitas bajo condiciones de saturación en agua. Este hecho hace de la Sierra del Convento unos de los pocos complejos a nivel mundial de corteza oceánica subducida parcialmente fundida retornada a la superficie terrestre.

Las estimaciones termobarométricas indican que la fusión parcial de las anfibolitas tuvo lugar a 750ºC y 14-16 kbar, y que la cristalización de las trondhjemitas ocurrió en profundidad (ca. 700-750ºC y 12-15 kbar). Los cálculos de balance de masas y las relaciones de fases sugieren que el proceso de fusión se caracterizó por una gran cantidad relativa de plagioclasa reactante, que fue eventualmente consumida durante la fusión, y porque la fracción de fusión fue pequeña. Muy interesante es el hecho de que la fusión de material máfico metaluminoso formó fundidos peraluminosos. Esto tiene importantes consecuencias para la interpretación de los fundidos de la lamina subducente. La peraluminosidad y la cristalización en profundidad explican la presencia de paragonita magmática en las trondhjemitas.

La geoquímica de elementos mayores y trazas de las anfibolitas muestra características geoquímicas de tipo normal-MORB ligeramente modificadas por la fusión parcial y la extracción del fundido. La geoquímica de las trondhjemitas se compara con la de las rocas volcánicas adakíticas del Cenozoico, generalmente interpretadas como los productos de la fusión parcial de una corteza oceánica subducida que reaccionaron con la cuña mantélica suprayacente durante su ascenso hacia el arco volcánico. Las trondhjemitas estudiadas tienen SiO_2 >56% en peso, $3.5<Na_2O<7.5$ % en peso, $(K_2O/Na_2O) \sim 0.42$, Mg# ~ 50, ratios La/Yb y Sr/Y elevadas. Presentan patrones de REE fraccionados, con enriquecimiento en LREE y patrones planos o ligeramente empobrecidos en HREE. No obstante, las trondhjemitas de la mélange de La Sierra del Convento comparan mejor con las rocas acidas del complejo de mélange de los Esquistos Catalina (California), considerados como los fundidos primarios de una lamina subducente que no reaccionaron con la cuña de manto suprasubducción. Los modelos geoquímicos basados en los coeficientes de partición fundido-mineral disponibles, indican fracciones de fundido entre 1 y 30% en peso. De acuerdo con la geoquímica de elementos mayores y trazas, las características isotópicas de los isótopos de Sr y Nd tanto de las anfibolitas como de las trondhjemitas, sugieren que el material MORB sufrió fusión parcial durante la subducción. Cabe destacar el hecho de que las ratios de los isótopos de Sr indican que el fluido externo que fluyó entre las anfibolitas durante la fusión no era de agua del mar y/o componente sedimentario.

La asociación metamórfica retrógrada se compone de combinaciones de onfacita, glaucofana, actinolita, tremolita, paragonita, lawsonita, albita, (clino)zoisita, clorita, pumpellyita y fengita formadas

durante la condiciones retrógradas en facies de esquistos azules tanto para las anfibolitas como para las trondhjemitas. Las condiciones P-T calculadas indican trayectorias P-T antihorarias (i.e. exhumaciones "tipo Franciscano"), consistentes con la exhumación sincrónica con subducción en el canal de subducción.

La formación de la anfibolitas-trondhjemitas en condiciones de alta presión y alta temperatura indican un elevado gradiente geotérmico durante la subducción de la litosfera oceánica. Tanto los elevados gradientes geotérmicos durante la subducción como las trayectorias P-T antihorarias de los bloques de la mélange de La Sierra del Convento contrastan con la evolución térmica de los bloques de otras mélanges serpentiníticas de Cuba, en las que los bloques de alta presión registran evoluciones P-T horarias típicas de exhumaciones de "tipo Alpina". Esto indica que la formación tuvo lugar en distintos ambientes de subducción. La subducción caliente en Cuba oriental se interpreta como el resultado del comienzo de la subducción de una litosfera oceánica joven.

La determinación de fusión parcial de una corteza oceánica subducida en Cuba oriental es única en todo el margen caribeño y tiene consecuencias muy importantes para la interpretación de la tectónica de placas de la región. Nuevos datos de U-Pb SHRIMP y Ar-Ar permiten determinar la evolución de la zona de subducción. Zircones de una roca tonalítica del complejo proporcionaron una edad de cristalización de 112.8 ± 1.1 Ma. Datos de Ar-Ar en anfíboles de distintos bloques anfibolíticos y trondhjemíticos dieron dos grupos de edades de enfriamiento para las muestras, 106-97 Ma (interpretada como el enfriamiento de la pargasita magmática/metamórfica) y 87-83 (interpretada como el crecimiento/enfriamiento del anfíbol retrógrado). Estos datos se combinan con las trayectorias P-T antihorarias calculadas y permiten establecer la siguiente historia de subducción y exhumación en la región: (a) un estadio inicial de subducción caliente que va desde 120 a unos 115 Ma desarrollado justo después del comienzo de la subducción, (b) un enfriamiento relativamente rápido y próximo a ser isobárico tras la acreción de los bloques a la placa de manto, durante 115-107 Ma, (c) un enfriamiento y exhumación lentos, sincrónico con la subducción, en el canal de subducción durante 107-70 Ma, y, por ultimo, (d) un enfriamiento y exhumación, sincrónico con la colisión, rápidos, durante 70-60 Ma, cuando la subducción terminó en la región.

Preface

Cuba constitutes part of the Caribbean orogenic belt that runs from Guatemala through the Antilles to northern South America (Figure 1). In the Greater Antilles this orogenic belt documents the collision of a Mesozoic-Tertiary intra-oceanic volcanic arc system with the North American plate. In Cuba, collision endured from the latest Cretaceous to the middle Eocene (Iturralde-Vinent, 1996, 1998). Collision preceded a long lasting stage of oceanic subduction which started during the early Cretaceous (Aptian; Pindell et al, 2005, 2006). This subduction zone was S-SW dipping and consumed Atlantic (Protocaribbean) lithosphere. The present-day equivalents of the largest Mesozoic-Tertiary Caribbean subduction zone and volcanic arc are the Lesser Antilles trench and volcanic arc, respectively. Previous to the Aptian, subduction of the Pacific (Farallon) plate contributed to the formation of pre-Aptian-Albian volcanic rocks (Pindell et al., 2005, 2006).

In Cuba the orogenic belt is composed of oceanic material (ophiolites and intra-oceanic volcanic arc terranes) together with continental material from the borderlands of North-America (Bahamas platform) and the Maya (Yucatan) block (Figure 2). Metamorphic rocks documenting subduction crop out in serpentinite melanges classically considered as part of the ophiolites, as well as in subducted sedimentary terranes of unknown paleogeographic origin (e.g., the Escambray terrane; Somin and Millan, 1981). All these rocks form part of discrete N-NE directed tectonic units. In west and central Cuba, the basic architecture of the belt is defined by a stack of units made of (bottom to top in the pile) volcanic-arc, ophiolites and sedimentary units of the Caribbean, Caribbean forearc and Bahamian-Maya borderlands, respectively. In eastern Cuba, between the Nipe and Oriente faults, the ophiolitic units are emplaced on top of the Cretaceous volcanic arc rocks (Figure 3). The stacks are covered by Paleocene-Eocene syn-orogenic deposits typically of turbiditic and olistostromic character which are also overridden by the allochtonous units (Iturralde-Vinent, 1996, 1998).

The volcanic arc units are made of volcanic, volcano-sedimentary, and plutonic arc rocks. The magmatic rocks are basic to acid in composition, and document an early Cretaceous (late Neocomian-Aptian-Albian) oceanic island arc of tholeiitic (IAT) affinity which evolved to a voluminous calc-alkaline (CA) and high-alkaline arc in Albian to Campanian times (Iturralde-Vinent, 1996, 1998). Similar sequences have been identified all along the Caribbean realm, from Guatemala through the Antilles, Trinidad-Tobago, the Netherlands Antilles, and Venezuela to Colombia and, for this reason, they have been collectively named as the Great Arc of the Caribbean (Burke, 1988). During the Paleogene (upper Danian-lower Eocene), a new volcanic arc of calc-alkaline affinity was developed in eastern Cuba (Sierra Maestra). Similar Paleogene volcanic arc rocks occur in Jamaica, Hispaniola, and Puerto Rico (Lewis and Draper, 1990).

The ophiolitic material form elongated bodies located in the mid-northern part of Cuba. For this reason it has been termed “Northern Ophiolite Belt” (Iturralde-Vinent, 1989). The bodies are made of fragments of typical ophiolites (serpentinitic harzburgite tectonites, gabbroids, basalts, and oceanic sedimentary rocks). Dispersed within these bodies occur tectonic mélanges composed of serpentinitic matrix and exotic blocks of ophiolite, volcanic arc material, sediments of the Bahamian-Maya borderlands, and subduction-related high pressure metamorphic rocks. In eastern Cuba, the ophiolites form two large bodies termed Mayarí-Cristal and Moa-Baracoa complexes. Both were grouped in the “eastern Cuba ophiolites” (Iturralde-Vinent et al., 2006) to emphasize their geological differences relative to west-central Cuba ophiolites. The two complexes have geochemical supra-subduction signatures suggesting formation in a back-arc environment (Proenza et al., 2006; Marchesi et al., 2006). Serpentinite matrix mélanges containing subduction-related metamorphic blocks (i.e., La Corea and Sierra del Convento mélange, Figures 2 and 3) appear at the base of the ophiolite bodies and overriding the volcanic arc units of the region (Santo Domingo and Purial complexes, Figure 3).

Collectively, the metamorphic blocks of the mélanges document the history of subduction in the region. However, notwithstanding the important contributions by M.L. Somin and G. Millán (particularly, Somin and Millán, 1981), the evolution of metamorphism and its bearing to the geodynamic evolution of the northern margin of the Caribbean plate are perhaps the worst

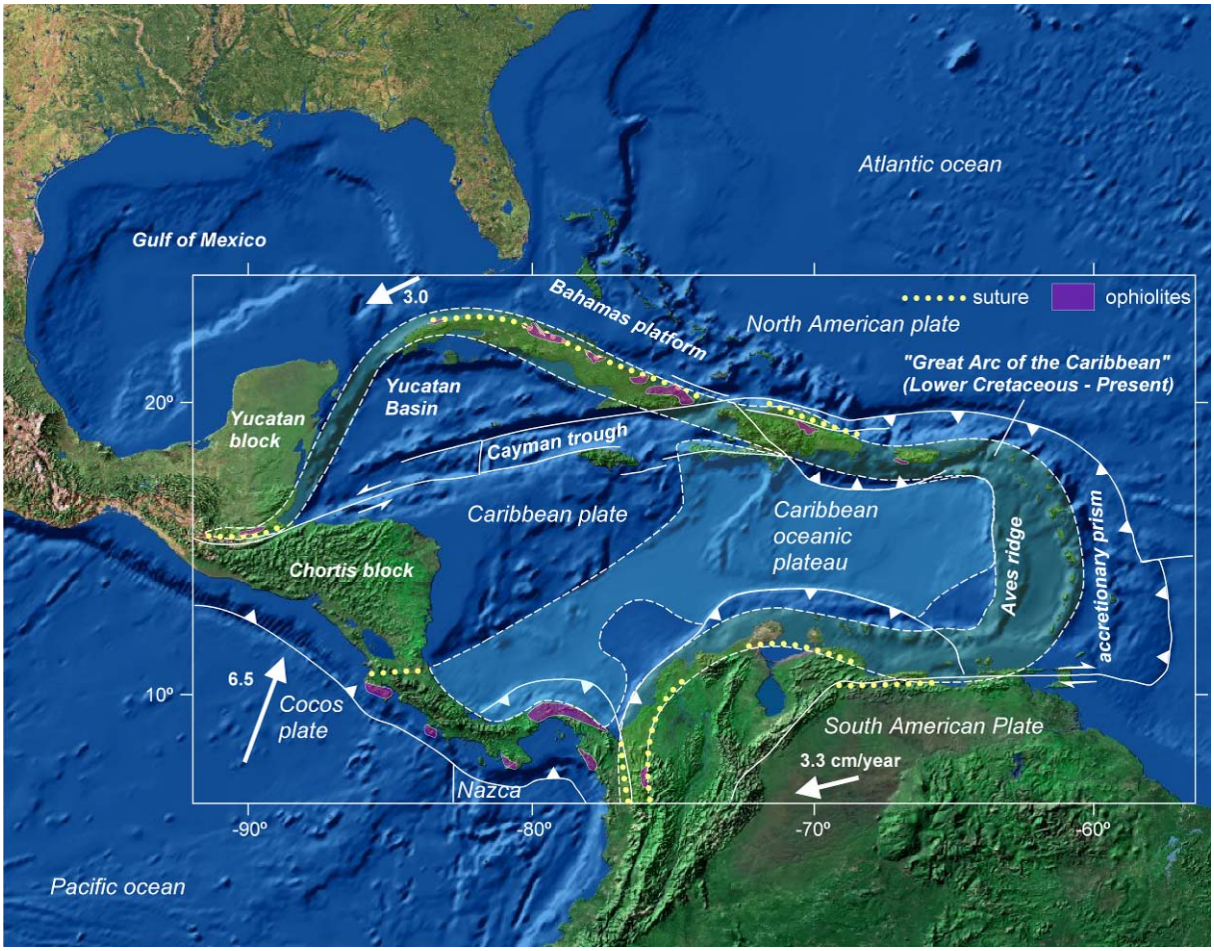

FIGURE 1. Plate tectonic configuration of the Caribbean region, with important geological features including ophiolitic bodies and Cretaceous- Tertiary suture zones (compiled after Draper et al., 1994; Meschede and Frisch, 1998; and Mann, 1999).

known geological issues of Cuba. García-Casco et al. (2006) showed that the subduction-related high pressure rocks of Cuba show variable metamorphic evolution. In west-central and eastern Cuba subduction-related metamorphic complexes appear as serpentinite-matrix mélanges containing high pressure blocks of subducted oceanic material. Eclogite, blueschist, and garnet amphibolite blocks from these mélanges document cold (i.e. mature) subduction of oceanic lithosphere. Some blocks of eclogite and garnet amphibolite followed clockwise P-T evolutions typical of "Alpine-type" exhumation. The age data and interpretation P-T paths suggest subduction during pre-Aptian times and arrest of subduction during the Aptian-Albian (García-Casco et al., 2002; 2006).

In eastern Cuba, metamorphic blocks of greenschist, blueschist, epidote amphibolite, and epidote-garnet amphibolite (but not eclogite) occur within similar subduction-related serpentinite-matrix mélanges. These blocks document both hot and cold subduction. Hot subduction is recorded in epidote ± garnet amphibolite blocks and associated tonalite-trondhjemite which followed counterclockwise P-T paths characterized by near-isobaric cooling and cold decompression (i.e., "Franciscan-type" exhumation). Available age data and interpretation of P-T paths suggest formation during the Aptian-Albian, likely during the onset of subduction of a young oceanic lithosphere or a ridge, and exhumation during the Upper Cretaceous (García-Casco et al., 2006). This work is focused to the petrogenesis of amphibolite and associated tonalite-trondhjemite blocks from the Sierra del Convento mélange.

The Sierra del Covento mélange is located in the Guantánamo province of eastern Cuba. Eastern Cuba is perhaps the worst known geological region of Cuba. Orographic and administrative accessibility difficulties, together with very intense tropical weathering, and tectonic and lithological complexities have made the geologic study of this region difficult. However, the

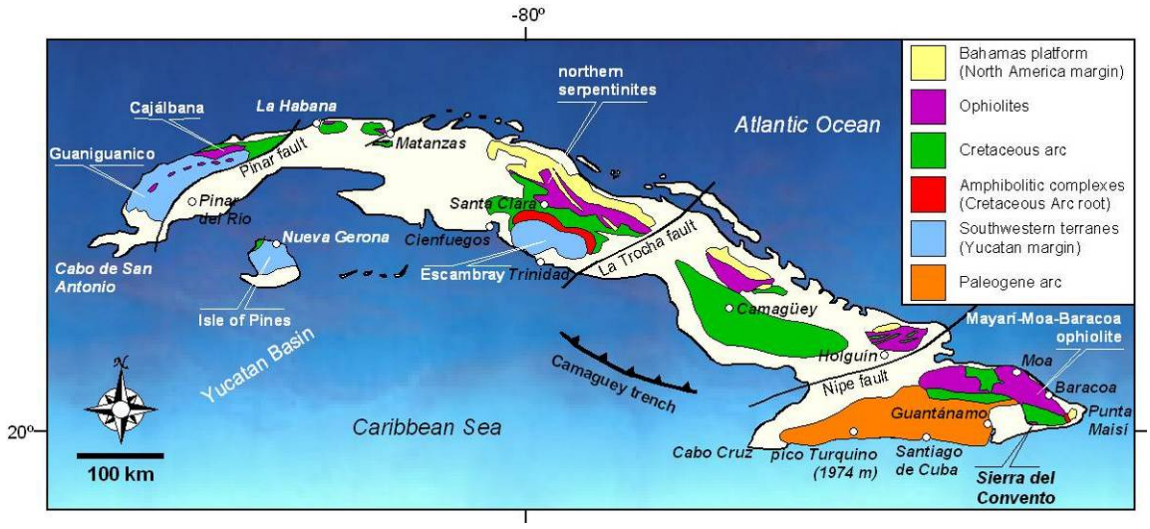

FIGURE 2. Geological sketch map of Cuba (after Iturralde-Vinent, 1996) showing location of the Sierra del Convento mélange and other important geologic and geographic elements.

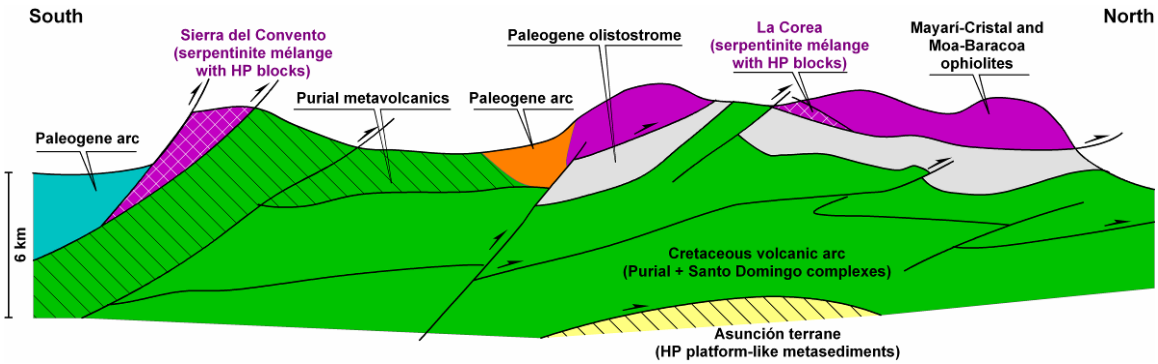

FIGURE 3. Generalized sketch cross-section of eastern Cuba (after Iturralde-Vinent, 1998) showing the relation of major geological complexes in the region.

geology of the region is still poorly known, and detailed geologic, structural, and petrologic analysis is lacking. Literature references to the geology and petrology of the Sierra del Convento mélange are very scarce. To give an idea of such lack of knowledge it could be mentioned that Gyarmati (1983) do not even mention the mélange in his review of metamorphic rocks of eastern Cuba. Basically, the literature concerning the Sierra del Convento mélange is restricted to a few papers by a fairly short number of authors: Boiteau et al. (1972) and Somin & Millán (1981), who identified the mélange and described a variety of metamorphic blocks; Cobiella et al. (1984), Kulachlov & Leyva (1990), Hernández & Canedo (1995), Millán (1996) and Leyva (1996) who provided additional basic field and petrographic descriptions; and Somin et al. (1992) who provided a few K-Ar age data.

Perhaps, the best description of the Sierra del Convento mélange is found in Somin and Millán (1981). As noted above, this book is the best (and only) comprehensive work on the metamorphic geology (field relations, mineral assemblages, textures, and age) of Cuba published to date. These authors presented petrographic descriptions of rocks from the Sierra del Convento mélange and identified its relation to a subduction environment. However, a detailed petrological and geochemical characterization of this subduction mélange was lacking. Such a study is important because of two main reasons: (a) the significance of this subduction mélange for the knowledge of the interactions among the Caribbean and adjacent plates during the Mesozoic-Tertiary and (b) the presence of a subduction-related migmatitic complex, which makes this complex exceptional as only few partially melted subduction complexes have been described to date. These two issues constitute the main objectives of the work presented.

This PhD Thesis is entitled **"Petrological and Geochemical study of a subduction mélange (Sierra del Convento, Eastern Cuba). A case of partially melted slab"**. The work has been supervised by Dr. Antonio García Casco

(Departamento de Mineralogía y Petrología, Universidad de Granada) and has received financial support from the research projects BTE2002-01011 "*Terrenos metamórficos en el margen septentrional del Caribe (Cuba)*" and CGL2006-08527/BTE "*Evolución metamórfica en márgenes de placa convergentes: Desde el inicio de la subducción oceánica hasta la colisión arco-continente en el margen septentrional de la placa del Caribe, Cuba*" of the Ministerio de Ciencia y Tecnología and Ministerio de Educación y Ciencia, respectively, the Junta de Andalucía Research Group RNM 302 "*Petrología y modelización de procesos litosféricos*", and the UNESCO research projects nº433 "*Caribbean plate tectonics*" and nº 546 "*Subduction zones of the Caribbean*".

Throughout the four years of development of this project we carried out a preliminary fieldtrip in order search the study area and collect 27 samples, and two sampling campaigns when we collected 93 samples (June 2003) and 122 samples (December 2003), respectively, from the Sierra del Convento mélange and nearby complexes. Of this sample set, 62 samples were selected for detailed petrographic study (Table A). Some of these 62 samples were selected for subsequent electron microscopy and geochemical work carried on in the "Centro de Instrumentación Científica", University of Granada. Also, Ar/Ar isotopic analyses were carried on during a three-month stay in the ARGONAUT laboratory, Universität Salzburg (Austria). These actions have permitted a direct collaboration with researches from several institutions, including Guillermo Millán and Kenya Núñez, (Instituto de Geología y Paleontología, Ministerio de la Industria Básica, Cuba), Manuel Iturralde-Vinent (Museo Nacional de Historia Natural, Cuba), Franz Neubauer (Universität Salzburg, Austria), and Alfred Kröner and Yamirka Rojas (University of Mainz, Germany). I am proud to say that this study has been conducted in the frame of a large collaborative project among all these researchers and institutions.

A compilation and revision of previous and new age and P-T-t data of metamorphic blocks from serpentinite mélanges all along Cuba was conducted and is presented here as **Chapter I Geological and Petrological Settings**. This Chapter I, published in *Geologica Acta* (García-Casco et al., 2006), offers the basic geological and petrological setting of this study. It is shown that the most significant mélange complexes from eastern Cuba, i.e., the Sierra del Convento and La Corea mélanges, share a similar lithological assemblage which differs from that of mélanges from west-central Cuba.

The most outstanding characteristic of eastern Cuba mélanges is the occurrence of partially melted rocks subducted to moderate depths (ca. 50 km). This indicates a hot subduction scenario uncommon in fossil subduction complexes. In anomalously hot conditions subduction environments, flux of water from subjacent lithologies allows the geothermal gradient to intersect the wet-solidus of metabasite, making possible the production of slab melts (Prouteau et al., 1999, 2001). These slab melts were first described by Kay (1978) in the Aleutian arc and have been defined as new magma type termed adakite (Martin, 1986; Defant and Drummond, 1990). During their ascent to the surface the slab melts react with the overlying peridotite wedge and change their original composition, producing adakitic rocks. Thus, the study of the products of partial melting in the Sierra del Convento mélange contribute to the petrogenesis of slab melts and adakites.

The petrogenesis of the amphibolite-trondhjemite association from the Sierra del Convento mélange is given in chapters II and III. In **Chapter II: Petrology** (accepted for publication in the *Journal of Petrology*) we present descriptions of field relations, mineral assemblages and textures, and major element compositions of rocks and minerals, as well as P-T estimates for the various stages of evolution of amphibolites and their partial melting trondhjemitic-tonalitic products. These data are used to derive a petrogenetic model based on phase relations. The findings are used to propose a tectonic model of formation.

In **Chapter III: Geochemistry** (submitted for publication in *Chemical Geology*) the elemental and Sr and Nd isotope geochemistry of amphibolite and associated tonalite-trondhjemite is provided. The petrogenesis of the trondhjemites is discussed in terms of melting models using available distribution coefficients of key elements between the melt and coexisting phases. The implications for adakite petrogenesis are discussed.

The evolution of subduction in the northern margin of the Caribbean realm is presented in **Chapter IV: Geochronology and P-T-t paths** (to be submitted for publication in the *Journal of Metamorphic Geology*). Calculated burial, exhumation, heating, and cooling rates of studied blocks are derived from new Ar-Ar amphibole and SHRIMP U-Pb zircon data (provided by Y. Rojas and A. Kröner) and previously published K-Ar data. The calculated rates allow establishing the full history of subduction and exhumation in the associated subduction channel, from the onset of subduction during the early Cretaceous (ca. 120 Ma) to its demise in the late Cretaceous-early Tertiary (70-60 Ma) when collision started in the region.

REFERENCES

Boiteau, A., Michard, A., Saliot, P. 1972. Métamporphisme de haute pression dans le complexe ophiolitique du Purial (Oriente,Cuba). Comptes

Rendus de l'Académie des Sciences Paris 274 (série D), 2137-2140.

Burke, K., 1988. Tectonic evolution of the Caribbean. Annual Reviews of Earth and Planetary Sciences, 16, 201-230.

Cobiella, J., Quintas, F., Campos M., Hernández, M. 1984. Geología de la Región Central y Suroriental de la Provincia de Guantánamo. Santiago de Cuba: Editorial Oriente, Santiago de Cuba, 125 pp.

Defant, M.J., Drummond, M.S., 1990. Derivation of Some Modern Arc Magmas by Melting of Young Subducted Lithosphere. Nature 347(6294), 662-665.

Draper, G., Jackson, T. A. & Donovan, S. K., 1994. Geologic provinces of the Caribbean Region. In: Caribbean Geology: An Introduction. (eds Donovan, S. K. & Jackson, T. A.), pp. 3-12, U.W.I. Publishers' Association, Kingston (Jamaica).

García-Casco, A., Torres-Roldán R. L., Iturralde-Vinent, M. A., Millán, G., Núñez Cambra, K., Lázaro, C. & Rodríguez Vega, A. 2006. High pressure metamorphism of ophiolites in Cuba. Geologica Acta 4, 63-88.

García-Casco, A., Torres-Roldán, R.L., Millán, G., Monié, P., Schneider, J., 2002. Oscillatory zoning in eclogitic garnet and amphibole, Northern Serpentinite Melange, Cuba: a record of tectonic instability during subduction? Journal of Metamorphic Geology, 20, 581-598.

Gyarmati, P., 1983. Las rocas intrusivas intermedias de Cuba oriental. In E. Nagy et al. (eds.). Contribución a la geología de Cuba Oriental, Edit. Cient.-Técnica, 99-111.Iturralde-Vinent, M. A. 1998. Sinopsis de la constitución Geológica de Cuba. Acta Geologica Hispanica 33, 9-56.

Hernández, M., Canedo, Z., 1995. Geoquímica de las ofiolitas meridionales de Cuba oriental. University of Moa, Moa (Cuba).

Iturralde-Vinent, M. A. 1996. Introduction to Cuban Geology and Geophysics. In: Iturralde-Vinent, M. A. (ed.) Ofiolitas y Arcos Volcánicos de Cuba. Miami, USA, IGCP Project 364 Special Contribution 1, 3-35.

Iturralde-Vinent, M.A., 1989. Role of ophiolites in the geological constitution of Cuba. Geotectonics, 4, 63-74.

Iturralde-Vinent, M. A., Díaz Otero, C., Rodríguez Vega, A. & Díaz Martínez , R., 2006. Tectonic implications of paleontologic dating of Cretaceous-Danian sections of Eastern Cuba. Geologica Acta, 4, 89-102.

Kay, R.W., 1978. Aleutian Magnesian Andesites - Melts from Subducted Pacific Ocean Crust. Journal of Volcanology and Geothermal Research 4(1-2), 117-132.

Kulachkov, L. V. & Leyva, R. C. (1990). Informe sobre los resultados de los trabajos de reconocimiento geológico para cuarzo filoniano en la parte oriental de Cuba. Unpublished report of the Instituto Superior Minero-Metalúrgico de Moa (Cuba).

Lewis, J.F., Draper, G., 1990. Geological and tectonic evolution of the northern Caribbean margin. In: Dengo, G., Case, J.E. (Eds.), The Geology of North America, The Caribbean Region. Geological Society of America, Colorado, pp. 77–140.

Leyva, R. C. 1996. Características geológicas, regularidades de distribución y perspectivas de utilización del cuarzo filoniano de la región oriental de Cuba. Unpublished report of the Instituto Superior Minero-Metalúrgico de Moa (Cuba), 90 pp.

Mann, P., 1999. Caribbean sedimentary basins: Classification and tectonic setting. In: Caribbean Basins. Sedimentary Basins of the World 4 (ed Mann, P.), pp. 3-31, Elsevier Science B.V., Amsterdam.

Marchesi, C., Garrido, C.J., Godard, M., Proenza, J.A., Gervilla, F., & Blanco-Moreno, J., 2006. Petrogenesis of highly depleted peridotites and gabbroic rocks from the Mayarí-Baracoa Ophiolitic Belt (eastern Cuba). Contributions to Mineralogy and Petrology 151(6), 717-736.

Meschede, M. & Frisch, W., 1998. A plate tectonic model for the Mesozoic and Early Cenozoic history of the Caribbean plate. Tectonophysics, 296, 269-291.

Martin, H., 1986. Effect of steeper Archaean geothermal gradient on geochemistry of subduction-zone magmas. Geology 14, 753-756.

Millán, G. (1996). Metamorfitas de la asociación ofiolítica de Cuba. In: Iturralde-Vinent, M. A. (ed.). Ofiolitas y Arcos Volcánicos de Cuba. Miami, USA, IGCP Project 364 Special Contribution 1, 131-146.

Pindell, J. L, Kennan, L., Maresch, W. V., Stanek, K. P., Draper, G. & Higgs, R. 2005. Plate-kinematics and crustal dynamics of circum-Caribbean arc-continent interactions: Tectonic controls on basin development in Proto-Caribbean margins. In: Avé Lallemant, H.G. & Sisson, V.B. (eds.) Caribbean-South American plate interactions, Venezuela. Geological Society of America Special Paper 394, 7-52.

Pindell, J. L, Kennan, L., Stanek, K. P., Maresch, W. V. & Draper, G. (2006). Foundations of Gulf of Mexico and Caribbean evolution: eight controversies resolved. Geologica Acta 4, 303-341.

Proenza, J. A., Díaz-Martínez, R., Iriondo, A., Marchesi, C., Melgarejo, J. C., Gervilla, F., Garrido, C. J., Rodríguez-Vega, A., Lozano-Santacruz, R. & Blanco-Moreno, J. A., 2006. Primitive Cretaceous island-arc volcanic rocks in eastern Cuba: the Téneme Formation. Geologica Acta, 4, 103-121.

Prouteau, G., Scaillet, B., Pichavant, M., Maury, R., 2001. Evidence for mantle metasomatism by hydrous silicic melts derived from subducted oceanic crust. Nature 410(6825), 197-200.

Prouteau, G., Scaillet, B., Pichavant, M., Maury, R.C., 1999. Fluid-present melting of ocean crust in subduction zones. Geology 27(12), 1111-1114.

Somin, M.L., Millán, G. 1981. Geology of the Metamorphic Complexes of Cuba (in Russian). Nauka, Moscow, 219 pp. [Сомин, М., Милъян, Г. (1981). Геология Метаморфических Комплексов Кубы. Наука, Москва, 219.]

Somin, M.L., Arakelyants, M.M., Kolesnikov, E.M., 1992. Age and tectonic significance of high-pressure metamorphic rocks in Cuba. International Geology Review, 34, 105-118.

Table 1. Mineral abundance in the studied amphibolite samples (visual estimates).

	peak metamorphic												retrograde										
SAMPLES	Amp	Ep	Grt	Cpx	Qtz	Pl	Pa	Rt	Ttn	Ilm	Ap	Others	Ca Amp	Gl	Chl	Pmp	Ab	Lws	Pa	Czo	Phe	Kfs	Other
CV53-I	60	30			10			x					x		x					x			
CV53X-I	58	40			x			x					x	x	2	x				x			
CV53b-I	55	35			10			x	x				x	x	x	x	x			x	x		
CV54a	60	38						x					x		2	x				x			
CV61	100	x											x	x	x	x				x	x		
CV61a	70	15			x			x	x				x	2	13	x				x			
CV61b	90	5							x				x	2	2	x				x	1		
CV62	60	30			10			x					x	x	x	x				x	x		
CV62a	60	25			13			x					x		x	x				x	2		
CV62b-I	60	30			10			x	x		x		x	x	x	x	x			x	x		
CV139a	45	20	20		5				x				x	x	x	x	x				10		
CV139b	90	9						x	1				x	x	x	x				x	x		
CV139d	100	x			x			x					x	x		x							
CV53o-I	55	35	x					x					x	x	x	x				x			
CV54e	60	20	5		15			x					x	x	x	x				x	x		
CV140a	45	10	10		x			x					x	x	x	x	5			x	30		
CV139f	30	25	5		x				5				10	10	10	x				x	5		
CV227a	60	40						x			x		x	x	x	x				x			
CV228d	60	25	5		10			x	x		x		x	x	x	x	x			x	x		
CV228e	50	35	5		10			x	x		x		x	x	x	x	x			x			
CV230a	74	10	10						1				x	x	x	x			x	x	5		
CV230b	60	25	15		x			x	x		x		x	x	x	x	x			x			
CV230c	55	25	15						5				x	x	x	x				x			
CV237c	40		5						2				20	20	8	x				5			
CV237e	40		5						2				20	20	8	x				5			
CV237h	30								x				20	20	10	x				10			
CV237i	100								x	x			x	x	x	x				x			
CV237j	50	5	15	15	x			x	5	x			x	5	5	x	x			x			Omp
CV237m-I	50	40											x	x	x	x	x			x			
CV237n	60	30			x				x				x	x	x	x				x	10		
CV237p-I	40							x	x				30	30	x	x				x			
CV279a	50		10						5	x			15	15	5	x							Cal

Table 1 (continued). Mineral abundance in the studied trondhjemite samples (visual estimates).

	magmatic												retrograde										
SAMPLES	Amp	Ep	Grt	Cpx	Qtz	Pl	Pa	Rt	Ttn	Ilm	Ap	Others	Ca Amp	Gl	Chl	Pmp	Ab	Lws	Pa	Czo	Phe	Kfs	Others
SC20		8	x		20	55	x								x		x	3	10	4	x		
SC21	5	10			10	60	10	x			x		x		x	x	x		2	1	x	x	
SC22		10			10	60	10	x							x		x	x	5	5	x		
SC23	5	10			15	60	5	x	x				x		x	x	x		2	3	5		
CV53-III		5			20	65	2				x						x		3	5	x		
CV53X-II		30			10	40	20		x								x		x	x	x		
CV53a	10	15			5	60	2	x					x		x	x	x		8	x	x		
CV53b-II					30	60	x								x		x		7	3	x	x	
CV53c		15			5	60	x										x		15	5	x		
CV53e					60																40	x	
CV53f	25	25			5	35	x	x				Ky	x		x	x	x		10	x			
CV54b	10	15			5	60	x				x		x		x	x	x		5	x	x		
CV60a		8			30	40	5	x			x	Ky			x	x	x	5	10	2	x	x	
CV60b		5			20	55	x	x			x						x	x	10	10	x		
CV62b-II	x	3			20	70	x				x		x		x		x		5	2	x		
CV201a		2			30	40									x		x	x		8	20	x	
CV201d					50	5															45	x	
CV201f					65																35	x	
CV201g			x		30	50											x				20	x	
CV53o-II		10			15	60	2	x									x		8	5			
CV227b	8	10			5	70	x	x	x				x		x		x	x	3	4			
CV228a	9	10			5	65	2	x			x		x		x		x		6	3			
CV228b		10			10	60	5	x									x	x	2	3			
CV228c	3	15			15	55	5		x		x		x		x		x	x	3	4			
CV230e					35	55														5	5	x	
CV233b		5			30	45			x												20	x	
CV237p-II	x				10	58	1		1				x		30		x			x			
CV237r	10			x		40							x		x		x			50	x		
CV201h					30	50			x						x		x		x		20		
CV278a-I			30		25																35	x	

Chapter I. Geological and Petrological Settings

This Chapter has been published in ***Geologica Acta***, Vol.4, Nº1-2, 2006, 63-88.

High pressure metamorphism of ophiolites in Cuba

A. GARCÍA-CASCO[(1)] R.L. TORRES-ROLDÁN[(1)] M.A. ITURRALDE-VINENT[(2)] G. MILLÁN[(3)] K. NÚÑEZ CAMBRA[(3)] C. LÁZARO[(1)] and A. RODRÍGUEZ VEGA[(4)]

(1) Departamento de Mineralogía y Petrología, Universidad de Granada
Fuentenueva s/n, 18002-Granada, Spain García-Casco E-mail: agcasco@ugr.es Torres-Roldán E-mail: rafael@ugr.es Lázaro Email: clazaro@ugr.es.

(2) Museo Nacional de Historia Natural
Obispo no. 61, Plaza de Armas, La Habana 10100, Cuba. E-mail: iturralde@mnhnc.inf.cu

(3) Instituto de Geología y Paleontología
Via Blanca y Carretera Central, La Habana, Cuba. E-mail: kenya@igp.minbas.cu

(4) Departamento de Geología, Instituto Superior Minero-Metalúrgico
Las Coloradas Moa, Holguín, Cuba. E-mail: arvega48@yahoo.com

ABSTRACT

High-pressure metamorphic complexes of ophiolitic material in Cuba trace the evolution of the northern margin of the Caribbean Plate during the Mesozoic. In the northern ophiolite belt of western and central Cuba, these complexes document cold (i.e., mature) subduction of oceanic lithosphere. Age data indicate subduction during pre-Aptian times followed by mélange formation and uplift during the Aptian-Albian. The P-T evolution is clockwise with relatively hot geothermal gradient during exhumation (i.e., "Alpine-type"), suggesting that exhumation may have been triggered by unroofing processes ensuing arrest of subduction. It is hypothesized that tectonic processes related to termination of subduction led to formation of characteristic oscillatory zoning of garnet recorded in blocks separated by ca. 800 km along strike of the belt. In eastern Cuba, the complexes document hot subduction with peak conditions at ca. 750 ºC, 15-18 kbar followed by near-isobaric cooling (i.e., counterclockwise P-T path). The contrasting petrologic evolution in the two regions indicates that the correlation of eastern and western-central Cuban mélanges is doubtful. The age and tectonic context of formation of these hot-subduction complexes is uncertain, but available data are consistent with formation during the Aptian-Albian due to a) the birth of a new subduction zone and/or b) subduction of young oceanic lithosphere or a ridge. Furthermore, tectonic juxtaposition of high-pressure ophiolitic material and subducted platform metasediments in the Escambray complex (central Cuba) that were decompressed at relatively cold geothermal gradients ("Franciscan-type" P-T paths) indicates syn-subduction exhumation during the uppermost Cretaceous (ca. 70 Ma). The diversity of P-T paths, ages and tectonic settings of formation of the high-pressure complexes of ophiolitic material in Cuba document a protracted history of subduction at the northern margin of the Caribbean Plate during the Mesozoic.

KEYWORDS: High-pressure. Metamorphism. Ophiolite. Subduction. Caribbean.

INTRODUCTION

Volcanic-arc and ophiolitic rocks constitute important geological elements of the Caribbean realm (Fig. 1A), and deciphering their origin and evolution is fundamental to achieving well-founded plate-tectonic reconstructions for the region. Volcanic-arcs provide insights into the age of subduction and the processes triggering it. In contrasts, ophiolites are related to generation of oceanic lithosphere either at mid-ocean ridges or at suprasubduction environments. However, ophiolitic rock assemblies, in the Caribbean and elsewhere, normally enclose high pressure (HP) metamorphic complexes indicative of the location, age and tectonic processes accompanying subduction. When associated with non-metamorphosed ophiolitic bodies, as in Cuba, high-pressure complexes are exotic relative to their enclosing ophiolitic matrix, and can be used in combination with associated non-metamorphosed ophiolites and volcanic arc terranes to constrain the geometry of plate boundaries.

In Cuba, ophiolitic material metamorphosed to high-pressure is found as blocks within serpentinite-matrix mélanges in a number of geological settings (Somin and Millán, 1981; Millán, 1996a). The most important ophiolitic assembly is the "northern ophiolite belt" (Iturralde-Vinent, 1989; 1996a and b; 1998), a discontinuous belt of more than 1000 km in length composed of discrete, variously sized bodies exposed in the north of the island, from W to E, Cajálbana, Mariel-La Habana-Matanzas, Las Villas, Camagüey, Holguín, Mayarí, Moa-Baracoa (Fig. 1B). All these bodies have been widely considered to represent a single geologic element formed within the same paleogeographic/paleotectonic setting during the Mesozoic, although more recently Iturralde-Vinent et al. (this volume) argued that eastern Cuba bodies should not be included as part of this belt. In this paper, we follow this subdivision.

The ophiolitic bodies are composed mostly of chrysotile-lizardite serpentinites, which are the metamorphic products of harzburgite, dunite and, less abundantly, pyroxenite, wehrlite and lherzolite, though they also contain fragments of the crustal sections of ophiolite, including layered and isotropic gabbros and associated cumulate rocks, chromite ores, diabase, basalt and pelagic sediments (see Iturralde-Vinent, 1996b for review; additionally, see Khudoley, 1967; Khudoley and Meyerhoff, 1971; Pardo, 1975; Somin and Millán, 1981; Fonseca et al., 1985; Iturralde-Vinent, 1989; Millán, 1996a; Kerr et al., 1999; Proenza et al., 1999). These bodies of serpentinite have been the subject of controversy concerning the origin of Alpine-type ultramafic rocks since the 1950's, when H.H. Hess proposed a primary hydrated ultramafic magma but N.L Bowen disputed this hypothesis and interpreted the bodies as solid intrusions of serpentinized peridotite (see Young, 1998, p. 201-209). In the 1970's the bodies were recognized as oceanic fragments accreted to the Yucatan/North American margin during late Upper Cretaceous to Paleogene collision of this margin with the Upper Cretaceous volcanic arc of Cuba. Oceanic transformations resulted in serpentinization and low-pressure metamorphism (Somin and Millán, 1981; Millán, 1996a; Auzende et al., 2002; Proenza et al., 2003, García-Casco et al., 2003). During accretion, the bodies were strongly sliced off, fractured and brecciated. In fact, most of them can be considered as tectonic serpentinite-matrix mélanges that contain, in addition to co-genetic igneous and sedimentary materials, exotic blocks incorporated from adjacent platform sedimentary sequences, volcanic-arc and subduction complexes. Other ophiolitic assemblies appear as tectonic slices within continental terranes that probably represent fragments of the Mesozoic platform of the Maya block (i.e., Escambray and Guaniguanico terranes of central and western Cuba, respectively; Iturralde-Vinent, 1989, 1996a; Pszczólkowski, 1999; Fig. 1B). These ophiolitic slices are composed of chrysotile-lizardite serpentinite-matrix mélanges in the Guaniguanico terrane, while in the Escambray massif they are made of a) massive garnet amphibolites (Yayabo amphibolites, sensu Millan, 1997b) and b) antigorite-bearing serpentinite-matrix mélanges containing high-pressure rocks (Somin and Millán, 1981; Millán, 1996a, 1997b; Auzende et al., 2002; Schneider et al., 2004).

Notwithstanding the important contributions by M.L. Somin and G. Millán (1981), the evolution of metamorphism is perhaps one of the least known geological issues of Cuba. In this paper, we review and provide new data concerning the metamorphic evolution of high-pressure rocks of basic composition and oceanic origin present in mélanges forming part of a) the northern ophiolite belt, b) the eastern Cuba ophiolites and c) tectonically intercalated slices within the Guaniguanico and Escambray terranes. Our principal focus is the nature, age and tectonic significance of high pressure metamorphism.

SUMMARY OF CUBAN GEOLOGIC HISTORY

The Cuban orogenic belt formed as a result of convergence between the North American and Caribbean plates in Mesozoic to Tertiary times (Iturralde-Vinent, 1988, 1994, 1996a). The process involved a large amount of oceanic material including ophiolites and intra-oceanic volcanic arc rocks that appear as complexly imbricated tectonic slices for the most part of the Cuban orogenic belt.

The earliest age of formation of the northern ophiolite belt is constrained to be Upper Jurassic by Tithonian through Albian-Cenomanian oceanic sediments that locally cover the igneous rocks in

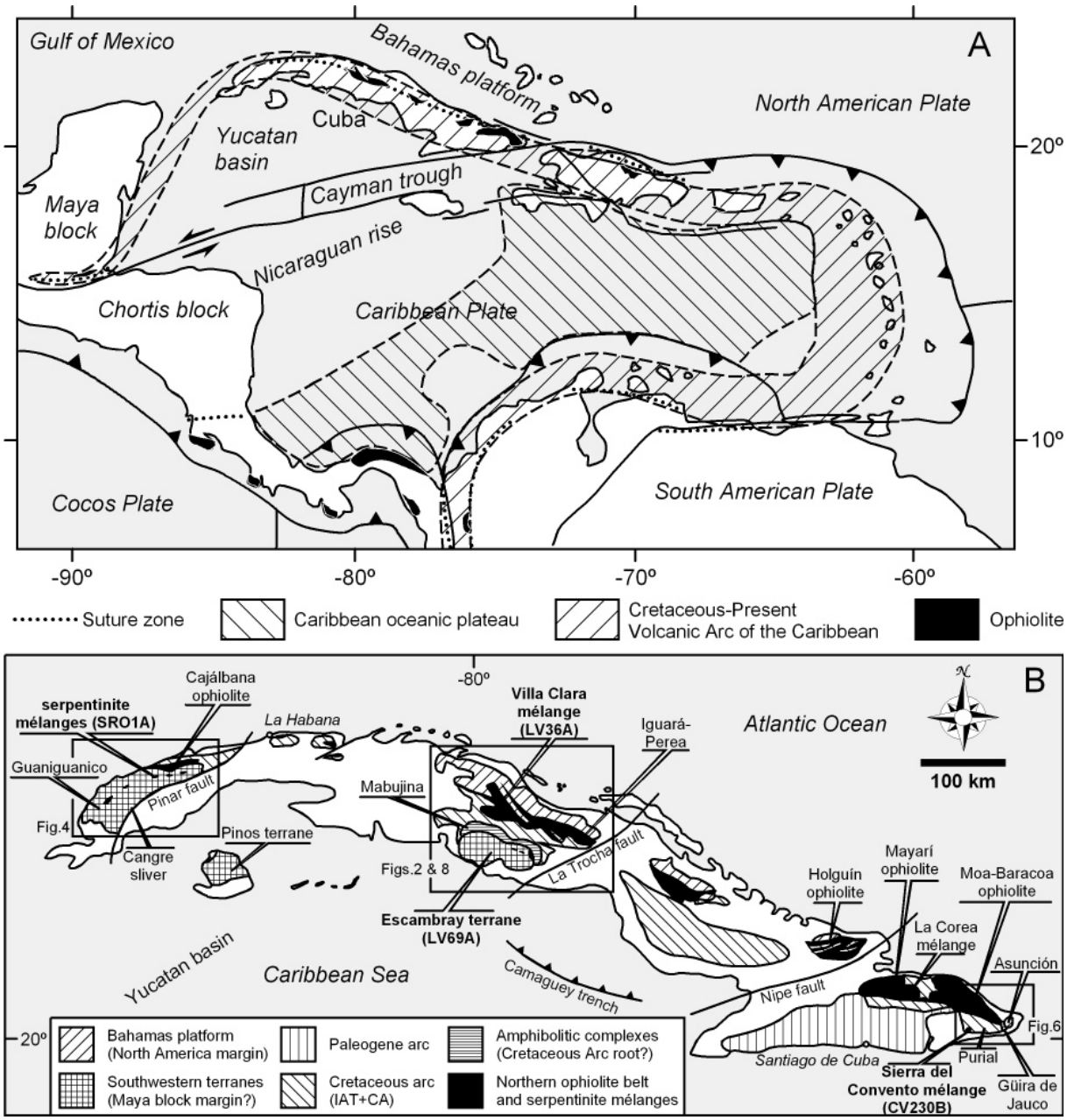

FIGURE 1 A) Plate tectonic configuration of the Caribbean region, with important geological features including ophiolitic bodies and Cretaceous- Tertiary suture zones (compiled after Draper et al., 1994; Meschede and Frisch, 1998; and Mann, 1999). B) Geological sketch of Cuba (after Iturralde-Vinent, 1996a) showing location of the northern ophiolite belt and other important geologic elements mentioned in the text, and the studied areas with indication of studied samples (see Figs. 2, 4, 6 and 8 for further detail).

different parts of the belt (Iturralde-Vinent and Morales, 1988; Iturralde-Vinent, 1994, 1996b; Llanes et al., 1998). Isotopic (mostly K-Ar) ages of igneous rocks span an interval of 160-50 Ma (see review by Iturralde-Vinent et al., 1996). Of these data, only the Upper Jurassic to Lower Cretaceous dates are commonly considered to represent formation of oceanic lithosphere, while Upper Cretaceous to Paleogene K-Ar dates are thought to represent subsequent arc-related magmatism or isotopic resetting due to post-formation alteration and deformation events. Middle-Upper Jurassic is the time of break-off of Pangea in the region and the onset of formation of an oceanic basin connected with the Atlantic, the Proto-Caribbean (sensu Pindell, 1985, 1994; see also Mann, 1999 and references therein), which opened as the Americas drifted away since that time until the Maastrichtian. According to most workers, the northern and eastern ophiolite belts of Cuba formed in the inter-Americas gap (e.g. Somin and Millán, 1981; Iturralde-Vinent, 1996a; Kerr et al., 1999), a conclusion that is

strengthened by the scarcity of associated plateau basalts (or B" material; Burke et al., 1984; Kerr et al., 1999) which are typical of the Caribbean crust. However, increasing geochemical evidence accumulated recently from Early and Late Cretaceous basaltic rocks associated with these ophiolitic complexes favours supra-subduction environments (including back-arc, fore-arc and arc settings) instead of mid-ocean ridges as the locus of basalt generation. García-Casco et al. (2003) indicated IAT signatures of basaltic rocks from the Cajálbana ophiolite body metamorphosed in an Early Cretaceous (130 Ma) volcanic arc environment. Fonseca et al. (1989) and Kerr et al. (1999) described boninitic rocks in the northern ophiolite belt (Havana region) of unknown age, but the latter authors suggested that they may represent an Early Cretaceous (Aptian-Albian or older) boninite volcanic arc. In this same belt the Margot Formation (Matanzas region) consists in back arc basalts (Kerr et al., 1999) dated as Cenomanian-Turonian (Pszczólkowski, 2002). García-Casco et al. (2003) indicated probable calc-alkaline signatures in basaltic rocks from the Iguará-Perea region (northern ophiolite belt, Las Villas) metamorphosed in a Turonian-Coniacian (88 Ma) volcanic arc environment. Andó et al. (1996) indicated calc-alkaline trend in magmatic rocks of suggested Upper Cretaceous age in the Holguín ophiolite body. Cenomanian-Turonian island arc tholeiitic basalts are recorded in eastern Cuba ophiolites (Proenza et al., 1998, 1999, this volume, Iturralde-Vinent et al., this volume). Thus, volcanic material in the northern and eastern ophiolite belts document suprasubduction environments during the Early and Late Cretaceous and, possibly, a number of intra-oceanic subduction events. The paleotectonic/paleogeographic location of the tectonic slices of (meta)ophiolitic material in the Guaniguanico and Escambray terranes, on the other hand, remains uncertain due to their complex tectonic relationships and lack of detailed geochemical studies.

A belt of tectonic units consisting of volcanic, volcanic-sedimentary and plutonic arc rocks of basic through acid composition all along the island (Fig. 1B) documents an Early Cretaceous (Late Neocomian-mid Albian age) island arc of tholeiitic (IAT) affinity rooted by oceanic lithosphere that developed into a voluminous calc-alkaline (CA) and high-alkaline arc (Albian-Campanian; Iturralde-Vinent, 1996c and d; Díaz de Villalvilla, 1997; Kerr et al., 1999, Iturralde-Vinent et al., this volume, and references therein). This sequence of Cretaceous arc volcanism in Cuba is similar to that identified all along the Caribbean region (Donnelly and Rogers, 1978; Burke, 1988; Donnelly et al., 1990; Lebron and Perfit, 1993, 1994; Jolly et al., 2001). Burke (1988) named this arc the Great Arc of the Caribbean, which would have evolved as a response to Cretaceous subduction in the region, but the relationship between this volcanic-arc terrane and the various types of suprasubduction magmatic events recorded in northern and eastern ophiolite belts is uncertain.

Intense collision tectonics, ophiolite obduction and olistostrome formation of latest Cretaceous through Paleocene-Middle Eocene age relate to the collision of the oceanic volcanic arc terranes with the ophiolites and the continental margins of the Maya and Bahamas blocks (Pszczólkowski and Flores, 1986; Iturralde-Vinent, 1994, 1996a, 1998; Bralower and Iturralde-Vinent, 1997; Gordon et al., 1997). The Campanian termination of the volcanic arc and the Upper Cretaceous isotopic ages of continental metamorphic terranes (Escambray, Isle of Pines) and of the oceanic roots of the volcanic arc (Mabujina complex) (Iturralde-Vinent et al., 1996; García-Casco et al., 2001; Grafe et al., 2001; Schneider et al., 2004) indicate onset of arc-continent collision in the Cuban segment of the Caribbean orogenic belt in Upper Cretaceous times. However, Kerr et al. (1999) suggested that the earliest collision event in Cuba is of Aptian-Albian age and of intra-oceanic nature, unrelated to the Upper Cretaceous-Paleogene arc-continent collision event. This intra-oceanic event was identified by García-Casco et al. (2002) in mélanges of the northern ophiolite belt of central Cuba.

ANALYTICAL METHODS

Mineral compositions were obtained with a CAMECA SX-50 microprobe (University of Granada) operated at 20 kV and 20 nA, and synthetic SiO_2, Al_2O_3, $MnTiO_3$, Fe_2O_3, MgO and natural diopside, albite and sanidine, as calibration standards, and a ZEISS DSM 950 scanning microscope equipped with a LINK ISIS series 300 Analytical Pentafet system operated at 20 kV and 1-2 nA beam current, with counting times of 50-100 s, and the same calibration standards. Representative analyses are given in Table 1. Elemental XR images were obtained with the same CAMECA SX-50 machine operated at 20 kV and conditions indicated in figures 5, 7 and 9. The images were processed using unpublished software by Torres-Roldán and García-Casco. Fe^{3+} in clinopyroxene, amphibole, garnet and epidote was calculated after normalization to 4 cations and 6 oxygens (Morimoto et al., 1988), 23 oxygens (Leake et al., 1997), 8 cations and 12 oxygens, and 8 cations and 12.5 oxygens (Fe_{total}=Fe^{3+}) per formula unit (pfu), respectively. Mineral and end-member abbreviations are after Kretz (1983), except for amphibole (Amp).

TABLE 1. Representative composition of mineral phases in studied samples (see also García-Casco et al., 2002, and Schneider et al., 2004).

Sample	CV230b	LV69	SRO1A	SRO1A	LV69	LV69	CV230b	LV69	SRO1A
Phase	Grt	Grt	Grt	Pl	Omp	Ms	Ep	Ep	Ep
Tie line	peak	peak	peak	peak	peak	peak	peak	peak	peak
SiO2	37.83	38.28	37.60	68.36	55.73	49.56	38.43	38.48	38.01
TiO2	0.07	0.02	0.06		0.08	0.41	0.06	0.09	0.10
Al2O3	21.32	21.84	21.32	19.68	10.19	30.49	31.82	28.37	25.83
FeOtot*	21.90	23.92	26.87	0.44	4.40	1.80	1.96	5.82	9.29
MnO	1.28	0.50	0.13		0.04	0.00	0.02	0.17	0.02
MgO	3.62	7.75	1.67		8.52	3.18	0.02		0.02
CaO	13.03	7.22	12.31	0.19	13.51	0.00	24.34	24.00	23.81
Na2O				11.73	6.69	1.08			
K2O				0.01	0.00	9.39			
Sum	99.09	99.52	99.97	100.42	94.44	95.91	95.75	92.32	96.11
Oxygen	12	12	12	8	6	22	12.5	12.5	12.5
Si	2.97	2.95	2.98	2.98	2.00	6.53	2.97	3.00	2.99
Ti	0.00	0.00	0.00		0.00	0.04	0.00	0.01	0.01
Al	1.97	1.98	1.99	1.01	0.43	4.74	2.90	2.61	2.39
Fe3+	0.07	0.11	0.05	0.02	0.04	0.00	0.13	0.38	0.61
Fe2+	1.37	1.43	1.73	0.00	0.09	0.20	0.00	0.00	0.00
Mn	0.08	0.03	0.01		0.00	0.00	0.00	0.01	0.00
Mg	0.42	0.89	0.20		0.46	0.62	0.00		0.00
Ca	1.10	0.60	1.04	0.01	0.52	0.00	2.01	2.00	2.00
Na				0.99	0.46	0.28			
K				0.00		1.58			

Sample	CV230b	CV230b	CV230b	LV69	LV69	LV69	SRO1A	SRO1A	SRO1A
Phase	Pargasite	Gl	Act	Bar	Gl	Act	MgKat	Gl	Act
Tie line	peak	retro	retro	peak	retro	retro	peak	relict (inclusion)	retro
SiO_2	43.48	57.21	55.29	50.81	57.06	52.87	47.52	57.88	55.47
TiO_2	0.87	0.09	0.05	0.21	0.05	0.10	0.29	0.00	0.00
Al_2O_3	13.69	11.33	1.57	10.70	9.56	5.93	12.64	11.07	2.71
FeO_{tot}*	13.33	12.73	11.83	8.73	10.01	9.06	14.83	11.28	10.93
MnO	0.15	0.14	0.20	0.05	0.07	0.11	0.06	0.03	0.00
MgO	11.29	8.61	16.20	14.39	11.56	16.22	9.61	9.25	16.13
CaO	11.49	0.60	11.71	8.17	1.91	10.04	8.25	1.09	11.44
Na_2O	2.48	7.17	0.92	3.87	6.38	2.19	4.29	6.85	1.11
K_2O	0.47	0.01	0.03	0.23	0.03	0.11	0.26	0.00	0.07
Sum	95.57	96.09	96.94	97.15	95.66	96.64	97.81	99.94	100.90
Oxygen	23	23	23	23	23	23	23	23	23
Si	6.41	7.91	7.88	7.18	7.92	7.52	6.91	8.00	7.86
Ti	0.10	0.01	0.00	0.02	0.00	0.01	0.03		
Al	2.38	1.85	0.26	1.78	1.57	0.99	2.17	1.80	0.45
Fe^{3+}	0.11	0.13	0.08	0.16	0.18	0.17	0.06	0.03	0.03
Fe^{2+}	1.53	1.34	1.33	0.87	0.99	0.91	1.74	1.28	1.26
Mn	0.02	0.02	0.02	0.01	0.01	0.01	0.01	0.00	
Mg	2.48	1.78	3.44	3.03	2.39	3.44	2.09	1.90	3.41
Ca	1.81	0.09	1.79	1.24	0.28	1.53	1.29	0.16	1.74
Na	0.71	1.92	0.25	1.06	1.72	0.60	1.21	1.83	0.31
K	0.09	0.00	0.01	0.04	0.00	0.02	0.05		0.01

* Total Fe expressed as FeO.

NORTHERN OPHIOLITE BELT

Central Cuba

Central Cuba is used informally to embrace the area from Havana to Holguín, which bears the most complete representation of geologic complexes in the island (Figs. 1B and 2A). In this region, the continental North American margin and foreland to the north includes middle Jurassic to Eocene sedimentary formations of Cayo Coco, Remedios, Camajuaní and Placetas belts, of which the latter is of deep water affinity and related to the oceanic Proto-Caribbean realm (Iturralde-Vinent, 1996a, 1998). The northern ophiolite belt is formed by a number of tectonic slices thrusted northward and partially intermingled with the Placetas belt. To the south, the Cretaceous volcanic-plutonic arc belt is tectonically emplaced above the northern ophiolite belt, but in the Havana-Matanzas and Holguín regions it is tectonically intermingled with the northern ophiolites. The Cretaceous volcanic arc belt contains Neocomian?-Albian tholeiitic rocks covered by Albian-Campanian calc-alkaline and high-alkaline rocks. The suites are formed by volcanic, plutonic and volcanic-sedimentary sequences. The

volcanic-arc units tectonically overlie the Mabujina complex, composed mainly of arc-derived medium- to high-grade, low to intermediate pressure, metamorphic rocks of ultrabasic, basic, intermediate and acid composition that are crosscut by slightly to strongly metamorphosed and deformed plutonic bodies (Somin and Millán, 1981; Millán, 1996b; Grafe et al., 2001; Blein et al., 2003). This complex is interpreted as the metamorphosed roots of the island arc and its oceanic sole (Somin and Millán, 1981; Millán, 1996b) or as a separate arc system (Blein et al., 2003). The Mabujina complex is in turn tectonically underlain by the Escambray terrane, described below. The thrust-and-fold belt was complexly assembled during late Upper Cretaceous-Middle Eocene times, when syn-tectonic sedimentary-olistostromic formations of Paleogene age were deposited above the northern ophiolite belt and the continental margin sections (Iturralde-Vinent, 1998).

Mélanges containing m- to dm-sized blocks of eclogite, garnet amphibolite, amphibolitite, blueschist, greenschist, quartzite, metapelite and antigoritite occur within the northern ophiolite belt. Important localities are in the Villa Clara (Fig. 2B) and the Holguín-Gibara regions (Kubovics et al., 1989), which are separated by ca. 450 km along strike of the major geological structure (Fig. 1B). Available K-Ar ages from samples of high-pressure (HP) blocks in the region range from 130 to 60 Ma, but data cluster about 110±10 Ma (Somin and Millán, 1981; Somin et al., 1992; Iturralde-Vinent et al. 1996) suggesting an Early Cretaceous age for the subduction zone; younger ages are inferred to represent reworking during Upper Cretaceous-Paleogene tectonism associated with collision.

García-Casco et al. (2002) provided detailed descriptions of representative eclogite samples from blocks of mélanges associated with the northern ophiolite belt in Villa Clara and Holguín regions (Figs. 1B and 2B). The rocks conform to the type-C eclogites of Coleman et al. (1965) and the low-T eclogites of Carswell (1990), consisting of an assemblage containing garnet porphyroblasts up to 3 mm width set in a matrix of faintly oriented medium grained omphacite, calcic to sodic-calcic amphibole (locally also porphyroblastic), epidote, rutile, sphene, apatite and occasional phengite. These rocks are not classified as eclogite s.s. as defined by Carswell (1990), but rather as amphibole-eclogite (cf. Newton, 1986) since they contain less than 75% of garnet plus omphacite, and amphibole bears textural relationships (position, inclusions, chemical zoning, replacements) that clearly indicate its stability during pre-, syn- and post-peak-eclogitic metamorphism. Porphyroblasts of garnet and amphibole commonly bear inclusions of epidote, rutile, sphene, omphacite, amphibole, albite, quartz and chlorite. The main eclogitic assemblage (Grt+Omp+NaCa Amp+Ep+Rt+Spn) is affected by localized replacement by albite (Ab), actinolitic amphibole, epidote and sphene generated by a late-stage albite-epidote amphibolite to greenschist facies overprint (Fig. 3). The general P-T path of the samples is clockwise, with prograde increase in temperature and pressure followed by strong decompression accompanied by moderate cooling during the retrograde exhumation path (Fig. 3). However, XR-mapping of the samples demonstrated the presence of complex oscillatory zoning in garnet and amphibole porphyroblasts. Based on a) the chemical nature of the oscillations and b) phase relationship modelling, García-Casco et al. (2002) concluded that oscillatory zoning formed as a result of widespread and recurrent changes in P-T conditions during prograde metamorphism (Fig. 3). Such thermal disturbances are incompatible with steady state subduction of the slab and it was proposed that they were produced instead by tectonic processes related to the demise of a subduction system.

Age determinations for the eclogite sample LV36A yielded 103.4±1.4 ($^{40}Ar/^{39}Ar$ plateau age of amphibole), 115.0±1.1 ($^{40}Ar/^{39}Ar$ plateau age of phengite; 123.1±1.0 to 117.1±0.9 intragrain laserprobe fusion ages) and 118.2±0.6 Ma (Rb/Sr isochron for phengite-omphacite-whole-rock; Schneider, 2000, see also García-Casco et al., 2002). These data indicate that the minimum age of eclogite facies metamorphism is pre-118 Ma (Aptian or older), while final uplift and cooling dates to Aptian-Albian times (118-103 Ma). Thus, it is concluded that block LV36A formed in a subduction system of pre-Aptian age and that it was incorporated into the mélange and exhumed during the Aptian-Albian. The tectonic nature of the mélange-forming event is uncertain. However, the near-isothermal decompression sections of the retrograde part of the P-T paths followed by the HP block offer some insights into this problem. The decompression-dominated retrograde paths are similar to that termed Alpine type (Ernst, 1988), which are normally interpreted as the result of rapid exhumation in a relatively hot geothermal gradients imposed by tectonic unroofing after arrest of subduction. Though arrest of subduction is generally thought to have been the result of collision of the subduction-forearc system with a buoyant down-going continental, oceanic, or arc lithosphere (e.g. Ernst, 1988; Ring et al., 1999; Wakabayashi, 2004), other collision tectonic processes, such as reversals of subduction polarity, have similar consequences, as discussed below. In either case, however, the retrograde paths of exotic blocks within the northern ophiolite belt in central Cuba are consistent with collision tectonics accompanying termination of subduction during the mid-Cretaceous.

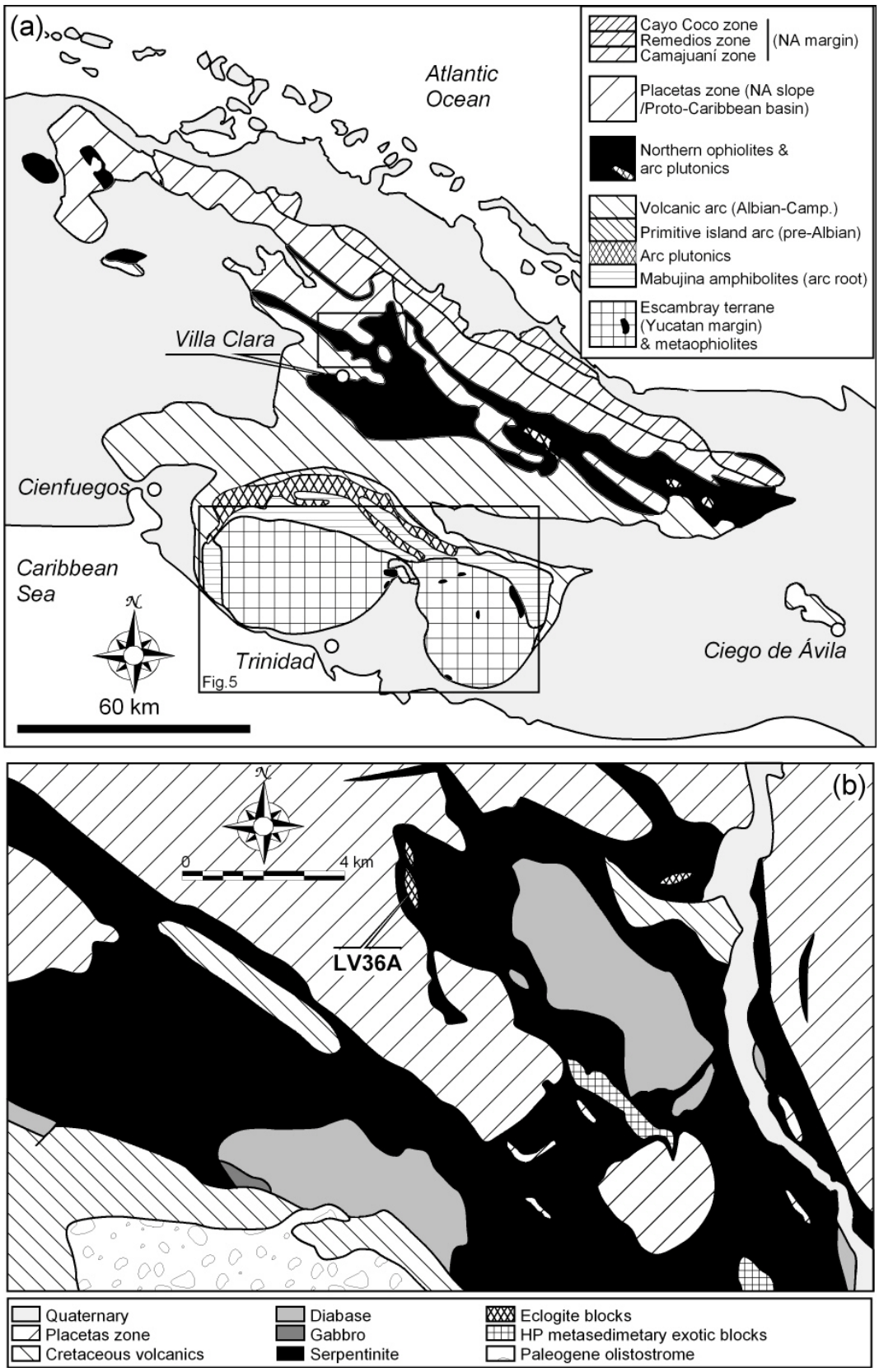

FIGURE 2. (A) Basic geologic features of central Cuba (from Iturralde-Vinent, 1996a), and (B) geologic map of the studied area (slightly modified and simplified after García Delgado et al., 1998) with indication of sample locality.

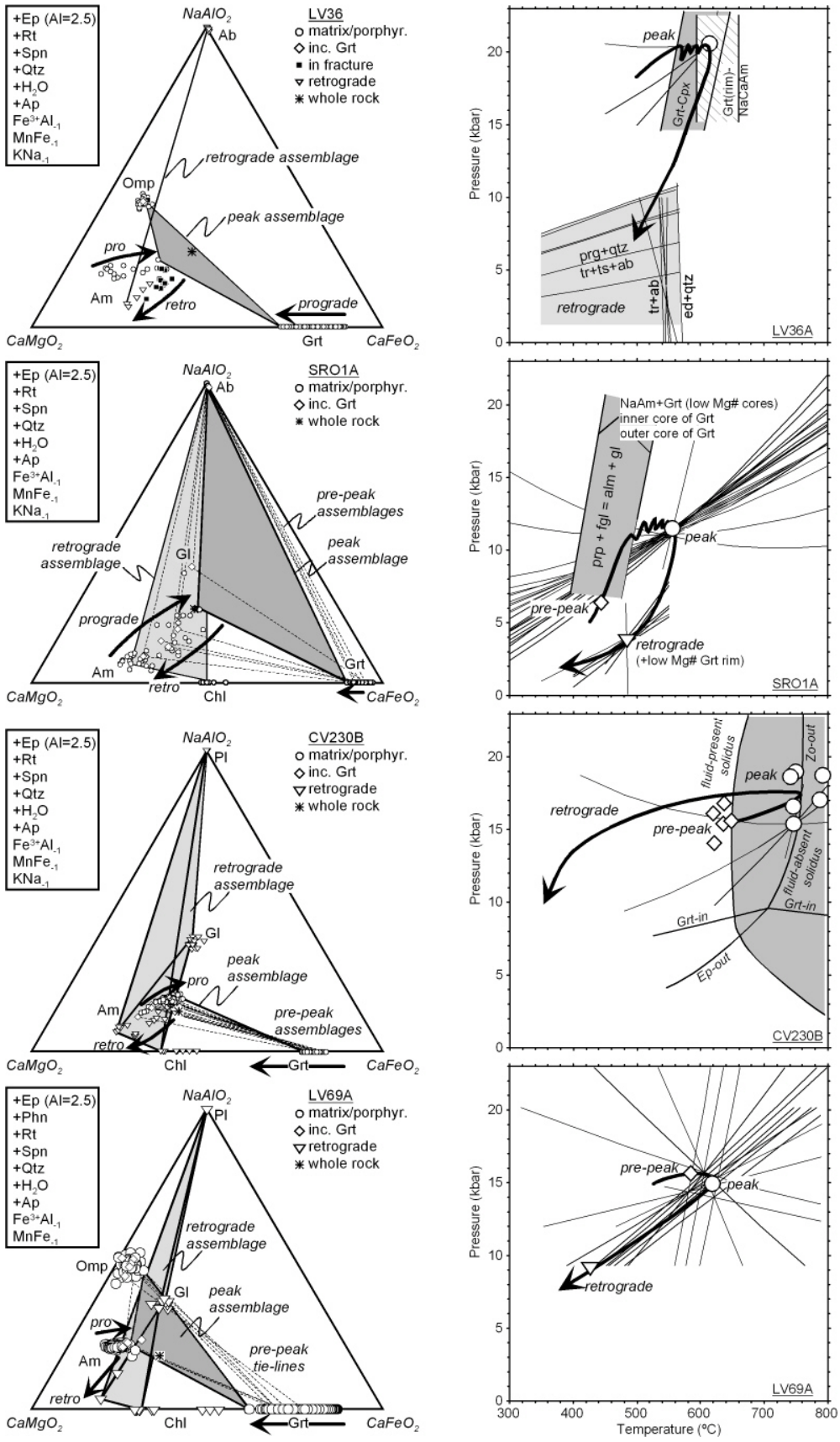

FIGURE 3. $AlNaO_2$-$CaMgO_2$-$CaFeO_2$ phase diagrams and associated P-T calculations and paths for the studied samples. The phase diagram was constructed after projection from average epidote, rutile, sphene, quartz, apatite, H_2O (±phengite) and the exchange vectors $Fe^{3+}Al_{-1}$ and $MnFe_{-1}$ (±KNa_{-1}). The thin lines in the P-T diagrams correspond with results of Thermocalc (see also García-Casco et al., 2002, and Schneider et al., 2004, for samples LV36A and LV69A, respectively).

Western Cuba

Western Cuba is here used informally to represent the geological units which crop out mostly in the Pinar del Río province (Figs. 1B and 4A). The Geology of this region diverges from that of central Cuba in that the continental Guaniguanico terrane represents the Mesozoic margin of the Maya block (Iturralde-Vinent, 1994; Pszczólkowski, 1999), though the oceanic terranes correlate with central Cuba. The Cajálbana ophiolite body is the western counterpart of the northern ophiolite belt. The body is noticeably elongated and tectonically sandwiched in between tectonic slices of two Cretaceous arc sequences: the Albian-Campanian volcanic-sedimentary sequences of the Bahía Honda belt to the north and the Albian-Cenomanian Felicidades belt to the south (Fig. 4). The Bahía Honda belt constitutes the western equivalent of the calc-alkaline Albian-Campanian volcanic arc belt while the Felicidades belt is interpreted as an adjacent marginal-sea basin of nearly the same age (Iturralde-Vinent, 1996a and b; Kerr et al., 1999). The Cajálbana ophiolite and the Bahía Honda and Felicidades belts are grouped within the oceanic Bahía Honda allochthonous terrane, which overrides the Guaniguanico terrane along NW-directed thrusts (Iturralde-Vinent, 1994; 1996a). The Guaniguanico terrane is formed by north-northeast verging thrust belts, namely the Quiñones, Sierra del Rosario, Sierra de los Órganos and Cangre belts (Fig. 4A), composed of Jurassic and Cretaceous sedimentary sequences related to the eastern margin of the Maya block (North American Plate) and syntectonic Paleocene to Middle Eocene foreland sediments (Iturralde-Vinent, 1994, 1996a; Rosencrantz, 1990, 1996; Bralower and Iturralde-Vinent, 1997; Pszczólkowski, 1999). Iturralde-Vinent (1994, 1996a) and Pszczólkowski (1999) considered that thrusting and gravitational sliding during the Paleogene completely reversed the original relative paleogeographic positions of the Guaniguanico thrust units. Gordon et al. (1997) identified a complex Paleogene tectonic history with at least five phases of deformation. The terrane is non-metamorphic, except the Cangre belt, metamorphosed to high pressure low temperature conditions (Somin and Millán, 1981; Pszczólkowski and Albear, 1985; Millán, 1988, 1997a). The age of metamorphism has not been precisely determined. Somin et al. (1992, sample M-3) reported a K-Ar whole-rock data of 113 ± 5 Ma in a sample of mica-quartz schist that probably represents a mixture of detritic and metamorphic ages (see Hutson et al., 1998).

In the Guaniguanico terrane, mostly in the Sierra del Rosario belt, metamorphosed and non-metamorphosed ophiolitic material appears as medium- to large-sized exotic blocks and olistoplates incorporated into syn-tectonic olistostromic formations having a Lower Eocene sedimentary matrix (Pszczólkowski, 1978; Somin and Millán, 1981; Somin et al., 1992; Millán, 1996a, 1997a; Bralower and Iturralde-Vinent, 1997). The metamorphosed blocks consist of serpentinite-matrix mélanges containing HP exotic blocks. Available age data from the HP metamorphic blocks range form 128 to 58 Ma, with recurrence of 110±10 Ma ages (Somin and Millán, 1981; Somin et al., 1992; Iturralde-Vinent et al., 1996) as in central Cuba (see above). The coincidence of age data of HP blocks from western and central Cuba suggests that the occurrence of HP ophiolitic rocks within Lower Eocene sedimentary matrix in western Cuba is a peculiarity of this region related to the late stages of Tertiary orogenic evolution and not to the primary evolution of the subduction system where the HP blocks originated. Additionally, the Early Cretaceous radiometric ages in western and central Cuba mélanges suggest that HP metamorphism developed in the same subduction system.

That the Early Cretaceous subduction system of central Cuba extended to western Cuba is also indicated by the petrologic features of HP bocks from serpentinite mélanges of the Guaniguanico terrane. Here we describe a garnet amphibolite block (SRO1A) collected from a Paleogene olistostromic deposit located ca. 8 km to the south of the village of Bahía Honda (Fig. 4B). Figure 5 depicts the relevant textural and mineral composition information of this sample (see also the phase diagram of Fig. 3 for further information). The amphibolite is fine-grained, composed of garnet, calcic to sodic-calcic amphibole (actinolite-magnesiohornblende-barroisite-magnesiokatophorite), clinozoisite/epidote, rutile, sphene, albite, chlorite and glaucophane. Of these, amphibole, epidote and chlorite are oriented along the foliation. Glaucophane appears as scarce xenomorphic blasts set in the matrix of calcic to sodic-calcic amphibole and is interpreted as relict. Garnet porphyroblasts (≈500 μm in width) contain inclusions of glaucophane, calcic amphibole, epidote, albite and sphene. Albite is fine to medium grained, locally porphyroblastic, and has non-oriented inclusions of all the phases (including garnet) with which it is in textural equilibrium. However, garnets appear slightly corroded by the matrix assemblage, particularly actinolitic amphibole, epidote and chlorite. The absence of omphacite and the coexistence of garnet+albite indicate this block was metamorphosed at lower pressure and temperature than eclogites from central Cuba described above, within the albite-epidote amphibolite facies, while relict glaucophane suggests the prograde path evolved through the blueschist facies. The retrograde

assemblage (actinolite+epidote+chlorite+albite) denotes greenschist facies overprint.

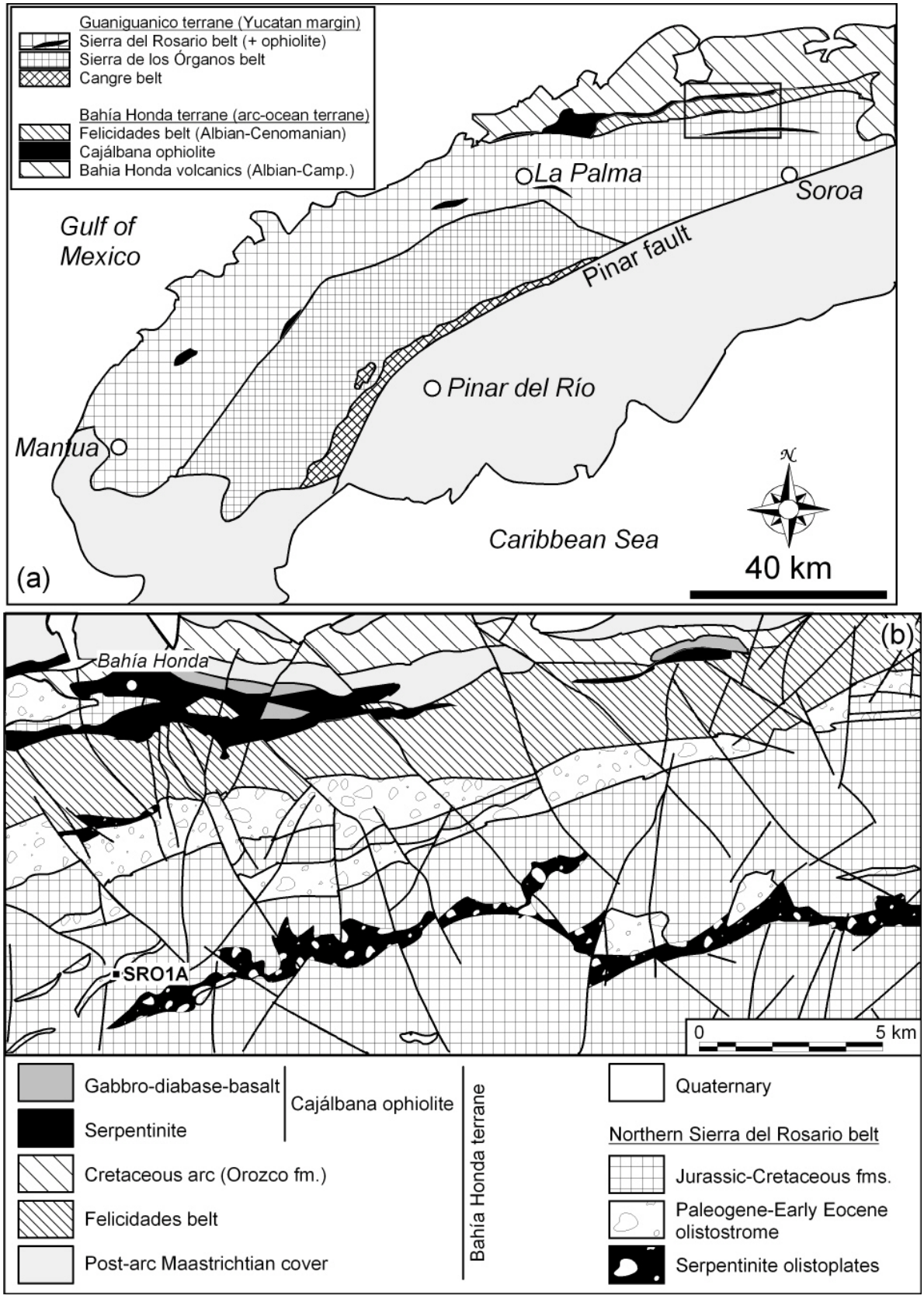

FIGURE 4. (A) Basic geologic features of western Cuba (compiled after Pszczólkowski, 1994 and Iturralde-Vinent, 1996a), and (B) geologic map of the studied area (slightly modified and simplified after Martínez González et al., 1994) with indication of sample locality.

Although sample SRO1A formed at a distinct shallower level in the subduction system compared with the eclogites from central Cuba, their metamorphic evolutions prove to be similar. This interpretation is confirmed by prograde growth zoning of garnet from this W-Cuba sample, which is disturbed by several euhedral concentric oscillations in Mn, Mg, Ca and Fe (Fig. 5). These oscillations developed in the course of prograde metamorphism towards peak albite-epidote amphibolite facies conditions (Fig. 3). The distribution of the elements define relatively homogeneous cores that have high Mn (that slightly decreases outward) and low Ca and Mg# contents, and overgrowths poorer in Mn and richer in Ca but only slightly richer in Mg# where the oscillations take place. In terms of Mg (and Mg#), the overgrowths display two major reversals (resolved in the detailed right-hand side section of the profile of Fig. 5) that match upturns in Mn and Ca, in addition to other reversals of lower intensity. As in the eclogites of central Cuba, the increase in Mn and decrease in Mg# at the reversed layers indicate formation upon recurrent prograde-retrograde episodes taking place in the course of subduction. Matrix amphibole shows a distinctively irregular patchy zoning in many grains (Fig. 5). When concentric zoning is developed the cores are actinolitic and the overgrowths are magnesiohornblende to barroisite-magnesiokatophorite, indicating prograde growth. The outermost rims are retrograde as they trend backwards to magnesiohornblende and actinolite with increasing Mg# relative to peak sodic-calcic amphibole. The inclusions of amphibole within garnet cores are similar to the actinolitic cores of matrix amphibole. Consequently, the prograde zoning of matrix amphibole correlates, at least in part, with the oscillatory zoning of garnet. Indeed, the preservation of prograde patchy zoning in this sample is consistent with the adjustment of amphibole composition to recurrent changes in pressure and/or temperature in the course of subduction-related metamorphism. Glaucophane has intermediate Mg# (ca. 0.6) contents, slightly higher than prograde barroisitic amphibole and lower than calcic amphibole. Chlorite has Mg# = 0.54-0.52.

Metamorphic temperatures and pressures were estimated using Thermocalc (Holland and Powell, 1998, version 3.21). Calculations using different combinations of the composition of the phases have large errors, probably due to equilibrium problems and the poorly-known activity-composition relations of complex amphibole and chlorite solid solutions. The calculated pre-peak and peak P-T conditions are 444 ± 82 ºC, 6.4 ± 2.4 kbar, and 556 ± 107 ºC, 11.5 ± 3.1 kbar, respectively. Relative to the eclogites of central Cuba (Fig. 3), these figures are in accordance with the Mg#-poorer composition of garnet rims and the lack of omphacite in sample SRO1A. A range of 400-500 ºC was calculated using the Fe-Mg exchange equilibrium among relict glaucophane and garnet cores, although the pressure calculations using glaucophane in combination with other phases were rather imprecise. Consequently, the shape of the prograde path towards peak conditions depicted in Fig. 3 is uncertain. A similar range of temperature and 2-4 kbar was calculated using combinations of chlorite, garnet rims with lower Mg#, and retrograde amphibole, albite and epidote. The P-T path depicted in Fig. 3 is clockwise with a) P-T oscillations (that account for the Mg and Mn reversals in garnet) during the prograde subduction-related path and b) decompression-dominated retrogression. It should be noted that the P-T oscillations of the path suggest tectonic instability of the down-going slab, and that the Alpine-type retrograde portion of the path implies rapid exhumation and a relatively steep geothermal gradient, in all aspects similar to paths followed by eclogite blocks of central Cuba. These features strongly suggest the serpentinite-mélanges of western and central Cuba formed during the same Early Cretaceous subduction system that extended for a distance of about 800 km (present geographic coordinates), and that this system suffered a generalized (Aptian-Albian) tectonic event that terminated subduction.

Eastern Cuba

Eastern Cuba extends towards the East from the Nipe fault (Fig. 1B). The huge Mayarí-Cristal and Moa-Baracoa ophiolite bodies of this region have been classically viewed as the eastern counterpart of the northern ophiolite belt, but Iturralde-Vinent et al. (this volume) have characterized them as "eastern ophiolites". These bodies have been considered as suprasubduction ophiolite that underwent widespread infiltration by melts of island arc tholeiitic and boninitic composition that interacted with the ultramafic rocks (Proenza et al., 1998, 1999; Gervilla et al., 2005). The region contains a number of volcanic arc formations having distinct island arc tholeiitic, boninitic and calc-alkaline signatures, though in most cases they appear to be of Upper Cretaceous age (Iturralde-Vinent et al., this volume; Proenza et al., this volume). Whether these geochemically distinct arc volcanics formed within a single or different subduction zones is uncertain. The Purial volcanic complex, south of the ophiolitic bodies (Fig. 6A), includes island arc tholeiitic and calc-alkaline signatures and has been classically considered the eastern prolongation of the Cretaceous arc belt of western-central Cuba (Iturralde-Vinent, 1996c). However, important geological contrasts with other parts of Cuba are that this Cretaceous volcanic arc terrane is a) tectonically overridden by the ophiolitic complexes and b) metamorphosed to the greenschist and blueschist facies (Boiteau et al., 1972; Cobiella et al., 1977;

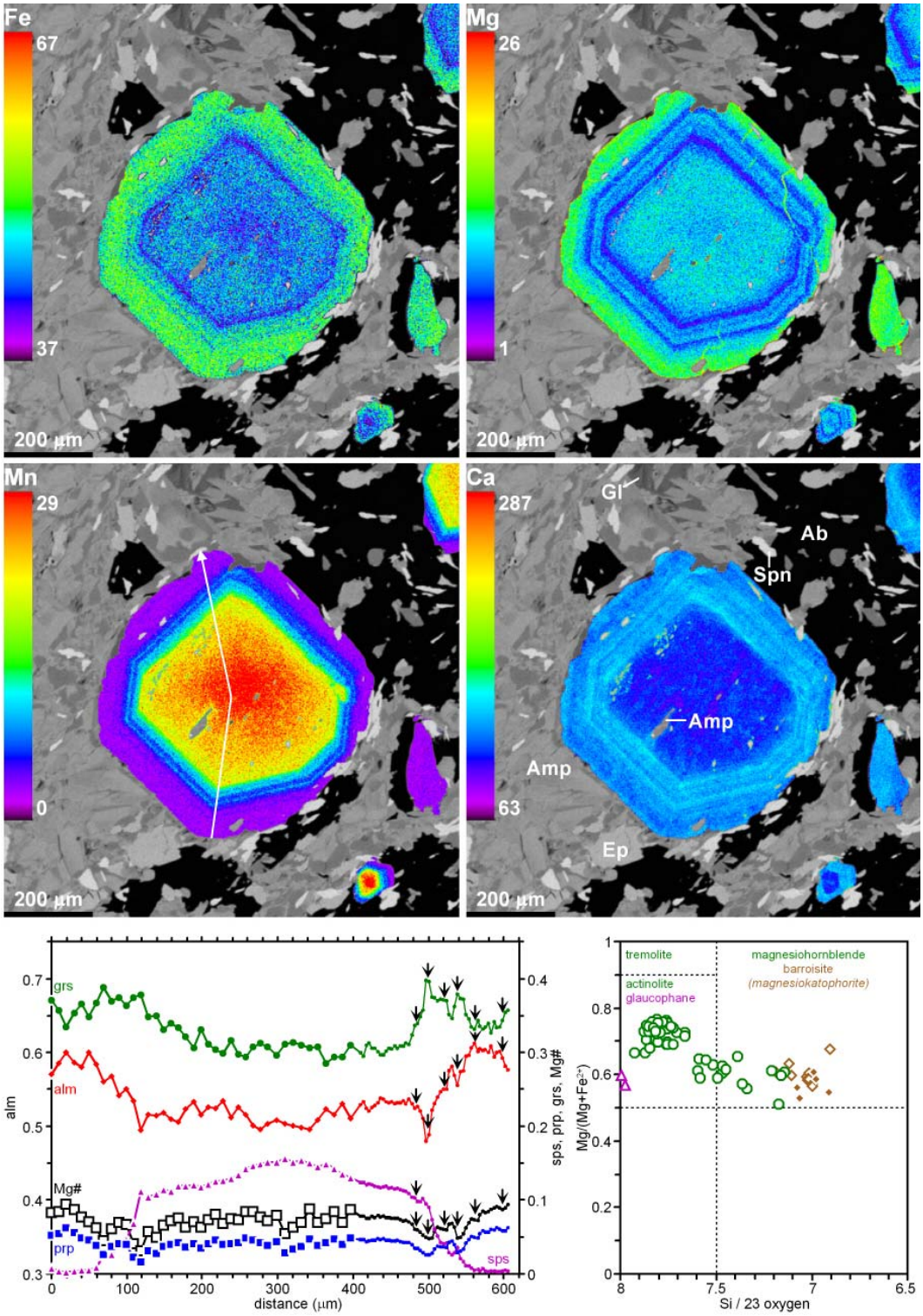

FIGURE 5. Key textural and mineral composition data of sample SRO1A. The synthetic XR images were generated with *Imager* software (Torres-Roldán and García-Casco, unpublished) and consist of the XR signals for Kα lines of Fe, Mn, Mg, and Ca in garnet (colour coded counts/nA/sec) corrected for 3.5 μs deadtime; voids, polish defects, and all other mineral phases masked out), overlaid onto a grey-scale base-layer that contains the basic textural information calculated with the expression $\Sigma[(counts/nA/s)_i \cdot A_i]$, A=Atomic number, i= Fe, Mn, Mg, Ca. Acceleration potential: 20 kV. Beam current: 151 nA. Step (pixel) size: 2 μm. Counting time: 30 ms. The compositional profile of garnet (Step size: 10 μm -left hand side of the profile-, and 4 μm -right hand side) is indicated in the XR image of Mn. The arrows indicate the location of Mg# reversals in the detailed profile. The composition of amphibole is plotted within the classification scheme of Leake et al. (1997). The green, brown and magenta symbols and labels correspond to calcic, sodic-calcic and sodic amphiboles, respectively. The empty symbols and normal typeface labels correspond to compositions with Sum(A) < 0.5. The filled symbols and italic typeface labels correspond to compositions with Sum(A) > 0.5.

Somin and Millán, 1981; Millán et al., 1985). Importantly, metamorphism in this complex is dated as late Upper Cretaceous by Somin et al. (1992; 75 ± 5 Ma K-Ar whole-rock) and Iturralde-Vinent et al. (this volume; 75-72 Ma based on paleontological dating). The Mesozoic North American margin (Florida-Bahamas platform) is likely represented in this region by the sedimentary sequences of the Asunción terrane, though an exotic origin cannot be excluded. This complex is metamorphosed to high-P low-T conditions (Millán et al., 1985). Regionally, the ophiolite bodies override the Asunción metasediments. The major displacements appear to be NE to NW-directed thrusts (Cobiella et al., 1984; Quintas, 1987, 1988; Nuñez Cambra et al., 2004). However, the structure of the region is complex and has not been studied in detail.

The ophiolitic bodies of eastern Cuba include serpentinite-matrix mélanges containing high-pressure blocks. The largest complexes are La Corea and Sierra del Convento mélanges, both having similar lithological assemblages (Millán, 1996a). La Corea mélange is located in Sierra de Cristal and is associated with the Mayarí-Cristal ophiolitic body (Fig. 1B). The Sierra del Convento mélange, located southward (Figs. 1B and 6), overrides the Purial metavolcanics. The nature of the metamorphic blocks is varied but, in contrast with other mélanges from central and western Cuba, high temperature epidote±garnet amphibolites bearing small bodies of leucocratic (mostly trondhjemitic) material dominate. Other types of block are blueschist, greenschist, quartzite, metagreywacke and metapelite, while eclogite is rare (Cobiella et al., 1977; Somin and Millán, 1981; Kulachkov and Leyva, 1990; Hernández and Canedo, 1995; Leyva, 1996; Millán, 1996a). Available age data for HP rocks range from 125 to 66 Ma in La Corea and 116-82 Ma in Sierra del Convento (Adamovich and Chejovich, 1964; Somin and Millán, 1981; Somin et al., 1992; Iturralde-Vinent et al., 1996; Millán, 1996a). As in central and western Cuba, the recurrence of Early Cretaceous ages indicates Early Cretaceous subduction. However, the geological singularities of eastern Cuba make the correlation of the associated subduction systems doubtful. These doubts are strengthened by the petrologic differences of the metamorphic blocks from both regions, as described below.

The most typical rock type of eastern Cuba mélanges is epidote-amphibolite, commonly bearing garnet. We shall describe here a representative garnet amphibolite sample (CV230b) of Sierra del Convento complex collected from the area of El Palenque (Fig. 6B). Figure 7 depicts the relevant textural and mineral composition information of this sample (see also the phase diagram of Fig. 3). The prograde assemblage consists of calcic (pargasitic) amphibole, epidote, garnet, sphene, rutile and apatite. Prograde plagioclase is lacking, as in most metabasite samples metamorphosed to the epidote-amphibolite facies of the Sierra del Convento mélange, suggesting relatively high pressure of formation. Retrograde overprints in the studied sample are faint and consist of albite, actinolite, glaucophane, chlorite and pumpellyite. Similar overprints are common in other samples, though the extent of retrogression is highly variable. Pargasitic amphibole comprises most of the matrix and is oriented parallel to the foliation. Individual crystals have a smooth core-to-rim prograde zoning (minimum Si = 6.38 atoms pfu; max. NaB= 0.33; max. SumA= 0.68; max. Ti = 0.11; min. Mg# = 0.62). The rims are commonly partly replaced by actinolite, glaucophane, chlorite and albite. Epidote displays a faint patchy zoning (Fe^{3+} = 0.12-0.17 atoms pfu). Garnet forms large porphyroblasts (up to >1.5 cm in diameter) that include pargasitic amphibole, epidote, rutile and sphene, and is slightly replaced at the rims and along fractures by pargasite-magnesiohornblende-actinolite, chlorite, pumpellyite and albite. Its composition is rich in almandine and grossular (X_{alm}= 0.45; X_{grs}=0.35-0.40), and the grains bear a smooth prograde growth zoning with decreasing Mn (down to 0.06 atoms pfu) and increasing Mg# (up to 0.24) towards the rims. The outermost 200-300 μm of the grains display reverse diffusive zoning (noted by upturns in Mg# and Mn; Fig. 7) formed during retrograde exchange with the matrix. This type of zoning indicates relatively high temperature at the onset of retrogression. Importantly, oscillatory zoning has not been observed in garnet from this and other samples of amphibolite from the Sierra del Convento mélange

Metamorphic conditions were estimated using Thermocalc (version 3.21). As for sample SRO1A, the results have a large uncertainty. In addition, errors are increased by the high-variance of the peak assemblage garnet-pargasite-epidote (Fig. 3). Using different combinations of the composition of inclusions within garnet and of the rims of garnet (not affected by retrograde diffusion) and matrix pargasite, the conditions of the pre-peak and peak assemblages were estimated at 600-650 ºC and 14-16 kbar, and 750-800 ºC and 15-18 kbar respectively. The conditions of retrogression could not be estimated with certainty, though the growth of retrograde glaucophane indicates cooling at relatively high pressure. The P-T path is counterclockwise, with high-grade conditions attained during subduction and blueschist conditions attained during accretion and exhumation.

Similar P-T conditions and counterclockwise paths can be inferred from other samples of amphibolite from the Sierra del Convento and La

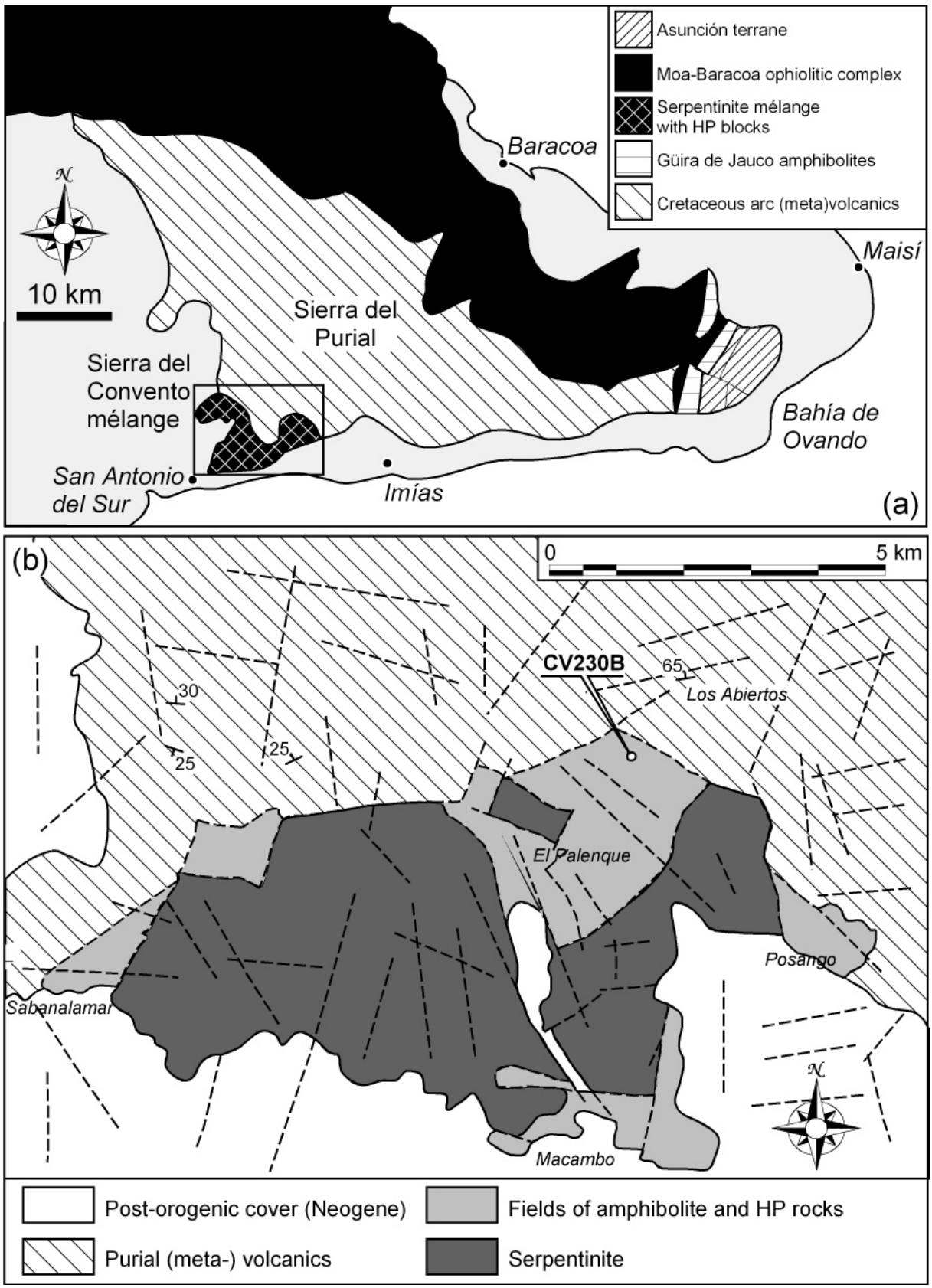

FIGURE 6. (A) Basic geologic features of eastern Cuba (Iturralde-Vinent, 1996a), and (B) geologic map of the Sierra del Convento mélange (Kulachkov and Leyva, 1990) with indication of sample locality.

Corea mélanges. These findings, which indicate hot subduction and cold exhumation for the amphibolite blocks of eastern Cuba mélanges, contrast with P-T conditions and paths observed in blocks from mélanges in western-central Cuba. Thus, the Early Cretaceous subduction systems of the two regions either were different or were associated with different geodynamic scenarios. Indeed, hot-subduction can be rationalized within the framework of either a) initiation of subduction or b) subduction of young oceanic lithosphere or an active oceanic ridge (e.g. Oh and Liou, 1990; Wakabayashi, 1990; 2004; Gerya et al., 2002; Willner et al., 2004). In the first case, the mélanges of eastern Cuba document initiation of a new subduction system during the mid-Cretaceous simultaneously with termination of subduction in central and western Cuba. In the second case, the mélanges of western-central and eastern Cuba were generated within the same Early Cretaceous subduction system, but a triple junction interaction (ridge-trench-transform or trench-transform-transform, Wakabayashi, 2004) should have occurred at its eastern branch. An important constraint that may contribute to solving this problem is the progressively refrigerated system implied by the observed retrograde paths in the high-grade blocks from eastern Cuba mélanges, which is consistent with continued subduction during incorporation of the blocks into the associated overlying subduction channel. This mechanism is not consistent with the mid-Cretaceous arrest of subduction inferred for western-central Cuba, favouring the "initiation of subduction scenario" for eastern Cuba and, consequently, the lack of correlation between the subduction systems of both regions.

ESCAMBRAY

The Escambray terrane crops out south of Central Cuba within the Cretaceous volcanic arc belt, in a tectonic window below the metamorphosed arc-related Mabujina complex (Figs, 1B and 8). It is composed of an ensemble of strongly deformed tectonic slices that comprise continental margin metasediments and metaophiolites (Somin and Millán, 1981; Millán and Somin, 1985; Millán, 1997b). Millán (1997b) subdivided the massif into four major tectonic units (I to IV, numbered from bottom to top in the pile; Fig. 8), each of which comprises a number of smaller tectonic units. The lithological sequences consist of metacarbonatic and metapsammopelitic rocks, with local metabasite intercalations. These rocks have been correlated with non-metamorphosed Jurassic-Cretaceous continental margin sequences in the Guaniguanico terrane of western Cuba, which formed part of the borderland of the Maya block (Millán, 1997a and b; see also Iturralde-Vinent, 1996a, Pszczólkowski, 1999). However, other reconstructions locate the terrane farther southwest in the borderland of the Chortis block (Pindell and Kennan, 2001).

P-T conditions during metamorphism in the Escambray were variable (Millán, 1997b; Fig. 8), ranging from low grade at intermediate-P (greenschist facies) and high-P (blueschist facies) to medium grade at high-P (eclogite facies). The internal deformation is intense and complex, with numerous tectonic-metamorphic inversions. The massif has an inverted metamorphic zoning, with greenschist facies at the base in unit I, greenschist and lawsonite blueschist facies in unit II, and epidote-blueschist and eclogite facies at the top in unit III. The uppermost unit IV in contact with the overlying Mabujina complex diverges from this pattern (greenschist-blueschist facies). High pressure conditions indicate subduction of the associated continental margin. Subduction of oceanic lithosphere is also documented by serpentinite-matrix mélanges bearing high-pressure exotic blocks (Fig. 8). Available age data range from Upper Jurassic (U-Pb age of zircon in eclogite, Maresch et al., 2003) through mid-Cretaceous (U-Pb: 106-100 Ma; Hatten et al., 1988, 1989) to Upper Cretaceous (K-Ar: 85-68 Ma; $^{40}Ar/^{39}Ar$: 71-68 Ma; Rb/Sr: 65-69 Ma; Somin and Millán, 1981; Hatten et al., 1988; Somin et al., 1992; Iturralde et al., 1996; Schneider et al., 2004). Except for the Upper Jurassic age (discussed below), these ages are consistent with subduction in the course of the Upper Cretaceous and exhumation during the late Upper Cretaceous. This suggests that the associated subduction system may be independent of the Lower Cretaceous subduction system recorded in the HP blocks of mélanges from the northern ophiolite belt in western and central Cuba. Petrologic evidence presented below also support this view.

Millán (1997b) reported that eclogite facies rocks of tectonic unit III underwent blueschist facies retrogression, and related this overprinting to the low-grade high-pressure metamorphism of unit II. This type of blueschist retrogression is not common in the HP exotic blocks of the northern ophiolite belt from western-central Cuba, a fact that may relate to tectonic processes exclusive of the Upper Cretaceous subduction system where the Escambray complex impinged. Millán (1997b) and Schneider et al. (2004) identified blueschist retrogression as a result of syn-subduction exhumation during the late Upper Cretaceous. These authors also noted that the prograde metamorphic evolution of coherent eclogite samples present in the metasedimentary formations is more complex than that of the eclogite blocks of the tectonically intercalated strips of serpentinite-mélanges, but that their peak eclogite conditions and retrograde evolutions are similar, the latter characterized by substantial cooling upon exhumation. Since subduction of buoyant continental

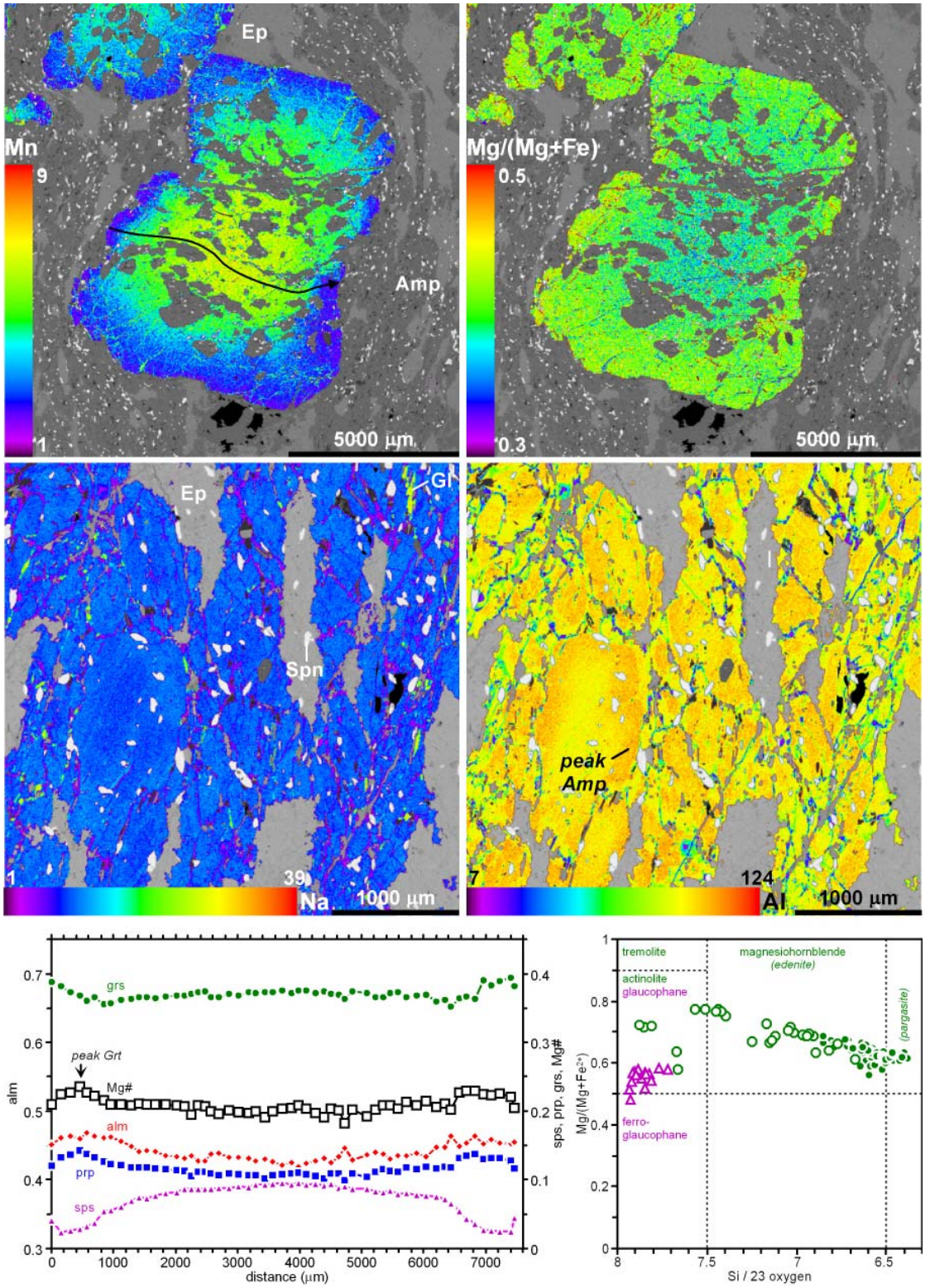

FIGURE 7. Key textural and mineral composition data of sample CV230B. The top synthetic XR images correspond to Mn(Kα) and Mg(Kα)/(Fe(Kα)+Mg(Kα)) of garnet (beam current: 292 nA; step size: 26 μm; counting time: 50 ms (Na, Mn, Ti, Mg) and 25 ms (Si, Al, Fe, Ca); all other operating conditions and procedures as in figure 5, except that the grey-scale base is calculated with the expression $\Sigma[(counts/nA/s)_i \cdot A_i]$, A=Atomic number, i= Si, Ti, Al, Fe, Mn, Mg, Ca, and Na). The bottom synthetic XR images (step size: 7 μm; all other operating conditions and procedures as above) correspond to Na(Kα) and Al(Kα) of amphibole (sodic and calcic; in the Na image, prograde pargasite-edenite-magnesiohornblende compositions appear with shades of blue, retrograde glaucophane is green-yellow, and retrograde actinolite is magenta). The compositional profile of garnet is indicated in the XR image of Mn. The composition of amphibole is plotted within the classification scheme of Leake et al. (1997), with symbols and labels as in figure 5.

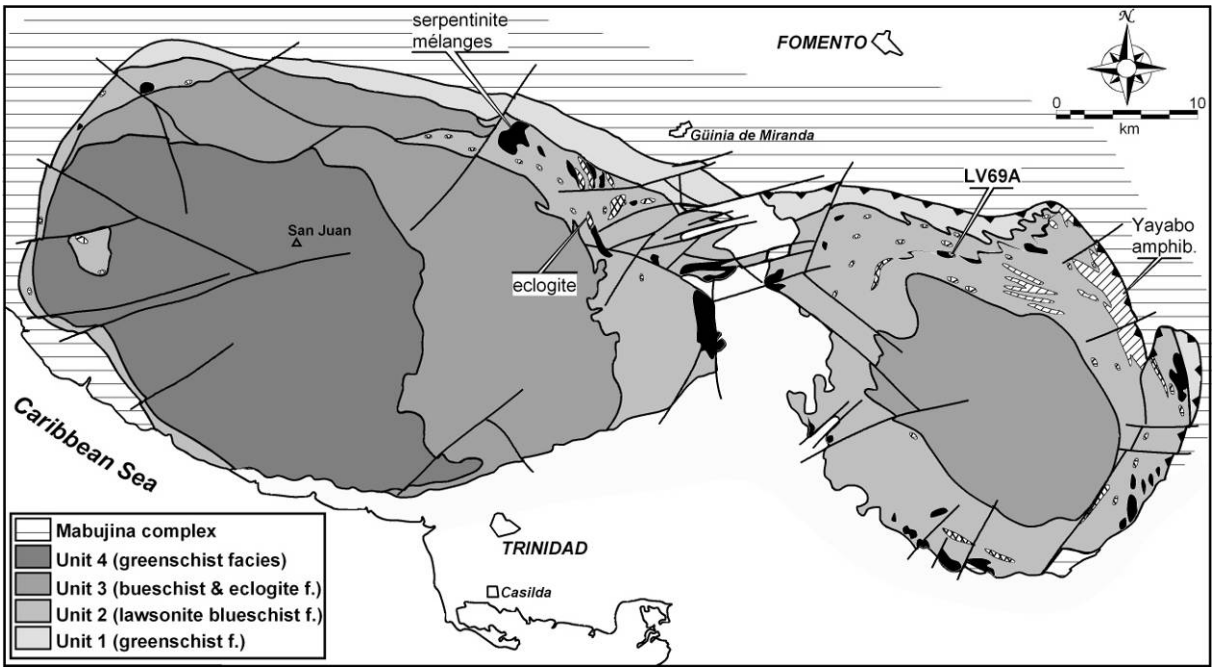

FIGURE 8. Geologic map of the Escambray (Millán, 1997b and unpublished data) with indication of major tectonic units, serpentinite mélanges and amphibolite and eclogite bodies within unit 3, and sample locality.

crust should have lead to tectonic-thermal processes different from those of normal oceanic lithosphere, we concentrate here on the metamorphic evolution of the HP exotic blocks within serpentinite-mélanges representing oceanic material present in unit III, using one sample of an eclogite block (LV69A) located towards the NE of the massif (Fig. 8). This sample was studied in detail by Schneider et al. (2004), though we shall give here additional petrologic evidence pertaining to its retrograde metamorphic evolution. The age data provided by Schneider et al. (2004) are $^{40}Ar/^{39}Ar$ (phengite): 69.3±0.6, $^{40}Ar/^{39}Ar$ (barroisite): 69.1±1.3 and Rb/Sr (whole-rock-phengite-barroisite): 66.0±1.7 Ma, and were interpreted as cooling ages close to thermal peak.

Figure 9 illustrates textural and mineral composition data from sample LV69A (see also Fig. 3 and Schneider et al., 2004). The peak mineral association is composed of almandinic (type-C) garnet, sodic-calcic (barroisite) amphibole, omphacite, epidote, muscovite, quartz, rutile and apatite, which is typical of amphibole-eclogites. Amphibole, omphacite, epidote, phengite, quartz and rutile comprise the matrix, though omphacite develops porphyroblasts up to 2 mm in length. Garnet is porphyroblastic, 1-2 mm in diameter, and includes epidote, sphene, rutile and, occasionally, amphibole, omphacite and quartz. These inclusions are oriented along an internal foliation oblique to the external foliation. The primary assemblage is irregularly replaced by a post-kinematic retrograde assemblage consisting of actinolite, glaucophane, albite, (clino)zoisite and chlorite, indicative of blueschist facies conditions.

Garnet zoning is concentric, typical of prograde growth, with cores richer in Fe, Mn and Ca, and rims richer in Mg and Mg#. This zoning pattern is disturbed by mechanical rupture of grains during deformation and, locally, by weak diffusional readjustments of Fe-Mn-Mg along fractures and rims of the grains and along the garnet-inclusions and garnet-garnet interfaces (Fig. 9). The mechanical rupture of the grains took place before attainment of the metamorphic peak, as indicated by broken grain boundaries rich in Mg and Mg# and poor in Mn. The diffusional process took place close to the thermal peak since the modified composition of the garnet interiors trends towards high Mg#. The composition of omphacite is almost homogeneous, though subtle variations in Al, Na, Ca, Fe, Mg and Mg# occur in patches. At places where omphacite is replaced by retrograde albite, the associated patches are poorer in Al and Na (i.e., lower jadeite content). Grains of omphacite included within garnet have lower Mg# than those of the matrix and porphyroblasts, though the jadeite contents are similar. Thus, the composition of peak omphacite corresponds with high Al, Na and Mg# contents. Amphibole in the matrix and enclosed within omphacite and garnet is sodic-calcic (barroisite, locally magnesiokatophorite). The compositional zoning is faint and concentric, with rims richer in Ti, Al, Fe and Na+K(A) indicative of prograde growth. The amounts of Na(B) decrease slightly towards the rims.

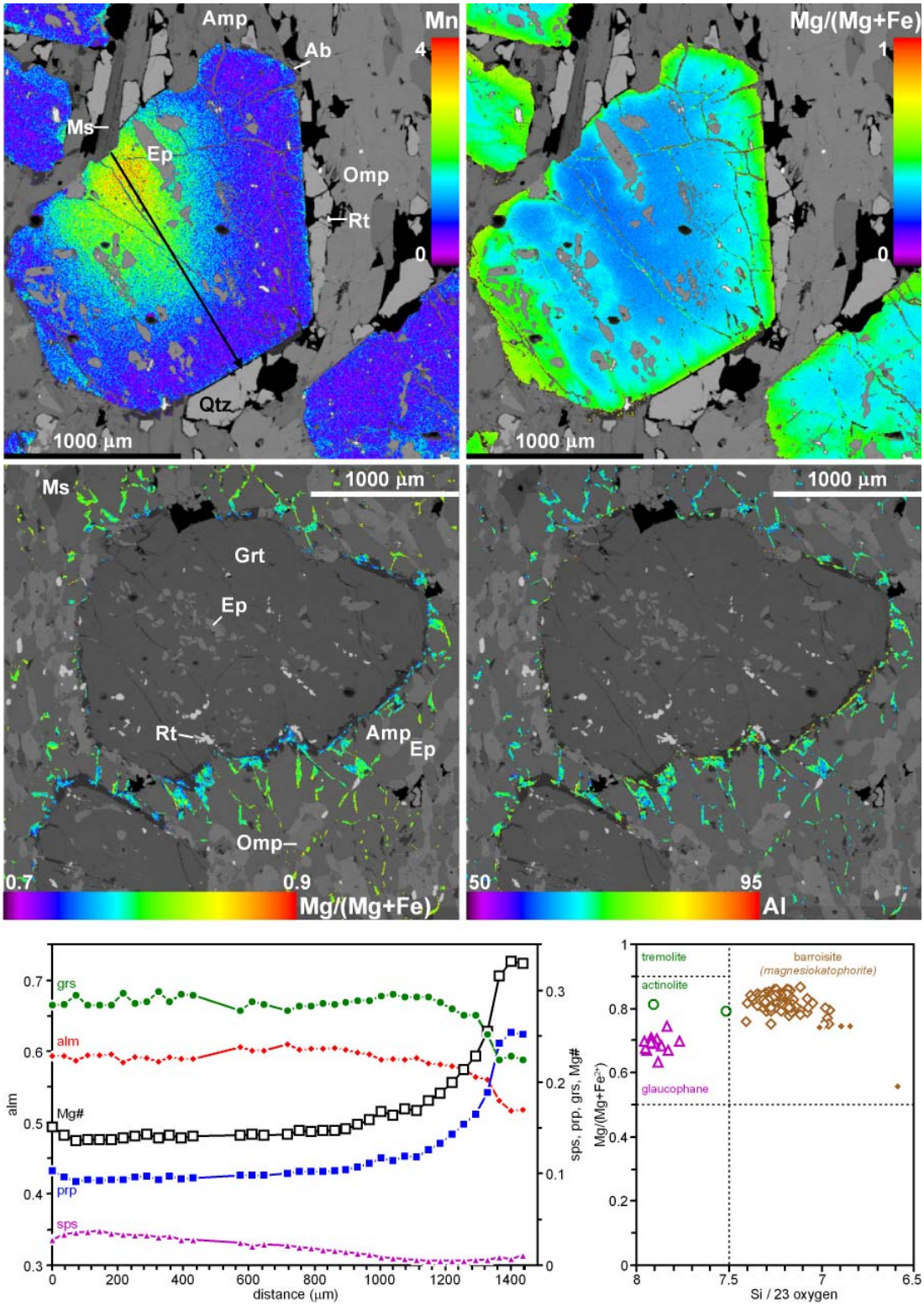

FIGURE 9. Key textural and mineral composition data of sample LV69A. The top synthetic XR images (beam current: 251 nA; step size: 5 µm; counting time: 50 ms; all other operating conditions and procedures as in figure 7) correspond to Mn(Kα) and Mg(Kα)/(Fe(Kα)+Mg(Kα)) of garnet. Note that the grain in the center of the images is fractured. The bottom synthetic XR images (step size: 6 µm; counting time: 50 ms (Na, Mn, Ti, Si) and 35 ms (Al, Fe, Mg, Ca; all other operating conditions and procedures as above and Fig. 7) correspond to Al(Kα) and Mg(Kα)/(Fe(Kα)+Mg(Kα)) of retrograde glaucophane. The compositional profile of garnet is indicated in the XR image of Mn. The composition of amphibole is plotted within the classification scheme of Leake et al. (1997), with symbols and labels as in figure 5.

Locally, amphibole rims are calcic (magnesiohornblende-actinolite), with a composition similar to that of retrograde grains associated with chlorite, albite and glaucophane. Inclusions of epidote within garnet have the Al-richest composition, the grains of the matrix show a faint zoning with cores richer in Al and rims richer in Fe^{3+} and some grains associated with retrograde overprints have lower Fe^{3+}, all indicating positive correlation of Fe^{3+} with temperature. Phengite shows a faint concentric zoning with cores richer in Si and Mg and rims richer in Al and Ti. This pattern is consistent with prograde growth at high pressure. Small grains of glaucophane overprint prograde barroisite, omphacite and garnet. At sites where glaucophane grew adjacent to garnet, its composition is richer in Fe and Al, while it is richer in Mg at sites dominated by amphibole and/or omphacite. This is clearly shown in Fig. 9, where grains of Al-Fe-richer glaucophane grown at the rims of garnet become richer in Mg as they intrude the matrix formed by barroisite+omphacite. Since garnet is rich in Al and Fe, and barroisite and glaucophane are poorer in Al and richer in Mg, this texture indicates that the heterogeneous composition of glaucophane is the result of diffusion problems during retrogression and not because of different stages of growth. Similarly, retrograde chlorite occurs adjacent to garnet and within the barroisite+omphacite matrix, and its composition mimics the site of growth with higher Fe contents in the former and higher Mg contents in the latter (not shown) indicating equilibrium problems.

Metamorphic conditions have been estimated using Thermocalc (version 3.21). With the new data outlined above, we refined the calculations of Schneider et al. (2004) with identical results within error. Conditions calculated for the pre-peak inclusion assemblage and the peak assemblage are 573 ± 66 º C and 14.6 ± 2.8 kbar, and 657 ± 47 ºC and 15 ± 2.1 kbar, respectively. Conditions calculated for the retrograde assemblage are 460 ± 87 ºC and 8.8 ± 1.7 kbar, though these figures are uncertain because of equilibrium problems of glaucophane and chlorite mentioned above. The resulting P-T path describes a prograde section within the eclogite field followed by strong cooling during decompression. That the retrograde P-T path involves substantial cooling, as is typical for Franciscan-type paths, is indicative of a low geothermal (i.e., refrigerated) gradient during exhumation, implying that subduction did not stop during mélange formation and exhumation. This situation resembles that inferred for eastern Cuba, but is the reverse from that inferred for the mélanges of western-central Cuba.

PLATE-TECTONIC IMPLICATIONS

Alternative plate-tectonic models have been proposed for the Caribbean region (see Morris et al., 1990; Pindell, 1994; Meschede and Frisch, 1998 for reviews, and the IGCP 433 "Origin of the Caribbean Plate" site http://www.ig.utexas.edu/CaribPlate/CaribPlate.html). However, most authors agree in a) formation of an oceanic inter-Americas gap (i.e., Proto-Caribbean) during Jurassic break-up of Pangea and Cretaceous drift of North and South America, b) progressive consumption of the Proto-Caribbean during the Cretaceous-Tertiary in one or several subduction zones, c) insertion of the Pacific-derived Caribbean plate into the inter-Americas gap and d) collision of the Caribbean plate with the North and South American plate margins during the uppermost Cretaceous and Tertiary (e.g. Wilson, 1966; Malfait and Dinkelman, 1972; Mattson, 1979; Pindell and Dewey, 1982; Burke et al., 1984; Duncan and Hargraves; 1984; Burke, 1988; Pindell and Barrett, 1990; Pindell, 1985, 1994; Mann, 1999; Iturralde-Vinent, 1998; Kerr et al., 1998, 1999; Pindell and Kennan, 2001). This process may have been accompanied by a change in polarity of subduction, from eastward-dipping subduction of the Pacific below the Proto-Caribbean to westward-dipping subduction of the Proto-Caribbean below the Pacific (Caribbean), but the age and tectonic scenario of the flip is debated.

Burke (1988), Duncan and Hargraves (1984) and Kerr et al. (1998) have argued for an Upper Cretaceous flip of subduction, while Mattson (1979), Pindell and Dewey (1982), Pindell (1994) and Pindell and Kennan (2001) have proposed an Aptian age. Mid-Cretaceous unconformities recorded in volcanic arc sequences along the Antilles and Venezuela have been related to an important mid-Cretaceous orogenic event by Pindell and Kennan (2001), but the unconformity is absent in Puerto Rico (Schellekens, 1998; Jolly et al., 2001) and Virgin Islands (Rankin, 2002). In La Habana, Villa Clara and Camagüey regions of central Cuba, unconformities and conglomerates of Albian age locally separate the tholeiitic and calc-alkaline island arc suites of the Cretaceous volcanic belt of central Cuba (i.e., pre-Camujiro/Los Pasos and Camujiro/Mataguá formations, respectively), but conglomerates and unconformities of Coniacian-Santonian age are also present within this volcanic belt (Iturralde-Vinent, 1996c and; Diaz de Villalvilla, 1997; Piñero Pérez et al., 1997). Lebron and Perfit (1993, 1994) argued for a mid-Cretaceous flip based on an abrupt change from IAT to CA affinity in volcanic arc rocks, but this argument has been disputed by Kerr et al. (1999), Jolly et al. (2001) and Iturralde-Vinent et al. (this volume) based on evidence from Cuba and Puerto Rico. Mid-

Cretaceous reversal of subduction has been related to northward overthrusting of the arc by oceanic crust in the Cordillera Central of Hispaniola (Draper et al., 1996, see also Lewis et al., 1999, 2002), but according to Lapierre et al. (1997, 1999) this tectonic event took place in Upper Cretaceous times. Our data and interpretations add to this debate.

Mid-Cretaceous arrest of subduction (western-central Cuba)

The P-T path and age data from high pressure blocks within serpentinite mélanges of the northern ophiolite belt in western and central Cuba provide evidence for pre-Aptian (pre-118 Ma) subduction, Aptian tectonic instability of the subduction system and Aptian-Albian arrest of subduction and mélange formation and exhumation. This mélange-forming event may relate to Aptian collision between Chortis and western Mexican blocks documented in exotic blocks of eclogite within serpentinite mélanges south of the Motagua fault zone in Guatemala (Harlow et al., 2004). If correlation exists, the lack of evidence for ocean basin closure and continent-continent collision in Cuba indicates prolongation of the continent-continent collision belt of Guatemala into a southern intra-oceanic belt.

The possible Cuban prolongation of mid-Cretaceous Guatemalan collision can be integrated into the tectonic model of Kerr et al. (1999). This model diverges from others proposed for the Caribbean region in postulating two simultaneous subduction systems during the Lower Cretaceous, the western one involving NE-directed consumption of the Pacific and associated with the formation of the tholeiitic island arc and the eastern one involving SW-directed consumption of the Proto-Caribbean and associated with the formation of a boninitic arc. Based on the extinction of the boninitic arc, the model incorporates termination of the subduction of the Proto-Caribbean and an orogenic event during the Aptian-Albian that formed an intra-oceanic suture. Thus, correlation of mid-Cretaceous sutures in Cuba and Guatemala is possible. Because the suture is located within the northern ophiolite belt, between the Cretaceous volcanic arc belt (to the South) and the Bahamas Platform (to the North) in central Cuba, the associated subduction zone likely involved subduction of the Proto-Caribbean, as suggested by Kerr et al. (1999). However, Harlow et al. (2004) suggested NE dipping subduction of the Pacific (Farallon) plate in Guatemala. To clarify this problem, age data of the boninitic rocks from Cuba are needed.

Alternatively, the mid-Cretaceous event of arrest of subduction and mélange formation in western-central Cuba may represent arrest of subduction of Pacific lithosphere related to Aptian flip of subduction as proposed by Pindell (1994) and Pindell and Kennan (2001). However, the model of Aptian flip of subduction predicts formation of western-central Cuba mélanges to the southwest (pre-Aptian scenario) of the volcanic arc. This prediction conflicts with the structural arrangement of central Cuba, where the Cretaceous volcanic arc belt overrides the northern ophiolite belt and associated mélanges along N-directed thrusts. Though this structure formed during the uppermost Late Cretaceous to Paleogene collision, the reconstruction of the relative position of the complexes during pre-Upper Cretaceous times places the mélanges northeast of the arc. The conflict is resolved if the mélanges are of Upper Cretaceous age, as proposed, for example, by Andó et al. (1996). But, while an additional Upper Cretaceous event of mélange formation is not excluded, the metamorphic data from the high-pressure blocks in the Holguín region indicate subduction during the Lower Cretaceous. Thus, model of Aptian flip of subduction can only accommodate our inferences concerning metamorphism in western-central Cuba mélanges if a fragment of the pre-Aptian fore-arc (located in the Pacific side of the arc) was tectonically incorporated to the post-Aptian fore-arc (located in the Proto-Caribbean side of the arc) during the flip of subduction, perhaps as a result of important sinistral strike-slip movements traversing the magmatic arc.

Mid-Cretaceous onset of subduction (eastern Cuba)

High-grade metamorphism in amphibolite blocks from eastern Cuba mélanges indicates formation in a hot subduction environment suggesting initiation of subduction. Initiation of subduction in the Caribbean realm has been proposed for parts of the Cordillera de la Costa accretionary prism, Venezuela (Smith et al., 1999). However, these authors dated the onset of subduction as Upper Cretaceous, while it is probably of Aptian age in eastern Cuba. Consequently, rocks from eastern Cuba support models of flip of subduction during the Aptian. This type of model predicts the birth of a new SW-dipping subduction system that consumed hot oceanic lithosphere of the Proto-Caribbean basin, which was opening at that time and subduction of a ridge was possible, as suggested by Pindell and Kennan (2001) who depict subduction of the Proto-Caribbean ridge in their model. Furthermore, continued subduction and, consequently, refrigeration of the subduction system during the Upper Cretaceous is consistent with counterclockwise P-T paths of eastern Cuba amphibolite blocks.

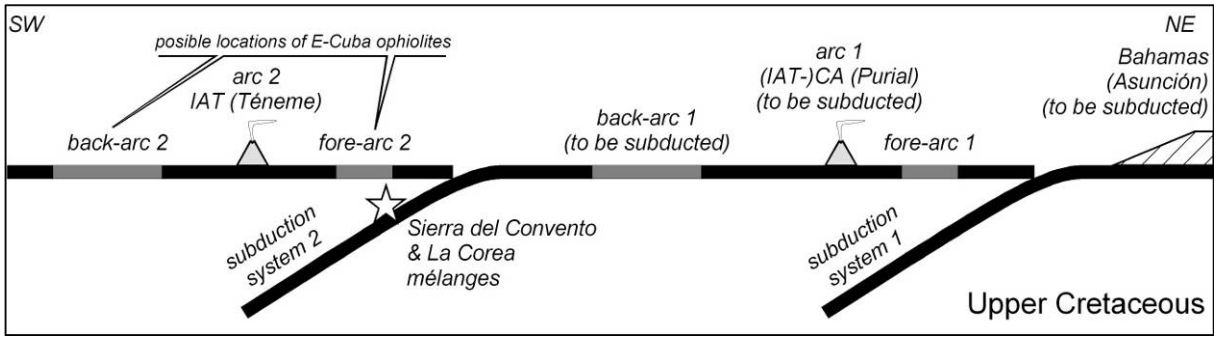

FIGURE 10. Model of the tectonic configuration of eastern Cuba during the Upper Cretaceous. Oceanic and suprasubduction volcanisms are indicated in black and grey, respectively. The Sierra del Convento and La Corea amphibolites (star) would have been formed upon the (Aptian) onset of subduction system 2, and the Purial complex (volcanic arc 1) would collide with this subduction system in the Late Campanian. The age of collision of the Asunción terrane (Bahamas?) with subduction system 2 is uncertain. Possible locations of eastern Cuba ophiolites and associated volcanics (suprasubduction system 2) are also indicated.

Upper Cretaceous subduction of the Purial volcanic arc

Though a sound structural analysis of eastern Cuba has not been undertaken, the basic structural arrangement of the region is dominated by NE-directed thrusts of (meta)ophiolitic material over the (meta)volcanic arc terrane of the Purial complex. This arrangement implies that the ophiolitic material and associated serpentinite mélanges were located to the SW of the Cretaceous volcanic arc belt previous to thrusting, conflicting with the predictions of models of Aptian flip of subduction. In this type of model, the mélanges should have been accreted to the fore-arc of the Caribbean plate and, consequently, should have been located to the NE of the volcanic arc. In addition, it should be noted that this model does not satisfactorily explain Late Campanian metamorphism of the Purial volcanic arc. This metamorphism was developed during collision of the Cretaceous volcanic arc belt with a subduction zone, as indicated by the attainment of high-pressure metamorphism and associated intense ductile deformation. In order to explain this orogenic process during the late Upper Cretaceous and the structural arrangement of eastern Cuba, it appears that two subduction zones are required as depicted in figure 10. This two-fold configuration explains a) volcanic arc sequences of Upper Cretaceous age with contrasted geochemical signatures including boninitic and tholeiitic in the eastern ophiolites and (mostly) calc-alkaline in the Cretaceous volcanic arc belt of the Purial complex, b) high-pressure metamorphism of oceanic material in La Corea and Sierra del Convento mélanges associated with the eastern ophiolites, c) high-pressure metamorphism of Cretaceous volcanic arc belt (Purial complex) and continental-margin sequences (Asunción), and d) thrusting of the ophiolitic bodies over the Cretaceous volcanic arc belt (Purial complex). The proposed arrangement of subduction during the Upper Cretaceous for eastern Cuba strengthens our view that mélanges of eastern and western-central Cuba are not correlated.

Upper Cretaceous subduction of the Escambray

Before our data and interpretations are discussed, the Late Jurassic (140-160 Ma) U-Pb ages of zircon of eclogites from the Escambray merits comment. This age is enigmatic and may represent either the magmatic crystallization of the precursor gabbro or an early (pre-Caribbean) metamorphic event (Maresch et al., 2003). Pindell and Kennan (2001) considered that this age correlates with Late Jurassic high pressure rocks from Baja California and suggested that the continental rocks of the Escambray (and Isle of Pines) may be located south of Chortis block during the late Jurassic. Furthermore, these authors depict the continental part of the Escambray massif to the SW of the Proto-Caribbean subduction zone during the Upper Cretaceous, implying that it was not subducted during this stage. This configuration is inconsistent with our interpretation of on-going subduction of oceanic and continental material during the late Upper Cretaceous and with independent studies that suggest correlation of a) the dragged basement of the eastern margin of the Yucatan peninsula with the Guaniguanico terrane (Pyle et al., 1973) and b) the latter with the Escambray and Isle of Pines terranes (Millán, 1997a and b; Iturralde-Vinent, 1996a, Pszczólkowski, 1999, and references therein). Further geochronological work is needed to solve this problem.

Assuming the continental portion of the Escambray ensemble forming part of the margin of the Maya block during the Mesozoic, subducted ophiolitic material within the complex (i.e. serpentinite-mélanges containing HP blocks) should

correspond to Proto-Caribbean oceanic crust. K-Ar, $^{40}Ar/^{39}Ar$ and Rb/Sr ages of metasediments from the margin and of subducted oceanic crust (e.g. eclogite block LV69A) suggest subduction during the Upper Cretaceous and exhumation during the late Upper Cretaceous. This configuration is consistent with models that incorporate flip of subduction either during the Upper Cretaceous or the Aptian, though pre-100 Ma U-Pb ages constitute a problem of the former type of models. In the latter type of model, the 100-106 Ma U-Pb ages of zircons (Hatten et al., 1988, 1989) of eclogite blocks within serpentinite mélanges are explained as earlier subducted Proto-Caribbean crust (see Millán, 1996a).

CONCLUDING REMARKS

The metamorphic evolution of subducted ophiolitic material from Cuba and the geologic setting of the different complexes do not support a single subduction system in the region during the Cretaceous. We propose that:

a) High-pressure blocks from the northern ophiolite belt in western and central Cuba formed in a pre-Aptian subduction zone that arrested during the Aptian-Albian due to an intra-oceanic collision event related to either Early Cretaceous continent-continent collision event in Guatemala or Aptian flip of subduction,

b) high-pressure high-temperature amphibolite blocks from the eastern Cuba ophiolites formed in a new Aptian (SW-dipping) hot subduction zone which evolved to mature subduction during the Upper Cretaceous and arrested during the Late Campanian when the Purial segment of the Cretaceous volcanic arc belt impinged into the subduction zone (Fig. 10), and

c) high-pressure rocks from the Escambray complex formed in a mature (SW-dipping) subduction zone of Upper Cretaceous age which consumed Proto-Caribbean oceanic crust and arrested during the late Upper Cretaceous, when the margin of the Maya block impinged into the subduction zone.

These conclusions suggest a variety of tectonic arrangements that may represent complications in space and time of a dynamic plate-tectonic scenario strongly influenced by adjacent continental masses of North and South America. It may be no coincidence that the inferred Aptian-Albian arrest of subduction in western and central Cuba and initiation of hot subduction in eastern Cuba is synchronous with the onset of opening of Equatorial-South Atlantic and the westward drift of South America during mid-Cretaceous times. This was a global event that may have had significant consequences for the plate-tectonic evolution of the Caribbean region, such as the demise and birth of subduction systems, subduction polarity reversals, intraoceanic collision, closure of small oceanic basins flanking continental blocks, changes in location and geochemical signature of arcs and of ocean-basin magmatic activity. The overlap in time of these events and of the episodes of subduction-related metamorphism and serpentinite-matrix mélange formation in Cuba makes conceivable that the latter had shared the same origin. This could mean that a number of independent subduction zones evolved in the Caribbean-eastern Pacific region during the Cretaceous. Plate tectonic models that incorporate Aptian flip of subduction better accommodate our data and interpretations, though some adaptations of the models are needed. In particular, the Early Cretaceous Cuban-Guatemalan subduction-collision event and two simultaneous Upper Cretaceous subduction zones should be considered. Thus, the subduction zone where the blocks from the northern ophiolite belt of western-central Cuba were formed document a Lower Cretaceous subduction system different from that of eastern Cuba and the Escambray, and the subduction zones where the HP rocks of the latter two regions formed do not necessarily represent different parts (separated along strike) of a single Upper Cretaceous subduction system.

ACKNOWLEDGEMENTS

We acknowledge Ed Lidiak and an anonymous reviewer for perceptive comments and suggestions. This paper is part of the IGCP project 433 (Caribbean Plate Tectonics) and has received financial support from the Spanish DGES-MEC project BTE2002-01011.

REFERENCES

Adamovich, A., Chejovich, V., 1964. Principales características de la geología y de los minerales útiles de la región nordeste de la Provincia de Oriente. Revista Tecnológica, 2, 14-20.

Andó, J., Harangi, Sz., Szakmány, By., Dosztály, L., 1996. Petrología de la asociación ofiolítica de Holguín. In: Iturralde-Vinent, M.A. (ed.), Ofiolitas y Arcos Volcánicos de Cuba. Miami, USA, IGCP Project 364 Special Contribution 1, 154-176.

Auzende, A.L., Devouard, B., Guillot S., Daniel, I., Baronnet, A., Lardeaux J.M., 2002. Serpentinites from central Cuba; petrology and HRTEM study. European Journal of Mineralogy, 14, 905-914.

Blein, O., Guillot, S., Lapierre, H., Mercier-de-Lepinay, B., Lardeaux, J.M., Millán, G., Campos, M., García, A., 2003. Geochemistry of the Mabujina Complex, central Cuba; implications on the Cuban Cretaceous arc rocks. Journal of Geology, 111, 89-101.

Boiteau, A., Michard, A., Saliot, P., 1972. Métamporphisme de haute pression dans le complexe ophiolitique du Purial (Oriente,Cuba). Comptes Rendus de l'Académie des Sciences Paris, 274 (série D), 2137-2140.

Bralower, T.J., Iturralde-Vinent, M.A., 1997. Micropaleontological dating of the collision between the North American plate and the Greater Antilles arc in western Cuba. Palaios, 12, 133-150.

Burke, K., 1988. Tectonic evolution of the Caribbean. Annual Reviews of Earth and Planetary Sciences, 16, 201-230.

Burke, K., Cooper, C., Dewey, J.F., Mann, P., Pindell, J.L., 1984. Caribbean tectonics and relative plate motions. In: Bonini, W., Hargraves, R.B., Shagam, R. (eds.) The Caribbean-South American Plate Boundary and Regional Tectonics. Geological Society of America, Boulder, Colorado, Memoir 162, 31-63.

Carswell, D.A., 1990. Eclogites and the eclogite facies: definitions and classifications. In: Carswell, D.A. (ed.) Eclogite Facies Rocks, Blackie, Glasgow, 1-13.

Cobiella, J., Campos M., Boiteau, A., Quintas, F., 1977. Geología del flanco sur de la Sierra del Purial. Revista La Minería de Cuba, 3, 54-62.

Cobiella, J., Quintas, F., Campos M., Hernández, M., 1984. Geología de la Región central y Suroriental de la Provincia de Guantánamo. Editorial Oriente, Santiago de Cuba, 125 pp.

Coleman, R.G., Lee, D.E., Beatty, L.B. Brannock, W.W., 1965. Eclogites and eclogites: their differences and similarities. Geological Society of America Bulletin, 76, 483–508.

Díaz de Villalvilla, L., 1997. Caracterización geológica de las formaciones volcánicas y volcano-sedimentarias en Cuba central, provincias Cienfuegos, Villa Clara, Sancti Spiritus. In: Furrazola Bermúdez, G.F., Núñez Cambra, K.E. (eds.). Estudios sobre Geología de Cuba. Centro Nacional de Información Geológica, La Habana, Cuba, 259-270.

Donnelly, T.W., Rogers, J.W., 1978. The distribution of igneous rock suites throughout the Caribbean. Geologie en Mijnbouw, 57, 151-162.

Donnelly, T.W., Beets, D., Carr, M., Jackson, T., Klaver, G., Lewis, J., Maury, R., Schellenkens, H., Smith, A.L., Wadge, G., Westercamp, D., 1990. History and tectonic setting of Caribbean magmatism. In: Dengo, G., Case, J.E. (eds.). Geology of North America. Volume H. The Caribbean region. Geological Society of America, Boulder, Colorado, 339–374.

Draper, G., Jackson, T.A., Donovan, S.K., 1994. Geologic provinces of the Caribbean Region. In: Donovan, S.K., Jackson, T.A. (eds.). Caribbean Geology: An Introduction. U.W.I. Publishers' Association, Kingston, Jamaica, 3-12.

Draper, G., Gutiérrez, G., Lewis, J.F., 1996. Thrust emplacement of the Hispaniola peridotite belt: Orogenic expression of the mid-Cretaceous Caribbean arc polarity reversal? Geology, 24, 1143-1146.

Duncan, R.A., Hargraves, R.B., 1984. Plate tectonic evolution of the Caribbean region in the mantle reference frame. In: Bonini, W., Hargraves, R.B., Shagam, R. (eds.) The Caribbean-South American Plate Boundary and Regional Tectonics. Geological Society of America, Boulder, Colorado, Memoir 162, 81-93.

Ernst, W.G., 1988. Tectonic history of subduction zones inferred from retrograde blueschists P-T paths. Geology, 16, 1081-1084.

Fonseca, E., Zelepugin, V.N., Heredia, M., 1985. Structure of the ophiolite association of Cuba. Geotectonics, 19, 321-329.

Fonseca, E., González, R., Delgado, R., Savieleva, G., 1989. Presencia de efusivos ofiolíticos y de boninitas en las provincias de La Habana y Matanzas. Boletín Técnico, Geología, 1, 1-9.

García-Casco, A., Torres-Roldán, R.L., Millán, G., Monié, P., Haissen, F., 2001. High-grade metamorphism and hydrous melting of metapelites in the Pinos terrane (W Cuba): Evidence for crustal thickening and extension in the northern Caribbean collisional belt. Journal of Metamorphic Geology, 19, 699-715.

García-Casco, A., Torres-Roldán, R.L., Millán, G., Monié, P., Schneider, J., 2002. Oscillatory zoning in eclogitic garnet and amphibole, Northern Serpentinite Melange, Cuba: a record of tectonic instability during subduction? Journal of Metamorphic Geology, 20, 581-598.

García-Casco, A., Pérez de Arce, C., Millán, G., Iturralde-Vinent, M.A., Fonseca, E., Torres-Roldán, R.L., Núnez, K., Morata, D., 2003. Metabasites from the northern serpentinite belt (Cuba) and a metamorphic perspective of the plate tectonic models for the Caribbean region. Taller del Proyecto nº 433 del PICG / UNESCO "Tectónica de placas en el Caribe", Memorias GEOMIN 2003, La Habana, ISBN 959-7117-11-8, 1-9.

García Delgado, D.E., Pérez Pérez, C., Delgado Damas, R., Díaz Otero, C., Millán, G., Furrazola, G., Díaz de Villalvilla, L., García Cadiz, I., Sukar, K., Delgado Carballo, I., Bernal, L., Pardo, M., Rojas Agramonte, Y., Suárez Leyva, V., Duani Duarte, E., 1998. Mapa geológico de Cuba central (provincias Cienfuegos, Villa Clara y Sancti Spiritus), escala 1:100000. Instituto de Geología y Paleontología, La Habana.

Gervilla, F., Proenza, J.A., Frei, R., González-Jiménez, J.M., Garrido, C., Melgarejo, J.C., Meibom, A., Díaz-Martínez, R., Lavaout, W., 2005. Distribution of platinum-group elements and Os isotopes in chromite ores from Mayarí-Baracoa ophiolitic belt (eastern Cuba). Contribution to Mineralogy and Petrology, in press.

Gerya, T.V., Stöckhert, B., Perchuk, A.L., 2002. Exhumation of high-pressure metamorphic rocks in a subduction channel -a numerical simulation. Tectonics, 21, (6), 1-19.

Gordon, M.B., Mann, P., Cáceres, D., Flores, R., 1997. Cenozoic tectonic history of the North America-Caribbean plate boundary in western Cuba. Journal of Geophysical Research, 102, 10055-10082.

Grafe, F., Stanek, K.P., Baumann, A., Maresch, W.V., Hames, W.E., Grevel, C., Millán, G., 2001. Rb-Sr and $^{40}Ar/^{39}Ar$ mineral ages of granitoid intrusives in the Mabujuna unit, central Cuba: Thermal exhumation history of the Escambray massif. Journal of Geology, 109, 615-631.

Harlow, G.E.., Hemming, S.R., Avé Lallemant, H.G., Sisson, V.B., Sorensen, S.S., 2004. Two high-pressure–low-temperature serpentinite-matrix mélange

belts, Motagua fault zone, Guatemala: A record of Aptian and Maastrichtian collisions. Geology, 32, 17-20.

Hatten, C. W., Somin, M. L., Millan, G., Renne, P., Kistler, R.W., Mattison, J.M., 1988. Tectonostratigraphic units of Central Cuba. Proceedings of the 11th Caribbean Geological Conference, Barbados, 35, 1-13.

Hatten, C.W., Mattison, J.M., Renne, P.R., Somin, M.L., Millán, G., Araqueliants, M.M., Kolesnikov, E.M., Sumin, L.V., 1989. Rocas metamórficas de alta presión: nuevos datos acerca de sus edades. Primer Congreso Cubano de Geología, La Habana, Cuba, 118-119.

Hernández, M., Canedo, Z., 1995. Geoquímica de las ofiolitas meridionales de Cuba oriental. Revista Minería y Geología, 3, 3-9.

Holland, T.J.B., Powell, R., 1998. An internally consistent thermodynamic data set for phases of petrological interest. Journal of Metamorphic Geology, 16, 309-343.

Hutson, F., Mann, P., Renne, P., 1998. $^{40}Ar/^{39}Ar$ dating of single muscovite grains in Jurassic siliclastic rocks (San Cayetano Formation): Constraints on the paleoposition of western Cuba. Geology, 26, 83-86.

Iturralde-Vinent, M.A., 1988. Naturaleza geológica de Cuba. Editorial Científico-Técnica, La Habana, Cuba, 246 pp.

Iturralde-Vinent, M.A., 1989. Role of ophiolites in the geological constitution of Cuba. Geotectonics, 4, 63-74.

Iturralde-Vinent, M.A., 1994. Cuban geology: A new plate tectonic synthesis. Journal of Petroleum Geology, 17, 39-70.

Iturralde-Vinent, M.A., 1996a. Introduction to Cuban Geology and Geophysics. In: Iturralde-Vinent, M.A. (Ed.). Ofiolitas y Arcos Volcánicos de Cuba. Miami, USA, IGCP Project 364 Special Contribution 1, 3-35.

Iturralde-Vinent, M.A., 1996b. Geología de las ofiolitas de Cuba. In: Iturralde-Vinent, M.A. (ed.). Ofiolitas y Arcos Volcánicos de Cuba. Miami, USA, IGCP Project 364 Special Contribution 1, 83-120.

Iturralde-Vinent, M.A., 1996c. El arco de islas volcánicas del Cretácico. In: Iturralde-Vinent, M.A. (ed.). Ofiolitas y Arcos Volcánicos de Cuba. Miami, USA, IGCP Project 364 Special Contribution 1, 179-189.

Iturralde-Vinent, M.A., 1996d. Evidencias de un arco primitivo (Cretácico Inferior) en Cuba. In: Iturralde-Vinent, M.A. (ed.). Ofiolitas y Arcos Volcánicos de Cuba. Miami, USA, IGCP Project 364 Special Contribution 1, 227-230.

Iturralde-Vinent, M.A., 1998. Sinopsis de la Constitución Geológica de Cuba. In Melgarejo J.C., Proenza, J.A. (eds.) Geología y Metalogénia de Cuba: Una Introducción. Acta Geologica Hispanica, 33, 9-56.

Iturralde-Vinent, M.A., Morales, T.M., 1988. Toleitas del Titoniano medio en la Sierra de Camaján, Camagüey. Posible datación de la corteza oceánica. Revista Tecnológica, 18, 25-32.

Iturralde-Vinent, M.A., Millán, G., Korkas, L., Nagy, E., Pajón, J., 1996. Geological interpretation of the Cuban K-Ar data base. In: Iturralde-Vinent, M.A. (ed.). Ofiolitas y Arcos Volcánicos de Cuba. Miami, USA, IGCP Project 364 Special Contribution 1, 48-69.

Iturralde-Vinent, M.A., Díaz Otero, C., Rodríguez Vega, A., Díaz Martínez , R., this volume. Tectonic Implications of Paleontologic Dating of Cretaceous-Danian Sections of Northeastern Cuba. Geologica Acta, ??, ??-??

Jolly, W.T., Lidiak, E.G., Dickin, A.P., Wu, T.W., 2001. Secular geochemistry of central Puerto Rican island arc lavas; constraints on Mesozoic tectonism in the eastern Greater Antilles. Journal of Petrology, 42, 2197-2214.

Kerr, A.C., Tarney, J., Nivia, A., Marriner, G.F., Saunders, A.D., 1998. The internal structure of oceanic plateaus: Inferences from obducted Cretaceous terranes in western Colombia and the Caribbean. Tectonophysics, 292, 173-188.

Kerr, A.C., Iturralde-Vinent, M., Saunders, A.D., Babbs, T.L., Tarney, J., 1999. A new plate tectonic model of the Caribbean: Implications from a geochemical reconnaissance of Cuban Mesozoic volcanic rocks. Geological Society of America Bulletin, 111, 1581-1599.

Khudoley, K. M., 1967. Principal features of Cuban geology. AAPG Bulletin, 51, 668-677.

Khudoley, K. M., Meyerhoff, A. A., 1971. Paleogeography and geological history of Greater Antilles. Geological Society of America, Boulder, Colorado, Memoir 129, 1-199.

Kretz, R., 1983. Symbols for rock-forming minerals. American Mineralogist, 68, 277-279.

Kubovics, I., Andó, J., Szakmány, Gy., 1989. Comparative petrology and geochemistry of high pressure metamorphic rocks from eastern Cuba and western Alps. Acta Mineralogica-Petrographica Szeged, 30, 35-54.

Kulachkov, L.V., Leyva, R.C., 1990. Informe sobre los resultados de los trabajos de reconocimiento geológico para cuarzo filoniano en la parte oriental de Cuba. Unpublished report of the Instituto Superior Minero-Metalúrgico de Moa.

Lapierre, H., Dupuis, V., Lepinay, B.M., Tardy, M., Ruiz, J., Maury, R.C., Hernández, J., Loubet, M., 1997. Is the Lower Duarte Complex (Española) a remmant of the Caribbean plume generated oceanic plateau? Journal of Geology, 105, 111-120.

Lapierre, H., Dupuis, V., Lepinay, B.M., Bosch, D., Monié, P., Tardy, M., Maury, R.C., 1999. Late Jurassic oceanic crust and Upper Cretaceous Caribbean plateau picritic basalts exposed in the Duarte igneous complex, Hispaniola. Journal of Geology, 107, 193-207.

Leake, B.E., Woolley, A.R., Arps, C.E.S,., Birch, W.D., Gilbert, M.C., Grice, J.D., Hawthorne, F.C., Kato, A., Kisch, H.J., Krivovichev, V.G., Linthout, K., Laird, J., Mandarino, J.A., Maresch, W.V., Nickel, E.H., Rock, N.M.S., Schumacher, J.C., Smith, D.C., Stephenson, N.C.N., Ungaretti, L., Whittaker, E.J.W., Touzhi, G., 1997. Nomenclature of amphiboles: Report of the Subcommittee on Amphiboles of the International Mineralogical Association, Commission on New

Minerals and Mineral Names. American Mineralogist, 82, 1019-1037.

Lebron, M.C., Perfit, M.R., 1993. Stratigraphic and petrochemical data support subduction polarity reversal of the Cretaceous Carribean island arc. Journal of Geology, 101, 389-396.

Lebron, M.C., Perfit, M.R., 1994. Petrochemistry and tectonic significance of Cretaceous island-arc rocks, Cordillera Oriental, Dominican Republic. Tectonophysics, 229, 69-100.

Lewis, J.F., Hames, W.E., Draper, G., 1999. Late Jurassic oceanic crust and Upper Cretaceous Caribbean plateau picritic basalts exposed in the Duarte igneous complex, Hispaniola: A discussion. Journal of Geology, 107, 505-508.

Lewis, J.F., Escuder Viruete, J., Hernaiz Huerta, P.P., Gutierrez, G., Draper, G., Pérez-Estaún, A., 2002. Subdivisión geoquímica del Arco Isla Circum-Caribeño, Cordillera Central Dominicana: Implicaciones para la formación, acreción y crecimiento cortical en un ambiente intraoceánico. Acta Geologica Hispanica, 37, 81-122.

Leyva, R.C., 1996. Características geológicas, regularidades de distribución y perspectivas de utilización del cuarzo filoniano de la región oriental de Cuba. Unpublished report of the Instituto Superior Minero-Metalúrgico de Moa, 90 pp.

Llanes, A.L., García, D.E., Meyerhoff, D.H., 1998. Hallazgo de fauna jurásica (Tithoniano) en ofiolitas de Cuba central. Memorias del III Congreso Cubano de Geología y Minería 2, Sociedad Cubana de Geología, La Habana, 241-244.

Malfait, B.T., Dinkelman, M.G., 1972. Circum-Caribbean tectonic and igneous activity and the evolution of the Caribbean plate. Geological Society of America Bulletin, 83, 251-272.

Mann, P., 1999. Caribbean sedimentary basins: Classification and tectonic setting. In: Mann, P. (ed.). Sedimentary Basins of the World, 4, Caribbean Basins, Elsevier Science B.V., Amsterdam, 3-31.

Maresch, W.V., Stanek, K.P., Grafe, F., Idleman, B., Baumann, A., Krebs, M., Schertl, H.P., Draper, G., 2003. Age systematics of high-pressure metamorphism in the Caribbean: confronting existing models with new data. 5th Cuban Geological Congress, GEOMIN 2003, La Habana, Cuba, Memorias, 296-298.

Martínez González, D., Vázquez Torres, M., Chang Carvajal, J.C., Denis Valle, R., Fernández Méndez, O., Fernández de Lara, R., Barrios Cardentey, E., 1994. Informe sobre la Generalización del Mapa Geológico del occidente de Cuba a escala 1:100000. Empresa Geologominera de Pinar del Río. 104 pp.

Mattson, P.H., 1979. Subduction, buoyant breaking, flipping and strike-slip faulting in the northern Caribbean. Journal of Geology, 87, 293-304.

Meschede, M., Frisch, W., 1998. A plate tectonic model for the Mesozoic and Early Cenozoic history of the Caribbean plate. Tectonophysics, 296, 269-291.

Millán, G., 1988. La asociación glaucofana-pumpellita en metagrabroides de la faja metamórfica Cangre. Boletín de Geociencias, 3, 35-36.

Millán, G., 1996a. Metamorfitas de la asociación ofiolítica de Cuba. In: Iturralde-Vinent, M.A. (ed.). Ofiolitas y Arcos Volcánicos de Cuba. Miami, USA, IGCP Project 364 Special Contribution 1, 131-146.

Millán, G., 1996b. Geología del complejo de Mabujina. In: Iturralde-Vinent, M.A. (ed.). Ofiolitas y Arcos Volcánicos de Cuba. Miami, USA, IGCP Project 364 Special Contribution 1, 147-153.

Millán G., 1997a. Posición estratigráfica de las metamorfitas cubanas. In: Furrazola Bermúdez, G.F., Núñez Cambra, K.E. (eds.). Estudios sobre Geología de Cuba. Centro Nacional de Información Geológica, La Habana, Cuba, 251-258.

Millán G., 1997b. Geología del macizo metamórfico del Escambray. In: Furrazola Bermúdez, G.F., Núñez Cambra, K.E. (eds.). Estudios sobre Geología de Cuba. Centro Nacional de Información Geológica, La Habana, Cuba, 271-288.

Millán, G., Somin, M.L., 1985. Contribución al conocimiento geológico de las metamorfitas del Escambray y Purial. Reportes de Investigación de la Academia de Ciencias de Cuba, 2, 1-74.

Millán, G. Somin, M.L., Díaz, C, 1985. Nuevos datos sobre la geología del macizo montañoso de la Sierra del Purial, Cuba Oriental. Reporte de Investigación del Instituto de Geología y Paleontología, 2, 52-74.

Morimoto, N., Fabries, J., Ferguson, A.K., Ginzburg, I.V., Ross, M., Seifert, F.A., Zussman, J., Aoki, K., Gottardi, G., 1988. Nomenclature of pyroxenes: Report of the Subcommittee on Pyroxenes of the International Mineralogical Association, Commission on New Minerals and Mineral Names. American Mineralogist, 73, 1123-1133.

Morris, A.E.L., Taner, I., Meyerhoff, H.A., Meyerhoff, A.A., 1990. Tectonic evolution of the Caribbean region; Alternative hypothesis. In: Dengo, G., Case, J.E. (eds.). Geology of North America. Volume H. The Caribbean region. Geological Society of America, Boulder, Colorado, 339–374.

Newton, R.C., 1986. Metamorphic temperatures and pressures of Group B and C eclogites. In: Evans, B.W., Brown, E.H. (eds.) Blueschists and Eclogites. Geological Society of America, Boulder, Colorado, Memoir 164, 17–30.

Nuñez Cambra, K.E., García-Casco, A., Iturralde-Vinent, M.A., Millán, G., 2004. Emplacement of the ophiolite complex in Eastern Cuba. Proceedings of the 32nd International Geological Congress, Florencia. Session: G20.11 Caribbean Plate Tectonics.

Oh, C.-W., Liou, J.G., 1990. Metamorphic evolution of two different eclogites in the Franciscan Complex, California, USA. Lithos, 25, 41-53.

Pardo, G., 1975. Geology of Cuba. In: Nairn, A.E.M., Stehlei, F.G. (eds.). The Ocean basins and margins, 3, The Gulf of Mexico and the Caribbean. Plenum Press, New York, 553-615.

Pindell, J.L., 1985. Alleghenian reconstruction and the subsequent evolution of the Gulf of Mexico, Bahamas and Proto-Caribbean Sea. Tectonics, 4, 1-39.

Pindell, J.L., 1994. Evolution of the Gulf of Mexico and the Caribbean. In: Donovan, S.K., Jackson, T.A. (eds.).

Caribbean Geology: An Introduction. U.W.I. Publishers' Association, Kingston, Jamaica, 13-39.

Pindell, J.L., Barrett, S.F., 1990. Geologic evolution of the Caribbean region; A plate-tectonic perspective. In: Dengo, G., Case, J.E. (eds.). The Geology of North America, Volume H. The Caribbean Region. Geological Society of America, Boulder, Colorado, 405– 432.

Pindell, J.L., Dewey, J.F., 1982. Permo-Triassic reconstruction of western Pangea and the evolution of the Gulf of Mexico/Caribbean region. Tectonics, 1, 179-212.

Pindell, J.L., Kennan, L., 2001. Kinematic Evolution of the Gulf of Mexico and Caribbean. In: Fillon, R., Rosen, N., Weimer, P., Lowrie, A., Pettingill, H., Phair, R., Roberts, H., van Hoorn, B. (eds.) Transactions of the Gulf Coast Section Society of Economic Paleontologists and Mineralogists (GCSSEPM) 21st Annual Bob F. Perkins Research Conference, Petroleum Systems of Deep-Water Basins, Houston, Texas, 193-220.

Piñero Pérez, E., Quintana, M. A., Marí Morales, T., 1997. Caracterización geológica de los depósitos vulcanógeno-sedimentarios de la región Ciego-Camagüey-Las Tunas. In: Furrazola Bermúdez, G., Núñez Cambra, K. (eds.) Estudios sobre Geología de Cuba. Centro Nacional de Información Geológica, La Habana, 345-356.

Proenza, J., Melgarejo, J.C., Gervilla, F., Lavaut, W., Revé, D., Rodríguez, G., 1998. Cromititas podiformes en la Faja ofiolítica Mayarí-Baracoa (Cuba). Acta Geologica Hispanica, 33, 153-177.

Proenza, J., Gervilla, F., Melgarejo, J.C. Bodinier, J.L., 1999. Al-and Cr-rich chromitites from the Mayarí-Baracoa ophiolitic belt (eastern Cuba): consequence of interaction between volatile-rich melts and peridotites in suprasubduction mantle. Economic Geology, 94, 547-566.

Proenza, J., Alfonso, P., Melgarejo, J.C., Gervilla, F., Tritlla, J., Fallick, A.E., 2003. D, O and C isotopes in podiform chromitites as fluid tracers for hydrothermal alteration processes of the Mayari-Baracoa ophiolitic belt, eastern Cuba. In: Verweij, J.M., Doust, H., Peach, C.J., Spiers, C.J., Swennen, R.A.J (eds.) Proceedings of Geofluids IV. Journal of Geochemical Exploration, 78-79, 117-122.

Proenza. J.A., Díaz-Martínez, R., Marchesi, C., Melgarejo, J.C., Gervilla, F., Rodríguez-Vega, A., Lozano-Santacruz, R., Blanco-Moreno, J., this volume. Primitive Island-Arc Volcanic Rocks in Eastern Cuba: The Téneme Formation. Geologica Acta, ??, ??-??

Pszczólkowski, A., 1978. Geosynclinal sequences of the Cordillera de Guaniguanico in western Cuba, their lithostratigraphy, facies development and paleogeography. Acta Geologica Polonica, 28, 1-96.

Pszczólkowski, A., 1994. Interrelationship of the terranes in western and central Cuba – Comment. Tectonophysics, 234, 339-344.

Pszczólkowski, A., 1999. The exposed passive margin of North America in western Cuba. In: Mann, P. (ed.). Sedimentary Basins of the World, 4, Caribbean Basins, Elsevier Science B.V., Amsterdam, 93-121.

Pszczólkowski, A., 2002. The Margot Formation in western Cuba: a volcanic and sedimentary sequence of (mainly) Cenomanian-Turonian Age. Bulletin of the Polish Academy of Sciences, 50, 193-205.

Pszczólkowski, A., Albear, J. F., 1985. Sobre la edad del metamorfismo y la estructura tectonica de la faja Cangre, Provincia de Pinar del Rio, Cuba. Ciencias de la Tierra y del Espacio, 10, 31-36.

Pszczólkowski, A., Flores, R., 1986. Fases tectónicas del Cretácico y del Paleógeno de Cuba occidental y central. Bulletin of the Polish Academy of Science (Earth Sciences), 34, 95-111.

Pyle, T.E., Meyerhoff, A.A., Fahlquist, D.A., Antoine, J.W., McCrevey, J.A., Jones, P.C., 1973. Metamorphic rocks from northwestern Caribbean Sea. Earth and Planetary Science Letters, 18, 339-344.

Quintas, F., 1987. Formación Mícara en Yumurí Arriba, Baracoa, Clave para la interpretación de la Geología Histórica pre-Paleocénica de Cuba Oriental. Revista Geología y Minería, 5, 3-20.

Quintas, F., 1988. Formación Mícara en Yumurí Arriba, Baracoa, Clave para la interpretación de la Geología Histórica pre-Paleocénica de Cuba Oriental. 2ª Parte. Revista Geología y Minería, 6, 3-16.

Rankin, D., 2002. Geology of St. John, U.S. Virgin Islands. USGS Professional Paper 1631, 1-36.

Ring, U., Brandon, M.T., Willett, S.D., Lister, G.S., 1999. Exhumation processes. In: Ring, U., Brandon, M.T., Lister, G.S., Willett S.D. (eds.) Exhumation Processes: Normal Faulting, Ductile Flow and Erosion, Geological Society, London, Special Publications, 154, 1-27.

Rosencrantz, E., 1990. Structure and tectonics in the Yucatan basin, Caribbean Sea, as determined from seismic reflection studies. Tectonics, 9, 1037-1059.

Rosencrantz, E., 1996. Basement structure and tectonics in the Yucatan basin. In: Iturralde-Vinent, M.A. (ed.). Ofiolitas y Arcos Volcánicos de Cuba. Miami, USA, IGCP Project 364 Special Contribution 1, 36-47.

Schellekens, J.H., 1998. Geochemical evolution and tectonic history of Puerto Rico. In: Lidiak, E.G., Laure, D.K. (eds.) Tectonic and Geochemistry of the Northern Caribbean. Geological Society of America, Boulder, Colorado, Special Paper 322, 35-66.

Schneider, J., 2000. Origines et chemins P, T, t d'éclogites de Cuba (Caraïbes) exhumes en contexte de subduction. DEA report. University of Montpellier II, France, 43 pp. Unpublished.

Schneider, J., Bosch, D., Monie, P., Guillot, S., García-Casco, A., Lardeaux, J.M., Torres-Roldán, R.L., Millán, G., 2004. Origin and evolution of the Escambray Massif (central Cuba); an example of HP/ LT rocks exhumed during intraoceanic subduction. Journal of Metamorphic Geology, 22, 227-247.

Smith, C.A., Sisson, V.B., Avé Lallemant, H.G.A., Copeland, P., 1999. Two contrasting pressure-temperature-time paths in the Villa de Cura blueschist belt, Venezuela: Possible evidence for Late Cretaceous initiation of subduction in the Caribbean: Geological Society of America Bulletin, 111, 831-848.

Somin, M.L., Millán, G., 1981. Geology of the metamorphic complexes of Cuba (in russian). Nauka, Moscow, 219 pp.

Somin, M.L., Arakelyants, M.M., Kolesnikov, E.M., 1992. Age and tectonic significance of high-pressure metamorphic rocks in Cuba. International Geology Review, 34, 105-118.

Wakabayashi, J., 1990. Counterclockwise PTt paths from amphibolites, Franciscan Complex, California: relics from the early stages of subduction zone metamorphism. Journal of Geology, 98, 657-680.

Wakabayashi, J., 2004. Tectonic mechanisms associated with P–T paths of regional metamorphism: Alternatives to single-cycle thrusting and heating. Tectonophysics, 392, 193-218.

Willner, A.P., Glodny, J., Gerya, T.V., Godoy, E., Massonne, H.-J., 2004. A counterclockwise PTt path of high-pressure/low-temperature rocks from the Coastal Cordillera accretionary complex of south-central Chile: constraints for the earliest stage of subduction mass flow. Lithos, 75, 283-310.

Wilson, J.T., 1966. Are the structures of the Caribbean and the Scotia arcs analogous to ice rafting? Earth and Planetary Science Letters, 1, 335-338.

Young, D.A., 1998. N.L. Bowen and crystallization-differentiation. The evolution of a theory. Mineralogical Society of America, Monograph Series, 4, Washington, D.C. 276 pp.

Chapter II. Petrology

This Chapter has been accepted for publication in the ***Journal of Petrology***

Partial melting and counterclockwise P-T path of subducted oceanic crust (Sierra del Convento mélange, Cuba)

A. GARCÍA-CASCO[(1)] C. LÁZARO[(1)] R.L. TORRES-ROLDÁN[(1)] K. NÚÑEZ[(2)] Y. ROJAS-AGRAMONTE[(3)] A. KRÖNER[(3)] F. NEUBAUER[(4)] G. MILLÁN[(2)] and I. BLANCO-QUINTERO[(1,5)]

(1) Departamento de Mineralogía y Petrología, Universidad de Granada
Fuentenueva s/n, 18002-Granada, Spain García-Casco E-mail: agcasco@ugr.es Lázaro E-mail: clazaro@ugr.es Torres-Roldán E-mail: rafael@ugr.es Blanco-Quintero E-mail: idael@ugr.es

(2) Instituto de Geología y Paleontología
Via Blanca y Carretera Central, San Miguel del Padrón, 11000 Ciudad Habana, Cuba. E-mail: kenya@igp.minbas.cu

(3) Institut für Geowissenschaften, Universität Mainz
55099 Mainz, Germany. Rojas-Agramonte E-mail: rojas@uni-mainz.de Kröner E-mail: kroener@mail.uni-mainz.de

(4) Fachbereich Geographie, Geologie und Mineralogie, Universität Salzburg
Hellbrunner Strasse 34, A-5020 Salzburg, Austria E-mail: Franz.Neubauer@sbg.ac.at

(5) Departamento de Geología, Instituto Superior Minero-Metalúrgico
Las Coloradas Moa, Holguín, Cuba.

ABSTRACT

Partial melting of subducted oceanic crust has been identified in the Sierra del Convento mélange (Cuba). This serpentinite-matrix mélange contains blocks of MORB-derived plagioclase-lacking epidote±garnet amphibolite intimately associated with peraluminous trondhjemitic-tonalitic rocks. Field relations, major element bulk-rock compositions, mineral assemblages, peak metamorphic conditions (ca. 750 ºC, 14-16 kbar), experimental evidence, and theoretical phase relations support that the trondhjemitic-tonalitic rocks formed by wet melting of subducted amphibolites. Phase relations and mass balance calculations indicate eutectic- and peritectic-like melting reactions characterized by large stoichiometric coefficients of reactant plagioclase and suggest that this phase was completely consumed upon melting. The magmatic assemblages of the trondhjemitic-tonalitic melts, formed by plagioclase, quartz, epidote, ±paragonite, ±pargasite, and ±kyanite, crystallized at depth (14-15 kbar). The peraluminous composition of the melts is consistent with experimental evidence, explains the presence of magmatic paragonite and (relict) kyanite, and place important constraints for the interpretation of slab-derived magmatic rocks. Calculated P-T conditions indicate counterclockwise P-T paths during exhumation, when retrograde blueschist-facies overprints made of combinations of omphacite, glaucophane, actinolite, tremolite, paragonite, lawsonite, albite, (clino)zoisite, chlorite, pumpellyite, and phengite were formed in the amphibolites and trondhjemites. Partial melting of subducted oceanic crust in eastern Cuba is unique in the Caribbean realm, and has important consequences for the plate tectonic interpretation of the region as it supports a scenario of onset of subduction of a young oceanic lithosphere during the early Cretaceous (ca. 120 Ma). The counterclockwise P-T paths were caused by ensuing exhumation during continued subduction.

KEYWORDS: amphibolite; exhumation; partial melting; trondhjemite; subduction.

INTRODUCTION

Formation and consumption of oceanic lithosphere at ridges and trenches, respectively, are the most important geodynamic processes that cause energy and material recycling (transfer) between the lithosphere and the mantle. Subduction consumes lithosphere that sinks into the mantle, but material fractionated into fluids or/and melts formed at various depths in the subducting slab is transferred to the mantle wedge, eventually triggering partial melting of ultramafic material and the formation of volcanic arcs. Because material deeply subducted down to sub-arc depths of 100-200 km rarely returns to the surface (Ernst, 1999), deciding whether fluids or melts are formed at sub-arc depths is a matter of geochemical inference, experimental work, and thermal modelling. Fluid fluxing out of the subducting slab is generally considered the main control for material transport to, and melting of peridotite in, the mantle wedge (e.g., Schmidt & Poli, 1998; Stern, 2002; Grove *et al*., 2006 and references therein). However, geochemical data (e.g., Defant & Drummond, 1990; Drummond *et al*., 1996; Stolz *et al*., 1996; Elliott *et al*., 1997), thermal modelling (e.g., Peacock *et al*., 1994; van Keken *et al*. 2002; Gerya & Yuen, 2003; Peacock, 2003; Kincaid & Griffiths, 2004; Conder, 2005; Abers *et al*., 2006), and experimental studies (e.g., Johnson & Plank 1999; Prouteau *et al*., 2001; Kessel *et al*., 2005; Hermann *et al*, 2006) have shown that partial melting of subducted sedimentary and/or mafic oceanic crust plays a major role in transferring matter from the slab to the mantle wedge. However, even if partial melting of subducted slabs may be a common phenomenon, natural examples of partially molten subduction complexes returned to the Earth's surface are scarce.

The amphibolite blocks of the "Catalina Schist" mélange, California, constitute perhaps the best known example of exhumed fragments of subducted oceanic crust where partial melting and metasomatic mass-transfer processes took place during subduction and accretion to the upper plate mantle (Sorensen & Barton, 1987; Sorensen, 1988; Sorensen & Grossman, 1989; Bebout & Barton, 2002). The study of these processes in this and other complexes is thus critical to unravel the geochemical evolution of the subduction factory (Bebout, 2007). Here we examine partial melting processes of subducted oceanic mafic crust in the Sierra del Convento serpentinite mélange, in eastern Cuba, which represents a subduction channel related to Mesozoic subduction on the northern margin of the Caribbean plate (García-Casco *et al*., 2006). We present descriptions of field relations, mineral assemblages and textures, and major element compositions of rocks and minerals, as well as P-T estimates for the various stages of evolution of amphibolites and their partial melting trondhjemitic-tonalitic products. These data are used to derive petrogenetic and tectonic models of formation.

GEOLOGICAL OVERVIEW

Geodynamic setting

Cuba forms part of the circum-Caribbean orogenic belt, which extends from Guatemala through the Greater and Lesser Antilles to northern South America (Fig. 1a). The belt encompasses the active volcanic arc of the Lesser Antilles, where the Atlantic lithosphere subducts below the Caribbean plate. However, Cretaceous to Tertiary volcanic-arc rocks all along the belt (Fig. 1a) document a long-lasting history of subduction in this margin of the Caribbean plate. Although the details of the Mesozoic evolution of this plate margin are debated (see Iturralde-Vinent & Lidiak, 2006; Pindell *et al*., 2005, 2006), geological and geophysical data indicate that the arc probably occupied a position in between the Americas, similar to that of the present-day Central American Arc, during the early Cretaceous. This implies that the Caribbean plate formed in the western Pacific and drifted eastwards relative to the Americas during the Mesozoic and Tertiary (Pindell *et al*., 2005). As a consequence of this drift, the volcanic arc finally collided with the continental margins of North America and South America during the latest Cretaceous-Tertiary.

Eastward drift of the Caribbean plate began in the Aptian (ca. 120 Ma; Pindell *et al*. 2005), when westward subduction of the Protocaribbean (i.e., Atlantic) also began. Ocean- and continent-derived high-pressure rocks found all along the edges of the Caribbean plate formed during the early Cretaceous to Tertiary and trace the history of subduction in the region (see review by Pindell *et al*., 2005; also García-Casco *et al*., 2002, 2006; Harlow *et al*., 2004; Escuder-Viruete & Pérez Estaún, 2006; Krebs *et al*., 2007). In Cuba, metamorphic rocks documenting subduction and accretion of oceanic crust during the Cretaceous are found in serpentinite mélanges associated with ophiolitic tectonic units (collectively termed "northern ophiolite belt"; Iturralde-Vinent, 1996, 1998) distributed E-W along the >1000 km length of the island (Somin & Millán, 1981; Millán, 1996; García-Casco *et al*., 2002, 2006; Fig. 1b). Based on an analysis of ages and P-T paths of metamorphic blocks from these mélanges, García-Casco *et al.* (2006) proposed that hot subduction related to Aptian onset of subduction of the Protocaribbean is recorded in eastern Cuba mélanges. The rocks described in this paper come from one of these mélanges located in the Sierra del Convento (Fig. 1c).

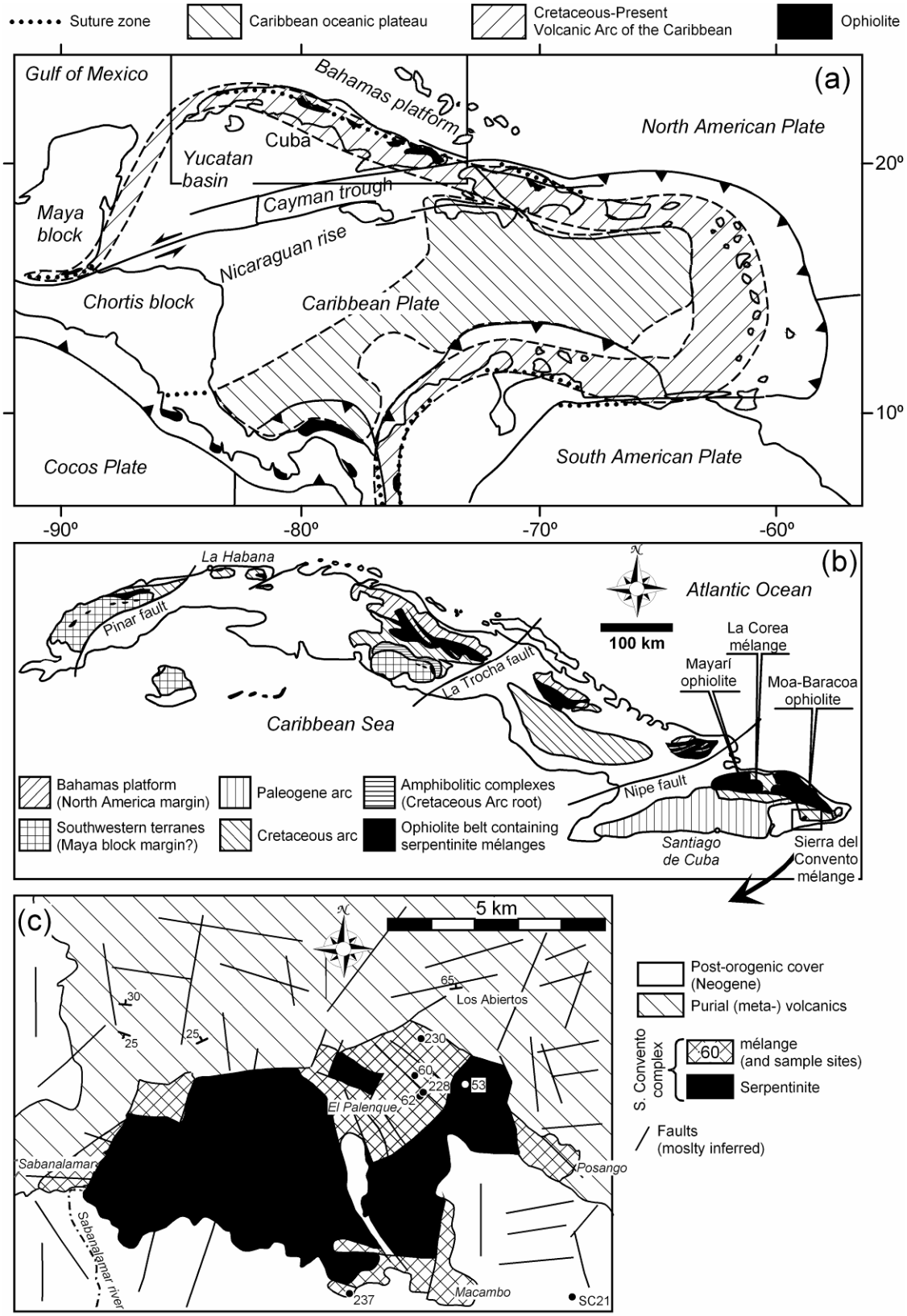

Fig. 1. (a) Plate tectonic configuration of the Caribbean region, with important geological features including ophiolitic bodies and Cretaceous-Tertiary suture zones. (b) Geological sketch map of Cuba (after Iturralde-Vinent, 1998) showing location of the northern ophiolite belt, other important geologic elements mentioned in the text, and the study area. (c) Simplified geologic map of the Sierra del Convento mélange (Kulachkov & Leyva, 1990) showing sample localities.

Geological setting

The geology of Eastern Cuba is characterized by large amounts of volcanic arc and ophiolitic materials. The ophiolite bodies (Mayarí-Cristal and Moa-Baracoa; Fig. 1b) were grouped in the "eastern Cuba ophiolites" by Iturralde-Vinent *et al.* (2006) to emphasize their geologic-petrologic differences with respect to the "northern ophiolite belt" of west-central Cuba. The former have geochemical supra-subduction signatures (Proenza *et al*., 2006; Marchesi *et al*., 2007) and override Cretaceous volcanic arc complexes along N-directed thrusts. Thrusting occurred during the late Cretaceous to earliest Paleocene (Cobiella *et al.*, 1984; Iturralde-Vinent *et al*., 2006). This structural arrangement differs from that of west-central Cuba, where the volcanic arc units override the northern ophiolite belt units. Another important difference with respect to west-central Cuba is that the volcanic arc units of eastern Cuba are locally metamorphosed to the blueschist facies (Purial Complex; Boiteau *et al.,* 1972; Somin & Millán, 1981; Cobiella *et al.,* 1984; Millán & Somin, 1985). This type of metamorphism, dated as late Cretaceous (ca. 75 Ma; Somin *et al.* 1992; Iturralde-Vinent *et al.*, 2006), documents subduction of the volcanic arc terrane due to a complicated plate-tectonic configuration (García-Casco *et al*., 2006) or to subduction erosion processes (J. Pindell, personal communication 2006). Platform-like Mesozoic sedimentary rocks forming the Asuncion terrane were also metamorphosed under high-P low-T conditions (Millán *et al*., 1985), but the timing of metamorphism is unknown.

The Sierra del Convento and La Corea mélanges (Fig. 1b) occur at the base of the ophiolite bodies of eastern Cuba, overriding the volcanic arc complexes. Both mélanges are similar and contain subduction-related metamorphic blocks of blueschist and epidote-garnet amphibolite; eclogite is rare or absent. Available K-Ar mineral and whole-rock ages in these melanges are 125-66 and 116-82 Ma in La Corea and Sierra del Convento, respectively (Somin *et al.*, 1992; Iturralde-Vinent *et al*., 1996; Millán, 1996 and references therein). These data and our unpublished Ar/Ar and SHRIMP zircon ages (ranging 114-83 Ma) from the Sierra del Convento mélange demonstrate that the history of subduction in the eastern Cuban can be traced from the early Cretaceous (Aptian) to the late Cretaceous.

The Sierra del Convento mélange

The Sierra del Convento mélange is located in the south of eastern Cuba (Fig 1b). It is tectonically emplaced on top of the Purial metavolcanic arc complex. The geology of the region is poorly known and detailed structural and petrologic analysis is lacking. Basic field and petrographic descriptions are provided by Boiteau *et al*. (1972), Somin & Millán (1981), Cobiella *et al.* (1984), Kulachkov & Leyva (1990), Hernández & Canedo (1995), Millán (1996), and Leyva (1996).

The field relationships of the mélange are obscured by intense weathering, tropical vegetation, and recent fracturing related to important post-Eocene activity along the sinistral transcurrent Oriente Fault that connects the Puerto Rico trench with the Cayman trough (Rojas-Agramonte *et al*., 2005, and references therein). The mélange is made of sheared serpentinite formed by hydration of harzburgite. It lacks exotic bocks in its central and topographically highest portion (max. height 755 m). Towards its borders, however, exotic blocks occur forming four submélange bodies of km-scale, namely (Fig. 1c) Posango (to the East), El Palenque (to the North), Sabanalamar (to the West), and Macambo (to the South). Our field observations suggest that these submélange bodies occur at the base of the Sierra del Convento mélange, in contact with the underlying volcanic arc Purial complex.

These submélange bodies are similar and contain low-grade tectonic blocks of metabasite, metagreywacke, metapelite-semipelite, and pelitic gneiss metamorphosed to the blueschist facies with greenschist facies overprints. The submélange bodies also contain blocks of metabasites that have been metamorphosed to the epidote amphibolite facies. These are the "high grade" amphibolite blocks described below. Our unpublished trace element analyses of the high-grade blocks show N-MORB signatures, indicating subducted oceanic lithosphere, as opposed to other low-grade blocks of metabasite, metagreywacke, metapelite-semipelite which represent metamorphosed volcanic-arc derived rocks of the Purial complex.

Importantly, the high-grade amphibolite blocks are made of plagioclase-lacking peak mineral assemblages consisting of pargasite, epidote, ±quartz, ±garnet, ±clinopyroxene (the latter is rare). The white material seen in the matrix of these rocks (e.g., Figs. 2a and b, except for the leucocratic segregations) is not plagioclase but epidote. Following the common usage and recent recommendations of the IUGS Subcommission on the Systematics of Metamorphic Rocks (Coutinho *et al.*, 2007) the lack of peak metamorphic plagioclase prevents using the term amphibolite to name these rocks. On the other hand, the abundance of epidote prevents using the term hornblendite, which would also convey a wrong connotation. Thus, the term amphibolite is used here to name the studied rocks even if their mineral assemblages do no conform to its classical use for rocks made of amphibole and plagioclase.

Another prominent petrological feature of the

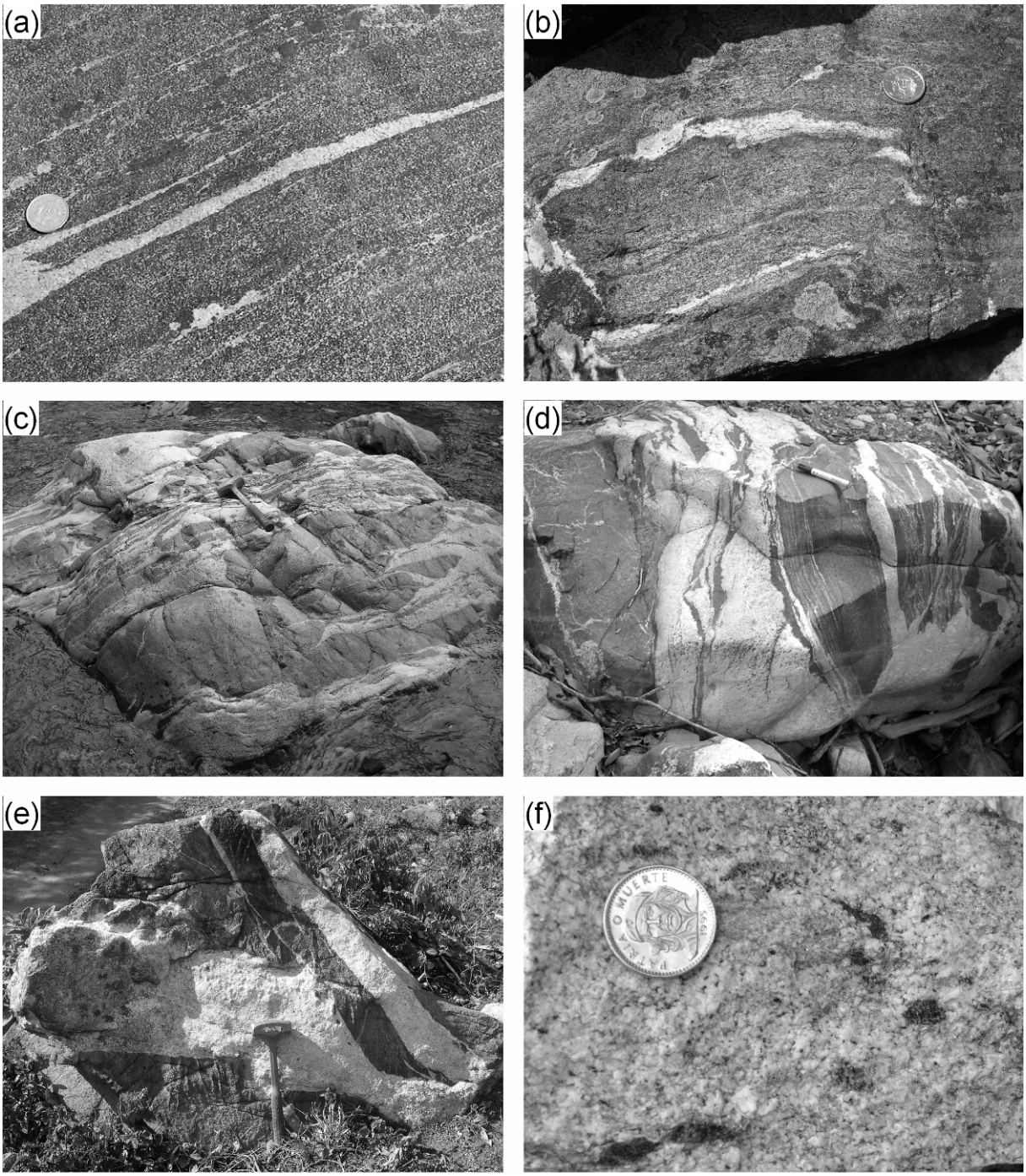

Fig. 2. Field relations of amphibolite blocks and associated tonalite-trondhjemite. (a) Banded amphibolite hosting sheared veins of trondhjemite. (b) Banded structure in migmatitic amphibolite showing hornblendite bands adjacent to trondhjemite segregation. (c) Block of amphibolite invaded by trondhjemite. Intrusion is ductile and contemporaneous with the main foliation of amphibolite. (d) Detail of block of amphibolite invaded by trondhjemite. (e) Brittle intrusion of trondhjemite into amphibolite forming agmatitic structure. (f) Detail of trondhjemite containing small enclaves of amphibolite and hornblendite. Shining crystals of paragonite stand out of the leucocratic groundmass.

Sierra del Convento mélange is the intimate association of amphibolite with cm-to-m size layers, pockets, and veins of trondhjemite-tonalite (Fig. 2). The nature and origin of these rocks has not been addressed in detail. Somin & Millán (1981) and Millán (1996) suggested that they represent ophiolitic plagiogranite pods formed during differentiation of MOR gabbros which were later subducted and metamorphosed together with the enclosing mafic rocks. In contrast, Hernández & Canedo (1995) suggested that the leucocratic material is post-metamorphic and identified it as

material of the Cretaceous volcanic-arc intruding the mélange. Based on field relations, Kulachkov & Leyva (1990) and Leyva (1996) conceded that there is a genetic relationship between the amphibolites and the leucocratic material, but did not indicate the type of relationship. In this paper we concentrate on these high-grade amphibolite blocks and associated trondhjemitic-tonalitic rocks.

FIELD RELATIONSHIPS

The high-grade blocks of amphibolite are of meter to tens of meter size, medium to coarse grained, and massive to banded (Figs. 2a-c). In the Macambo region, however, the blocks appear to be larger. In the Palenque region the amphibolites form discrete blocks, commonly m-sized. This region offers the largest amount of leucocratic material intimately associated with the amphibolites. In the Posango and Sabanalamar regions the blocks are best observed as detrital material forming part of recent alluvial deposits along the Yacabo and Sabanalamar rivers rather than as tectonic blocks within serpentinite.

The tonalitic-trondhjemitic bodies are of cm- to m-size. They are exclusively associated with the amphibolites and not with other types of exotic blocks within the mélange, and do not appear to crosscut the serpentinite matrix. The structure of the bodies varies from concordant layers to crosscutting veins relative to the metamorphic foliation of the amphibolites. Banded, stromatic, vein-like, and agmatitic structures typical of migmatites are common (Figs. 2a-e).

The banded structure is characterized by the association of mesosome (Ep±Grt amphibolite) – leucosome (trondhjemite-tonalite) parallel to the main syn-metamorphic foliation. Locally, melanosomic material consisting of >90% modal pargasitic amphibole (plus small amounts of epidote, rutile, titanite, apatite, ±quartz) is spatially associated with banded mesosome-leucosome pairs resembling stromatic structure of migmatites (Fig. 2b). The texture of this melanosome is variable, with grain size averaging less than one mm in some samples to several cm in others. Because of the abundance of pargasite, the melanosome material is termed here hornblendite following the recent recommendations of the IUGS Subcommission on the Systematics of Metamorphic Rocks (Coutinho *et al.*, 2007). Our unpublished major and trace element and Rb/Sr and Sm/Nd isotope data provide evidence that these hornblendites do not represent true restites but a metasomatic rock formed by interaction (i.e., back-reaction) of the amphibolites and fluids evolved from associated melts.

Stretched, boudinaged, and folded veins and pockets of trondhjemite-tonalite indicate that the amphibolites and associated segregations experienced ductile deformation (Figs. 2a-c). However, cross-cutting veins and agmatitic (magmatic breccia-like) structures also document brittle behaviour of the amphibolites during melt extraction (Figs. 2d and e). In all types of structures, but most typically in the agmatitic ones, the segregations contain small (generally cm-size) nodules of amphibolite with sharp to diffuse boundaries, suggesting disaggregation of amphibolite within the silicic melt (Fig. 2f).

Below we present detailed information on six representative samples of plagioclase-lacking amphibolite and five representative samples of associated trondhjemite-tonalite. Samples CV53b-I and CV62b-I are quartz-epidote amphibolite, CV228d and CV228e are quartz-epidote-garnet amphibolite, CV230b is epidote-garnet amphibolite, and CV237j is epidote-garnet-clinopyroxene amphibolite. Samples CV62b-II, CV228c, and SC21 are epidote-amphibole trondhjemite/tonalite, and CV53b-II and CV60a are epidote trondhjemite. The numbers in the sample labels refer to sample sites (see Fig. 1c; sample SC21 is a pebble collected in the bed of the Yacabo River). Closely associated amphibolite-trondhjemite pairs were sampled in sites CV62 and CV228. These samples are used below to examine melting relations.

ANALYTICAL TECHNIQUES

Whole-rock compositions were determined on glass beads by XRF using a PHILIPS Magix Pro (PW-2440) spectrometer at the University of Granada (Table 1; trondhjemite sample CV53b-II could not be analyzed because of its small size). LOI was determined on pressed powder pellets. Mineral compositions were obtained by WDS with a CAMECA SX-50 microprobe (University of Granada), operated at 20 kV and 20 nA, and synthetic SiO_2, Al_2O_3, $MnTiO_3$, Fe_2O_3, MgO, and natural diopside, albite, and sanidine, as calibration standards, and by EDS with a ZEISS DSM 950 scanning microscope, equipped with a LINK ISIS series 300 Analytical Pentafet system, operated at 20 kV and 1-2 nA beam current, with counting times of 50-100 s, and the same calibration standards. All analyses listed in Tables 3-10 were obtained by WDS. Clinopyroxene and amphibole compositions were normalized following the schemes of Morimoto *et al*. (1988) and Leake *et al*. (1997), respectively. Garnet was normalized to 8 cations and 12 oxygens and Fe^{3+} was estimated by stoichiometry. Epidote, feldspar, lawsonite, and kyanite were normalized to 12.5, 8, 8, and 5 oxygens, respectively, and $Fe_{total}=Fe^{3+}$. Mica, chlorite, and pumpellyite were normalized to 22, 28, and 24.5, oxygens, respectively, and $Fe_{total} = Fe^{2+}$. Mineral and end-member abbreviations are after Kretz (1983), except

for amphibole (Amp), silicate melt (L) and fluid (H_2O), with end-members of phases written entirely in the lower case. The atomic concentration of elements per formula units is abbreviated apfu.

Elemental XR images were obtained with the same CAMECA SX-50 microprobe operated at 20 kV, 200-300 nA beam current, with step (pixel) size of 3-10 μm, and counting time of 15-100 ms. We have found that high beam current combined with short counting time (milliseconds rather than seconds) avoids the problem of beam damage to silicates (cf. De Andrade *et al*., 2006). The images were processed with *Imager* software (Torres-Roldán & García-Casco, unpublished) and consist of the XR signals of Kα lines of the elements or element ratios (colour coded; expressed in counts/nA/s) corrected for 3.5 μs deadtime and with voids, polish defects, and all other mineral phases masked out, overlain onto a grey-scale base-layer calculated with the expression $\Sigma[(counts/nA/s)_i \cdot A_i]$, (A=Atomic number, i= Si, Ti, Al, Fe, Mn, Mg, Ca, Na, and K) that contains the basic textural information of the scanned areas.

BULK ROCK COMPOSITION

A detailed assessment of the bulk-rock chemistry of the blocks in the mélange will be presented elsewhere. Here, we briefly comment on some aspects of their major element geochemistry which help explain key features of their mineral assemblages.

The studied amphibolite samples have subalkaline, low-K (tholeiitic) basaltic composition (Figs. 3a and b). Their SiO_2 content ranges 43.25–48.02 wt.%, with lower values in the quartz-free samples. The latter samples trend toward (apparent) picritic composition. Notably, all samples have relatively low Na_2O contents (1.29–1.85 wt.%) making the samples to have relatively high inverse agpaitic index as compared to MORB (Fig. 3d). The garnet bearing samples have lower Mg# ($Mg/[Mg+Fe^{2+}_{total}]$ atomic proportions; Table 1).

The composition of the tonalite-trondhjemite samples is varied. In the TAS diagram they range from andesite through trachyandesite, trachyte and trachydacite to dacite (Fig. 3a). They are rich in Na_2O (5.58-.55 wt.%) and have very low K_2O contents (0.08-0.26 wt.%; Fig. 3b, Table 1), resembling rocks of the low-K tholeiite series. The FeO and MgO contents are low and Mg# is relatively high ranging from 0.38 to 0.67 (Fig. 3c). All samples are classified as trondhjemite in the O'Connor-Barker (O'Connor, 1965; Barker, 1979) An-Ab-Or classification scheme for granitic rocks (not shown) except sample SC21, which is classified as tonalite. However, sample SC21 is in fact leucocratic having somewhat major amounts of epidote (due to their higher CaO contents). For this reason all samples are henceforth collectively termed trondhjemites. Importantly, the trondhjemites are Al-saturated (i.e., peraluminous; ASI = 1.023-1.142; Fig. 3d) and plot close to the alkali feldspar-white mica mixing line delineated in Fig. 3d. Note that this line indicates albite-paragonite mixtures in K-poor rocks.

TEXTURES AND MINERAL ASSEMBLAGES

Amphibolites

Peak metamorphic mineral assemblages consist of pargasitic amphibole, epidote, ± garnet, ± quartz, ± diopsidic clinopyroxene (rare), rutile, titanite, and accessory apatite (Figs. 4a-f; Table 2). These assemblages define a crude foliation. Quartz appears as small dispersed grains and mm-sized "pockets" elongated along the foliation, though quartz-lacking samples are also common. Syn- to post-kinematic garnet is abundant but not present in all samples (Figs. 4a-f; Table 2). Its occurrence is influenced by bulk composition, as indicated by the lower Mg# of garnet-bearing samples (Table 1). It forms large porphyroblasts 0.5-3 cm in diameter containing inclusions of amphibole and epidote (Figs. 4a-f). Na-rich diopsidic clinopyroxene has been found in quartz-free samples of the Macambo region. It occurs as medium grained mm-sized grains in the matrix (Figs. 4d-f). Titanite appears as idiomorphic peak metamorphic crystals elongated along the foliation, but it also replaces rutile.

Retrograde overprints are made of combinations of glaucophane, actinolite, albite, (clino)zoisite, chlorite, pumpellyite, and, less abundantly, phengitic mica and omphacite, the latter being observed only in samples bearing peak metamorphic diopsidic clinopyroxene (Figs. 4a-f, Table 2). All these retrograde minerals are fine-grained and corrode the peak-metamorphic minerals, but they also are dispersed in the matrix or located in fractures. Retrograde glaucophane is typically aggregated with actinolite, chlorite and albite and commonly overprints peak amphibole (Figs. 4c and f). Retrograde omphacite replaces peak diopsidic clinopyroxene and is also present in retrograde assemblages made of glaucophane + magnesiohornblende-actinolite + albite + epidote which appear dispersed in the matrix and replacing pargasitic amphibole and garnet (Fig. 4f). Chlorite and pumpellyite replace garnet and pargasite. Scarce phengitic mica appears dispersed in the matrix of some samples. Retrograded crystals of pargasite commonly contain small needles of "exsolved" rutile/titanite.

Table 1. Chemical composition (wt.%) of studied samples.

	Amphibolites						trondhjemites			
	CV53b-I	CV62b-I	CV228d	CV228e	CV230b	CV237j	CV60a	CV228c	CV62b-II	SC21
SiO_2	45.84	46.78	46.26	48.02	43.25	43.94	67.83	60.08	66.32	60.46
TiO_2	1.72	1.26	2.26	2.16	1.94	2.57	0.22	0.19	0.06	0.22
Al_2O_3	16.40	16.98	14.68	14.99	16.70	13.33	18.24	23.65	21.13	22.30
FeO_{tot}	10.71	9.32	13.01	11.65	11.42	14.97	0.84	1.06	0.49	1.68
MnO	0.18	0.17	0.20	0.18	0.39	0.20	0.02	0.02	0.01	0.03
MgO	7.36	7.78	6.98	6.57	7.72	7.56	0.93	0.68	0.17	1.18
CaO	12.33	12.99	11.40	11.51	13.99	12.97	3.54	5.58	3.71	6.01
Na_2O	1.58	1.58	1.61	1.53	1.29	1.85	5.58	7.29	7.55	6.45
K_2O	0.27	0.20	0.26	0.21	0.31	0.05	0.26	0.08	0.15	0.17
P_2O_5	0.15	0.11	0.22	0.21	0.18	0.24	0.08	0.05	0.04	0.05
LOI	1.57	1.80	0.95	1.14	1.18	0.73	1.65	1.15	0.61	1.23
total	98.11	98.97	97.83	98.17	98.37	98.41	99.19	99.83	100.24	99.78
Mg#	0.551	0.598	0.489	0.501	0.547	0.474	0.665	0.533	0.380	0.557

Note: LOI: Lost on ignition. Mg# = $Mg/(Fe^{2+}_{total}+Mg)$.

Table 2. Mineral abundances in the studied samples (visual estimates).

	peak metamorphic / magmatic												Retrograde										
	Amp	Ep	Grt	Cpx	Qtz	Pl	Pa	Rt	Ttn	Ilm	Ky	Ap	CaAmp	Gl	Omp	Chl	Pmp	Ab	Lws	Pa	Czo	Phe	Kfs
Amphibolites																							
CV53b-I	55	35			10			x	x				x	x		x	x	x			x	x	
CV62b-I	60	30			10			x	x			x	x	x		x	x	x			x	x	
CV228d	60	25	5		10			x	x			x	x	x		x	x	x			x	x	
CV228e	50	35	5		10			x	x			x	x	x		x	x	x			x		
CV230b	60	25	15					x	x			x	x	x		x	x	x			x		
CV237j	50	5	15	15	x			x	5	x			x	5	x	5	x	x			x		
Trondhjemites																							
CV53b-II					30	60	x?					x				x		x		7	3	x	x
CV62b-II	x	3			20	70	x?					x	x			x		x		5	2	x	
CV228c	3	15			15	55	5		x			x	x			x	x	x	X	3	4		
CV60a		8			30	40	5	x			x	x				x	x	x	5	10	2	x	x?
SC21	5	10			10	60	10	x				x	x			x	x	x		2	1	x	x

Note: x: Present in small amounts.

Trondhjemitic segregations

The magmatic mineral assemblage of the trondhjemites is formed by medium-grained plagioclase and quartz with subordinate medium-grained paragonite, epidote, ± pargasite, plus accessory apatite, titanite, and rutile (Figs. 4g-m; Table 2). Kyanite is locally present as tiny relict inclusions within magmatic epidote (Fig. 4m). Epidote and pargasite are idiomorphic and medium-grained (1-3 mm in length). Pargasite frequently has a large aspect ratio of 5:1 (Fig. 4j). Paragonite has medium grain size (2-3 mm in length) and idiomorphic habit frequently corroded by plagioclase and fine-grained quartz, ±K-feldspar, ±phengite (Fig. 4h and l). Magmatic paragonite has been identified in samples SC21, CV228c, and CV60a, whereas its presence is more uncertain in samples CV62b-II and CV53B-II.

Retrograde mineral assemblages overprint the magmatic assemblages. Magmatic plagioclase appears largely transformed into retrograde albite plus fine-grained (clino)zoisite, paragonite and locally, lawsonite (Figs. 4g and k; Table 2). Magmatic epidote is overprinted by fine-grained overgrowths of (clino)zoisite + quartz symplectite which spray out of the magmatic epidote crystal and invade nearby plagioclase (Figs. 4i, k, and m). Pargasitic amphibole is partly replaced by magnesiohornblende-tremolite, chlorite, and pumpellyite (Fig. 4j). Glaucophane is not present. Titanite replaces rutile. If present, small laths of retrograde phengitic mica are dispersed in the matrix, associated with retrograde paragonite-

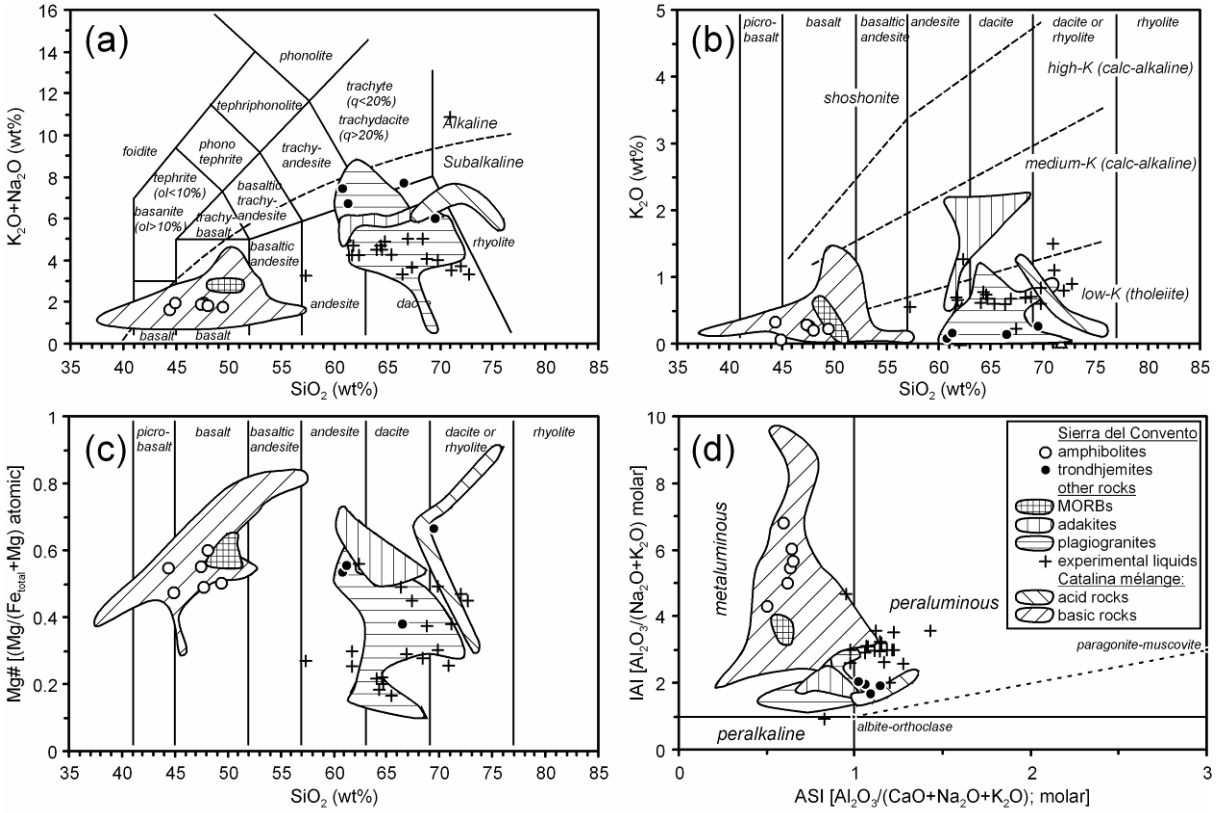

Fig. 3. Bulk composition of studied samples and of other rocks for comparison, including average and altered MORB (Hofmann, 1988; Kelemen *et al*, 2003; Staudigel *et al*., 1996), adakites (compiled by Drummond *et al*., 1996; Martin, 1999; and Smithies, 2000), oceanic and ophiolitic plagiogranites (compiled by Koepke *et al*., 2004), mafic and felsic (pegmatites and leucocratic segregate) rocks from the Catalina Schist (Sorensen & Grossman, 1989), and experimental liquids (glasses) obtained by partial melting of low-K mafic material under H_2O-present conditions at 800-900 ºC, 2-30 kbar (Nakajima & Arima, 1998; Prouteau *et al*., 2001; Selbekk & Skjerlie, 2002; Koepke *et al*., 2004). a) TAS diagram (Le Maitre *et al*., 2002). b) K_2O-SiO_2 diagram. c) Mg#-SiO_2 diagram. d) IAI (inverse agpaitic index)-ASI (alumina saturation index) diagram with indication of the projection of alkali-feldspar and white micas for reference. The TAS-based names of rocks of the low-K_2O+Na_2O series are shown in (b) and (c) for reference. Symbols for (a), (b), and (c) as in (d).

chlorite, and replacing magmatic plagioclase and paragonite (Fig 4l). Very small amounts of retrograde K-feldspar, typically replacing magmatic paragonite, are present in some samples.

MINERAL COMPOSITION

Amphibole

Amphibolites

Matrix amphibole is edenitic-pargasitic in composition (Fig. 5a). Zoning is faint (Figs. 4a and c), either shown as patches or, occasionally, as faint ill-defined concentric bands. Concentric zoning is defined by cores of edenite and outer shells of pargasite, indicating prograde growth (Fig. 6). Peak metamorphic pargasitic compositions are rich in Na-in-A (max. 0.85 apfu), total Al (max. 2.70 apfu), and Ti (max. 0.3 apfu), and poor in Si (min. 6.19 apfu), Na-in-M4 (min. 0.10 apfu), and Mg# (min. 0.506; Figs. 5a and 6; Table 3). As would be expected for high-variance mineral assemblages, the composition of amphibole is strongly controlled by bulk-rock composition, with Mg#-richer amphibole present in rocks with higher bulk Mg# (Fig. 5a). Notably, Na(M4) is relatively high in pre-peak (edenitic) compositions (Fig. 6), in particular in garnet-free samples where it amounts up to 0.47 apfu and almost reaches magnesiokatophorite compositions. This edenite-to-pargasite prograde zoning correlates with the composition of amphibole inclusions within garnet, which ranges from edenite to pargasite but does not reach peak pargasitic composition as recorded in matrix amphibole.

The outermost rims (50-100 μm in width) of matrix amphibole show zoning from pargasite through edenite-magnesiohornblende to actinolite (Figs. 4b and 5a), indicating retrograde growth/overprint. Actinolitic compositions are poor in Na(A) (max. 0.02 apfu), total Al (max. 0.26 apfu), and Ti (max. 0.001 apfu), and rich in Si (min. 7.88 apfu) and Mg# (min. 0.78; Fig. 5a; Table 3). Na(M4)

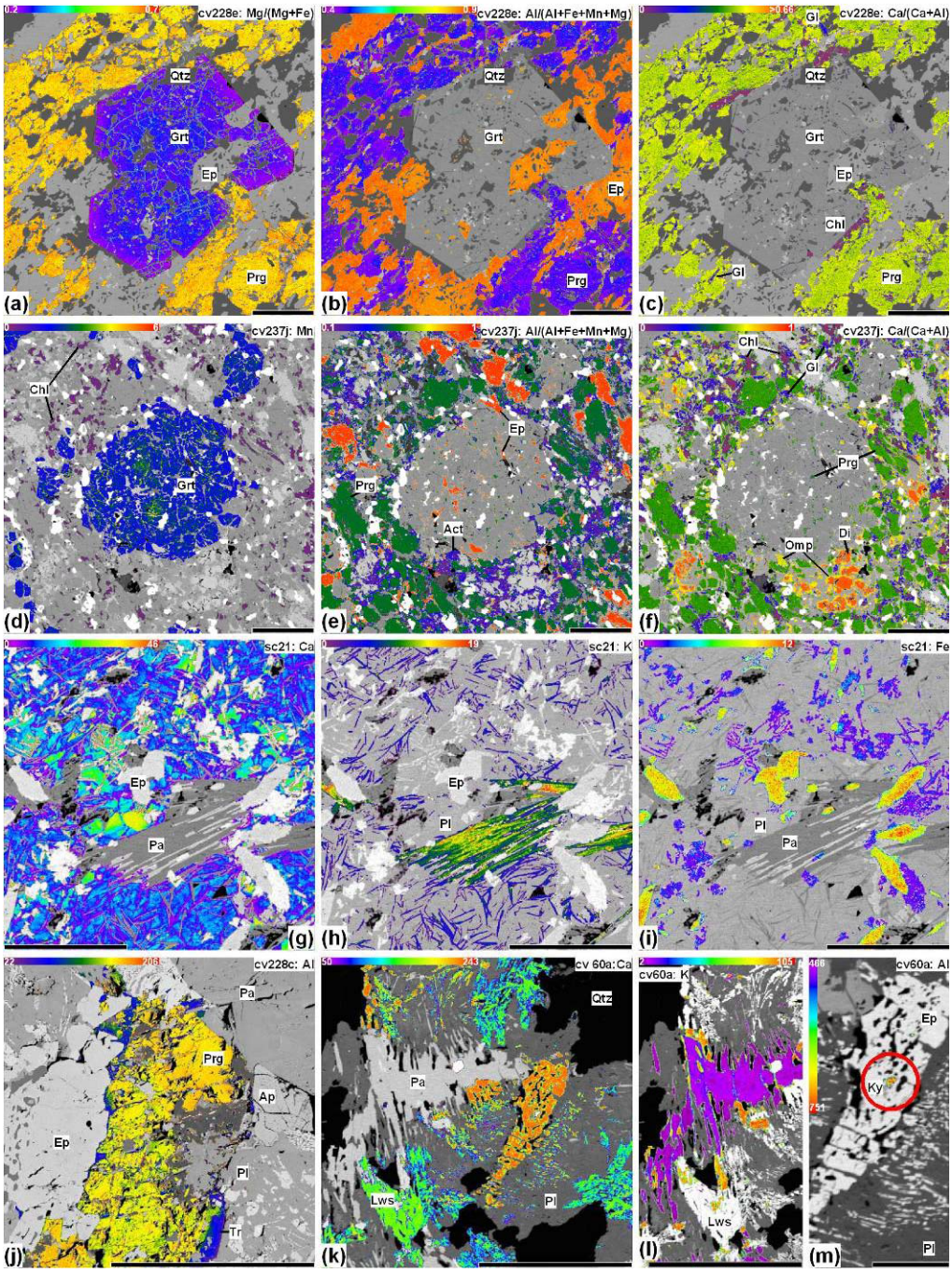

Fig. 4. XR images showing key textural and compositional data of amphibolite samples CV228e (a-c) and CV237j (d-f) and trondhjemite samples SC21 (g-i), CV228c (j) and CV60a (k-m). Scale bar: 1 mm, except (m): 0.25 mm. Colour scale bar (counts/nA/s) indicates high (red) and low (purple) concentrations. (a) Mg/(Mg+Fe) image showing pargasite (yellow-orange) and garnet with reverse zoning defined by lower Mg# at the rims (purple). (b) Al/(Al+Fe+Mn+Mg) image showing epidote (orange-red) with patchy zoning and pargasite (blue) overprinted by retrograde magnesiohornblende-actinolite (purple). (c) Ca/(Ca+Al) image showing retrograde glaucophane (blue) and chlorite (purple) overprinting pargasite (greenish). (d) Mn image showing garnet (blue) with relict core slightly richer in Mn (greenish) and retrograde chlorite (purple). (e) Al/(Al+Fe+Mn+Mg) image showing epidote (red) in the matrix and included in garnet, and peak pargasite (green) and retrograde actinolite (blue-purple). (f) Ca/(Ca+Al) image showing peak diopside (red) and pargasite (green) overprinted by retrograde omphacite (yellow), glaucophane (blue), and chlorite (purple). (g) Ca image showing magmatic oligoclase (yellow-orange) strongly overprinted by retrograde albite (bluish-purple). (h) K image showing magmatic paragonite (green-red) with high-K regions (red) and retrograde paragonite (blue) overprinting magmatic paragonite and plagioclase. (i) Fe image showing magmatic epidote (orange red) with Fe-rich cores (red) and retrograde (clino)zoisite (blue-purple) overprinting magmatic epidote and plagioclase. (j) Al image showing magmatic pargasite (green-orange) overprinted by tremolite (blue). (k) Ca image showing epidote (orange) and retrograde lawsonite (green) overprinting plagioclase. (l) K image showing magmatic paragonite (blue-purple) overprinted by retrograde phengite (red). (m) Al image showing relict inclusion of kyanite (enclosed in red circle) within magmatic epidote.

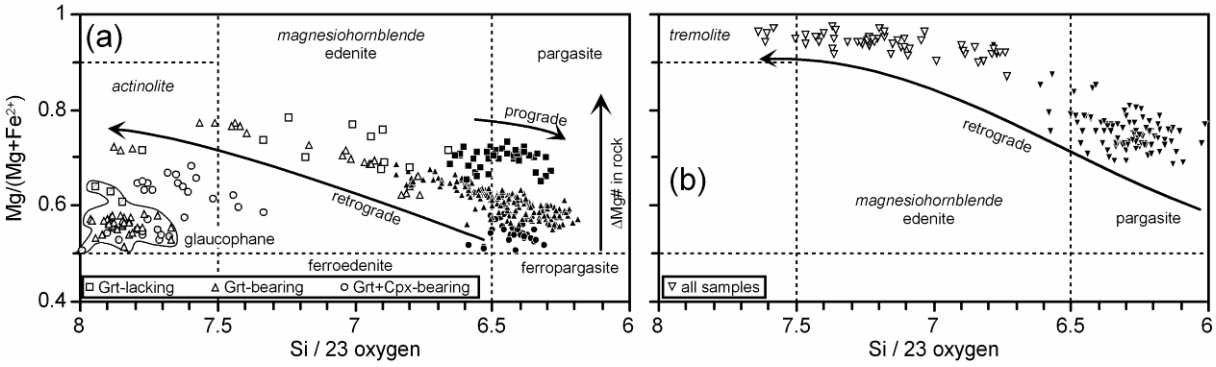

Fig. 5. Composition of amphibole from (a) amphibolites and (b) trondhjemites plotted in the classification scheme of Leake *et al*. (1997). The filled symbols and regular typeface labels correspond to calcic compositions with Sum(A) > 0.5 (pargasite-edenite), the empty symbols and italic typeface labels correspond to calcic compositions with Sum(A) < 0.5 (magnesiohornblende-actinolite-tremolite), and the hatched symbols (enclosed in field) and regular typeface labels correspond to sodic compositions (glaucophane). For clarity, some analyses with sodic-calcic compositions (magnesiokatophorite and barroisite) have not been differentiated from calcic amphiboles. Note that much of the compositional variation is due to retrograde overprinting.

of retrograde edenite and magnesiohornblende reach 0.49 apfu (Fig. 6), and a few analyses attain magnesiokatophorite and barroisite compositions.

The patchy zoning of most matrix crystals reflects a compositional spectrum comprising pargasite-magnesiohornblende-actinolite and indicates that it developed during retrograde adjustment/growth. These retrograde adjustments are clearly developed in single crystals of pargasite containing small needles of exsolved rutile/titanite.

The compositional variability of retrograde glaucophane is relatively large (Si: 7.67-7.99, Al: 1.46-1.98, Ca: 0.04-0.43, Na(M4): 1.54-1.91, Na(A): 0.01-0.17 apfu, and Mg#: 0.51-0.64; Fig. 5a; Table 4). This compositional range reflects compositional heterogeneity within single samples due to the effects of local effective bulk-composition at reaction sites and the timing of formation during the retrograde path. The first effect is best illustrated by Mg#-richer and Mg#-poorer glaucophane grains present in single samples and grown adjacent to matrix amphibole and garnet, respectively.

Trondhjemites

Magmatic amphibole shows no growth zoning. Its composition is pargasitic (Si down to 6.01, Al up to 2.87, Ti up to 0.26, Na(A) up to 0.72, K(A) up to 0.11, Na(M4) ca. 0.35 apfu, Mg# ca. 0.75; Fig. 5b; Table 3), similar to that of peak metamorphic amphibole from the amphibolites except for being richer Mg# (Fig. 5b). The composition of these grains is overprinted by patchy retrograde zoning, developed along fractures, exfoliation planes, and crystal rims (Fig. 4j). The retrograde composition of amphibole ranges from pargasite through edenite, magnesiohornblende to tremolite (Fig. 5b; Table 3). Notably, Na(M4) first increases along this path (pargasite to edenite), reaching 0.44 apfu and approaching sodic-calcic (magnesiokatophorite-magnesiotaramite) composition, then decreasing down to almost zero in the magnesiohornblende-tremolite compositions. This trend suggests a retrograde path with a first step of decreasing temperature at near constant pressure, followed by decreasing temperature and pressure.

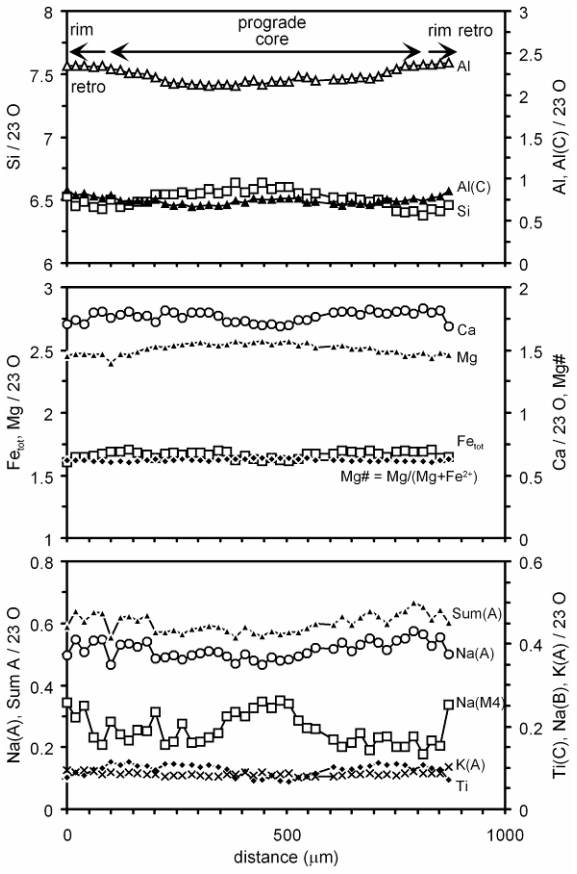

Fig. 6. Profile of amphibole from amphibolite sample CV230b recording a smooth prograde growth zoning (denoted by Si, Al(C), and Ti) from edenite to pargasite, and a retrograde overprint at the rims (edenite). Note that Na(M4) is relatively high in the pre-peak core and the post-peak rim.

Garnet

Garnets in the amphibolites are relatively rich in almandine (X_{alm} = 0.50-0.55) and, to some extent, grossular (0.2-0.3), and poor in pyrope (and 0.15-0.20) and spessartine (0.02-0.10), comparable with type C (i.e., low temperature) eclogitic garnet (Fig. 7a; Table 5). As in amphibole, the composition of garnet is influenced by bulk-rock composition; higher Mg# is observed in garnets from Fe-poorer bulk-rock composition (Fig. 7b).

Garnet zoning is faint. In most samples the cores are near-homogeneous. The rims and regions adjacent to fractures show retrograde readjustments denoted by increase in spessartine and decrease in Mg# (Figs. 4a and d, 7b-d). However, garnet in sample CV230b shows spessartine-poor and Mg#-rich rims denoting prograde growth (see García-Casco *et al*., 2006). Faint prograde zoning and the lack of low-temperature phases included within garnet suggest a relatively late stage of garnet growth during prograde metamorphism (i.e., close to and during peak conditions). Thus, much of the compositional variation of garnet is the result of retrograde readjustments characterized by increase in Mn and decrease in Mg# (Fig. 7b). Grossular contents may not be significantly affected by retrograde readjustments, but they increase sharply (up to $X_{grs} \sim 0.6$) in fractures traversing garnet in sample CV237j (Fig. 7e; Table 5).

Epidote

Matrix epidote from amphibolite shows variable Fe^{3+} contents, with pistacite contents (X_{ps} = $Fe^{3+}/[(Al-2)+Fe^{3+})]$ ranging from 0.2 to 0.7, except in sample CV230b where it amounts 0.1-0.2 (Table 6). Zoning is generally patchy, though some grains may show concentric zoning with lower X_{ps} at the rims (Fig. 4b) probably reflecting retrograde readjustments/growth.

In the trondhjemitic segregations magmatic epidote is richer in Fe^{3+} than retrograde grains of (clino)zoisite (X_{ps} up to 0.5 and 0.1, respectively; Figs. 4i and k; Table 6). The exception is sample CV60a, which contains magmatic epidote with low X_{ps} (<0.1; Table 6). Magmatic crystals show patchy zoning, with irregular high Fe^{3+} areas in the interior, probably formed at higher temperature. Intermediate compositions of magmatic epidote are interpreted as the result of crystallization upon cooling and/or subsolidus retrograde readjustments.

Clinopyroxene

Peak metamorphic clinopyroxene from sample CV237j is diopsidic in composition (Fig. 8; Table 5), with Mg# = 0.67-0.74, $Fe^{3+}/(Fe^{3+}+Fe^{2+})$ = 0.18-0.37, Ti up to 0.03 apfu, and Na = 0.07-0.09 apfu (X_{jd} = 0.04-0.06). This suggests a relatively high pressure of formation at high temperature. The composition of retrograde omphacite is Ca = 0.51-0.63 apfu, Mg# = 0.67-0.82, $Fe^{3+}/(Fe^{3+}+Fe^{2+})$ = 0.23-0.62, which translates into X_{jd} = 0.32-0.39 and X_{ae} = 0.06-0.14 (Fig. 8; Table 5).

Plagioclase

Plagioclase in the amphibolites is retrograde and almost pure albite in composition ($X_{ab} > 0.92$, with most analyses reaching $X_{ab} > 0.99$; Table 7).

The composition of magmatic plagioclase in the trondhjemites is uncertain as it has been largely retrogressed to albite-rich plagioclase. The magmatic crystals display retrograde patchy zoning that preserves irregular calcic regions dispersed within albite-richer retrograde areas (Fig. 4g). The maximum X_{an} of these relict regions, identified with the aid of XR images, are 0.29 (CV228c), 0.18 (SC21), 0.18 (CV62b-II), and 0.17 (CV53b-II and CV60a) (Figs. 11b, Table 7). Though these figures do not necessarily represent the original magmatic composition of plagioclase, they suggest that it was sodic andesine to calcic oligoclase.

Paragonite

Magmatic crystals of paragonite from the trondhjemites are rich in the muscovite component (K up to 0.35 apfu, $X_K = K/(K+Na) = 0.18$; Table 8). These crystals show patchy zoning with relict high-K areas in the interior of the grains with relatively high Ca-contents (0.06-0.10 apfu) and K-poorer areas distributed irregularly but typically along (001) planes and close to the rims, indicating retrograde readjustments upon cooling (Fig. 4h). The retrograded regions are somewhat richer in the margarite component (Fig. 9). Discrete grains of retrograde paragonite have Ca-poor and K-poor compositions and are of almost pure paragonite end-member composition (Figs. 4h and 9, Table 8). A detailed assessment of the composition of paragonite from sample SC21 is given by García-Casco (2007).

Phengite

Retrograde phengitic mica in the amphibolites (samples CV53b-I and CV62b-I) is very rich in celadonite content, with Si = 6.89-6.96 apfu, Mg = 0.77-0.86, Fe^{2+}_{total} = 0.21-0.27, Na = 0.06-0.09, and Mg# ($Fe=Fe^{2+}_{total}$) = 0.76-0.79 (Fig. 9; Table 8) indicating high pressure during retrogression.

The composition of phengitic mica in the trondhjemites is heterogeneous (Fig. 9; Table 8) and varies from high celadonite content (Si up to 6.97, Fe up to 0.21, Mg up to 0.83 apfu) to almost pure muscovite (Si down to 6.05 apfu). Mg# ranges from 0.69 to 0.92 and shows a positive correlation with Si,

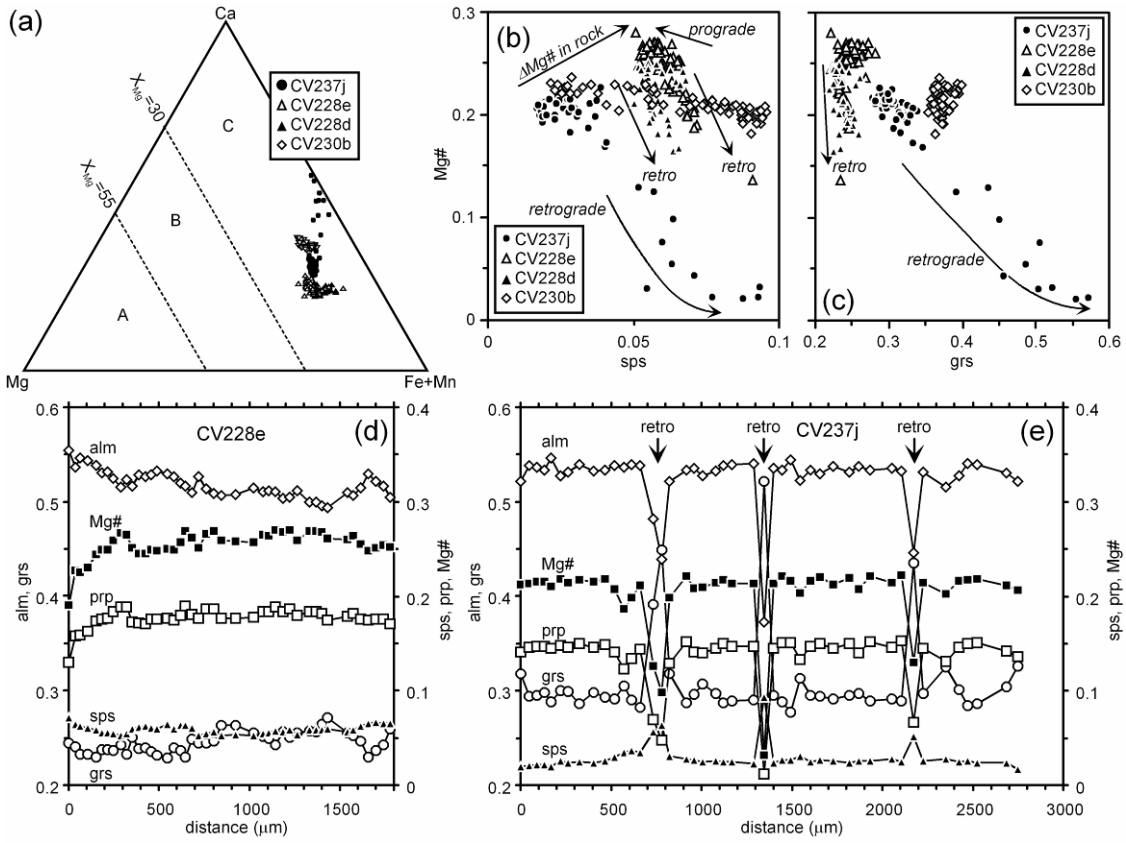

Fig. 7. Composition of garnet from amphibolites. (a) Garnet in the classification scheme of Coleman *et al*. (1965). Mg# vs. (b) spessartine and (c) grossular contents. Rim-to-rim profiles of porphyroblasts from samples (d) CV228e and (e) CV237j. Note the retrograde rims in (d) and the retrograde Ca-rich garnet developed along fractures in (e) indicated by arrows.

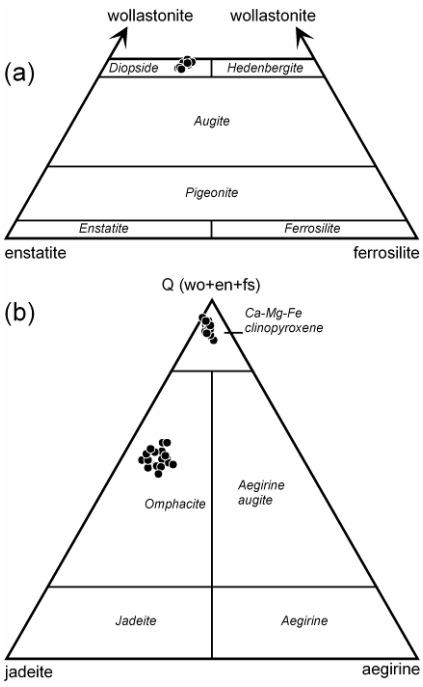

Fig. 8. Composition of clinopyroxene from sample CV237j in the classification scheme of Morimoto *et al*. (1988). (a) Peak calcic clinopyroxene (diopside). (b) Peak diopside and retrograde omphacite.

best shown when analyzing the chemical variation of phengite in single samples. Ba contents are low (0.06-0.01 apfu). The contents of Na (0.27-0.05 apfu) and Ti (0.014-0 apfu) are low to very low, with lower contents in celadonite-rich compositions (Fig. 9; Table 8). These compositional variations are consistent with continuing growth/readjustment during retrogression, with the onset of growth at relatively high temperature being represented by the lower Si and higher Na and Ti compositions.

Chlorite

Retrograde chlorite in the amphibolites bears Al = 4.34-5.17 apfu, Mn = 0.015-0.127 apfu, and Mg# (Fe^{2+}=Fe_{total}) = 0.50-0.71 (Table 9). Part of this compositional variability is due to the effect of bulk composition, with Mg#-rich compositions from Mg#-rich samples CV53b-I and CV62b-I and Mg#-poor compositions from Mg#-poor sample CV237j. The Al- and Mn-richer compositions are found in chlorite from Fe-richer samples bearing garnet. In these samples retrograde chlorite occurs adjacent to garnet and within the amphibolite matrix, and its

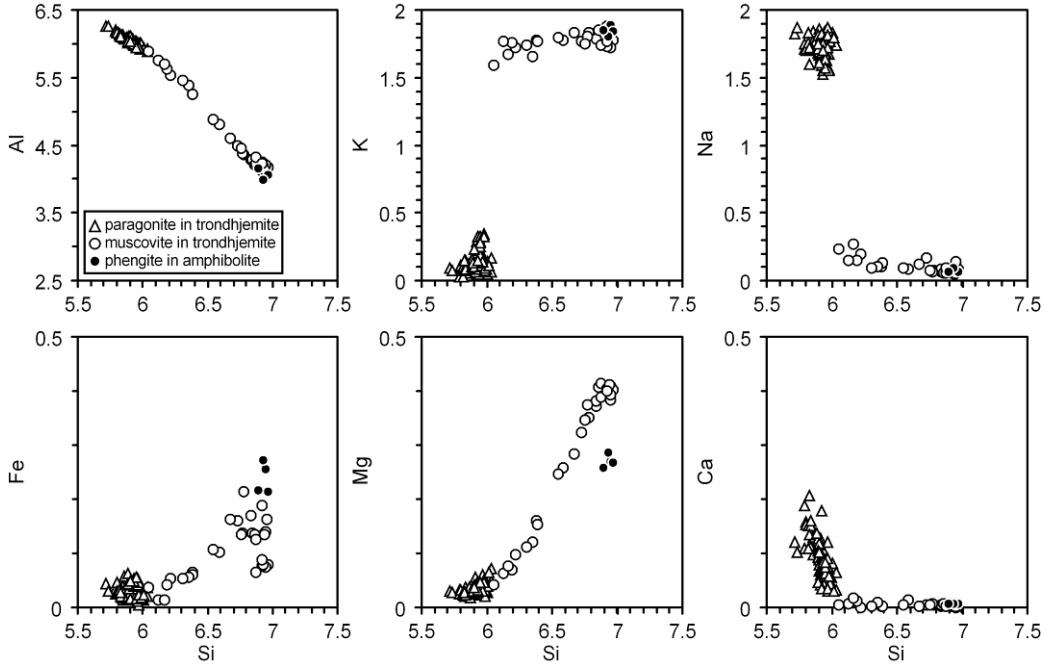

Fig. 9. Composition of micas from amphibolites (phengite) and trondhjemites (paragonite and muscovite-phengite). The high-K analyses of paragonite correspond to magmatic crystals.

composition mimics the site of growth with higher Fe, Al, and Mn contents in the former and higher Mg-contents in the latter.

Retrograde chlorite in the trondhjemites is similar to that of the amphibolites (Al = 4.49-5.11 apfu), except for being more magnesian (Mg# = 0.68-0.87; Table 9).

Other minerals

Retrograde pumpellyite in the amphibolite samples has Al = 4.81-4.92 apfu, Mg = 0.62-0.78 apfu, Fe^{2+}_{total} = 0.34-0.53 apfu, and Mg# (Fe^{2+}=Fe_{total}) = 0.56-0.70, whereas in the trondhjemite samples it has Al = 4.47-4.93, Mg = 0.82-1.09 apfu, Fe^{2+}_{total} = 0.20-0.40 apfu, and Mg# (Fe^{2+}=Fe_{total}) = 0.70-0.83 (Table 10). This again reflects the effect of bulk rock composition. Titanite has up to 0.072 Al (per 5 oxygens). Retrograde K-feldspar from the trondhjemites is almost pure orthoclase in composition, with X_{ab} = 0.004-0.025 and trace amounts of Ba (0.001-0.003 apfu; Table 7). Relict magmatic kyanite and retrograde lawsonite from the trondhjemites are almost pure in composition (Table 10).

PEAK METAMORPHIC AND MAGMATIC PHASE RELATIONS

Amphibolites

The peak metamorphic assemblages of the amphibolites are systematized in the ACF and AFN diagrams of Fig. 10. These diagrams are projected from coexisting phases and appropriate exchange vectors which allow condensation of the composition space. In order to give indications of the chemistry of the peak metamorphic minerals these phase diagrams also show the projection of relevant end-members of the solid solutions of interest. Because the ACF diagram is constructed after projection form quartz, the lack of quartz in sample CV237j helps explaining the apparent reaction relation among the peak metamorphic minerals plotted in Fig. 10c.

The ACF diagrams (Figs. 10a-c) show that epidote is paragenetic with peak pargasitic amphibole ± garnet ± clinopyroxene, indicating epidote-amphibolite facies conditions. These diagrams also help interpreting the lack of peak metamorphic plagioclase in the studied samples. This is best illustrated by the quartz-epidote amphibolite samples CV53b-I and CV62b-I (Fig. 10a). The bulk compositions of these samples plot within the tie-lines connecting peak metamorphic epidote and pargasite, implying no plagioclase stable in these bulk compositions at peak metamorphic conditions. The same conclusion is gained for the garnet bearing samples after inspection of the ACF diagram (Figs. 10b and c). However, the lack of peak metamorphic plagioclase in these samples is best appreciated in the AFN diagram projected from epidote of Fig. 10d. In this diagram, the bulk compositions of the epidote-garnet amphibolite samples CV228e and CV228e plot within the tie-lines connecting garnet and pargasite. Note that

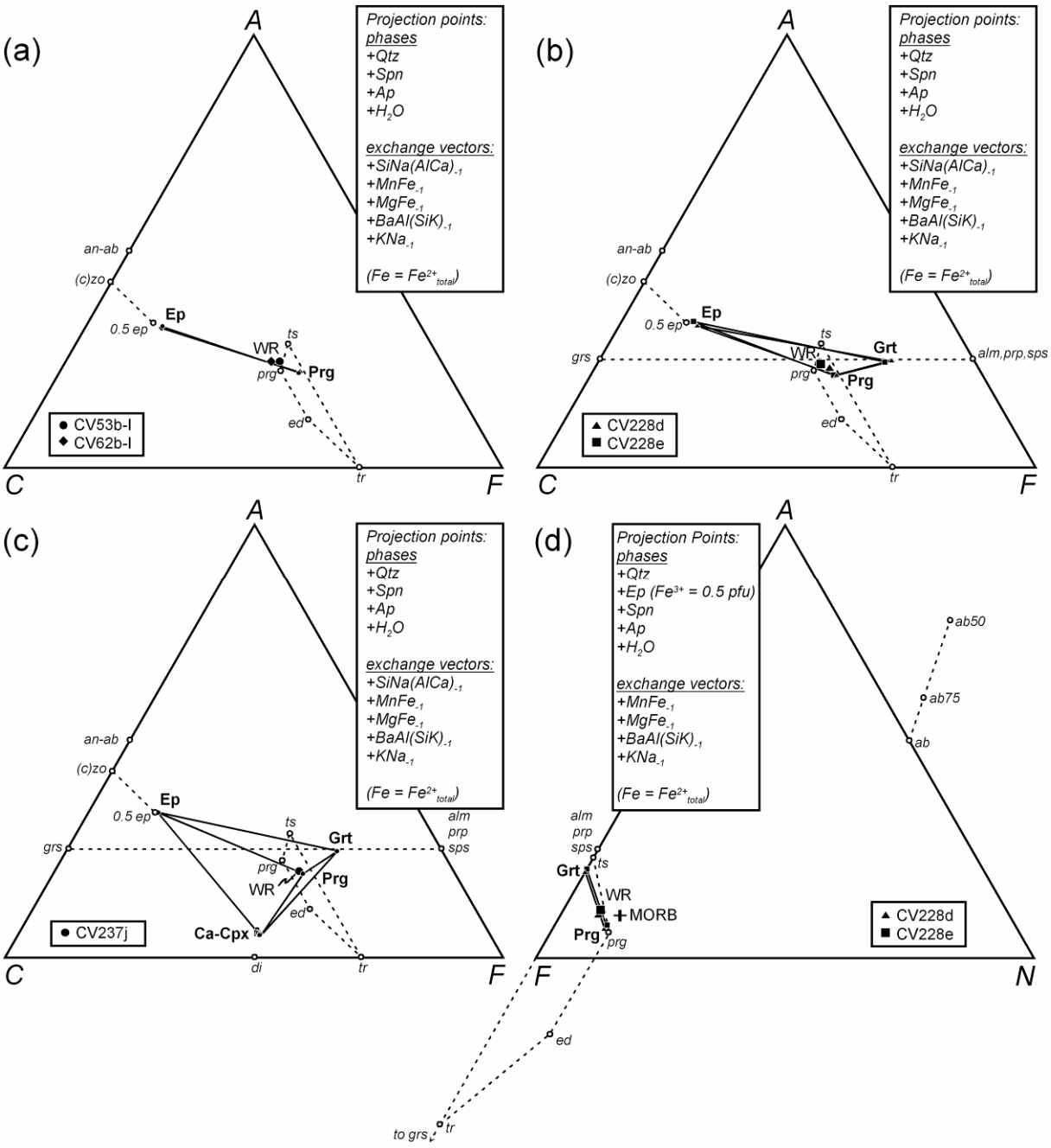

Fig. 10. (a)-(c) ACF and (d) AFN phase diagrams showing peak metamorphic assemblages of amphibolites (solid-tie lines, labels in bold typeface) and whole-rocks (WR). Average MORB (Hofmann, 1988; Kelemen *et al*, 2003) has been plotted in (d) for comparison. End-members (labels in italic lower case) of the solid solutions on interest are indicated by empty circles joined by dashed lines (0.5 ep: epidote with Fe^{3+} = 0.5 apfu). Note that anorthite and albite end members are collinear in the ACF diagram. The arrow in (d) indicates projection of grossular at infinity.

plagioclase would have been stable only in bulk compositions richer in Na_2O and/or Al_2O_3, such as those of average MORB plotted in Fig. 10d. The relations depicted in the AFN diagram of Fig. 10d strongly suggest that plagioclase consumption in, and alkali subtraction from, a MORB-like amphibolite by means of partial melting and subsequent melt extraction, respectively, are mechanisms that can account for the development of the studied bulk compositions and mineral assemblages.

Trondhjemitic segregations

The magmatic assemblages of the trondhjemites are systematized in the ACF and ACN diagrams of Figs. 11a and b, respectively, projected from coexisting phases and appropriate exchange vectors.

Note that the composition of the trondhjemite samples plot in the respective peraluminous fields of both diagrams. The tie-line crosscutting relations depicted in the ACF diagram (Fig. 11a) do not necessarily represent reaction among magmatic pargasite, epidote, plagioclase, and paragonite. These apparent reaction relations are best explained as a result of condensation of the composition space by projection from exchange vectors. A better representation of the magmatic assemblages is provided by the ACN diagram projected from pargasite (Fig. 11b). In this diagram no tie-line crosscutting relations exist among the magmatic minerals. Also, it clearly shows that the bulk composition of the trondhjemite magmas is appropriate for crystallization of magmatic paragonite from the melt.

The ACN diagram of Fig. 11b shows variable shapes of the plagioclase-epidote-paragonite tie-triangles. This is a consequence of the variable composition of magmatic plagioclase which, in turn, is a result of variable bulk composition of the samples (i.e., magmas). This is indicated by the fact that Na richer magmatic plagioclase is found in Na-richer samples (CV62b-II). However, as noted above, plagioclase is overprinted by albite, paragonite, and (clino)zoisite, with relict regions having higher Ca-contents (Fig. 4g). Even if these regions were identified with the aid of XR images, it is probable that they do not retain peak Ca-contents. Consequently, the variable shapes of the plagioclase-epidote-paragonite tie-triangles shown in Fig. 11b may be flawed. This has important consequences for thermobarometry, as discussed below.

P-T CONDITIONS AND P-T PATHS

Temperatures and pressures were estimated following the optimal P-T method of Powell & Holland (1994) using *THERMOCALC* (Holland & Powell, 1998, version 3.25, dataset 5.5, 12 Nov 04). Calculations were performed using different combinations of phases grown during pre-peak, peak, and post-peak conditions, as described below for each sample. A H_2O-fluid was included in all assemblages. All calculations are based on at least 4 independent reactions. The activities and (1σ) activity uncertainties of each end-member included in the calculations were obtained with software *AX* (T. Holland and R. Powell, 2000, unpublished). As indicated by Powell & Holland (1994), the uncertainties on the calculated P and T are not altered by a proportional change (e.g., doubling) of all the activity uncertainties, as long as the averaging is statistically consistent. The P-T uncertainties (σT and σP) given represent $\pm 1\sigma$ (95% confidence). The correlation between σT and σP for a given calculation is given below as "corr". High correlation indicates that with a T (or P) the other value is well constrained. Thus, large σT and σP imply well

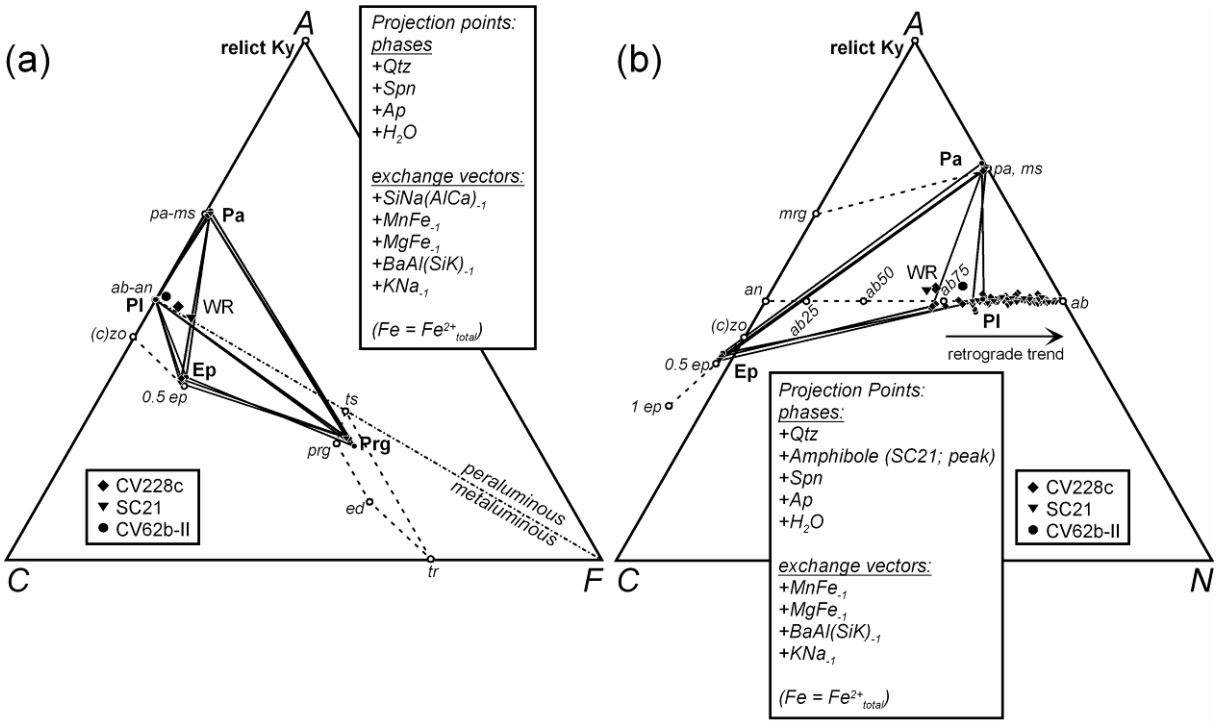

Fig. 11. (a) ACF and (b) ACN phase diagrams showing magmatic assemblages of pargasite-bearing trondhjemites (solid lines, bold typeface) and whole rocks (WR). In (b) the retrograde (subsolidus) trend of plagioclase is also shown. End-members (labels in italic lower case) of the solid solutions on interest are indicated by empty circles joined by dashed lines (0.5 ep and 1 ep: epidote with Fe^{3+} = 0.5 and 1.0 apfu, respectively). Note that the line connecting albite-anorthite in (b) corresponds with the limit of peraluminous vs. metaluminous compositions.

constrained P-T data if the former are highly correlated. The σT and σP uncertainties and correlations are appropriately incorporated into the uncertainty ellipses of Fig. 12 calculated following Powell & Holland (1994). In order to keep the calculated P-T error ellipses small and improve the statistics of the calculations, phase components with very low activities were neglected in the calculations and some phase components with errant behaviour (outliers) were occasionally rejected (see Powell & Holland, 1994 for justification). The calculations of pre-peak and peak conditions passed the "sigfit" test for statistical consistency, but some of the calculations of magmatic and retrograde conditions did not pass this test, suggesting equilibrium problems. The test implies that the "sigfit" values (quoted below for each calculation) should approach unity (see Powell & Holland, 1994 for further details).

Amphibolites

For thermobarometry, it is not possible to use the high-variance mineral assemblage amphibole + epidote + quartz of the garnet-free amphibolites because no set of linearly independent reactions can be found. Consequently, P-T calculations were performed only for the lower-variance (garnet-bearing) samples (Figs. 12a-c).

The calculated peak P-T conditions are based on the matrix assemblages Grt+Amp+Ep+Qtz (samples CV228d and CV228e), Grt+Amp+Ep (CV230b), and Grt+Amp+Ep+diopsidic Cpx (CV237j). The assemblages used for P-T calculations are shown in the ACF and AFN phase diagrams of Fig. 10 (see also Fig. 14). Pre-peak conditions were calculated using the composition of inclusions within garnet and the assemblages Grt+Amp+Ep+Qtz (sample CV228d) and Grt+Amp+Ep (CV230b). Retrograde conditions were calculated using actinolitic Amp+Gl+Chl+Ep+Grt (retrograded rims)+Qtz+Ab (samples CV228d and CV228e), actinolitic Amp+Gl+Chl+Ep+Grt (retrograded rims)+Ab (CV230b), and actinolitic Amp+Gl+Chl+Ep±Grt (retrograded rims)+Omp+Ab (CV237j).

The calculated peak conditions are 673±49 ºC, 14.6±2.2 kbar (corr 0.455, sigfit 1.13), 683±44 ºC, 15.7±2.1 kbar (0.476, 1.05), and 708±69 ºC, 13.8±2.2 kbar (-0.251, 0.81) in samples CV228d, CV228d, and CV230b, respectively, suggesting that these blocks underwent similar P-T conditions ranging 675-700 ºC and 14-16 kbar. However, peak conditions for CV273j are more uncertain. Using the assemblage indicated above with the composition of diopsidic clinopyroxene with the lowest, average, and highest Na contents, the calculated conditions are 859±46 ºC, 13±2.2 kbar (0.181, 1.04), 811±56 ºC, 14.4±2.7 kbar (0.134, 1.31) and 768±56 ºC 15±2.7 kbar (0.107, 1.36), respectively, suggesting higher temperatures and similar to somewhat lower pressures than the above three samples. As discussed below, the results calculated with the highest Na-content of diopsidic clinopyroxene are consistent with expected phase relations.

The calculated pre-peak conditions for samples CV228d and CV230b are slightly lower than those for peak conditions, down to 644±42 ºC, 13.1±1.9 kbar (0.514, 0.88) and 610±62 ºC, 13.9±2 kbar (-0.218, 0.96), respectively.

The calculated retrograde conditions are 525±28 ºC, 11.2±1.6 kbar (0.29, 2.35), 520±17 ºC, 11.2±1 kbar (0.345, 1.49), and 472±21 ºC, 10±1 kbar (0.473, 1.48) in samples CV228d, CV228d, and CV230b, respectively, suggesting that these blocks underwent similar retrograde P-T paths. The retrograde conditions for sample CV237j are 512±33 ºC, 11.9±1.3 kbar (0.155, 2.64) and 444±29 ºC, 10.6±1.1 kbar (0.437, 2.19) with or without retrograded garnet, respectively, included in the calculations.

These P-T calculations suggest counterclockwise P-T paths characterized by pre-peak prograde paths with increasing P and T within the epidote amphibolite facies, peak conditions within the epidote amphibolite facies, and retrogression within the blueschist facies (Figs. 12a-c).

Trondhjemitic segregations

As for the amphibolites, P-T calculations were performed using the lower-variance pargasite-bearing assemblages of samples CV228c, SC21, and CV62b-II (Fig. 12d). The calculated magmatic P-T conditions are based on the assemblages Amp+Ep+high-K Pa+Qtz+high-Ca Pl. The assemblages used for P-T calculations are shown in the ACF and ACN phase diagrams of Fig. 11. Retrograde conditions were calculated using tremolitic Amp+Chl+Ep+low-K Pa+Lws+Qtz+Ab (sample CV228c) and tremolitic Amp+Chl+Ep+ low-K Pa+Qtz+Ab (samples SC21 and CV62b-II).

The calculated magmatic conditions are 747±88 ºC, 14.7±3.2 kbar (0.988, 0.95), 793±96 ºC, 19.5±4 kbar (0.97, 0.65), and 730±81 ºC, 16.8±3.6 kbar (0.983, 0.51) in samples CV228c, SC21, and CV62b-II, respectively. The average calculated temperatures (ca. 750 ºC) are within error of calculated temperatures for the amphibolites. The pressure for CV228c overlaps with those for the common (Cpx-lacking) amphibolites. However, the pressures for samples SC21 and CV62b-II are higher. This is a consequence of the higher albite contents of plagioclase from these samples (Fig. 11b) and suggest that the equilibrium composition of magmatic plagioclase is probably not recorded in the analyses performed, as indicated above. Indeed, the

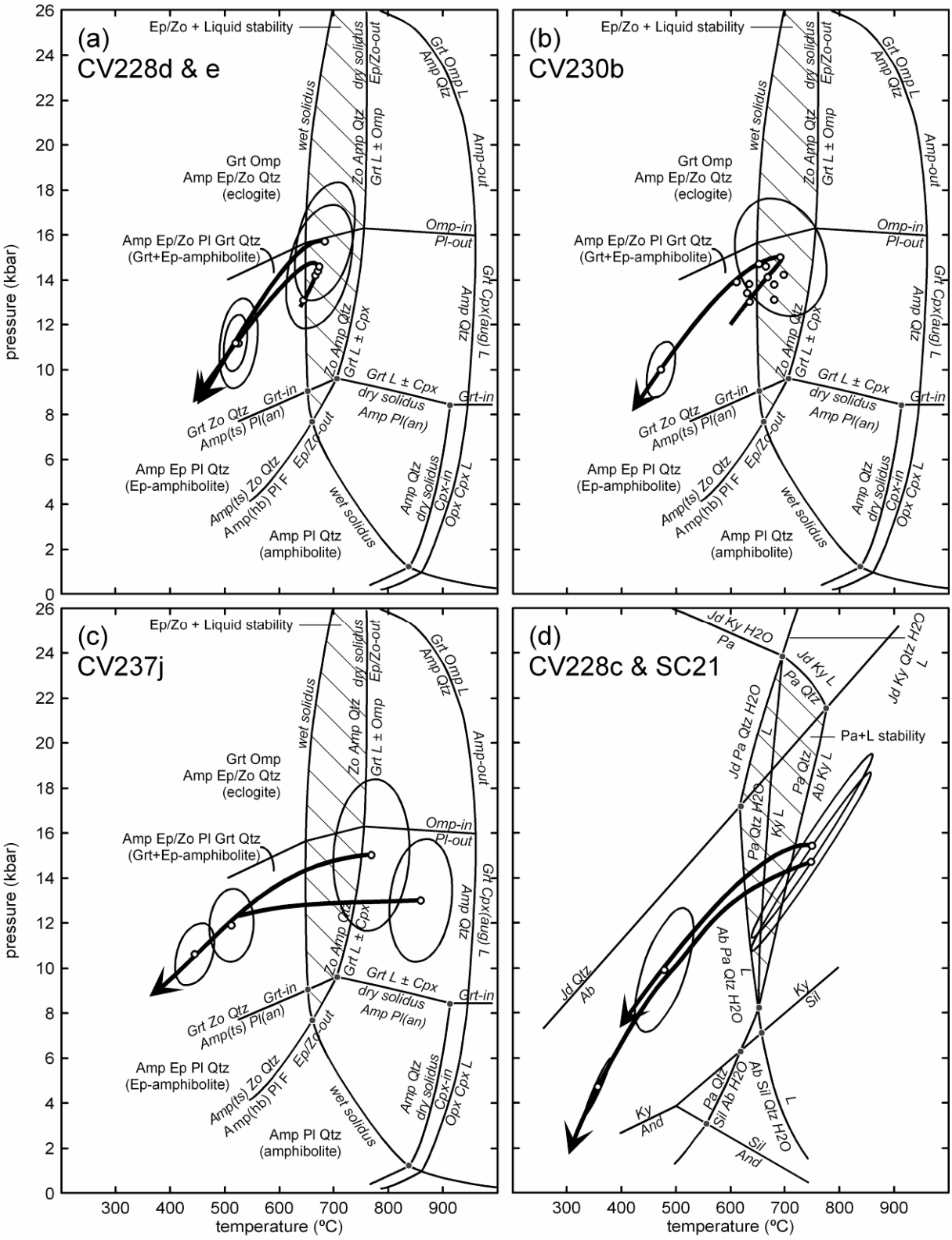

Fig. 12. P-T diagrams showing conditions calculated with *THERMOCALC* and paths for (a)-(c) Grt-bearing amphibolites and (d) Amp-bearing trondhjemites. Error ellipses: ±1σ. For reference, the grid for the basaltic system (Vielzeuf & Schmidt, 2001) is included in (a)-(c), and a grid for a simple trondhjemitic (NASH) system (Spear, 1993; García-Casco, 2007) is included in (d). The hatched regions in (a)-(c) and (d) represent the stabilities of epidote+liquid and paragonite+liquid, respectively. The two peak P-T conditions for the Cpx-bearing sample CV237j shown in (c) correspond to results using low (higher T) and high (lower T) Na contents of peak diopsidic clinopyroxene.

P-T conditions calculated for SC21 using the composition of plagioclase from sample CV228c (likely closer to the original composition of magmatic plagioclase) are 749±89 ºC at 15.4±3.3 kbar (0.988, 0.55), similar to those calculated for CV228c and approaching the pressures calculated for peak conditions in the amphibolites. Consequently, these latter P-T conditions for sample SC21 are plotted in Fig. 12d (ellipse with slightly higher peak P).

The conditions calculated for retrogression are 356±18 ºC, 4.7±1 kbar (0.963, 0.31), 478±43 ºC, 9.9±2.2 kbar (0.638, 2.15), and 550±21 ºC, 7.1±0.9 kbar (0.697, 0.79) in samples CV228c, SC21, and CV62b-II, respectively. These conditions are consistent with the retrograde conditions calculated for the amphibolites and indicate cooling at high pressure.

DISCUSSION

A subduction-related migmatitic complex

Field relations in the Sierra del Convento mélange show that the trondhjemitic-tonalitic bodies are closely related to blocks of amphibolite (Fig. 2) and do not crosscut other types of block and the serpentinite matrix of the mélange. This implies that the trondhjemitic-tonalitic melts do not represent exotic intrusions of volcanic-arc magmas and that these melts formed prior to incorporation of the amphibolite blocks into the mélange. On the other hand, the agmatitic structures and veins crosscutting the peak-metamorphic foliation of the amphibolite blocks (Figs. 2d and e) indicate that the melts did not form prior to subduction (i.e., they are not oceanic plagiogranites). The structures show that melt formation and segregation took place during and shortly after ductile deformation at near-peak metamorphic conditions, implying formation by partial melting of amphibolite in the subduction environment.

These inferences are in agreement with the major element composition of the trondhjemites. The peraluminous character of these rocks suggests that they do not represent oceanic plagiogranites or adakitic magmas, which are typically metaluminous (Fig. 3d). The low K_2O contents of the studied rocks also argue against typical adakite magma (Figs. 3b and d). Though less silicic, however, the trondhjemites of the Sierra del Convento mélange are comparable to peraluminous melts of the Catalina Schist formed during partial melting and metasomatism of subducted oceanic crust (Sorensen & Barton, 1987; Sorensen, 1988; Sorensen & Grossman, 1989; Bebout & Barton, 2002; Fig. 3d).

The major element bulk composition of the amphibolites, on the other hand, underlines their residual character attained after extraction of melt. The amphibolites have lower SiO_2 (trending toward apparent picritic compositions) and alkali components, notably Na_2O, and higher molar $Al_2O_3/(Na_2O+K_2O)$ than average MORB (Fig. 3). As discussed below, melting of amphibolite consumed relative large amounts of plagioclase up to its total consumption, a process consistent with these geochemical features if the primary tonalitic-trondhjemitic liquid was extracted after melting (cf. Fig. 10d). Not surprisingly, the aforementioned geochemical characteristics are similar to those of residual amphibolite from the Catalina Schist (Fig. 3).

Further evidence for partial melting of amphibolite is given by the calculated peak P-T conditions, which lie above the H_2O-saturated basaltic solidus (Figs. 12a-b, and 13a). These conditions suggest amphibolite melting at relatively low temperature, below the maximum stability of epidote in the basaltic system (Figs. 12a-b, and 13). This is in agreement with epidote forming part of the peak metamorphic supersolidus assemblage of the studied amphibolite samples (Fig. 10). In addition, such mineral assemblages and melting conditions indicate that melting took place under H_2O-present conditions, and that the dry solidus of amphibolite was not intersected (Figs. 12a-b) except perhaps in the Cpx-bearing sample (Fig. 12c).

Wet melting of amphibolite

H_2O-fluid strongly reduces the stability of plagioclase upon melting in the basaltic system, in particular at moderate to high pressure. This effect is appreciated in the H_2O-saturated and 5 wt% added H_2O "experimental pseudosections" compiled by Green (1982) for a standard tholeiitic basaltic composition (Fig 13). The relations shown in these pseudosections indicate that the stable assemblage appropriate for the calculated peak P-T conditions is Ep+Amp+Cpx+Grt+L±Qtz, and that the studied amphibolite samples should have contained plagioclase previous to partial melting.

The pseudosections of Fig. 13 also suggest that garnet and clinopyroxene are expected after wet melting of amphibolite. As discussed above, the lack of garnet in the Mg#-richer samples can be conceptualized as due to a bulk composition effect. The lack of clinopyroxene in most samples, however, suggests that this phase is not a necessary product of fluid-present melting of amphibolite. Indeed, while experiments indicate that clinopyroxene is a systematic product of melting of rocks of basaltic composition under H_2O-deficient conditions, they also suggest that this phase does not normally form upon wet melting near the solidus (Yoder & Tilley, 1962; Lambert & Wyllie, 1972; Heltz, 1973; 1976; Winther & Newton, 1991; Beard

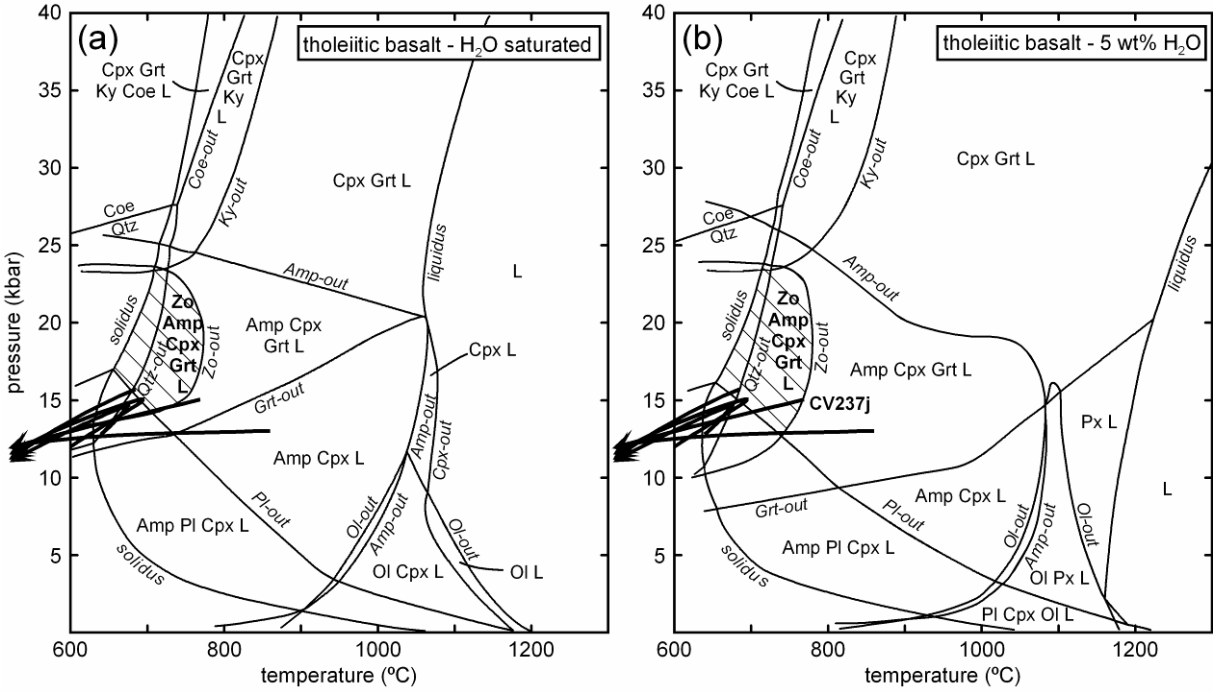

Fig. 13. Experimental pseudosections for the tholeiitic basaltic system constructed by Green (1982) for (a) water-saturated and (b) 5 wt% added H_2O conditions, and P-T paths calculated for the studied amphibolites. The hatched regions represent the stability fields of epidote+liquid above the stability limit of plagioclase, consistent with the mineral assemblages and calculated peak P-T conditions of the studied amphibolites. As shown in (b), the calculated P-T conditions and peak assemblage of the clinopyroxene-bearing sample CV237j suggest limited availability of H_2O.

& Lofgren, 1991; Selbekk & Skjerlie, 2002). Consequently, the studied rocks demonstrate that clinopyroxene is not a necessary product of wet-melting of amphibolite near the solidus at intermediate pressure, in agreement with proposals by Ellis & Thompson (1986) and Thompson & Ellis (1994).

The calculated conditions for the Cpx-bearing amphibolite sample CV237j (750-850 ºC 13-15 kbar) are above the maximum thermal stability of epidote in the water saturated basaltic system (Figs. 12c and 13a). This is not in agreement with textural evidence in this sample, where epidote forms part of the peak assemblage. This conflict is resolved if the peak conditions correspond to those calculated with the maximum Na content of diopsidic clinopyroxene (Fig. 12c) and water availability was more limited (Fig. 13b).

Melting reactions

Establishing the precise nature of the wet melting reactions underwent by the studied amphibolite samples is hampered by a) the lack of indication of the composition of peak metamorphic plagioclase present in the samples previous to melting and b) the possibility of post-melting processes, such as back reaction between melt and amphibolite (e.g., Kriegsman, 2001) and/or magmatic differentiation, which would have modified the composition of pristine primary melts. However, the phase relations depicted in the AFM-like diagrams of Fig. 14, combined with the analysis of the respective reaction space, allow constraining the nature of the melting reactions for each type of amphibolite. The analysis of reaction space has been performed in the 9-component system SiO_2-TiO_2-Al_2O_3-FeO-MgO-CaO-Na_2O-K_2O-P_2O_5 using software *CSpace* (Torres-Roldán *et al*., 2000). Component H_2O and, consequently, the fluid phase, were excluded from consideration because the H_2O-contents of the melts are unknown, though a H_2O-fluid should be considered part of the reactant assemblages. Also, Fe was treated as FeO_{total} and the exchange vector KNa_{-1} was included in the calculation because of the lack K-bearing phases during partial melting. With these and other constraints related to system degeneracy discussed below, the reaction space for each case discussed in the next paragraphs is uni-dimensional and the resulting single reaction represents a mass-balance that can be potentially identified as a melting reaction. All the reactions are expressed in oxy-equivalent units.

Garnet-lacking amphibolites

The mineral assemblage of the garnet-lacking amphibolite samples is represented in the AFM-like diagram of Fig. 14a by no more than peak pargasite

(note that the phase relations are projected from epidote). This allows deducing the composition of coexisting plagioclase previous to melting provided that the composition of the melt is known. As an example, Fig. 14a shows the relations for sample site CV62b. If a) trondhjemite vein CV62b-II represents the primary melt evolved from adjacent amphibolite CV62b-I, and b) plagioclase was totally consumed upon melting, the composition of peak metamorphic plagioclase is constrained to be collinear with peak pargasite and melt, implying a degenerate relation (Fig. 14a). The corresponding calculated composition of plagioclase is X_{ab} = 0.78 and the associated reaction is:

82.3 Pl (X_{ab} = 0.78) + 14.1 Qtz + 4.1 Ep + 1.9 Rt + 1.2 Amp+ 0.1 Ap (+ H_2O) = 100 L (CV62b-II) + 4.5 Spn.

Note that large relative amounts of reactant plagioclase contribute to melt formation. This is a consequence of melt and plagioclase being similar in composition, as clearly shown in the AFM diagram of Fig. 14a where both phases plot close to one each other.

The melting reaction deduced above is near-eutectic (i.e., Pl + Qtz + Amp + Ep = L). This general form remains unchanged even if the primary melt had a different composition to that of trondhjemite vein CV62b-II. Mass-balance constraints imply collinearity between amphibole, primary melt, and plagioclase and large relative amounts of reactant plagioclase in the associated degenerate reaction for any other tonalitic-trondhjemitic primary melt composition rich in plagioclase component. Consequently, we consider that the eutectic melting reaction Pl + Qtz + Amp + Ep = L is a good approximation to the wet-melting process underwent by the garnet-lacking amphibolites.

Garnet-bearing amphibolites

As an example, we discuss the relations for sample site CV228, where amphibolite CV228e is closely associated with trondhjemite segregate CV228c (Fig. 14b). The last sample is taken as a preliminary guess for the primary melt. Fixing the composition of the primary melt does not uniquely constrain the composition of plagioclase coexisting with the mineral assemblage of amphibolite CV228e.

Three reactions are possible depending on the composition of plagioclase. Plagioclase with X_{ab} = 0.69 is collinear with amphibole and melt, implying a degenerate reaction involving no garnet (i.e., Pl + Qtz + Amp + Ep = L, as above). For plagioclase with X_{ab} > 0.69 the melt plots to the left of the tie-line pargasite-plagioclase in the AFM-like diagram, as shown in Fig. 14b for plagioclase with X_{ab} = 0.72. This type of topology implies a peritectic AFM reaction of the form Amp + Pl (+ Ep + Qtz) = L + Grt. For plagioclase with X_{ab} < 0.69 the melt plots to the right of the tie-line pargasite-plagioclase and within the tie-triangle pargasite-garnet-plagioclase in the AFM-like diagram, implying a AFM melting reaction of the form Amp + Pl + Grt (+ Qtz) = L (+ Ep). The corresponding mass-balance reactions calculated for X_{ab} = 0.72, X_{ab} = 0.69, and X_{ab} = 0.66,

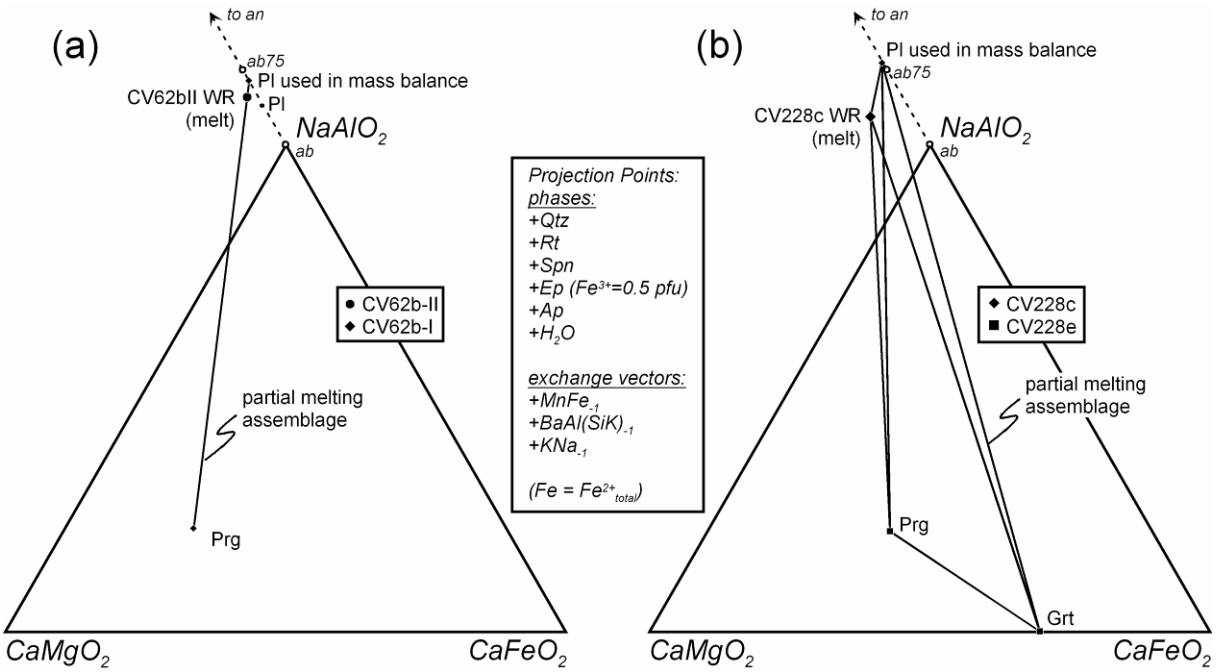

Fig. 14. AFM-like phase diagrams for sample sites (a) CV62 and (b) CV228. The solid tie-line/triangles represent the partial melting assemblages amphibole ± garnet + plagioclase + melt (see text for justification of plagioclase composition and mass balance calculations using these assemblages). The arrows indicate projection of anorthite component at infinity.

respectively, are:

84.2 Pl (X_{ab} = 0.72) + 11.5 Ep + 8.1 Amp + 4.5 Qtz + 3.6 Rt + 0.1 Ap (+ H_2O) = 100 L + 8.8 Spn + 4.4 Grt.

87.3 Pl (X_{ab} = 0.69) + 0.7 Ep + 5.9 Amp + 4.7 Qtz + 1.6 Rt + 0.1 Ap (+ H_2O) = 100 L + 3.6 Spn.

92.9 Pl (X_{ab} = 0.66) + 4.7 Amp + 2.6 Grt + 4 Qtz + 0.6 Rt + 0.1 Ap (+ H_2O) = 100 L + 1.3 Spn + 5.8 Ep.

For the same reasons indicated above, these reactions involve large relative amounts of reactant plagioclase and suggest total consumption of this phase upon melt formation.

Similar reactions would be deduced if trondhjemite CV228c does not represent a pristine primary melt. For other tonalitic-trondhjemitic primary melt compositions rich in plagioclase component it is possible to evaluate the melting relations fixing the composition of plagioclase. Our results indicate reactions with the same general forms as those deduced above (i.e., Pl + Qtz + Amp + Ep = L + Grt, Pl + Qtz + Amp + Ep = L, and Pl + Qtz + Amp + Grt = L + Ep). Therefore, melting of the studied garnet-bearing amphibolites should conform to one of these reactions.

The degenerate eutectic-like reaction Pl + Qtz + Amp + Ep = L involving no garnet is considered unlikely because there is no fundamental reason for a general collinear relation between plagioclase, amphibole, and melt in garnet-bearing assemblages. The other two reactions are peritectic. We favour reaction Pl + Qtz + Amp + Ep = L + Grt (Fig. 14b) because garnet is idiomorphic in sample CV228e (Fig. 4a), a feature that conflicts with reactant garnet as predicted by reaction Amp + Pl + Grt = L + Ep. Furthermore, the latter reaction has epidote in the product, a result which is inconsistent with theory and experiments (e.g., Ellis & Thompson, 1986; Thompson & Ellis, 1994; Quirion & Jenkins, 1998).

A variety of melting reactions are possible for the garnet+clinopyroxene-bearing amphibolite sample CV237j. The number of possible reactions is larger in this case because the presence of quartz in the pre-melting assemblage of this quartz-lacking sample is uncertain. Garnet, clinopyroxene, amphibole, and epidote may appear either as reactants or products in these reactions, depending on the composition of plagioclase and melt and the presence/absence of quartz. However, in all the possible reactions the amount of plagioclase involved is large, in agreement with the behaviour of this phase in other types of amphibolite studied.

Thus, it is concluded that the amount of plagioclase present in amphibolite previous to melting is a mayor control on the extent of wet melting. This inference applies to amphibolite with different their mineral assemblages undergoing different melting reactions. Because of the relatively high pressure of melting (ca. 15 kbar) the amount of plagioclase present in the pre-melting assemblages is inferred to have been small and, consequently, low melt fractions should have been produced. Low melt fractions are consistent with the Fe+Mg-poor nature of the studied trondhjemitic rocks. These inferences strongly suggest that plagioclase was completely consumed in the amphibolites upon melting and that the trondhjemites are (near-) primary melts.

Peraluminosity of primary slab melts

The studied rocks confirm that melts formed upon partial melting of metabasite at intermediate pressure under fluid-present conditions are peraluminous (cf. Ellis & Thompson, 1986, and Thompson & Ellis, 1994) and that this type of melt can form in a subducting slab. However, peraluminosity is not a typical characteristic of magmas thought to have formed upon partial melting of subducted slabs (e.g., Cenozoic adakites, Archaean tonalite-trondhjemite complexes; Defant & Drummond, 1990; Martin, 1999). This observation should be taken into consideration when the origin of slab-derived magmas is addressed.

Experimental work on melting of natural and synthetic metabasites has shown that peraluminous melts form at low-temperature conditions close to the wet basaltic solidus and metaluminous melts form under conditions largely deviated from the wet basaltic solidus, typically at > 850 ºC (Yoder & Tilley, 1962; Holloway & Burnham, 1972; Heltz, 1976; Ellis & Thompson, 1986, Beard & Lofgren, 1989; Rapp *et al*., 1991; Gaetani *et al.*, 1993; Winther & Newton, 1991; Thompson & Ellis, 1994; Kawamoto, 1996; Springer & Seck, 1997; Nakajima & Arima,1998; Prouteau *et al*., 2001; Selbekk & Skjerlie, 2002; Koepke *et al*., 2004). Under conditions close to the solidus, amphibole is abundant and plagioclase is scarce or not present in the residua, small melt fractions are formed, and the resulting melt is acid, in all aspects similar to characteristic amphibolite-trondhjemite associations of the Sierra del Convento mélange. Under conditions largely deviated from the solidus amphibole is scarce or not present, large melt fractions are formed, and the resulting melt is relatively basic (andesitic). It follows that metaluminous slab magmas, if formed by melting of mafic rocks close to the wet solidus, are not pristine slab melts. Metaluminosity of such magmas should be identified, instead, as a consequence of post-melting processes such as interaction with the mantle wedged and/or the base of the crust (cf. Kepezhinskas *et al*., 1995; Stern & Kilian, 1996; Martin, 1999; Yogodzinski *et al*. 2001; Prouteau *et al*., 2001).

Magmatic paragonite and kyanite

Magmatic paragonite is expected in peraluminous melts crystallized at moderate to high pressure. As shown in Fig. 12d, magmatic paragonite is stable in the model NASH system above 8 kbar. Similar relations are predicted in the more complex NCASH system (García-Casco, 2007). Using a NCASH pseudosection approach, García-Casco (2007) calculated that paragonite is stable above the solidus of sample SC21 in the range 680 – 730 ºC at ca. 14 kbar. This is consistent with the high K-content of magmatic paragonite (Fig. 9) indicating crystallization at high temperature (García-Casco, 2007). Crystallization of trondhjemitic melt at depth within the stability field of paragonite is also consistent with the occurrence of magmatic epidote in the studied rocks (Figs. 4i and k), a feature that is normally taken as an indication of moderate to high pressure of crystallization of magmatic rocks (Schmidt & Poli, 2004, and references therein). The model phase relations calculated by García-Casco (2007) show that magmatic epidote is not stable at < 13 kbar in bulk composition SC21, in agreement with the calculated crystallization pressure of 14-16 kbar (Fig. 12d).

The presence of kyanite relicts within magmatic epidote in some samples (Fig. 4m) also points to crystallization at high pressure. The NCASH pseudosection for sample SC21 shows stable kyanite + epidote above the solidus at > 720 ºC, 14-15 kbar and total consumption of kyanite upon reaction with melt to produce paragonite and more epidote during near-isobaric cooling (García-Casco, 2007). These relations explain the relict nature of kyanite within epidote in the studied rocks.

The consistency between natural mineral assemblages and theoretical phase relations allows concluding that paragonite is an expected product of crystallization of peraluminous trondhjemitic melt at intermediate to high pressure. Therefore, relatively low pressure (< 8 kbar) of crystallization explains the lack of paragonite in natural peraluminous trondhjemites (e.g., Johnson *et al*., 1997).

Tectonic implications

Recent thermal models incorporating appropriate temperature dependence of mantle rheology suggest that melting of subducted oceanic crust may occur at shallower depths and be more general over a range of plate velocities and ages, subduction angles, and other geophysical variables (i.e., not restricted to special cases of subduction) than previously assumed based on the relatively cool slabs calculated in earlier models (e.g., van Keken *et al*., 2002; Gerya & Yuen, 2003; Conder, 2005; Abers *et al*., 2006). Following these recent results, melting in the Sierra del Convento could be interpreted as the result of normal subduction. Thermal models, however, also point towards special subduction environments where melting is possible at relatively shallow depths, including the edge of a slab (e.g., Kincaid & Griffiths, 2004), subhorizontal subduction (e.g., Manea *et al*., 2005), subduction retreat (e.g., Kincaid & Griffiths, 2003, 2004), onset of subduction (e.g., Gerya *et al*., 2002), or subduction of a very young slab or a ridge (e.g., Okudaira & Yoshitake, 2004; Uehara & Aoya, 2005). Though it is difficult to decipher the precise subduction environment of formation of the studied rocks, regional arguments favour a scenario of onset of subduction of young oceanic lithosphere.

Regional geological data in the Caribbean realm point to initiation of subduction during the Aptian (ca. 120 Ma; Pindell *et al.*, 2005, 2006). The latter authors have developed a tectonic model for the evolution of the Caribbean realm which incorporates the birth of a SW-dipping subduction system during the Aptian which consumed oceanic lithosphere of the Protocaribbean (Atlantic) basin, which was opening at that time and, consequently, subduction of a hot young oceanic lithosphere and/or a ridge was possible. Indirect evidence for the existence of a (near-orthogonal) subducting Protocaribbean ridge during the Cretaceous is given by geochemical studies of magmatic rocks from the overriding Caribbean plate (e.g., Jolly & Lidiak, 2006; Escuder-Viruete *et al*., 2007; see also discussion by Pindell *et al*., 2005, 2006). Thus, since age data indicate that the earliest stage of subduction in eastern Cuba is of Aptian age (ca. 120 Ma; see García-Casco *et al*., 2006), the studied rocks likely formed in a scenario of onset of subduction of young lithosphere (Fig. 15).

After a thorough consideration of P-T-t data and thermal models, Krebs *et al*. (2007) have recently developed a similar scenario of onset of Aptian subduction of young (ca. 20 Ma-old) Protocaribbean lithosphere for eclogite blocks of the Río San Juan mélange (Dominican Republic). The descriptions and interpretations of these authors suggest that the Río San Juan and the Sierra del Convento mélanges are geologically correlated. The Río San Juan mélange contain eclogites formed during the early Cretaceous (103.6 ± 2.7 Ma) and blueschist formed during the late Cretaceous. The eclogites attained similar peak temperature (ca. 750) than the Sierra del Convento amphibolites, though the former attained substantially higher peak pressure (ca. 23 kbar) and did not apparently underwent partial melting. These differences in the earliest products of subduction point to strike-parallel variations in the thermal structure (i.e., age) of the subducting Protocaribbean

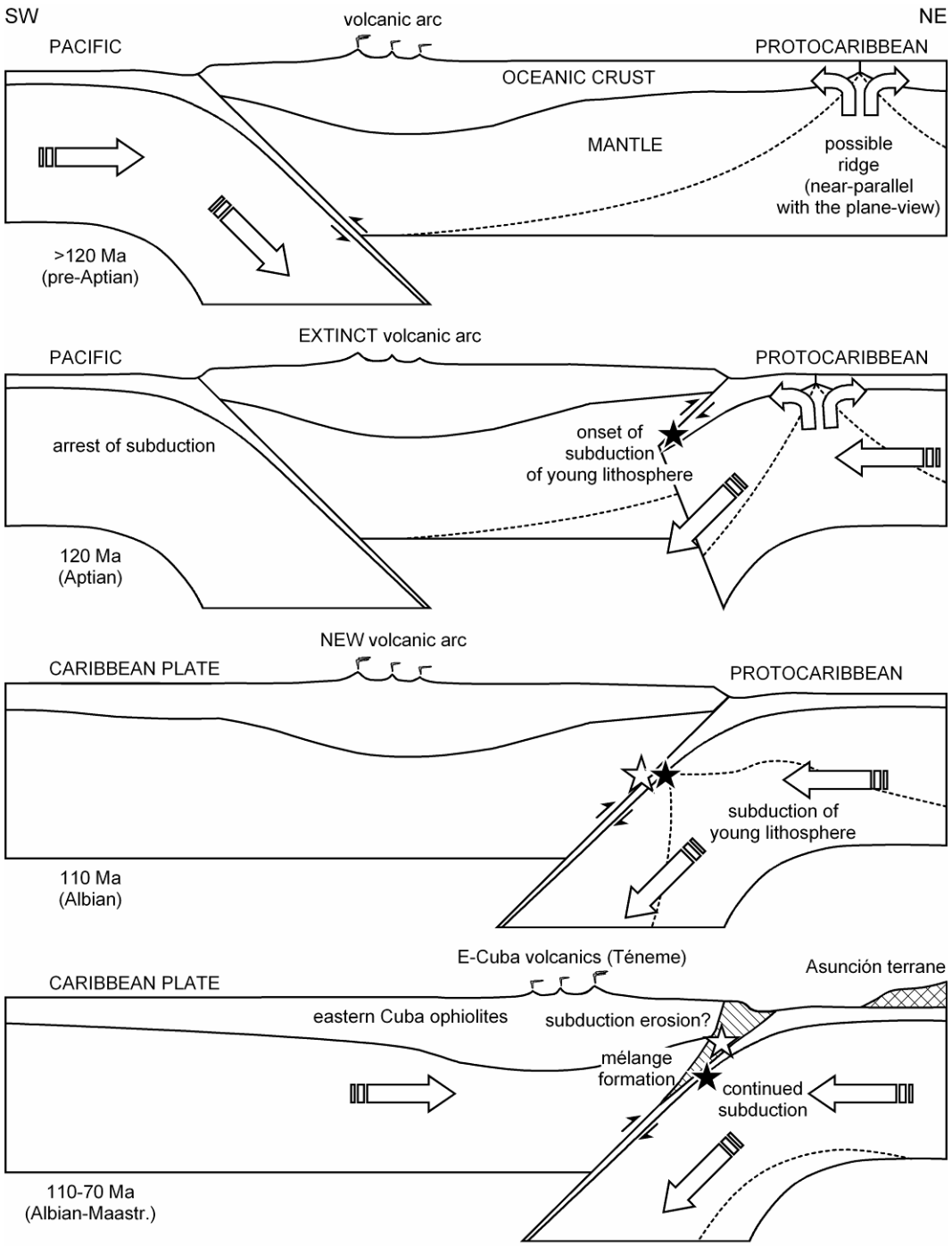

Fig. 15. Schematic representation of the tectonic evolution of eastern Cuba (cf. Pindell *et al*., 2005). The filled and empty stars indicate amphibolite in the course of Aptian onset of subduction of young lithosphere and late Cretaceous accretion/exhumation of the tectonic blocks, respectively. The Sierra del Convento mélange formed in the subduction channel (hatched). Subduction of volcanic-arc material (Purial complex) suggests subduction erosion during the late Cretaceous.

during the early Cretaceous. Plate-tectonic reconstructions locate eastern Cuba to the N-NW of Hispaniola by Aptian times (Pindell *et al*., 2005), implying that the subducting slab was hotter (i.e., younger) to the N-NW (relative to Hispaniola) and, consequently, that the ridge should have been located close to eastern Cuba by Aptian times.

This scenario for the onset of subduction explains the observed counterclockwise P-T paths of the Sierra del Convento amphibolite blocks. Onset of subduction produces a transient geothermal gradient at the slab-mantle interface which cools down upon continued subduction (Gerya *et al*., 2002). Our calculated P-T paths suggest that, after accretion to

the overriding plate, the blocks of amphibolite and associated trondhjemites were refrigerated at depth, in agreement with the expected effects of continued subduction (Fig. 12). At this stage in the Sierra del Convento mélange the trondhjemite magmas formed by partial melting of amphibolite cooled down and crystallized. The subduction models of Gerya *et al*. (2002) show that continued subduction leads to the formation of a serpentinitic layer (subduction channel) by hydration of the overriding mantle some Ma after the onset of subduction. These authors also indicated that formation of such a serpentinite layer allows formation of serpentinite-mélanges and the onset of exhumation of early accreted blocks along the subduction channel. In the Sierra del Convento mélange this stage is recorded by the blueschist facies overprints developed as the amphibolite and trondhjemite blocks followed counterclockwise P-T paths (Fig. 15).

As subduction proceeds, more material normally of lower-grade can be accreted to the subduction channel (Gerya *et al*., 2002). Blocks of blueschist not studied here record this stage in the Sierra del Convento. A similar picture arises from the Río San Juan mélange (Krebs *et al*., 2007). Thus, both mélanges constitute fragments of a subduction channel documenting a long-lasting history of subduction, accretion, mélange formation, and uplift, and both give direct evidence for Aptian onset of subduction of the Protocaribbean (Fig. 15).

CONCLUSIONS

The Sierra del Convento mélange (eastern Cuba) contains high-grade tectonic blocks of plagioclase-lacking epidote ± garnet amphibolite and associated tonalite-trondhjemite which formed during subduction of oceanic lithosphere. Field relations, major element bulk-rock compositions, textures, peak metamorphic, magmatic, and retrograde mineral assemblages, and P-T conditions, and the agreement between the observed mineral assemblages and those predicted by experimental and theoretical studies indicate that tonalite-trondhjemite formed by partial melting of amphibolite in the subduction environment, and that both shared a common P-T history during exhumation. Thus, these tectonic blocks represent a rare example of oceanic subduction-related migmatites which have returned to the Earth's surface. Regional arguments suggest a scenario of onset of subduction of young oceanic lithosphere (during the Aptian). Partial melting at ca. 15 kbar, 750 ºC was characterized by low melt fractions, was fluid-assisted, occurred close to the metabasite solidus, consumed large relative amounts of plagioclase in the amphibolites, and formed plagioclase-lacking residual amphibolite and peraluminous, K-poor, Mg#-rich leucocratic tonalitic-trondhjemitic melts that segregated into veins, layers, and agmatitic structures. Shortly after melt formation amphibolite + melt blocks were accreted to the overriding plate, where they started to cool as subduction proceeded, allowing the partial melts to crystallize at depth. This favoured the formation of magmatic paragonite, kyanite, epidote, plagioclase, pargasite, and quartz after crystallization of the melts. Later, syn-subduction exhumation in the mélange caused counterclockwise P-T paths, forming retrograde blueschist-facies assemblages in all types of rock. Blueschist-facies conditions prevailed during the ensuing history of subduction, when other blocks were incorporated into the mélange, attesting for a long-lasting history of accretion, mélange formation and uplift.

ACKNOWLEDGEMENTS

The authors wish to thank Walter Maresch, an anonymous reviewer, and editor Ron Frost for their perceptive comments and suggestions which substantially improved this paper. Walter Maresch is also thanked for providing us with a pre-print manuscript by Krebs and co-workers on the Río San Juan mélange. Manuel Iturralde-Vinent kindly reviewed an early version. This paper is a contribution to IGCP-546 "Subduction zones of the Caribbean". The work presented in this paper has received financial support from MEC project CGL2006-08527/BTE.

REFERENCES

Abers, G. A., van Keken, P. E., Kneller, E. A., Ferris, A. & Stachnik, J. C. (2006). The thermal structure of subduction zones constrained by seismic imaging: Implications for slab dehydration and wedge flow. Earth and Planetary Science Letters 241, 387-397.

Barker, F. (1979). Trondhjemites: Definition, environment and hypotheses of origin. In: Barker, F. (ed.) Trondhjemites, Dacites and Related Rocks. Elsevier, Amsterdam, 1-12.

Beard, J. S. & Lofgren, G. E. (1989). Effect of water on the composition of melts of greenstone and amphibolites. Science 244, 195-197.

Beard, J. S. & Lofgren, G. E. (1991). Dehydration melting and water-saturated melting of basaltic and andesitic greenstones and amphibolites at 1, 3, and 6.9 kb. Journal of Petrology 32, 365-401.

Bebout, G. E. (2007). Metamorphic chemical geodynamics of subduction zones. Earth and Planetary Science Letters 260, 373-393.

Bebout, G. E. & Barton, M. D. (2002). Tectonic and metasomatic mixing in a high-T, subduction-zone mélange - insights into the geochemical evolution of the slab-mantle interface. Chemical Geology 187, 79-106.

Boiteau, A., Michard, A. & Saliot, P. (1972). Métamporphisme de haute pression dans le complexe ophiolitique du Purial (Oriente,Cuba). Comptes

Rendus de l'Académie des Sciences Paris 274 (série D), 2137-2140.

Cobiella, J., Quintas, F., Campos M. & Hernández, M. (1984). Geología de la Región Central y Suroriental de la Provincia de Guantánamo. Santiago de Cuba: Editorial Oriente, Santiago de Cuba, 125 pp.

Coleman, R. G., Lee, D. E., Beatty, L. B. & Brannock, W. W. (1965). Eclogites and eclogites: their differences and similarities. Geological Society of America Bulletin 76, 483-508.

Conder, J. A. (2005). A case for hot slab surface temperatures in numerical viscous flow models of subduction zones with an improved fault zone parameterization. Physics of the Earth and Planetary Interiors 149, 155-164.

Coutinho, J. M. V., Kräutner, H. G., Sassi, F., Schmid, R. & Sen, S. (2007). A systematic nomenclature for metamorphic rocks: 8. Amphibolite and granulite. Recommendations by the IUGS Subcommission on the Systematics of Metamorphic Rocks. Web version of 01.02.2007 (http://www.bgs.ac.uk/SCMR/docs/papers/paper_8.pdf).

De Andrade V., Vidal, O., Lewin, E., O'Brien, P., & Aagard, P. (2006). Quantification of electron microprobe compositional maps of rock thin sections: an optimized method and examples. Journal of Metamorphic Geology 24, 655-668.

Defant, M. J. & Drummond, M. S. (1990). Derivation of some modern arc magmas by melting of young subducted lithosphere. Nature 347, 662-665.

Drummond, M. S., Defant, M. J. & Kepezhinskas, P. K. (1996). Petrogenesis of slab-derived trondhjemite-tonalite-dacite/adakite magmas. Transactions of the Royal Society of Edinburgh: Earth Sciences 87, 205-215.

Elliott, T., Plank, T., Zindler, A., White, W. & Bourdon, B. (1997). Element transport from slab to volcanic front at the Mariana arc. Journal of Geophysical Research 102 (B7), 14,991-15,019.

Ellis, D. J. & Thompson, A. B. (1986). Subsolidus and partial melting reactions in the quartz-excess $CaO+MgO+Al_2O_3+SiO_2+H_2O$ system under water-excess and water deficient conditions to 10 kb: Some implications for the origin of peraluminous melts from mafic rocks. Journal of Petrology 27, 91-121.

Ernst, W. G. (1999). Metamorphism, partial preservation, and exhumation of ultrahigh-pressure belts. The Island Arc 8, 125-153.

Escuder-Viruete, J. & Pérez-Estaún, A. (2006). Subduction-related P–T path for eclogites and garnet glaucophanites from the Samaná Peninsula basement complex, northern Hispaniola. International Journal of Earth Sciences 95, 995-1017.

Escuder-Viruete, J. Contreras, F., Stein G., Urien P., Joubert M., Pérez-Estaún A., Friedman R. & Ullrich, T. (2007). Magmatic relationships and ages between adakites, magnesian andesites and Nb-enriched basalt-andesites from Hispaniola: Record of a major change in the Caribbean island arc magma sources. Lithos (in press), doi:10.1016/j.lithos.2007.01.008.

Gaetani, G. A., Grove, T. L. & Bryan, W. B. (1993). The influence of water on the petrogenesis of subduction-related igneous rocks. Nature 365, 332-335.

García-Casco, A. (2007). Magmatic paragonite in trondhjemites from the Sierra del Convento mélange, Cuba. American Mineralogist 92, 1232-1237.

García-Casco, A., Torres-Roldán, R. L., Millán, G., Monié, P. & Schneider, J. (2002). Oscillatory zoning in eclogitic garnet and amphibole, Northern Serpentinite Melange, Cuba: a record of tectonic instability during subduction? Journal of Metamorphic Geology 20, 581-598.

García-Casco, A., Torres-Roldán R. L., Iturralde-Vinent, M. A., Millán, G., Núñez Cambra, K., Lázaro, C. & Rodríguez Vega, A. (2006). High pressure metamorphism of ophiolites in Cuba. Geologica Acta 4, 63-88.

Gerya, T. V. & Yuen, D. A. (2003). Rayleigh-Taylor instabilities from hydration and melting propel 'cold plumes' at subduction zones. Earth and Planetary Science Letters 212, 47-62.

Gerya, T. V., Stoeckhert, B. & Perchuk, A. L. (2002). Exhumation of high-pressure metamorphic rocks in a subduction channel - a numerical simulation. Tectonics 21, 6-1-6-19.

Green, T. H. (1982). Anatexis of mafic crust and high pressure crystallization of andesite. In: R. S. Thorpe (ed.) Andesites, John Wiley & Sons, 465-487.

Grove, T. L., Chatterjee, N., Parman, S. W. & Médard, E. (2006). The influence of H_2O on mantle wedge melting. Earth and Planetary Science Letters 249, 74–89.

Harlow, G. E., Hemming, S. R., Avé Lallemant, H. G., Sisson, V. B. & Sorensen, S. S. (2004). Two high-pressure–low-temperature serpentinite-matrix mélange belts, Motagua fault zone, Guatemala: A record of Aptian and Maastrichtian collisions. Geology 32, 17-20.

Heltz, R. T. (1973). Phase relations of basalt in their melting ranges at P_{H2O}=5 kb as a function of oxygen fugacity. Part I. Mafic phases. Journal of Petrology 14, 249-302.

Heltz, R. T. (1976). Phase relations of basalt in their melting ranges at P_{H2O}=5 kb. Part II. Melt compositions. Journal of Petrology 17, 139-193.

Hermann, J., Spandler, C., Hack, A., & Korsakov, A. V. (2006). Aqueous fluids and hydrous melts in high-pressure and ultra-high pressure rocks: Implications for element transfer in subduction zones. Lithos 92, 399-417.

Hernández, M. & Canedo, Z. (1995). Geoquímica de las ofiolitas meridionales de Cuba oriental. Revista Minería y Geología 3, 3-9.

Hofmann, A. W. (1988). Chemical differentiation of the Earth: the relationship between mantle, continental crust, and oceanic crust. Earth and Planetary Science Letters 90, 297-314.

Holland, T. J. B. & Powell, R. (1998). An internally consistent thermodynamic data set for phases of petrological interest. Journal of Metamorphic Geology 16, 309-343.

Holloway, J. R. & Burnham, C. W. (1972). Melting relations of basalt with equilibrium water pressure less than total pressure. Journal of Petrology 13, 1-29.

Iturralde-Vinent, M. A. (1996). Introduction to Cuban Geology and Geophysics. In: Iturralde-Vinent, M. A. (ed.) Ofiolitas y Arcos Volcánicos de Cuba. Miami, USA, IGCP Project 364 Special Contribution 1, 3-35.

Iturralde-Vinent, M. A. (1998). Sinopsis de la constitución Geológica de Cuba. Acta Geologica Hispanica 33, 9-56.

Iturralde-Vinent, M. A. & Lidiak, E.G. (2006). Caribbean tectonic, magmatic, metamorphic and stratigraphic events. Implications for plate tectonics. Geologica Acta 4, 1-5.

Iturralde-Vinent, M. A., Millán, G., Korkas, L., Nagy, E. & Pajón, J. (1996). Geological interpretation of the Cuban K-Ar data base. In: Iturralde-Vinent, M. A. (ed.). Ofiolitas y Arcos Volcánicos de Cuba. Miami, USA, IGCP Project 364 Special Contribution 1, 48-69.

Iturralde-Vinent, M. A., Díaz Otero, C., Rodríguez Vega, A. & Díaz Martínez , R. (2006). Tectonic implications of paleontologic dating of Cretaceous-Danian sections of Eastern Cuba. Geologica Acta 4, 89-102.

Johnson, K., Barnes, C. G. & Miller C. A. (1997). Petrology, Geochemistry, and Genesis of High-Al Tonalite and Trondhjemites of the Cornucopia Stock, Blue Mountains, Northeastern Oregon. Journal of Petrology 38, 1585-1611.

Johnson, M. C. & Plank, T. (1999). Dehydration and melting experiments constrain the fate of subducted sediments. Geochemistry Geophysics Geosystems 1, paper number 199GC000014.

Jolly W. T. & Lidiak E. G. (2006). Role of crustal melting in petrogenesis of the Cretaceous Water Island Formation (Virgin Islands, northeast Antilles Island arc). Geologica Acta 4, 7-33.

Kawamoto, T. (1996). Experimental constraints on differentiation and H_2O abundance of calc-alkaline magmas. Earth and Planetary Science Letters 144, 577-589.

Kelemen, P. B., Hanghoj, K. & Greene, A. R. (2003). One view of the geochemistry of subduction-related magmatic arcs with an emphasis on primitive andesite and lower crust. In: Rudnick, R. L. (ed) The crust. Oxford, U.K., Elsevier-Pergamon, Treatise on Geochemistry (eds. H. D. Holland & K. K. Turekian) 3, 593-659.

Kepezhinskas, P. K., Defant, M. J. & Drummond, M. S. (1995). Na metasomatism in the island-arc mantle by slab melt-peridotite interaction: evidence from mantle xenoliths in the north Kamchatka arc. Journal of Petrology 36, 1505-1527.

Kessel, R., Ulmer, P., Pettke, T., Schmidt, M. W. & Thompson, A. B. (2005). The water–basalt system at 4 to 6 GPa: Phase relations and second critical endpoint in a K-free eclogite at 700 to 1400 ºC. Earth and Planetary Science Letters 237, 873-892.

Kincaid, C. & Griffiths, R. W. (2003). Laboratory models of the thermal evolution of the mantle during rollback subduction. Nature 425, 58-62.

Kincaid, C. & Griffiths, R. W. (2004). Variability in flow and temperatures within mantle subduction zones, Geochemistry Geophysics Geosystems 5, Q06002, doi: 10.1029/2003GC000666.

Koepke, J., Feig, S. T., Snow, J. & Freise, M. (2004). Petrogenesis of oceanic plagiogranites by partial melting of gabbros: an experimental study. Contributions to Mineralogy and Petrology 146, 414-432.

Krebs, M., Maresch, W.V., Schertl, H.-P., Baumann, A., Draper, G., Idleman, B., Münker, C. & Trapp, E. (2007). The dynamics of intra-oceanic subduction zones: A direct comparison between fossil petrological evidence (Rio San Juan Complex, Dominican Republic) and numerical simulation. Lithos (in press).

Kretz, R. (1983). Symbols for rock-forming minerals. American Mineralogist 68, 277-279.

Kriegsman, L. M. (2001). Partial melting, partial melt extraction and partial back reaction in anatectic migmatites. Lithos 56, 75-96.

Kulachkov, L. V. & Leyva, R. C. (1990). Informe sobre los resultados de los trabajos de reconocimiento geológico para cuarzo filoniano en la parte oriental de Cuba. Unpublished report of the Instituto Superior Minero-Metalúrgico de Moa (Cuba).

Lambert, I. B. & Wyllie, P. J. (1972). Melting of gabbro (quartz-eclogite) wit excess water to 35 kilobars, with geological applications. Journal of Geology 80, 693-708.

Le Maitre, R. W. (ed), Streckeisen, A., Zanettin, B., Le Bas, M. J., Bonin, B., Bateman, P., Bellieni, G., Dudek, A., Efremova, S., Keller, J., Lameyre, J., Sabine, P. A., Schmid, R., Sørensen, H. & Woolley, A. R. (2002). Igneous Rocks: A Classification and Glossary of Terms. 2nd edition, Cambridge University Press, Cambridge, 236 pp.

Leake, B. E., Woolley, A. R., Arps, C. E. S,., Birch, W. D., Gilbert, M. C., Grice, J. D., Hawthorne, F .C., Kato, A., Kisch, H. J., Krivovichev, V. G., Linthout, K., Laird, J., Mandarino, J. A., Maresch, W. V., Nickel, E. H., Rock, N. M. S., Schumacher, J. C., Smith, D. C., Stephenson, N. C. N., Ungaretti, L., Whittaker, E. J. W. & Touzhi, G. (1997). Nomenclature of amphiboles: Report of the Subcommittee on Amphiboles of the International Mineralogical Association, Commission on New Minerals and Mineral Names. American Mineralogist 82, 1019-1037.

Leyva, R. C. (1996). Características geológicas, regularidades de distribución y perspectivas de utilización del cuarzo filoniano de la región oriental de Cuba. Unpublished report of the Instituto Superior Minero-Metalúrgico de Moa (Cuba), 90 pp.

Manea, V. C., Manea, M., Kostoglodov, V. & Sewell, G. (2005). Thermo-mechanical model of the mantle wedge in Central Mexican subduction zone and a blob tracing approach for the magma transport. Physics of the Earth and Planetary Interiors 149, 165-186.

Marchesi, C., Garrido, C.J., Bosch, D., Proenza, J.A., Gervilla, F. Monié, P. & Rodríguez-Vega, A. (2007). Geochemistry of Cretaceous Magmatism in Eastern Cuba: Recycling of North American Continental Sediments and Implications for Subduction Polarity in the Greater Antilles Paleo-arc. Journal of Petrology 48, 1813-1840.

Martin, H. (1999). Adakitic magmas: modern analogues of Archaean granitoids. Lithos 46, 411-429.

Millán, G. (1996). Metamorfitas de la asociación ofiolítica de Cuba. In: Iturralde-Vinent, M. A. (ed.). Ofiolitas y Arcos Volcánicos de Cuba. Miami, USA, IGCP Project 364 Special Contribution 1, 131-146.

Millán, G. & Somin, M. L. (1985). Contribución al conocimiento geológico de las metamorfitas del Escambray y Purial. Reportes de Investigación de la Academia de Ciencias de Cuba 2, 1-74.

Millán, G., Somin M.L. & Díaz, C. (1985). Nuevos datos sobre la geología del macizo montañoso de la Sierra del Purial, Cuba Oriental. Reporte de Investigación del Instituto de Geología y Paleontología 2, 52-74.

Morimoto, N., Fabries, J., Ferguson, A. K., Ginzburg, I. V., Ross, M., Seifert, F. A., Zussman, J., Aoki, K. & Gottardi, G. (1988). Nomenclature of pyroxenes: Report of the Subcommittee on Pyroxenes of the International Mineralogical Association, Commission on New Minerals and Mineral Names. American Mineralogist 73, 1123-1133.

Nakajima, K. & Arima, M. (1998). Melting experiments on hydrous low-K tholeiite: Implications for the genesis of tonalitic crust in the Izu-Bonin - Mariana arc. The Island Arc 7, 359-373.

O'Connor, J. T. (1965). A classification of quartz-rich igneous rocks based on feldspar ratios. U.S. Geological Survey Professional Paper 525B, B79-B84.

Okudaira, T. & Yoshitake. Y. (2004). Thermal consequences of the formation of a slab window beneath the Mid-Cretaceous southwest Japan arc: A 2-D numerical analysis. The Island Arc 13, 520-532.

Peacock, S. M. (2003). Thermal structure and metamorphic evolution of subducting slabs. In Eiler, J. (ed.) Inside the Subduction Factory. Geophysical Monograph 138, American Geophysical Union, Washington, D.C, p. 7-22.

Peacock, S. M., Rushmer, T. & Thompson, A. B. (1994). Partial melting of subducting oceanic crust. Earth and Planetary Science Letters 121, 227-244.

Pindell, J. L, Kennan, L., Maresch, W. V., Stanek, K. P., Draper, G. & Higgs, R. (2005). Plate-kinematics and crustal dynamics of circum-Caribbean arc-continent interactions: Tectonic controls on basin development in Proto-Caribbean margins. In: Avé Lallemant, H.G. & Sisson, V.B. (eds.) Caribbean-South American plate interactions, Venezuela. Geological Society of America Special Paper 394, 7-52.

Pindell, J. L, Kennan, L., Stanek, K. P., Maresch, W. V. & Draper, G. (2006). Foundations of Gulf of Mexico and Caribbean evolution: eight controversies resolved. Geologica Acta 4, 303-341.

Powell, R. & Holland, T. J. B. (1994). Optimal geothermometry and geobarometry. American Mineralogist 79, 120-133.

Proenza, J. A., Díaz-Martínez, R., Iriondo, A., Marchesi, C., Melgarejo, J. C., Gervilla, F., Garrido, C. J., Rodríguez-Vega, A., Lozano-Santacruz, R. & Blanco-Moreno, J. A. (2006). Primitive Cretaceous island-arc volcanic rocks in eastern Cuba: the Téneme Formation. Geologica Acta 4, 103-121.

Prouteau, G., Scaillet, B., Pichavant, M. & Maury, R.C. (2001). Evidence for mantle metasomatism by hydrous silicic melts derived from subducted oceanic crust. Nature 410, 197-200.

Quirion, D. M. & Jenkins, D. M. (1998). Dehydration and partial melting of tremolitic amphibole coexisting with zoisite, quartz, anorthite, diopside and water in the system H_2O-CaO-MgO-Al_2O_3-SiO_2. Contributions to Mineralogy and Petrology 130, 379-389.

Rapp, R. P., Watson, E. B. & Miller, C. F. (1991). Partial melting of amphibolite/eclogite and the origin of Archean trondhjemites and tonalites. Precambrian Research 51, 1-25.

Rojas-Agramonte, Y., Neubauer, F., Handler, R., García-Delgado, D. E., Friedl, G. & Delgado-Damas, R. (2005). Variation of paleostress patterns along the Oriente Transform Fault, Cuba: Significance for Neogene-Quaternary tectonics of the Caribbean realm. Tectonophysics 396, 161–180.

Schmidt, M. W. & Poli, S. (1998). Experimentally based water budgets for dehydrating slabs and consequences for arc magma generation. Earth and Planetary Science Letters 163, 361-379.

Schmidt, M. W. & Poli, S. (2004). Magmatic epidote. Reviews in Mineralogy & Geochemistry 56, 399-430.

Selbekk, R. S. & Skjerlie, K. P. (2002). Petrogenesis of the anorthosite dyke swarm of Tromsø, North Norway: Experimental evidence for hydrous anatexis of an alkaline mafic complex. Journal of Petrology 43, 943-962.

Smithies, R. H. (2000). The Archaean tonalite-trondhjemite-granodiorite (TTG) series is not an analogue of Cenozoic adakite. Earth and Planetary Science Letters 182, 115-125.

Somin, M. L. & Millán, G. (1981). Geology of the Metamorphic Complexes of Cuba. Moscow, Nauka, 219 pp. (in Russian).

Somin, M. L., Arakelyants, M. M. & Kolesnikov, E. M. (1992). Age and tectonic significance of high-pressure metamorphic rocks in Cuba. International Geology Review 34, 105-118.

Sorensen, S. S. (1988). Petrology of amphibolite-facies mafic and ultramafic rocks from the Catalina Schist, Southern California: metasomatism and migmatization in a subduction zone metamorphic setting. Journal of Metamorphic Geology 6, 405-435.

Sorensen, S. S. & Barton, M. D. (1987). Metasomatism and partial melting in a subduction complex: Catalina Schist, southern California. Geology 15, 115-118.

Sorensen, S. S. & Grossman, J. N. (1989). Enrichment in trace elements in garnet amphibolites from a paleo-subduction zone: Catalina Schist, southern California. Geochimica et Cosmochimica Acta 53, 3155-3177.

Spear, F. S. (1993). Metamorphic Phase Equilibria and Pressure-Temperature-Time Paths. Mineralogical Society of America Monographs, Washington, D. C. 799 p

Springer, W. & Seck, H. A. (1997). Partial fusion of basic granulites at 5 to 15 kbar: implications for the origin of TTG magmas. Contributions to Mineralogy and Petrology 127, 30-45.

Staudigel, H., Plank, T., White, B. & Schmincke, H. U. (1996). Geochemical fluxes during seafloor alteration of the upper oceanic crust: DSDP sites 417-418. In: Bebout, G. E., Scholl, D. W., Kirby, S. H. & Platt, J. P. (eds) Subduction top to bottom. Geophysical Monograph, American Geophysical Union, Washington, D.C., 96, 19-38.

Stern, R. J. (2002). Subduction zones. Reviews of Geophysics 40, (art. no.-1012, doi:10.1029/2001RG000108).

Stern, C. R. & Kilian, R. (1996). Role of the subducted slab, mantle wedge and continental crust in the generation of adakites from the Andean Austral Volcanic Zone. Contributions to Mineralogy and Petrology 123, 263-281.

Stolz, A. J., Jochum, K. P., Spttel, B. & Hofman, A. W. (1996). Fluid- and melt-related enrichment in the subarc mantle: evidence from Nb/Ta variations in island-arc basalts. Geology 24, 587-590.

Thompson, A. B. & Ellis, D. (1994). $CaO+MgO+Al_2O_3+SiO_2+H_2O$ to 35 kb: Amphibole, talc, and zoisite dehydration and melting reactions in the silica-excess part of the system and their possible significance in subduction zones, amphibole melting, and magma fractionation. American Journal of Science 294, 1229-1289.

Torres-Roldán, R. L., García-Casco, A. & García-Sánchez, P. A. (2000). CSpace: An integrated workplace for the graphical and algebraic analysis of phase assemblages on 32-bit Wintel platforms. Computers and Geosciences 26, 779-793.

Uehara, S. & Aoya, M. (2005). Thermal model for approach of a spreading ridge to subduction zones and its implications for high-P/high-T metamorphism: Importance of subduction versus ridge approach ratio. Tectonics 24, TC4007, doi: 10.1029/2004TC001715.

van Keken, P. E., Kiefer, B. & Peacock, S. M. (2002). High-resolution models of subduction zones: Implications for mineral dehydration reactions and the transport of water into the deep mantle. Geochemistry Geophysics Geosystems 3, 1056, doi: 10.1029/2001GC000256.

Vielzeuf, D. & Schmidt, M. W. (2001). Melting reactions in hydrous systems revisited: applications to metapelites, metagreywackes and metabasalts. Contributions to Mineralogy and Petrology 141, 251-267.

Winther, K. T. & Newton, R. C. (1991). Experimental melting of hydrous low-K tholeiite: evidence on the origin of Archaean cratons. Bulletin of the Geological Society of Denmark 39, 213-228.

Yoder, H. S. Jr. & Tilley, C. E. (1962). Origin of basalt magmas; an experimental study of natural and synthetic rock systems. Journal of Petrology 3, 342-532.

Yogodzinski, G. M., Lees, J. M., Churikova, T. G., Dorendorf, F., Wörner, G. & Volynets, O. N. (2001). Geochemical evidence for the melting of subducting oceanic lithosphere at plate edges. Nature 409, 500-504.

Table 3. Representative analyses of calcic amphibole (normalized to 22 O and 2 OH).

Rock type	amphibolites												trondhjemites					
Samp	CV228D		CV228E		CV230B		CV237J		CV53B-I		CV62B-I		CV228C		CV62B-II		SC21	
Type	peak	retro	peak	retro	peak	retro	peak	retro	peak	retro	peak	retro	peak	retro	peak	retro	peak	retro
SiO_2	42.04	46.59	42.64	46.42	42.94	54.45	42.53	53.82	44.58	49.59	44.01	51.13	42.16	54.02	45.44	53.36	42.90	55.22
TiO_2	2.47	0.32	0.78	0.35	0.97	0.01	1.05	0.08	0.68	0.36	0.64	0.24	1.61	0.51	0.57	0.20	1.07	0.06
Al_2O_3	13.72	11.24	14.38	11.02	13.45	1.93	13.31	2.62	13.16	7.50	15.59	8.04	16.72	3.86	15.56	7.38	16.29	4.03
FeO_{total}	15.55	15.31	15.13	14.30	13.57	12.03	16.70	14.61	13.01	12.78	11.47	10.11	10.32	3.95	8.02	3.30	9.68	2.71
MnO	0.22	0.21	0.18	0.18	0.15	0.20	0.05	0.11	0.20	0.22	0.24	0.23	0.22	0.41	0.16	0.13	0.11	0.04
MgO	10.12	10.99	10.25	11.74	11.18	15.77	9.62	14.10	11.96	13.84	12.06	15.43	11.84	21.17	14.02	19.57	12.57	21.69
CaO	10.10	9.07	10.20	9.68	11.49	11.23	11.13	11.00	10.01	10.09	9.93	9.66	10.54	12.01	10.29	11.55	10.50	12.27
BaO	0.08	0.00	0.00	0.23	0.02	0.04	0.01	0.00	0.04	0.00							0.00	0.00
Na_2O	2.79	2.66	3.03	2.90	2.43	0.89	3.09	1.29	3.23	2.43	3.34	2.56	3.73	0.97	3.47	1.73	3.38	1.02
K_2O	0.45	0.37	0.45	0.26	0.46	0.10	0.07	0.04	0.34	0.20	0.40	0.13	0.29	0.10	0.39	0.12	0.26	0.07
H_2O(*)	2.02	2.04	2.02	2.05	2.02	2.08	2.01	2.08	2.05	2.07	2.08	2.12	2.06	2.16	2.11	2.17	2.06	2.18
Total	99.55	98.80	99.06	99.12	98.67	98.73	99.56	99.75	99.26	99.07	99.76	99.65	99.50	99.17	100.03	99.50	98.83	99.27
Si	6.23	6.83	6.32	6.80	6.39	7.85	6.35	7.77	6.52	7.19	6.35	7.24	6.13	7.51	6.45	7.37	6.23	7.61
Ti	0.28	0.03	0.09	0.04	0.11	0.00	0.12	0.01	0.08	0.04	0.07	0.03	0.18	0.05	0.06	0.02	0.12	0.01
Al	2.40	1.94	2.51	1.90	2.36	0.33	2.34	0.45	2.27	1.28	2.65	1.34	2.87	0.63	2.60	1.20	2.79	0.65
Fe^{3+}	0.31	0.41	0.30	0.30	0.13	0.11	0.16	0.14	0.28	0.26	0.27	0.30	0.08	0.23	0.15	0.07	0.16	0.14
Fe^{2+}	1.61	1.47	1.58	1.45	1.56	1.34	1.93	1.62	1.31	1.29	1.11	0.90	1.17	0.23	0.80	0.31	1.01	0.18
Mn	0.03	0.03	0.02	0.02	0.02	0.02	0.01	0.01	0.02	0.03	0.03	0.03	0.03	0.05	0.02	0.01	0.01	0.00
Mg	2.23	2.40	2.27	2.57	2.48	3.39	2.14	3.04	2.61	2.99	2.59	3.26	2.57	4.39	2.97	4.03	2.72	4.45
Ca	1.60	1.42	1.62	1.52	1.83	1.74	1.78	1.70	1.57	1.57	1.53	1.47	1.64	1.79	1.56	1.71	1.63	1.81
Ba	0.00	0.00	0.00	0.01	0.00	0.00	0.00	0.00	0.00	0.00							0.00	0.00
Na	0.80	0.76	0.87	0.82	0.70	0.25	0.89	0.36	0.91	0.68	0.93	0.70	1.05	0.26	0.96	0.46	0.95	0.27
K	0.08	0.07	0.08	0.05	0.09	0.02	0.01	0.01	0.06	0.04	0.07	0.02	0.05	0.02	0.07	0.02	0.05	0.01
Mg#	0.58	0.62	0.59	0.64	0.61	0.72	0.53	0.65	0.66	0.70	0.70	0.78	0.69	0.95	0.79	0.93	0.73	0.96

(*)Calculated by stoichiometry.

Table 4. Representative analyses of sodic amphibole (normalized to 22 O and 2 OH).

Sample	CV228D	CV228E	CV230B	CV237J	CV53B-I	CV62B-I
SiO_2	54.92	55.98	56.54	56.35	57.77	57.10
TiO_2	0.12	0.30	0.09	0.02	0.06	0.16
Al_2O_3	9.73	10.04	11.07	10.67	11.28	10.45
FeO_{total}	15.23	13.74	12.70	13.48	10.92	11.85
MnO	0.13	0.16	0.11	0.02	0.09	0.10
MgO	8.11	8.97	8.60	8.48	9.78	9.98
CaO	1.82	1.76	1.28	1.57	0.30	1.47
BaO	0.00	0.03	0.00	0.00	0.02	
Na_2O	6.52	6.61	6.84	6.66	7.32	6.68
K_2O	0.04	0.02	0.02	0.04	0.00	0.02
H_2O(*)	2.10	2.14	2.15	2.14	2.18	2.17
Total	98.71	99.76	99.40	99.42	99.71	99.98
Si	7.84	7.85	7.90	7.90	7.95	7.89
Ti	0.01	0.03	0.01	0.00	0.01	0.02
Al	1.64	1.66	1.82	1.76	1.83	1.70
Fe^{3+}	0.18	0.16	0.08	0.09	0.12	0.16
Fe^{2+}	1.64	1.46	1.41	1.49	1.13	1.21
Mn	0.02	0.02	0.01	0.00	0.01	0.01
Mg	1.73	1.87	1.79	1.77	2.01	2.06
Ca	0.28	0.27	0.19	0.24	0.04	0.22
Ba	0.00	0.00	0.00	0.00	0.00	
Na	1.81	1.80	1.85	1.81	1.95	1.79
K	0.01	0.00	0.00	0.01	0.00	0.00
Mg#	0.51	0.56	0.56	0.54	0.64	0.63

(*)Calculated by stoichiometry.

Table 5. Representative analyses of garnet (normalized to 12 O) and clinopyroxene (normalized to 6 O).

Phase	garnet								Ca-Cpx	Omp
Sample	CV228D		CV228E		CV230B		CV237J		CV237J	
Type	peak	retro	peak	retro	peak	retro	peak	retro	peak	retro
SiO_2	37.31	37.57	37.74	37.44	37.83	37.63	37.90	37.86	50.86	54.60
TiO_2	0.27	0.03	0.20	0.07	0.07	0.07	0.07	0.21	0.30	0.75
Al_2O_3	21.33	21.28	21.48	21.31	21.32	21.56	21.33	20.91	3.35	9.14
FeO_{total}	25.37	27.13	24.74	26.15	21.90	21.95	25.16	16.86	11.18	8.21
MnO	2.56	2.83	2.49	3.12	1.28	1.99	1.11	3.93	0.13	0.05
MgO	4.44	2.97	4.79	3.23	3.62	2.96	3.81	0.19	11.04	6.60
CaO	8.16	7.89	8.79	8.58	13.03	13.46	10.15	19.69	21.69	13.86
Na_2O									1.09	6.66
Total	99.44	99.69	100.23	99.91	99.04	99.62	99.53	99.65	99.62	99.85
Si	2.94	2.99	2.94	2.96	2.97	2.95	2.98	2.98	1.91	1.98
Ti	0.02	0.00	0.01	0.00	0.00	0.00	0.00	0.01	0.01	0.02
Al	1.98	1.99	1.97	1.99	1.98	1.99	1.98	1.94	0.15	0.39
Fe^{3+}	0.10	0.03	0.11	0.08	0.07	0.09	0.05	0.06	0.09	0.08
Fe^{2+}	1.58	1.77	1.50	1.65	1.37	1.35	1.61	1.05	0.27	0.17
Mn	0.17	0.19	0.16	0.21	0.08	0.13	0.07	0.26	0.00	0.00
Mg	0.52	0.35	0.56	0.38	0.42	0.35	0.45	0.02	0.62	0.36
Ca	0.69	0.67	0.73	0.73	1.10	1.13	0.86	1.66	0.87	0.54
Na									0.08	0.47
Mg#	0.25	0.17	0.27	0.19	0.24	0.20	0.22	0.02	0.70	0.68

Table 6. Representative analyses of epidote (normalized to 12 O and 1 OH).

Type of rock	amphibolite						trondhjemite								
Sample	CV228D	CV228E	CV230B	CV237J	CV53B-I	CV62B-I	CV228C		CV53B-II		CV60A	CV62B-II		SC21	
Type	peak	peak	peak	peak	peak	peak	peak	retro	peak	retro	peak	peak	retro	peak	retro
SiO_2	37.96	38.11	38.73	38.42	37.93	38.46	38.63	40.21	38.05	38.95	39.31	38.73	39.67	38.89	39.36
TiO_2	0.22	0.22	0.04	0.12	0.14	0.23	0.18		0.10	0.00	0.04	0.17	0.02	0.15	0.01
Al_2O_3	27.05	27.50	31.91	27.25	26.68	26.59	27.87	32.74	28.36	32.59	32.73	28.16	33.46	28.92	33.18
FeO_{tot}	8.85	7.88	2.11	7.63	8.38	8.65	6.18	0.91	6.26	1.22	0.96	6.62	0.24	6.12	0.46
MnO	0.17	0.16	0.04	0.09	0.49	0.15	0.10		0.19	0.01	0.01	0.20	0.00	0.15	0.05
MgO	0.10	0.13	0.02	0.01	0.03	0.17	0.18	0.06	0.09	0.01	0.03	0.15	0.03	0.20	0.02
CaO	23.32	23.39	24.29	23.64	23.38	23.05	23.13	24.72	23.81	24.54	23.95	23.07	24.36	23.30	24.01
BaO			0.02	0.04			0.00		0.00	0.00	0.00			0.03	0.03
H_2O(*)	1.92	1.92	1.95	1.92	1.91	1.92	1.92	1.99	1.92	1.96	1.96	1.93	1.98	1.95	1.96
Total	99.58	99.31	99.12	99.12	98.94	99.22	98.18	100.63	98.77	99.29	98.99	99.03	99.75	99.70	99.09
Si	2.96	2.97	2.98	3.00	2.98	3.00	3.02	3.03	2.97	2.98	3.01	3.01	3.01	3.00	3.00
Ti	0.01	0.01	0.00	0.01	0.01	0.01	0.01		0.01	0.00	0.00	0.01	0.00	0.01	0.00
Al	2.48	2.53	2.89	2.51	2.47	2.45	2.57	2.90	2.61	2.94	2.95	2.58	2.99	2.63	2.98
Fe^{3+}	0.58	0.51	0.14	0.50	0.55	0.56	0.40	0.06	0.41	0.08	0.06	0.43	0.02	0.39	0.03
Mn	0.01	0.01	0.00	0.01	0.03	0.01	0.01		0.01	0.00	0.00	0.01	0.00	0.01	0.00
Mg	0.01	0.02	0.00	0.00	0.00	0.02	0.02	0.01	0.01	0.00	0.00	0.02	0.00	0.02	0.00
Ca	1.95	1.95	2.00	1.98	1.97	1.93	1.94	1.99	1.99	2.01	1.96	1.92	1.98	1.92	1.96
Ba			0.00	0.00			0.00		0.00	0.00	0.00			0.00	0.00

(*)Calculated by stoichiometry.

Table 7. Representative analyses of feldspars (normalized to 8 O).

Phase	plagioclase														Kfs
Type of rock	amphibolite				trondhjemite										trondhj.
Sample	CV230 B	CV237 J	CV53B -I	CV62B -I	CV228C		CV53B-II		CV60A		CV62B-II		SC21		SC21
Type	retro	retro	retro	retro	peak	retro	peak	retro	peak	retro	peak	retro	peak	retro	retro
SiO_2	67.90	68.54	67.97	65.84	61.55	67.39	63.58	68.82	63.97	68.71	64.39	68.85	63.48	67.88	64.28
Al_2O_3	19.38	19.57	19.37	20.60	23.41	20.07	22.19	19.30	22.37	19.34	22.41	19.64	22.61	19.84	18.18
FeO_{total}	0.05	0.30	0.14	0.32	0.00	0.03	0.03	0.02	0.00	0.00	0.03	0.01	0.01	0.02	0.02
MnO	0.00	0.00	0.01			0.00					0.00	0.01	0.01	0.00	0.01
CaO	0.02	0.07	0.19	1.09	5.89	0.60	3.53	0.04	3.62	0.01	3.27	0.08	3.77	0.41	0.01
BaO	0.00	0.01	0.00			0.00	0.01	0.01	0.00	0.00			0.02	0.00	0.07
Na_2O	11.77	11.81	11.60	10.76	8.21	11.34	9.76	11.67	9.73	11.80	9.85	11.85	9.49	11.70	0.05
K_2O	0.02	0.01	0.01	0.47	0.04	0.01	0.05	0.03	0.02	0.00	0.05	0.02	0.04	0.03	16.72
Total	99.14	100.31	99.29	99.08	99.10	99.45	99.15	99.89	99.72	99.87	100.00	100.47	99.43	99.89	99.35
Si	2.99	2.99	2.99	2.92	2.75	2.96	2.83	3.01	2.83	3.00	2.84	2.99	2.82	2.97	3.00
Al	1.01	1.00	1.00	1.08	1.23	1.04	1.16	0.99	1.17	1.00	1.16	1.01	1.18	1.02	1.00
Fe^{3+}	0.00	0.01	0.00	0.01	0.00	0.00	0.00	0.00	0.00	0.00	0.00	0.00	0.00	0.00	0.00
Mn	0.00	0.00	0.00			0.00					0.00	0.00	0.00	0.00	0.00
Ca	0.00	0.00	0.01	0.05	0.28	0.03	0.17	0.00	0.17	0.00	0.15	0.00	0.18	0.02	0.00
Ba	0.00	0.00	0.00			0.00	0.00	0.00	0.00	0.00			0.00	0.00	0.00
Na	1.01	1.00	0.99	0.93	0.71	0.97	0.84	0.99	0.83	1.00	0.84	1.00	0.82	0.99	0.00
K	0.00	0.00	0.00	0.03	0.00	0.00	0.00	0.00	0.00	0.00	0.00	0.00	0.00	0.00	1.00

Table 8. Representative analyses of micas (normalized to 20 O and 4 OH).

Phase	paragonite									phengite							
Type of rock	trondhjemite									amphibolite		trondhjemite					
Sample	CV228C		CV53B-II		CV60A		CV62B -II	SC21		CV53B -I	CV62B -I	CV53B-II		CV60A		CV62B-II	
Type	peak	retro	peak	retro	peak	retro	peak	peak	retro	retro	retro	retro	retro	retro	retro	retro	retro
SiO_2	45.99	45.23	46.14	46.63	45.97	46.18	47.02	46.43	47.46	51.96	52.29	49.84	52.28	46.89	52.27	46.24	52.28
TiO_2	0.07	0.14	0.02	0.00	0.29	0.05	0.21	0.17	0.10	0.07	0.09	0.03	0.01	0.13	0.04	0.08	0.01
Al_2O_3	39.95	40.70	39.58	39.89	39.83	40.57	40.13	39.06	39.70	25.42	25.83	29.22	26.33	36.19	26.32	36.88	26.48
FeO_{total}	0.41	0.27	0.35	0.29	0.27	0.13	0.50	0.39	0.21	2.28	1.92	1.46	1.47	0.38	1.25	0.13	1.22
MnO							0.01	0.02	0.00	0.04	0.00	0.02	0.04			0.00	0.01
MgO	0.14	0.13	0.16	0.27	0.19	0.16	0.21	0.26	0.35	4.05	4.04	2.85	3.88	0.71	4.13	0.63	4.17
CaO	0.77	0.79	0.35	0.36	0.86	0.34	0.49	0.42	0.22	0.03	0.04	0.02	0.00	0.08	0.06	0.05	0.02
BaO			0.12	0.03	0.06	0.06		0.25	0.02	0.29		0.46	0.16	0.21	0.48		
Na_2O	6.73	7.37	6.77	7.22	6.73	7.33	6.64	6.25	7.31	0.24	0.23	0.47	0.26	0.58	0.23	0.59	0.26
K_2O	0.97	0.19	1.36	0.55	1.08	0.55	0.96	2.11	0.67	11.09	10.84	10.74	10.88	10.42	10.66	10.44	10.93
H_2O(*	4.67	4.67	4.65	4.69	4.67	4.70	4.73	4.66	4.74	4.48	4.50	4.48	4.51	4.54	4.51	4.53	4.52
Total	99.70	99.48	99.50	99.95	99.97	100.08	100.90	100.01	100.78	99.94	99.78	99.58	99.83	100.15	99.95	99.58	99.88
Si	5.91	5.81	5.95	5.96	5.90	5.89	5.96	5.98	6.01	6.95	6.96	6.67	6.95	6.19	6.94	6.12	6.93
Ti	0.01	0.01	0.00	0.00	0.03	0.00	0.02	0.02	0.01	0.01	0.01	0.00	0.00	0.01	0.00	0.01	0.00
Al	6.05	6.17	6.01	6.01	6.02	6.10	5.99	5.93	5.93	4.01	4.05	4.61	4.13	5.63	4.12	5.76	4.14
Fe^{3+}																	
Fe^{2+}	0.04	0.03	0.04	0.03	0.03	0.01	0.05	0.04	0.02	0.25	0.21	0.16	0.16	0.04	0.14	0.01	0.14
Mn							0.00	0.00	0.00	0.00	0.00	0.00	0.00			0.00	0.00
Mg	0.03	0.02	0.03	0.05	0.04	0.03	0.04	0.05	0.07	0.81	0.80	0.57	0.77	0.14	0.82	0.12	0.82
Ca	0.11	0.11	0.05	0.05	0.12	0.05	0.07	0.06	0.03	0.00	0.01	0.00	0.00	0.01	0.01	0.01	0.00
Ba			0.01	0.00	0.00	0.00		0.01	0.00	0.02		0.02	0.01	0.01	0.03		
Na	1.68	1.84	1.69	1.79	1.67	1.81	1.63	1.56	1.80	0.06	0.06	0.12	0.07	0.15	0.06	0.15	0.07
K	0.16	0.03	0.22	0.09	0.18	0.09	0.16	0.35	0.11	1.89	1.84	1.83	1.85	1.75	1.81	1.76	1.85
Mg#	0.38	0.46	0.44	0.62	0.56	0.70	0.42	0.55	0.74	0.76	0.79	0.78	0.83	0.77	0.85	0.90	0.86

(*)Calculated by stoichiometry.

Table 9. Representative analyses of chorite (normalized to 20 O and 16 OH).

Type of rock	amphibolite						trondhjemite			
Sample	CV228D	CV228E	CV230B	CV237J	CV53B-I	CV62B-I	CV228C	CV60A	CV62B-II	SC21
SiO_2	25.99	26.36	27.29	26.38	27.85	28.61	29.84	29.38	30.59	29.38
Al_2O_3	20.63	20.61	20.45	18.47	19.10	20.44	19.86	19.77	20.47	20.40
FeO_{total}	22.94	23.02	21.86	27.51	20.08	17.57	14.22	14.62	9.02	12.48
MnO	0.19	0.35	0.26	0.08	0.27	0.26	0.04	0.21	0.18	0.16
MgO	17.73	17.58	17.56	14.80	19.86	21.08	23.71	23.15	27.43	24.83
H_2O(*)	11.52	11.56	11.60	11.19	11.66	11.97	12.17	12.05	12.51	12.20
Total	99.01	99.47	99.01	98.43	98.82	99.93	99.84	99.18	100.21	99.44
Si	5.42	5.47	5.64	5.66	5.73	5.73	5.88	5.85	5.87	5.78
Al	5.07	5.04	4.98	4.67	4.63	4.83	4.61	4.64	4.63	4.73
Fe^{2+}	4.00	3.99	3.78	4.93	3.46	2.94	2.34	2.43	1.45	2.05
Mn	0.03	0.06	0.05	0.02	0.05	0.04	0.01	0.03	0.03	0.03
Mg	5.51	5.44	5.41	4.73	6.09	6.30	6.97	6.87	7.84	7.28
Mg#	0.58	0.58	0.59	0.49	0.64	0.68	0.75	0.74	0.84	0.78

(*)Calculated by stoichiometry.

Table 10. Representative analyses of pumpellyite (normalized to 28 O and 7 H), lawsonite (normalized to 10 O and 4H), and kyanite (normalized to 5 O).

Phase	pumpellyite				lawsonite		kyanite	
Type of rock	Amphibolite		trondhjemite		trondhjemite		trondhjemite	
Sample	CV230B	CV53B-I	CV228C	CV60A	CV228C	CV60A	CV53F	CV60A
Type	retro	retro	retro	retro	retro	retro	peak	peak
SiO_2	36.86	36.80	38.40	37.70	38.97	38.43	36.06	36.57
TiO_2	0.20	0.07	0.20	0.16	0.05	0.11	0.01	0.04
Al_2O_3	25.27	26.16	25.03	26.16	31.87	32.27	62.48	62.56
FeO_{total}	2.56	2.65	2.30	1.78	0.02	0.04	0.60	0.40
MnO	0.99	0.61	0.59	0.45	0.00	0.00	0.00	0.00
MgO	3.45	3.26	3.96	3.45				
CaO	22.99	23.09	21.16	22.65	18.35	17.53		
BaO		0.00	0.01	0.02	0.00	0.00		
Na_2O		0.19	0.41	0.18				
K_2O		0.00	0.01	0.00				
H_2O(*)	6.53	6.58	6.55	6.58	11.54	11.46		
Total	98.85	99.41	98.60	99.14	100.73	99.84	99.14	99.57
Si	5.96	5.91	6.16	6.02	2.03	2.01	0.98	0.99
Ti	0.02	0.01	0.02	0.02	0.00	0.00	0.00	0.00
Al	4.82	4.95	4.73	4.93	1.95	1.99	2.01	2.00
Fe^{3+}	0.00	0.00	0.00	0.00	0.00	0.00	0.01	0.01
Fe^{2+}	0.35	0.36	0.31	0.24				
Mn	0.14	0.08	0.08	0.06	0.00	0.00	0.00	0.00
Mg	0.83	0.78	0.95	0.82				
Ca	3.99	3.98	3.64	3.88	1.02	0.98		
Ba		0.00	0.00	0.00	0.00	0.00		
Na		0.06	0.13	0.06				
K		0.00	0.00	0.00				
Mg#	0.71	0.69	0.75	0.78				

(*)Calculated by stoichiometry (including OH and H_2O).

Chapter III. Geochemistry

This Chapter has been submitted to ***Chemical Geology***

Geochemical and Sr-Nd isotope signatures of pristine slab melts and their residues (Sierra del Convento mélange, eastern Cuba)

C. LÁZARO[(1)] A. GARCÍA-CASCO[(1)]

(1) Departamento de Mineralogía y Petrología, Universidad de Granada
Fuentenueva s/n, 18002-Granada, Spain Lázaro E-mail: clazaro@ugr.es García-Casco E-mail: agcasco@ugr.es

ABSTRACT

Major and trace element geochemical signatures and Sr-Nd isotope data of MORB-like amphibolite blocks and associated leucocratic low-K trondhjemitic rocks from the Sierra del Convento mélange (Cuba) indicate that oceanic crust underwent partial melting processes during subduction. Theoretical melting models suggest that the trondhjemites are not oceanic plagiogranite formed after differentiation or partial melting of MORB at oceanic ridges, but instead they formed by water-saturated melting of an oceanic crust under hot subduction conditions. REE patterns of the trondhjemites are fractionated ($1 < (La/Yb)_n < 16.8$), with LREE enrichment and flat or slightly depleted HREE patterns which compare well with adakitic melts formed by partial melting of mafic material at moderate to high pressure. Indeed, trondhjemites from Sierra del Convento have some of the geochemical features of Cenozoic adakites, including SiO_2>56%, 3.5%<Na_2O<7.5%, (K_2O/Na_2O) ≈ 0.42, Mg# ≈ 50, Ni =20-40 ppm, Cr =30-50 ppm, LREE enrichment, HREE depletion, and high La/Yb and Sr/Y. However, the trondhjemites from Sierra del Convento are more comparable to acid rocks from Catalina Schist mélange (California) considered to be primary slab melts which did not react with the mantle wedge. In agreement with major and trace element geochemistry, the Sr-Nd isotope systematic of selected amphibolites and trondhjemites can be explained by a two stage model involving a) generation of MORB-like basalts and b) partial melting of subducted MORB.

KEYWORDS: slab melt; adakite; partial melting modeling; subduction; MORB; Sr-Nd isotopes.

INTRODUCTION

Kay (1978) identified a distinctive rock type, a magnesian andesite significantly different from boninite, in the volcanic arc rocks of Adak Island (Aleutian Islands) which defined as a new magma type and latter termed adakite (Martin, 1986; Defant and Drummond, 1990). Adakites are andesites and dacites characterized by low heavy rare earth element (HREE) contents combined with high Sr values, and have been shown to crop out in many oceanic and continental volcanic arcs, (e.g. Smith and Leeman, 1987; Defant et al., 1992; Morris, 1995; Sajona et al., 1996; Stern and Kilian, 1996; Sajona et al., 2000; Beate et al., 2001; Benoit et al., 2002; Bourdon et al., 2002; Bourdon et al., 2003; Samaniego et al., 2005; Stevenson et al., 2005). Their origin is generally considered to be the result of partial melting of subducted oceanic crust.

Under normal subduction zones the geothermal conditions of the slab may not attain P-T conditions for melting at sub-arc depths, but dehydrates and release large ion lithophile element (LILE)-enriched hydrous fluids that metasomatize the overlying mantle wedge and instigate its melting (e.g. Gill, 1981; Kushiro, 1990; Tatsumi and Kogiso, 1997). However, when the subducting slab is anomalously hot, the geothermal gradient may intersect the wet solidus of amphibolite/eclogite allowing the production of slab melts. Such hot conditions can be generated in the cases of subduction of young oceanic lithosphere (Defant and Drummond, 1990), due to fast and oblique (Yogodzinski et al., 1995; 2001), or flat subduction (Gutscher et al., 2000), while the H_2O-present conditions are attained when the slab is fluxed by water from subjacent hydrous lithologies (Prouteau et al., 1999; 2001).

Experiments have shown that melt compositions produced by water-saturated melting of metabasite show a great sensitivity to pressure, producing trondhjemitic (for 10-20 kbar) to tonalitic melts (for 30 kbar) (Prouteau et al., 1999; 2001). The origin of the free water may be dehydration of serpentinite underlying the oceanic crust. During ascent to the surface, slab melts will react with the hot mantle peridotite through which they migrate, thus changing their composition, and may even be entirely consumed via metasomatism (Beard et al., 1993; Rapp et al., 1999; Kilian and Stern, 2002; Kelemen et al., 2004). In particular, Na depletion in Cenozoic adakites relative to experimentally produced melts of hydrated basalt under P-T conditions comparable to adakite generation have recently been related to melt/rock reaction within the mantle wedge (Xiong et al., 2006).

Thus, examples of pristine slab melts reaching the Earth's surface are scarce. Only in rare cases of subduction complexes, such as the Catalina Schist mélange (California), partial melting of metabasite and metasomatic mass-transfer processes in the slab have been described (Sorensen, 1988; Sorensen and Grossman, 1989; Bebout and Barton, 1993; Grove and Bebout, 1995). The tonalitic-trondhjemitic melts produced in this mélange have been considered as primary adakitic liquids (e.g., Martin, 1999) generated at intermediate pressures due to the onset of hot subduction.

In this paper, we characterize the major, trace, and Sr-Nd isotope geochemistry of pristine primary melts and residual rocks produced in a hot subduction scenario. To this end, we use the example of the Sierra del Convento mélange (Eastern Cuba), where partial melting of a subducting slab has recently been described (García-Casco, 2005; García-Casco et al., submitted 2007). This mélange represents a subduction channel related to Mesozoic subduction in the northern margin of the Caribbean plate. Outcrop scale structures, mineral textures and compositions, P-T conditions (García-Casco et al., submitted 2007), and the major, trace, and isotope geochemical data presented in this paper indicate that subducted oceanic metabasites suffered wet-melting processes during subduction and produced primary tonalitic-trondhjemitic liquids that were trapped in the subducting slab. Consequently, these melts did not react with the mantle, allowing a unique geochemical characterization of pristine slab melts.

GEOLOGICAL SETTING AND FIELD RELATIONS

The Greater Antilles constitute an orogenic belt at the northern margin of the Caribbean plate. This belt formed during the Mesozoic-Tertiary and includes oceanic complexes (ophiolites and intra-oceanic volcanic arcs) and continental (platform-derived) material. In Cuba, this belt is made of fragments of the North-American and Caribbean plates (Iturralde-Vinent, 1998), comprising continental material (Bahamas platform and Yucatan peninsula) and oceanic ophiolites and volcanic arc(s) (Fig. 1a). Isotopic ages of metamorphosed continental-derived rocks indicate that the beginning of the arc-continent collision started in the late Cretaceous (Iturralde-Vinent et al., 1996; García-Casco et al., 2001).

In eastern Cuba, the ophiolitic belt is formed by two large bodies, Mayarí and Moa-Baracoa, which show supra-subduction signatures (Proenza et al., 1998; 1999; Marchesi et al., 2006). Mélange complexes made of serpentinitic matrix enclosing high pressures metamorphic exotic blocks are also present at the base of these ophiolitic massifs. The ophiolitic bodies and the serpentinitic mélanges form the highest structural complexes in the region,

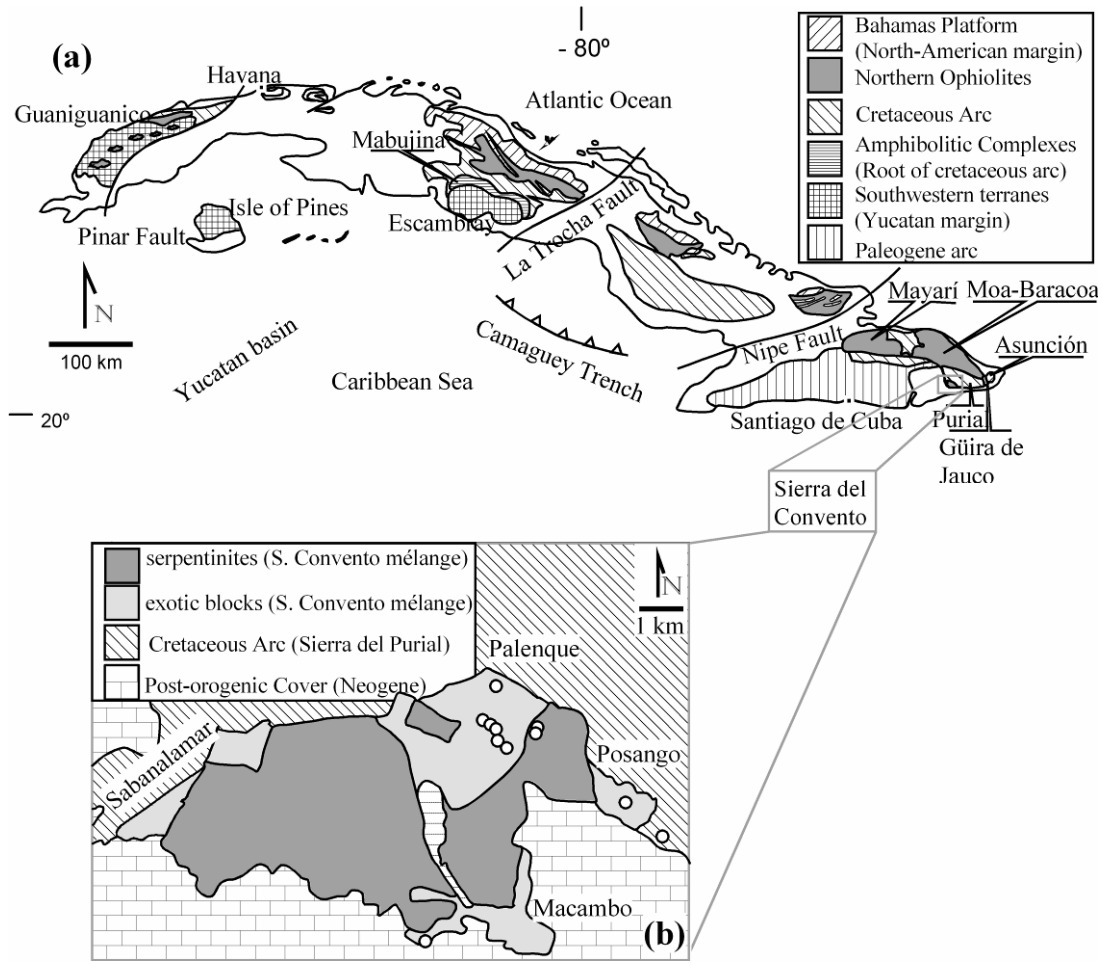

Fig. 1. (a) General geological map of Cuba (Iturralde-Vinent, 1998) showing the main geological units and (b) Geological map of Sierra del Convento (Kulachkov and Leyva, 1990) with location of sample sites.

overriding all other complexes. The Purial complex is composed of volcanic arc sequences which are generally metamorphosed to greenschist and, locally, to blueschist facies (Boiteau et al., 1972; Somin and Millán, 1981; Millán and Somin, 1985; Millán, 1996).

The Sierra del Convento mélange, located in the eastern part of the island (Fig. 1a), has a serpentinite matrix which includes exotic blocks of metamorphic rocks (Somin and Millán, 1981; Kulachkov and Leyva, 1990; Hernández and Canedo, 1995; Leyva, 1996; Millán, 1996; Blanco Quintero, 2003; García-Casco et al., 2006; submitted 2007). These blocks are preferentially concentrated in four different domains at the borders of a large mostly serpentinitic body (Fig. 1b). The ultramafic material show variable extent of serpentinization, ranging from serpentinized harzburgites bearing relicts of ortho- and clinopyroxene to serpentinites s.s. (Hernández and Canedo, 1995). Metamorphic exotic blocks are mainly amphibolites showing variable grain size and extent of deformation and recrystallization. They are foliated and mainly composed of amphibole + epidote ± quartz ± garnet. Hornblendites (following recent recommendations of the IUGS Subcommission on the Systematics of Metamorphic Rocks (Coutinho et al., 2007)) are a variety of these amphibolites made almost exclusively of medium to coarse grained amphibole. Leucocratic rocks of trondhjemitic-tonalitic composition are commonly associated with the amphibolites. These rocks typically appear as small veins or segregates within amphibolites, though locally they are larger and form metric-sized bodies which may have amphibolite enclaves (Figs. 2a and b). Agmatitic and stromatic structures, typical of migmatites, have also been recognized (Fig. 2b). The leucocratic rocks are formed by primary (magmatic) plagioclase + quartz + epidote ± paragonite ± amphibole, have variable grain size, and show minor deformation structures.

This paper examines the geochemistry of exotic blocks of amphibolites, hornblendites, and related leucocratic rocks (trondhjemites).

ANALYTICAL TECHNIQUES

Bulk-rock chemistry

Powered whole-rock samples were obtained by grinding in a tungsten carbide mill. Major element and Zr compositions were determined on glass beads, made of 0.6g of powered sample diluted in 6g of $Li_2B_4O_7$, by a PHILIPS Magix Pro (PW-2440) X-ray fluorescence (XRF) equipment at the University of Granada (Centro de Instrumentación Científica, CIC). Precision was better than ±1.5% for an analyte concentration of 10 wt.%. Precision for Zr and LOI is better than ±4% at 100 ppm concentration.

Trace element, except Zr, were determined at the University of Granada (CIC) by ICP-Mass Spectrometry (ICP-MS) after HNO_3 + HF digestion of 0.1000 g of sample powder in a Teflon-lined vessel at ~180ºC and ~200 p.s.i. for 30 min, evaporation to dryness, and subsequent dissolution in 100 ml of 4 vol.% HNO_3. Results for international standards PM-S and WS-E run as unknows during analytical sessions are shown in Table 1. Concentrations of these standards are not significantly different from recommended values (Govindaraju, 1994). Precision was better than ±2% and ±5% for analyte concentrations of 50 and 5 ppm.

Isotope analysis

Isotope analyses were carried out at the University of Granada (CIC). Whole rock samples for Sr and Nd isotope analyses were digested in the same way as for ICP-MS analysis, using ultra-clean reagents and analyzed by thermal ionization mass spectrometry (TIMS) in a Finnigan Mat 262 spectrometer after chromatographic separation with ion exchange resins. Normalization values were $^{86}Sr/^{88}Sr=0.1194$ and $^{146}Nd/^{144}Nd=0.7219$. Blanks were 0.6 and 0.09 nanograms for Sr and Nd, respectively. The external precision (2σ), estimated by analysing 10 replicates of the standard WS-E (Govindaraju, 1994), was better than 0.003% for $^{87}Sr/^{86}Sr$ and 0.0015% for $^{143}Nd/^{144}Nd$. The $^{87}Sr/^{86}Sr$ measured value in the laboratory for NBS 987 international standard was 0.710250 ± 0.0000044 for 89 cases. Measurements of La Jolla Nd international standard on this mass spectrometer yield a mean $^{143}Nd/^{144}Nd$ ratio of 0.511844 ± 0.0000065 for 49 cases.

PETROGRAPHY AND P-T EVOLUTION

Forty seven representative samples from the exotic blocks including twenty three amphibolites, eight coarse-grained hornblendites, and fifteen trondhjemites collected in the Sierra del Convento mélange were selected for this study (Fig. 1b). Detailed petrographic and mineral chemistry information of representative metabasites and trondhjemites is presented elsewhere (García-Casco et al., submitted 2007).

The primary mineral assemblage of the amphibolites is pargasitic amphibole (ca. 60%) and epidote-clinozoisite (ranging from 11% to 50%) (Fig. 2c). Quartz and garnet are also common primary minerals. Quartz is interstitial with respect to amphibole and epidote, while garnet forms large porphyroblasts (up to several cm in size). Primary plagioclase is not present in any of the rocks. Titanite and rutile are ubiquitous accessory phases, both present in the matrix and included in amphibole, epidote and garnet. Retrogression is less than 10% in the studied samples. Pargasitic amphibole (and garnet) may be altered to magnesiohornblende-actinolite, chlorite, glaucophane, and pumpellyite. Some samples also show retrograde albite.

The hornblendites are composed almost entirely (ca. 90-95%) of primary pargasitic amphibole. Clinozoisite/epidote, titanite, rutile (frequently included in amphibole), and quartz are present as accessory phases. These hornblendites are coarse grained, with varieties reaching centimetric grain size, and may appear somewhat foliated or, more commonly, isotropic. Pargasitic amphibole may be replaced by the same retrograde minerals as in the amphibolites.

The trondhjemites are leucocratic rocks mainly consisting of primary medium grained sodic plagioclase (ca. 65%), variable quartz, epidote-clinozoisite, and paragonite (Fig. 2d). Some samples also have primary pargasitic amphibole (1-8%). Rutile is accessory but ubiquitous (Fig. 2d). The crystals of primary plagioclase appear moderately to strongly retrograded to combinations of albite, (clino)zoisite, paragonite, and lawsonite. In some samples, the plagioclase is somewhat saussuritized. Primary epidote-clinozoisite is idiomorphic, showing well developed crystal faces and having a magmatic appearance. Generally, primary epidote/clinozoisite is overgrown by secondary metamorphic acicular (clino)zoisite grown perpendicular to the crystal faces of primary grains. Other retrograde minerals include magnesiohornblende-tremolite, chlorite, and pumpellyite after pargasitic amphibole, and occasional fine-grained phengitic muscovite.

The retrograde mineral phases in all types of rock, including glaucophane, lawsonite, clinozoisite and paragonite, document cooling at high pressure. García-Casco et al. (2006; submitted 2007) have indicated that the rocks followed counterclockwise P-T paths, with peak metamorphic conditions attained at 675-700 ºC and 14-16 kbar, that is above the wet solidus of typical MORB tholeiite, and retrograde conditions ranging from 10-12 kbar and

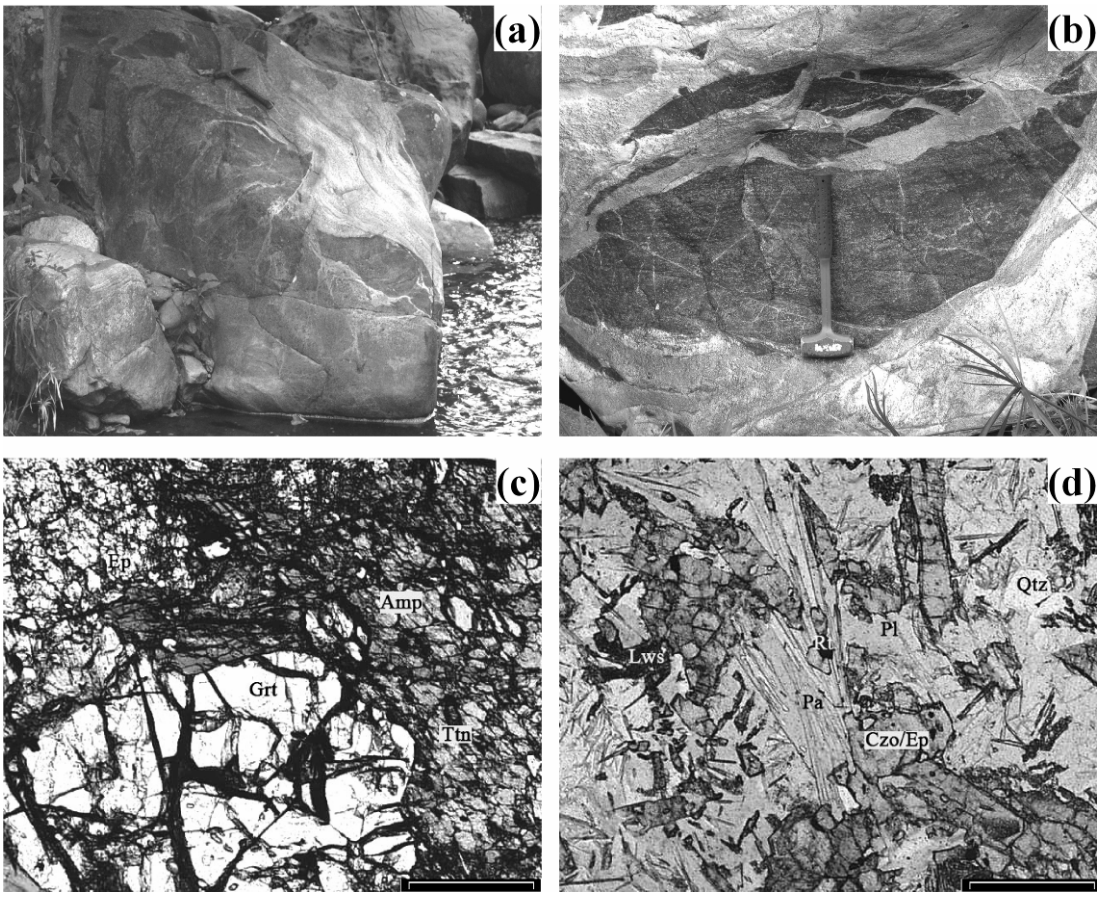

Fig. 2. (a) Amphibolite with leucocratic material showing stromatic structures (Palenque), (b) leucocratic rocks intrude and fracture the amphibolite producing agmatitic structures (Palenque), (c) photomicrograph of an amphibolite mainly composed of amphibole, epidote, garnet, and titanite (included both in the garnet and in the amphibole), (d) photomicrograph of a trondhjemite with plagioclase, paragonite, quartz, and clinozoisite-epidote, rutile and retrograde lawsonite are also shown. The scale bar is 500 μm in (c) and (d). Mineral abbreviations after Kretz (1983).

450-550 ºC. This type of path would have allowed the crystallization of trondhjemitic melts at high pressure (13-14 kbar, 650-680 ºC).

MAJOR AND TRACE ELEMENT GEOCHEMISTRY

Major and trace element geochemical data for the Sierra del Convento samples analyzed in this study are presented in Table 1.

Major elements

Amphibolites

Amphibolites have SiO_2 contents between 42.1 and 51.4 wt.%, ranging from picro-basaltic to basaltic compositions in TAS (total alkalis vs. silica) diagram (Le Maitre et al., 1989) (Fig. 3a) and have a low-K tholeiitic affinity (Peccerillo and Taylor, 1976) (Fig. 3b). Al_2O_3 contents vary from 12.6 to 20.5 wt.%. They have FeO_{tot} contents higher than 7.8 wt.%, MgO between 6.8-10.5 wt.%, MnO and TiO_2 below 0.4 and 3.5 wt.% respectively. CaO contents range between 10.7 and 15.3 wt.%, while Na_2O and K_2O contents are below 3.1 wt.% and 0.5 wt.%, respectively. Mg# (100 * molar MgO/(MgO+FeO_{tot})) values are variable ranging from 42.2 to 66.8. Harker diagrams show negative correlation between TiO_2, FeO_{tot}, P_2O_5 and SiO_2. On the other hand, Al_2O_3, MgO, CaO, Na_2O and K_2O do not show a clear correlation with SiO_2 (Fig. 4).

Hornblendites

Hornblendites plot in the basalt and basaltic-andesite fields of the TAS diagram, with SiO_2 contents ranging from 45.5 to 53 wt.%, and have low-K (tholeiite) to medium-K (calc-alkaline) affinities. In all cases, the contents of K_2O are lower than 0.64 wt.% (Figs. 3a and b). These rocks have higher MgO contents and Mg# values than the amphibolites (>10 wt.% and >60, respectively), and slightly lower Al_2O_3 contents (8-15.3 wt.%). FeO_{tot} is higher than 6.7 wt.%, TiO_2 is below 2 wt.%, and MnO is ca. 0.2 wt.%. The CaO contents are slightly lower than for the amphibolites, around 11 wt.%, but

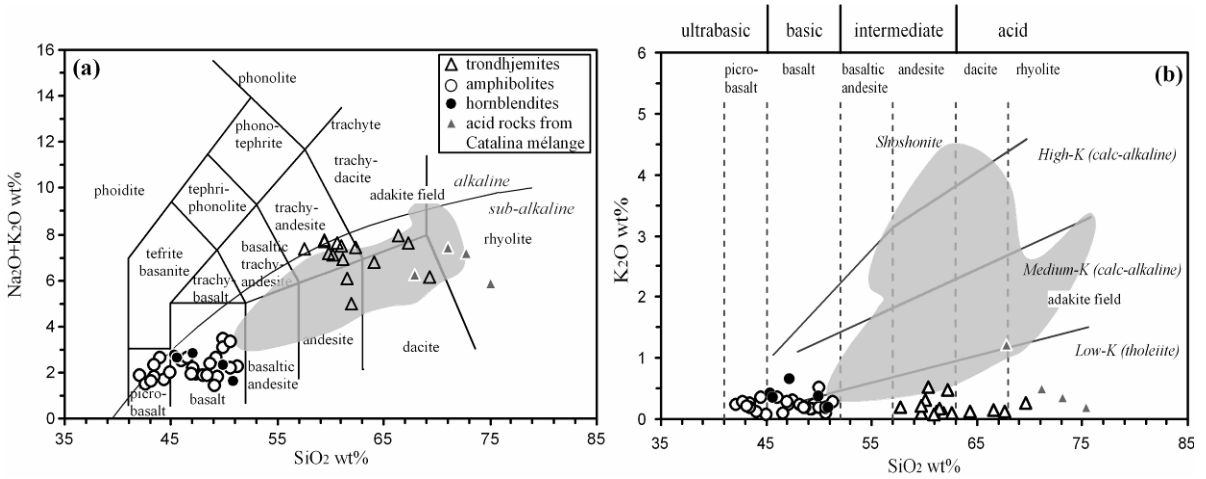

Fig. 3. (a) TAS diagram of classification of volcanic rocks from Le Maitre (1989) and (b) K_2O vs. SiO_2 diagram (Peccerillo and Taylor, 1976) with subdivision of volcanic series in shoshonite, high-K, medium-K and low-K and TAS based names of rocks of the sub-alkaline series. The diagrams contain the studied amphibolites, hornblendites, trondhjemites, and other rocks for comparison including: acid rocks from the Catalina Schist mélange, California (pegmatites and leucocratic segregate, Sorensen and Grossman, 1989); Cenozoic adakites from the Aleutians (Yogodzinski et al., 1995), Argentina (Benoit et al., 2002), Chile (Stern and Kilian, 1996), Ecuador (Beate et al., 2001; Bourdon et al., 2002; 2003; Samaniego et al., 2005), Philippines (Sajona et al., 1996; 2000), Japan (Morris, 1995), Panama-Costa Rica (Defant et al., 1992), USA (Smith and Leeman, 1987); and average adakite values (Martin, 1999; Smithies, 2000). All analyses normalized to 100 wt% anhydrous.

Na_2O (below 2.3 wt.%) is similar to that of the amphibolites. Variation diagrams show a negative correlation between TiO_2, Al_2O_3, FeO_{tot}, K_2O, P_2O_5 and SiO_2 (Fig. 4). CaO and Na_2O show a relatively homogeneous distribution with respect to SiO_2 contents and MgO contents increase with SiO_2.

Trondhjemites

The composition of trondhjemites in the TAS diagram ranges from andesite-trachyandesite to trachydacite-dacite (Fig. 3a), plotting in the low-K tholeiitic series field (Fig. 3b). They have SiO_2 contents ranging between 57.8-69.5 wt.%, Al_2O_3 higher than 18.4 wt.%, and CaO between 3.5 and 7.4 wt.%. They also have more than 4.3 wt.% in Na_2O and less than 0.5 wt.% in K_2O. The CaO/Na_2O ratio ranges from 0.48 to 1.48, though 80% of samples have values higher than 0.75. The contents of TiO_2, FeO_{tot}, and MgO are below 0.6, 4, and 3 wt.% respectively. The Mg# values are relatively high, varying from 38 to 67. In the cationic diagram K-Na-Ca (Barker and Arth, 1976), these leucocratic rocks follow the trondhjemitic trend (Fig. 5a). The studied samples are much depleted in K and enriched in Na, similarly to acid rocks from the Catalina Schist mélange but deviate slightly from the field defined by Cenozoic adakites. In the CIPW normative An-Ab-Or diagram of O´Connor (1965) with the classification of acid and intermediate rocks modified by Barker (1979) the samples plot in the tonalitic and trondhjemitic composition fields (Fig. 5b). Due to their leucotonalitic nature, these samples are termed trondhjemites. The major mineralogical divergence between the trondhjemites is the proportion of epidote-clinozoisite, which increases the CaO/Na_2O ratio in the leucotonalitic compositions. Importantly, all the studied samples are Al-saturated (i.e. peraluminous), with ASI (alumina saturation index) values ranging from 1.023 to 1.142.

Considering amphibolites to trondhjemites in the Harker diagrams, TiO_2, FeO_{tot}, MgO, CaO, and P_2O_5 show negative trends with increasing SiO_2, while Al_2O_3 and Na_2O show positive trends (Fig. 4). However, it is worth mentioning that the amphibolite-trondhjemites compositional spectrum displays a gap in silica content from 51.4 to 57.7 wt.% suggesting partial melting of amphibolites and melt extraction as the major process leading to the formation of the trondhjemitic rocks.

Trace elements

Amphibolites

The abundances of trace elements in this rock type are similar to those of N-MORB. This is clearly seen in normal MORB-normalized spider diagrams (Fig 6a). In this type of diagram, the general pattern of distribution of the elements is homogeneous through Sm to Ni, while the LILE and Pb, Th, and U show a larger scatter. The most important deviations from N-MORB composition are enrichment in Cs, Ba, and Pb, depletion in Th and Nb, and variable enrichment/depletion in U and Sr (Fig. 6a).

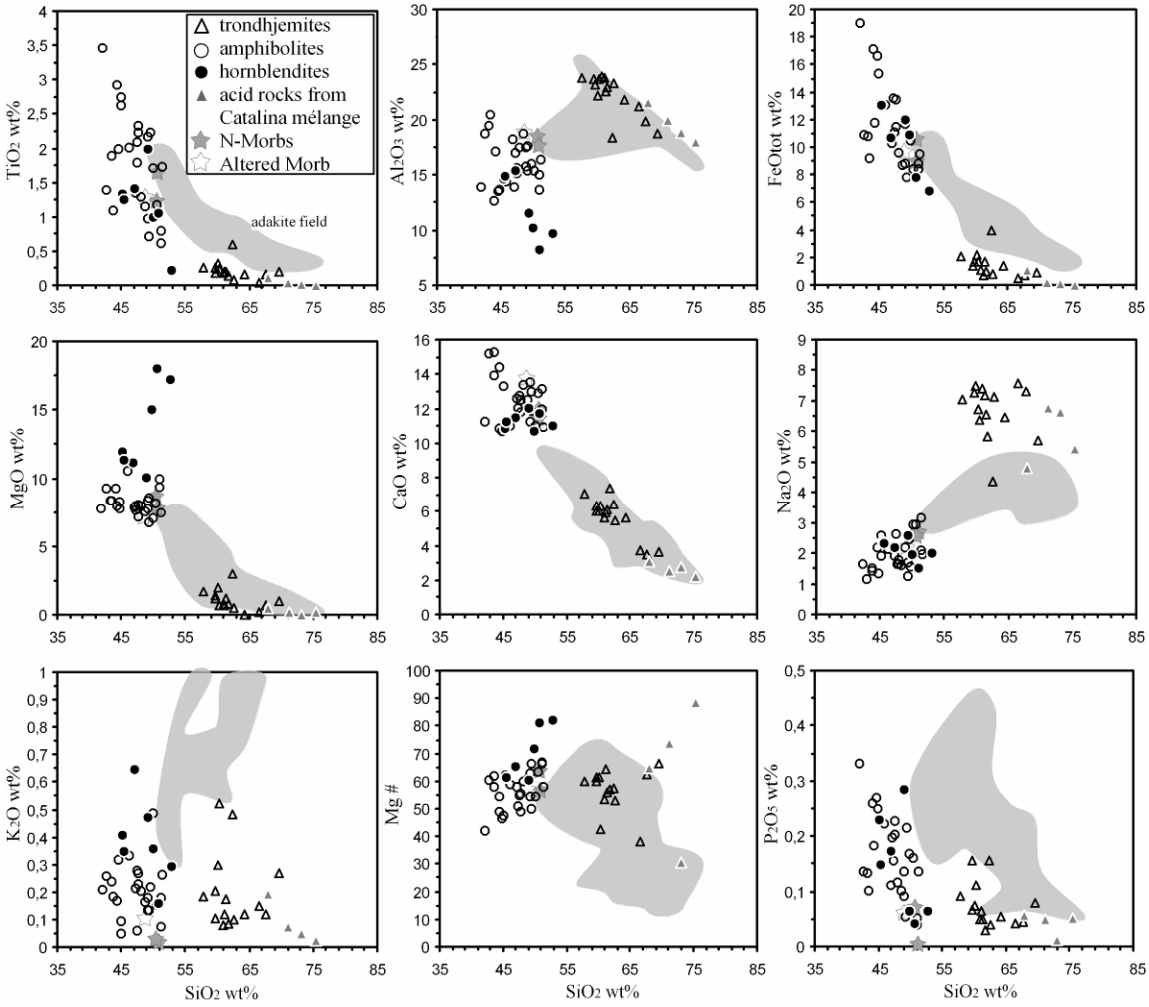

Fig. 4. Harker variation diagrams showing bulk composition of amphibolites, hornblendites, and trondhjemites of the Sierra del Convento and other rocks for comparison, including N-MORB (Hofmann, 1988; Kelemen et al., 2003), altered MORB (Staudigel et al., 1996), Cenozoic adakites (references as in Fig. 3), and acid rocks from the Catalina Schist mélange, California (Sorensen and Grossman, 1989).

Amphibolite LREE and HREE abundances range from 3 to 50 and from 10 to 50 times chondrite values, respectively (Fig. 7a). The chondrite-normalized REE patterns are characterized by slight depleted LREE patterns. The $(La/Yb)_n$ ratio (normalized to chondrite, McDonough and Sun, 1995) varies from 0.28 to 0.88, with most of the samples ranging 0.5-0.8. Only two samples show higher values (1.09 and 1.94) suggesting more fractionated REE patterns. In general, these are N-MORB-like signatures. Eu anomalies are variable. Most of samples have no or negative Eu anomaly (Eu/Eu* = 0.78-1), but 4 samples have values between 1.1 and 1.35. Negative Eu anomalies suggest plagioclase fractionation (during partial melting). None of the samples show significant enrichment in HREE and Y (with Y contents ranging from 15.5 ppm to 72.1 ppm), not even in those samples containing garnet. These data suggest little fractionation of garnet during partial melting.

N-MORB signatures are also evident when samples are plotted in diagrams commonly used to discriminate between various types of basaltic rocks. Because of the metamorphic imprint of the studied rocks, the diagrams used are those which involve elements generally considered immobile during metamorphism such as HFSE (Nb, Ta, Zr, Hf, Ti) and HREE. Though some samples may plot outside the respective MORB fields, in the Cr-Y (Pearce, 1982), the V-Ti (Shervais, 1982), and Th/Yb vs. Ta/Yb (Wood et al., 1979) diagrams (Figs. 8a, b and c) the rocks clearly show MORB signatures. Volcanic arc tholeiites (IAT) and within-plate basalts (WPB), two potential sources of amphibolites given by regional geology arguments (see Discussion), are thus excluded from consideration. In the Th/Yb vs. Ta/Yb diagram it is also apparent that the samples have N-MORB signatures (Fig. 8c).

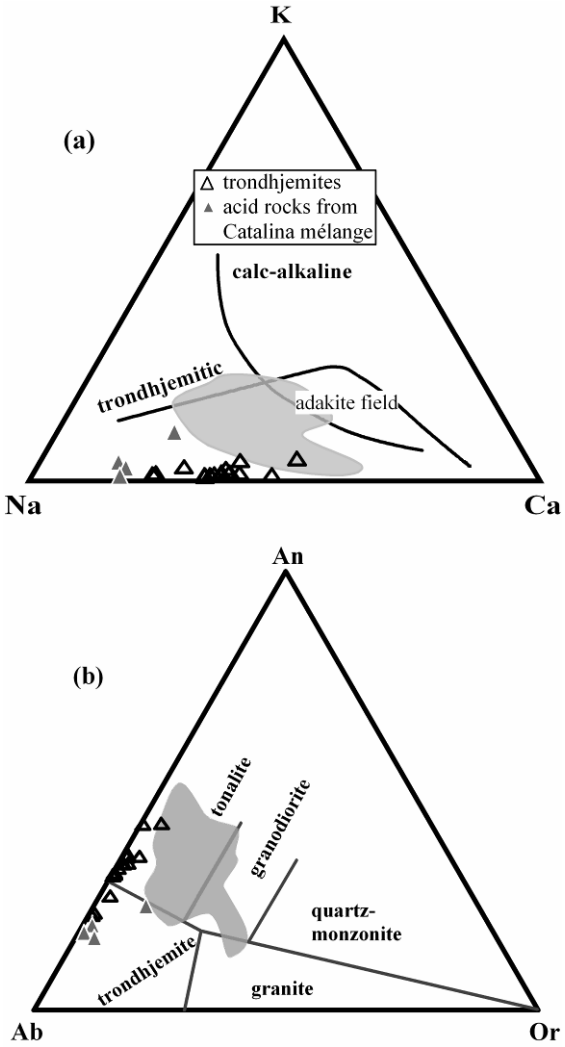

Fig. 5. (a) K-Na-Ca cationic diagram (Barker and Arth, 1976) and (b) molecular normative (CIPW) diagram (O´Connor, 1965), with fields after Barker (1979) of trondhjemites from Sierra del Convento mélange and other acid rocks for comparison including pegmatites and leucocratic segregate from the Catalina Schist mélange, California (grey triangles), and Cenozoic adakites (sources as in Fig. 3).

Hornblendites

The trace element abundances of this type of rock are similar to those of the amphibolites, except for being slightly depleted in Sr to Lu in the normal MORB-normalized diagram and slightly enriched in LILE (Fig. 6b). These features can hardly be reconciled with a restitic origin for this type of rock. Instead, the enrichment in LILE and Pb suggests that these rocks represent amphibolites modified by metasomatic processes accompanying partial melting.

Hornblendites show two different types of chondrite-normalized REE patterns. One group of samples displays patterns similar to those of the amphibolites, with convex upward shapes, $(La/Yb)_n$ ranging from 0.47 to 0.88 and no Eu anomaly (Eu/Eu* = 1.00). Respect to the amphibolite REE abundances, this group of hornblendites are in the lower range. A second group of samples displays a slightly more fractionated linear shape (Fig. 7b) with $(La/Yb)_n$ ranging from 1.5 to 1.9 and Eu/Eu* values between 1.00-1.04. This type of pattern is not typical of the amphibolites. Nevertheless, the HREE content of this group overlap with that of the former type of hornblendites.

Interestingly, the Cr-Y diagram (Fig. 8a) shows these rocks trending towards the volcanic-arc basalt field (mostly due to low Y contents), and the V-Ti diagram (Fig. 8b) allows discrimination between the two groups of samples and characterization of the hornblendites as MORB-like rocks. In the Th/Yb vs. Ta/Yb diagram (Fig. 8c), this group of samples trend, instead, towards E-MORB compositions and far from island arc basalts. These apparently contradictory features evidence that hornblendite compositions do not correspond to original igneous basaltic compositions, we suggest that they represent N-MORBs which have been modified during metasomatism processes.

Trondhjemites

The spider diagram for trondhjemites show fractionated patterns (Fig. 6c). Relative to the studied amphibolites and hornblendites, the trondhjemites show depletion in La, Ce, Pr, Nd, Sm, and Eu through to Ni in the normal MORB-normalized diagram. The contents of LILE, Th, U, Pb, and HFSE, however, are similar to those of the amphibolites, and Sr shows a significative enrichment (2-12 times N-MORB). Due to the very low contents of adjacent elements (Sm and Eu) a strong positive anomaly in Zr is apparent in the normal MORB-normalized diagram.

LREE and HREE contents range from 0.35 to 35.5 and from 0.4 to 6 times the chondrite values, respectively (Fig. 7c). In spite of Yb values being very low, less than 0.3 ppm (except one sample which has 1.034 ppm), the $(La/Yb)_n$ ratio values range from 0.9 to 16.8. So the chondrite-normalized REE patterns are slightly fractionated and, in a number of cases, tend to be concave upward. It is important to stress the general low REE contents and $(La/Yb)_n$ of most samples, in all cases lower than adakites. This can be explained in terms of a minor contribution of REE-bearing phases during melting of the amphibolites. On the other hand, most samples display positive Eu anomalies, with $1<Eu/Eu^*<2.5$. This, in turn, suggests the important participation of plagioclase in the melting process. The Nb-Y, Ta-Yb, Rb-(Y+Nb), and Rb-(Yb+Ta) diagrams of Pearce et al. (1984) have been used to characterize the trondhjemites in terms of setting of formation (Fig. 9). It is clear that the samples plot in the volcanic arc field and thus precluding similarity to ocean ridge plagiogranites (and within-plate and

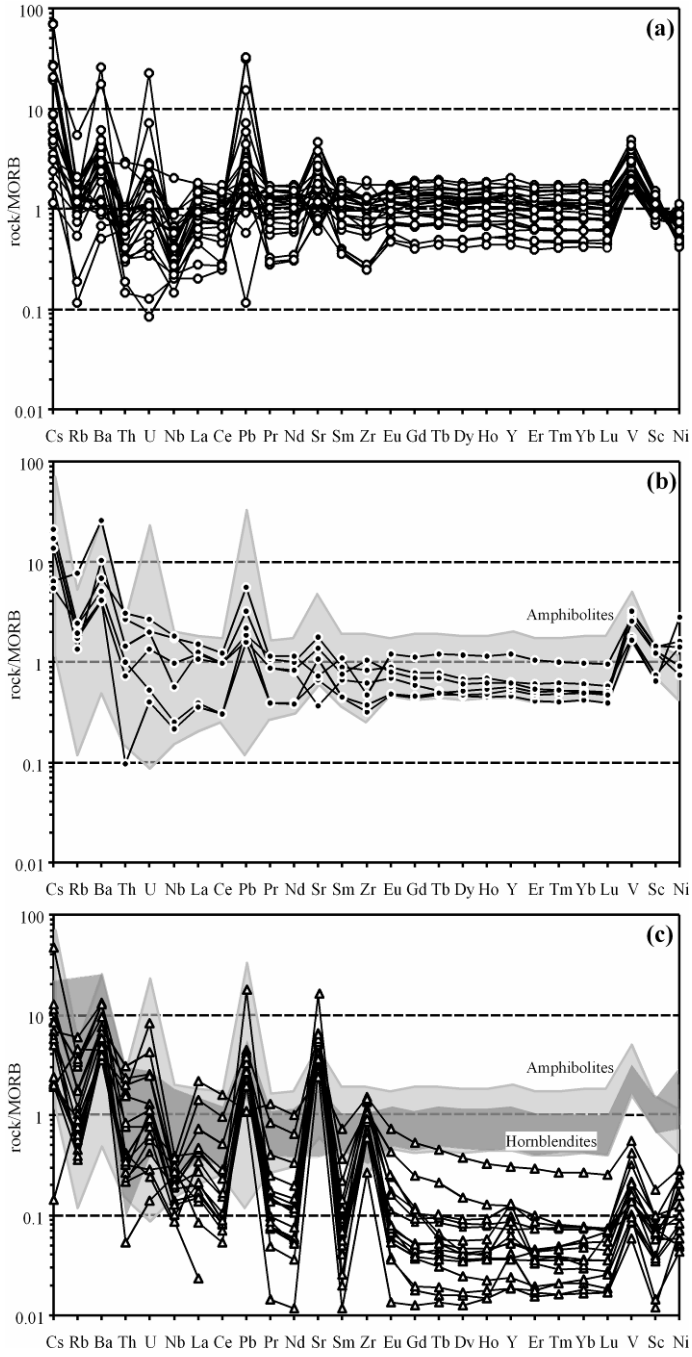

Fig. 6. N-MORB (Hofmann, 1988) normalized spider diagrams for: (a) amphibolites, (b) hornblendites, and (c) trondhjemites from Sierra del Convento mélange.

syn-collision granitic s.l. rocks). Adakites from a number of localities worldwide and acid rocks from the Catalina Schist mélange were also plotted for comparison. The trondhjemites from the Sierra del Convento are comparable to the Catalina rocks and to a lesser extent with adakites.

However, the Sr contents are high (>300 ppm, except one sample with 271.5 ppm) while the Y contents are low (<4.7 ppm, except 10.842 ppm for the aforementioned exception), as is typical of adakites (Table 2). This is clearly appreciated in the Sr/Y vs. Y diagram of Defant and Drummond (1990), where the trondhjemites mostly plot in the adakite field although some samples have very high Sr/Y values (>500) compared to the adakites (Fig. 10a). In the $(La/Yb)_n$ vs. $(Yb)_n$ diagram (Martin, 1986) the Sierra del Convento trondhjemites and the Catalina rocks plot outside the typical field of adakites as a result of their depletion in La (Fig. 10b).

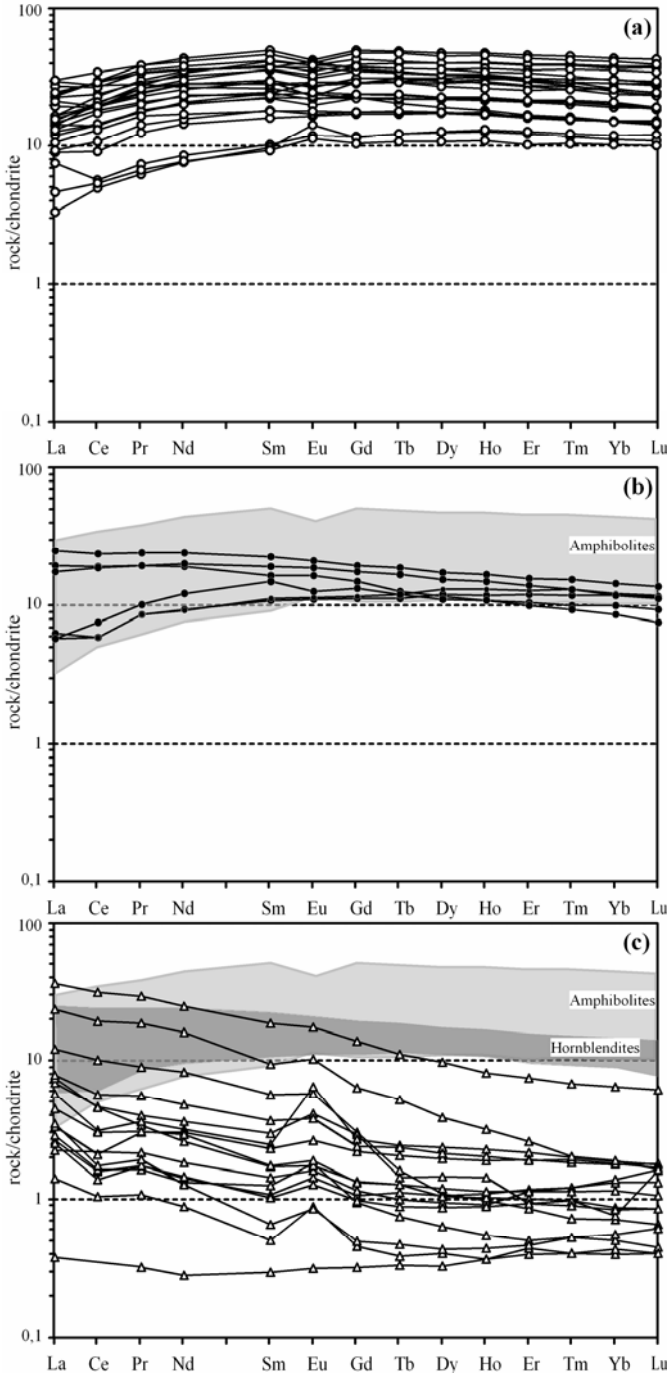

Fig. 7. Chondrite (McDonough and Sun, 1995) normalized REE patterns for: (a) amphibolites, (b) hornblendites, and (c) trondhjemites from Sierra del Convento mélange.

Thus, it can be concluded that the trondhjemites of the Sierra del Convento have chemical characteristics that allow them to be compared with adakites, but they are not typical differing in their unfractionated REE patterns, low La (and other LREE) contents, and very high Sr contents.

ISOTOPE GEOCHEMISTRY

Four amphibolite samples (CV53X-I, CV62b-I, CV62a, and CV228e), one hornblendite (CV61), and three trondhjemites (CV62b-II, SC21, and CV228a) have been analyzed for Sr and Nd isotope geochemistry (Table 3). Initial isotopic ratios were calculated, using ^{87}Rb and ^{147}Sm decay constants $1.42*10^{-11}$ yr^{-1} and $6.54*10^{-12}$ yr^{-1}, respectively, for

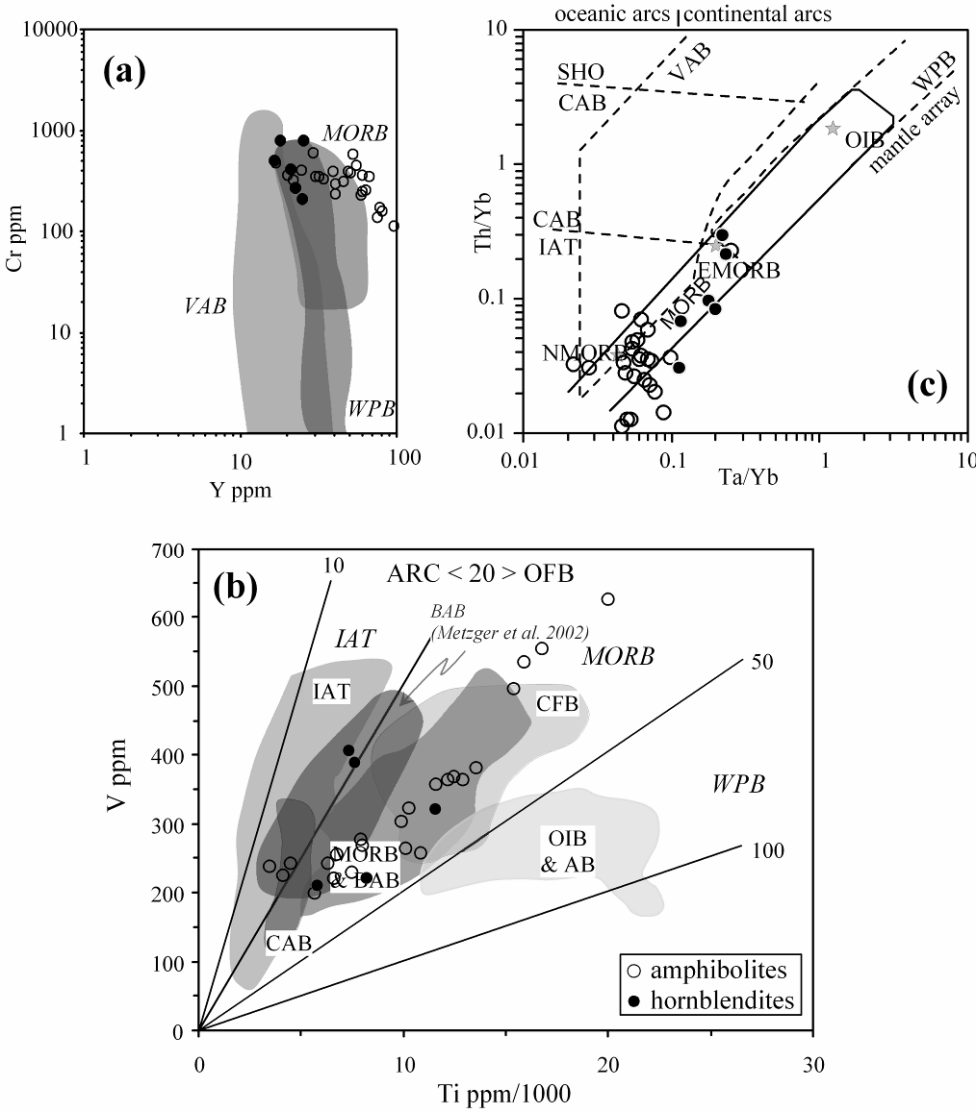

Fig. 8. Amphibolites and hornblendites plotted in: (a) Cr-Y discrimination diagram for basalts (Pearce, 1982), showing the fields for MORB, volcanic-arc basalts (VAB) and within-plate basalts (WPB), (b) Ti-V discrimination diagram for basalts (Shervais, 1982), showing the fields of island arc tholeiite (IAT), MORB, and back arc basalt (VAB), continental flood basalt (CFB), and ocean-island (OIB), and alkali basalt (AB) as a function of the V/Ti ratio. (c) Th-Ta discrimination diagram using Yb as a normalization factor (Wood et al., 1979) showing the fields of shoshonite (SHO), calc-alcaline basalt (CAB), island-arc tholeiite (IAT), volcanic-arc basalt (VAB), and within-plate basalts (WPB). In this latter, Ocean-island basalt (OIB), Enriched-MORB and N-MORB (Sun and McDonough, 1989) have been also projected for comparison.

the metamorphic peak and formation of trondhjemites after partial melting of amphibolites at ca. 110 Ma based on available K/Ar geochronological data (Somin and Millán, 1981), and unpublished SHRIMP zircon data U/Pb data (Yamirka Rojas-Agramonte, personal communication 2007), and for the timing of formation of subducted Proto-Caribbean oceanic crust at 150 Ma, based on regional arguments (see below and Pindell et al., 2005). Errors for initial ratios are given at 2-sigma uncertainty. Samples of other rock types used for comparison were corrected for the same ages.

Sr and Nd isotopes

The amphibolites $^{87}Sr/^{86}Sr$ ratio ranges from 0.703155 to 0.703317. The isotopic ratio of hornblendite is slightly higher, 0.703871, and those of the trondhjemites range from 0.703088 to 0.703234.

$^{143}Nd/^{144}Nd$ ratios of the amphibolites, hornblendite, and trondhjemites are 0.513091 to 0.51317, 0.513046, and 0.51292 to 0.513022, respectively. One sample of trondhjemite could not be analyzed due to very low concentration in elemental Nd. As described above, low Nd

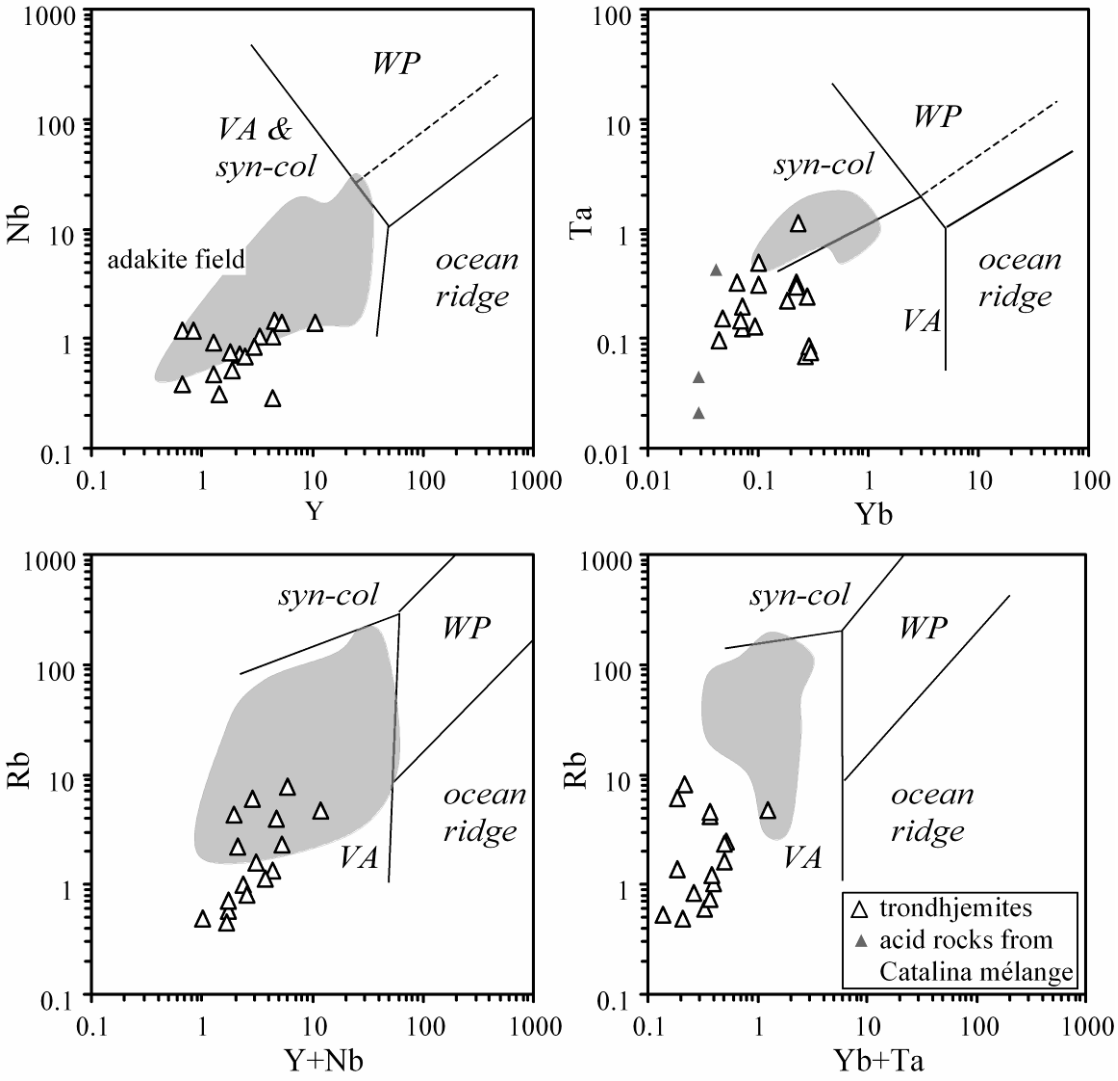

Fig. 9. Trondhjemites plotted in discrimination diagrams for granitic rocks (Pearce et al., 1984) showing the fields of ocean ridge, volcanic arc (VA), syn-collisional (syn-collisional), and within-plate (WP) granitic rocks. Grey fields correspond to Cenozoic adakite compositions (references as in Fig. 3). Acid rocks from the Catalina Schist mélange are plotted in the Ta-Yb diagram.

concentration is a common feature of trondhjemites of the Sierra del Convento, and is indicative of a depleted source with no sediment imprint.

Amphibolites have εNd (150Ma) values of +8.73 to +10.01, indicating a depleted source (i.e., depleted mantle) in the mantle array with no other component contribution. This supports the proposed MORB protolith for these amphibolites. The analyzed samples compare well to normal-mid ocean ridge basalt (N-MORB; Hart et al., 1999; Kelemen et al., 2003) and Cretaceous Atlantic MORB (Jahn et al., 1980) differentiated from a depleted MORB Mantle (DMM; Workman and Hart, 2005; Fig. 11a). No seawater alteration is detected in the analyzed samples.

The εNd (110Ma) values of trondhjemites (+7.2 and +9.11) point to a depleted source, such as a very young juvenile crust, i.e. ocean crust, differentiated from a depleted mantle without continental crust components. The εNd (110Ma) overlapping the trondhjemite and amphibolite (+9.76 to +11.11) fields, clearly links both types of rock and strengthens the view that the trondhjemites were produced by partial melting of the former with no apparent significant input of external sources (Fig. 11b). However, since the partial melting process involved fluid-present conditions, likely caused by the influx of external fluids into the amphibolites (García-Casco et al., submitted 2007), it must be concluded that the external fluid had isotopic composition typical of a depleted source and not of sea water or fluids evolved from metasedimentary sources.

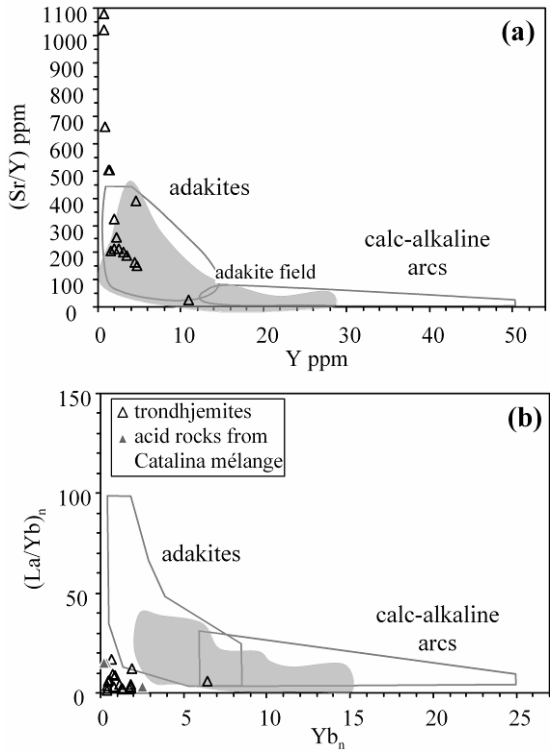

Fig. 10. Trondhjemitic rocks plotted in (a) (Sr/Y) vs. Y and (b) $(La/Yb)_n$ vs. Yb_n diagrams with adakite and calc-alkaline arc fields as defined by Defant and Drummond (1990) and Martin (1986), respectively. Grey fields correspond to Cenozoic adakite compositions (references as in Fig. 3). Acid rocks from the Catalina Schist mélange have been plotted in b).

The absence of a sedimentary component in the trondhjemites is indeed evident from the projection of the isotopic composition of the Atlantic Cretaceous Pelagic Sediment (AKPS, Jolly et al., 2006), which may be used as a proxi of potential subducted sediments (Fig. 11b). A similar conclusion can be reached for the hornblendite (εNd (150Ma) = +7.45 and εNd (110Ma) = +8.59). Formation of this rock type at peak metamorphic conditions through metasomatic processes did not involve fluids from metasedimentary sources. Thus, dehydration of serpentinized harzburgite and infiltration of this fluid through the mantle and lower crustal segment of the subducted lithosphere is a potential process that could produce the type of fluid that percolated the amphibolites during their partial melting and metasomatic processes.

In terms of Sr-Nd systematic, the trondhjemites are also comparable to adakitic rocks from Ecuador (Samaniego et al., 2005), Chile (Stern and Kilian, 1996), Argentina (Kay et al., 1993), Mexico (Aguillón-Robles et al., 2001), and Panama-Costa Rica (Defant et al., 1992) (Fig. 11b). This, however, does not mean a common source and process of formation since the depleted source of adakites must be interpreted in terms of partial melting of MORB followed by interaction with a depleted supra-subduction mantle wedge. Notably, the Sierra del Convento trondhjemites were trapped within the amphibolite source and did not undergo this latter process.

DISCUSSION

The origin of the protoliths

Amphibolites

Elemental and isotopic data indicate that the protoliths of the amphibolites are basaltic rocks of N-MORB composition that evolved from a depleted mantle source, and no trace of within-plate basalts and/or ocean plateau-like rocks is identified.

The Caribbean plate contains a large within-plate igneous province made of oceanic plateau basaltic rocks which formed episodically since the early Cretaceous in the range 140-70 Ma (Donnelly et al., 1990; Kerr et al., 1998; 1999; Lewis et al., 2002; Hoernle et al., 2004; Kerr and Tarney, 2005). The lack of plateau basalts in the Sierra del Convento amphibolites and their geochemical features would suggest that subduction of this plate was not involved. During pre-110 Ma times, island arc tholeiitic basalts were extruded in the "primitive" island arc of the Caribbean (Lebron and Perfit, 1993). Thus, subduction of the Proto-Caribbean, an oceanic basin connected with the Atlantic and formed during the break up of Pangea through late Jurassic to late Cretaceous times, is suggested. This is in agreement with general views of the tectonic evolution of the Caribbean realm (Pindell and Kennan, 2001; Pindell et al., 2005; 2006) which identify onset of subduction of the Proto-Caribbean below the Caribbean plate during the late Early Cretaceous (ca. 120 Ma). This onset of subduction scenario is consistent with a high geothermal gradient inferred in the subducting Sierra del Convento slab at 120-110 Ma (García-Casco et al., 2006; submitted 2007). As a corollary, it becomes apparent that the ophiolitic complexes (Mayarí and Moa-Baracoa) of eastern Cuba and the associated mélange complexes come from quite different plates and tectonic environments, even if they are closely associated at present, and that they probably amalgamated during the latest Cretaceous (late Campanian-Maastrichtian) collision in the region (see, García-Casco et al., 2006; submitted 2007).

Trondhjemites

Three different hypotheses may be proposed to explain the origin of trondhjemites in the Sierra del Convento: subducted oceanic plagiogranites, exotic arc magmas emplaced in the mélange, or partial

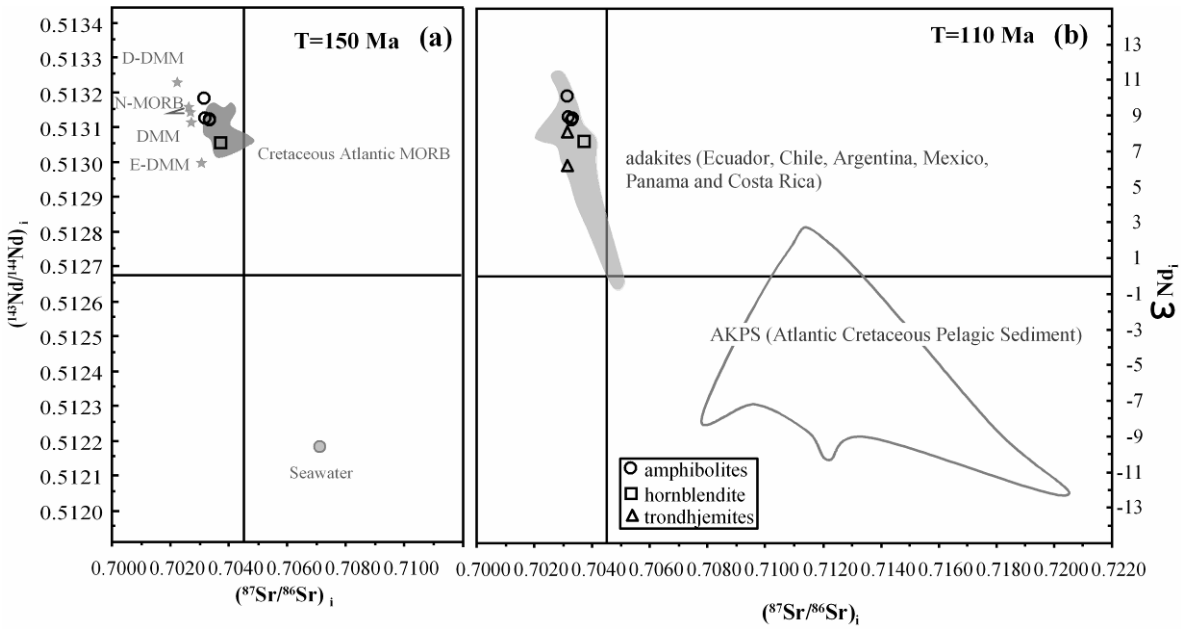

Fig. 11. $(^{87}Sr/^{86}Sr)_i$ vs. $(^{144}Nd/^{143}Nd)_i$ and εNd_i diagrams. $\varepsilon Nd = ((^{143}Nd/^{144}Nd_{sample}/^{143}Nd/^{144}Nd_{CHUR})-1)*10^4$, where CHUR = chondrite uniform reservoir (De Paolo, 1988). εNd and initial values calculated using $(^{143}Nd/^{144}Nd)_{CHUR} = 0.512638$, $(^{147}Sm/^{144}Nd)_{CHUR}=0.1967$ (Wasserburg et al., 1981). Composition of seawater is from McCulloch et al., (1981) and Sm/Nd data is from Piepgras and Wasserburg (1980). Samples were corrected for two different ages: (a) T=150 Ma and (b) T=110 Ma, appropriate for MOR basalt formation and peak metamorphism (and partial melting) shortly after onset of subduction, respectively. In (a) data for depleted MORB mantle (DMM), depleted DMM (D-DMM), and enriched DMM (E-DMM) are from Workman and Hart (2005); N-MORB data are from Hart et al. (1999) and Kelemen et al. (2003); and Cretaceous Atlantic MORB data are from Jahn et al. (1980). In (b) the adakite field (grey colour) includes data from Ecuador (Samaniego et al., 2005), Chile (Stern and Kilian, 1996), Argentina (Kay et al., 1993), Mexico (Aguillón-Robles et al., 2001), and Panama-Costa Rica (Defant et al., 1992), and the Atlantic Cretaceous Pelagic Sediment (AKPS) field constructed after data from Jolly et al. (2006).

melting products derived from the amphibolites. The petrological and geochemical characteristics of the trondhjemites exclude the plagiogranite and exotic volcanic arc origin hypothesis (García-Casco et al., submitted 2007). All aspects, including field relations, petrological analysis and elemental and isotope geochemistry indicate that these rocks generated by partial melting of amphibolites during subduction at ca. 15 kbar and 700 ºC.

We conclude that the partial melting was H_2O-present from the following observations. Notably, for water-undersaturated melting, a systematic presence of clinopyroxene would have been expected. Water-present melting is in agreement with thermodynamic calculations (García-Casco et al., submitted 2007) indicating P-T melting conditions within the epidote-amphibolite facies (ca. 700 ºC, 15 kbar), just above the water-saturated solidus of MORB composition. Accordingly, partial melting experiments of amphibolites in the presence of low-salinity aqueous fluid reproducing conditions of the Sierra del Convento mélange, such as those carried on by Xiong et al. (2005) at T <975ºC and intermediate P (10-20 kbar), show how similar partial melts (in terms of major elements) and residues (amphibole ± garnet ± rutile ± magnetite with little or no clinopyroxene) may be formed.

Hornblendites

The hornblendites have elemental and isotopic signatures corresponding, in general, to modified basalt. Though their features may appear, at first glance, typical of a composition residual to trondhjemitic melt extraction, the trace element systematic of the hornblendites and element abundances intermediate between those of amphibolites and trondhjemites (Figs. 6c and 7c) strongly support a non-residual character for this rock type. The process involved a first step of partial melting to yield a "normal" residue (amphibolites with pargasite) with latter fluid interaction modifying their mineral assemblages (forming abundant hornblende) and geochemical features.

Garnet amphibolites from the Catalina Schist mélange (California) present selvages (rinds) of amphibole and phylosilicates that resemble hornblendites from the Sierra del Convento. These rinds were explained by metasomatic phenomena reflecting the interaction between ultramafic and mafic-to-felsic rocks (Sorensen and Grossman, 1989; and references therein). The selvages show similar REE patterns to the Sierra del Convento hornblendites, some with fractionated patterns and others with MORB-like patterns, and their element

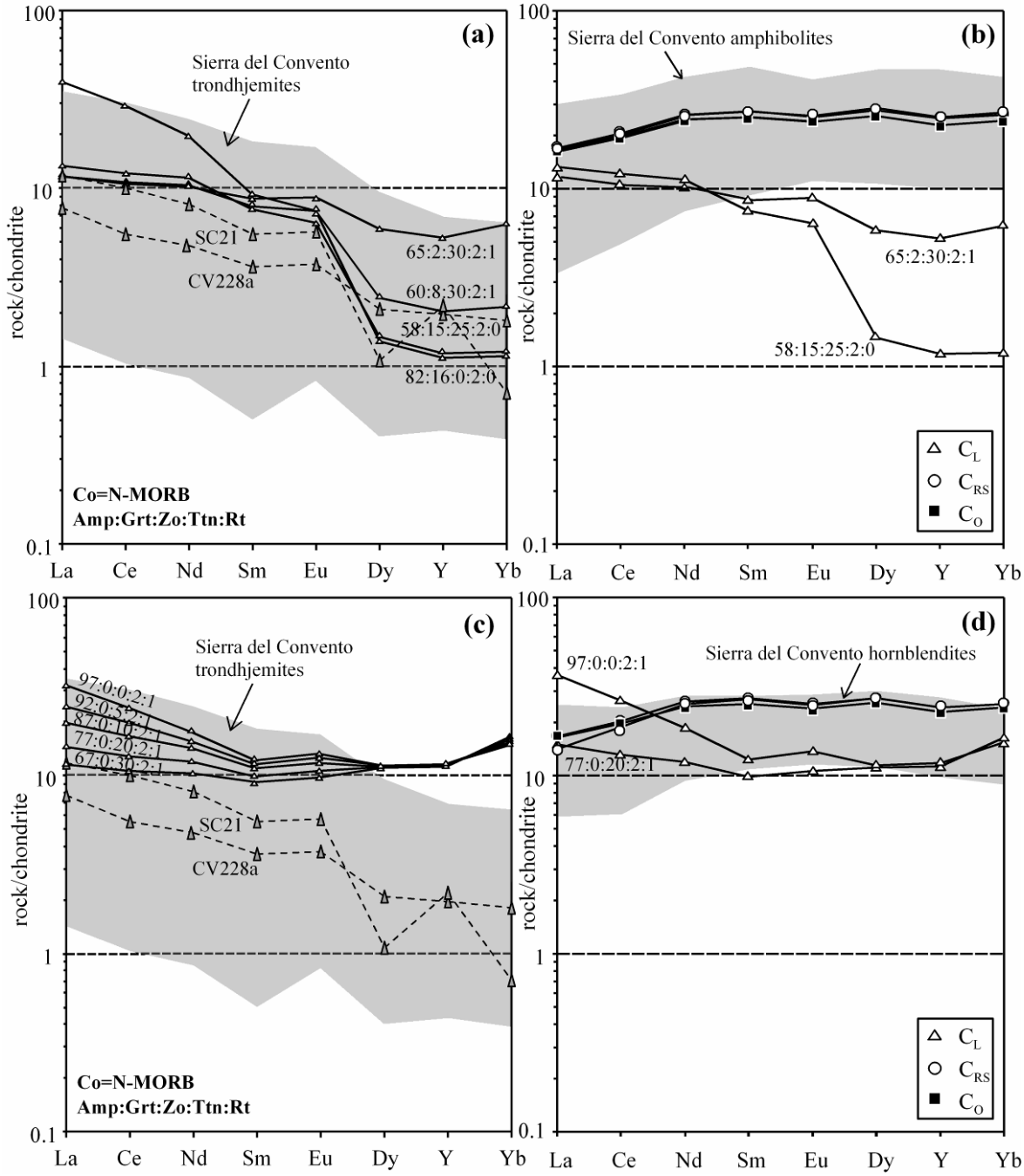

Fig. 12. Chondrite (McDonough and Sun, 1995) normalized REE + Y diagrams for batch-melting models with weight fraction of melt produced F = 0.1 and concentration of the elements in unmelted MORB (Hofmann, 1988) source (Co). (a) and (b) Results of calculations for amphibolitic residues ranging from: 58-82% Amp, 2-16% Grt, 0-30% Zo, 2% Ttn, and 0-1% Rt. (c) and (d) Results of calculations for hornblenditic residues ranging from 67-97% Amp, 0% Grt, 0-30% Zo, 2% Ttn, and 1% Rt. In (a) and (c) the calculated melt compositions, two representative trondhjemites (SC21 and CV228a), and the trondhjemitic field from Sierra del Convento are plotted. Also are shown the unmelted source and selected calculated residues and melt compositions for (b) amphibolitic residues Amp:Grt:Zo:Ttn:Rt = 65:2:30:2:1 and 58:15:25:2:0 and (d) hornblenditic residues Amp:Grt:Zo:Ttn:Rt = 77:0:20:2:1 and 97:0:0:2:1, and the (b) amphibolite and (d) hornblendite fields from Sierra del Convento mélange.

abundances are intermediate between those of amphibolites and felsic rocks (Sorensen and Grossman, 1989). Thus, a partial melting plus metasomatic origin is proposed for this rock type in the Sierra del Convento mélange.

Partial melting modeling

Trace and REE modeling was undertaken to provide insights into the extent of melting and the nature of the protoliths and restites. Batch-melting

has been assumed for the calculations. The concentration of a trace element in the calculated melt C_L is related to its concentration in the unmelted source C_O by the expression, $C_L/C_O = 1 / [D_{RS}+F*(1-D_{RS})]$, where D_{RS} is the bulk partition coefficient of the residual solid calculated for every element in the model and F is the weight fraction of melt produced (ranging from 0 to 1). Elements considered in the calculations were La, Ce, Nd, Sm, Eu, Dy, Y, and Yb, for which Kd values have been published for all the considered phases (amphibole, garnet, epidote, titanite, and rutile). Amphibole partition coefficients are from Klein et al. (1997), except $Kd_Y^{Amp/melt}$ that was taken from Hilyard et al. (2000). Partition coefficients for garnet are from Sisson and Bacon (1992). Due to the lack of data for $Kd^{Ep/melt}$ different models were calculated assuming that element partition coefficients behaves as that of zoisite-melt or as combination of zoisite+allanite-melt, for which partition have been published (Frei et al., 2003). In the latter type of calculations, $Kd^{Ep/melt}$ was calculated as a weighted linear combination of $Kd^{Zo/melt}$ and $Kd^{Allanite/melt}$, with factors strongly weighting $Kd^{Zo/melt}$. Partition coefficients for titanite were taken from Tiepolo et al. (2002). Partition coefficients for rutile were taken from Klemme et al. (2005), for La, Ce, and Sm, and from Foley et al. (2000), for Nd, Eu, Dy, Y, and Yb.

Because of the lack of an obvious protolith in the mélange (most, if not all, the analysed amphibolite samples are restitic, see below), the concentrations of the selected elements in the unmelted source were taken from that of normal MORB (Hoffman, 1988). All diagrams have been normalized to the chondrite of McDonough and Sun (1995).

Based on the variability of modal abundances of phases in the amphibolites and hornblendites in the Sierra del Convento mélange, different mineralogical assemblages and modes were devised as potential residues. The results show that the most important factor controlling melt composition is the proportion of garnet in the residue. We present calculations with residues ranging from 0 to 25% of garnet. The mineralogical assemblages of the residues considered are therefore composed of combinations of amphibole, garnet, zoisite, titanite, and rutile. The proportions of these phases in the models presented in Figures 12 and 13 are expressed as Amp:Grt:Zo:Ttn:Rt.

Results of partial melting calculations indicate that the extent of melting (F) was low, in any case not larger than 0.3. Anyway, calculations show that differences in calculated melt compositions using F = 0.01 - 0.3 are insignificant. A value of F = 0.1, considered as a good approximation, is used in Figure 12. Four different melt compositions are presented in Figure 12a for residues with variable amphibole (58-82%), garnet (2-16%), zoisite (0-30%), titanite (2%) and rutile (0-1%) contents. The calculated element abundances and patterns compare well with those of Sierra del Convento trondhjemite field. In particular, the melt compositions calculated for residues Amp:Grt:Zo:Ttn:Rt = 58:15:25:2:0 and 65:2:30:2:1 compares quite well with the composition of two representative samples as SC21 and CV228a, respectively (Fig. 12a).

The computed element concentrations and patterns of the residues used in the calculations are practically identical to those of the amphibolites of the Sierra del Convento mélange (Fig. 12b), suggesting that the amphibolites are in fact residues after a small fraction of partial melting. In contrast, calculated melts for hornblendite residues (Fig. 12c), which do not contain garnet and have large amounts of amphibole, have element abundances and show patterns different from those of the trondhjemites from the Sierra del Convento. The representative examples of calculated melt composition shown in Figure 12c are less fractionated and more enriched in Dy, Y and Yb. This eliminates the hornblendites of the Sierra del Convento as possible residues, as suggested above.

Results of calculations varying the extent of melting further, F= 0.05 – 1, are presented in the $(La/Yb)_n$ vs. $(Yb)_n$ diagram (Fig. 13). This diagram was originally proposed by Martin (1986) to discriminate between adakite and calc-alkaline magmas based on melting models of a MORB source and eclogite (50%Grt, 50%Cpx), hornblende-eclogite (35%Grt, 35%Cpx, 30%Hbl), and garnet-amphibolite (12%Grt, 44%Cpx, 44%Hbl) residues. We, instead, present calculations for the melting of epidote-amphibolite with varying garnet contents in the residue (X=0-25%; Fig. 13a). In these models, the variation in the amount of garnet is balanced by changes in the proportion of amphibole and epidote in the residue (i.e., Amp = 65-(X/2); Grt = X; Zo = 32-(X/2); Ttn = 2; Rt = 1, Fig. 13a). The results suggest that the extent of melting was low, and that residues with varying garnet-amphibole-epidote contents as observed in the Sierra del Convento amphibolites may have been formed. Again, the results of calculations using hornblendite assemblages and modes as residues suggest that the hornblendites of the Sierra del Convento are not residual rocks (Fig. 13b). In these models, the residues considered are garnet-free and their amphibole content range from 65 to 95% (Amp = 65+X; Grt = 0; Zo = 32-X; Ttn = 2; Rt = 1, with X varying from 0 to 30%; Fig. 13b). Figure 13b shows that the melts produced have a lower $(La/Yb)_n$ and higher $(Yb)_n$ contents than the trondhjemites of the Sierra del Convento.

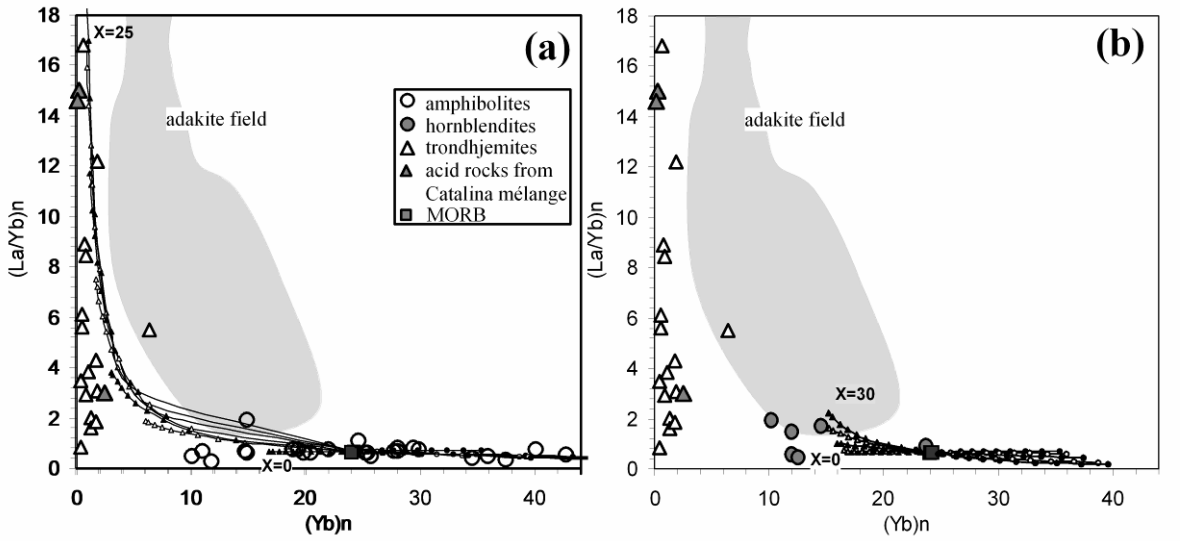

Fig. 13. $(La/Yb)_n$ vs. $(Yb)_n$ diagram with melting curves calculated varying the extent of melting (F= 0.05 – 1). (a) Calculations for epidote-amphibolite with varying garnet (X=0-25%) contents in the residue. The variation in the amount of garnet is balanced by changes in amphibole and epidote in the residue (i.e., Amp 65-(X/2): Grt X: Zo 32-(X/2): Ttn 2: Rt 1). (b) Calculations using hornblendite assemblages as residues. Residues considered are garnet-free and their amphibole content range from 65 to 95% (Amp 65+X: Grt 0: Zo 32-X: Ttn 2: Rt 1, with X varying from 0 to 30). Sources for adakites and acid rocks from the Catalina Schist mélange as in figure 3.

Trondhjemites from Sierra del Convento as primary slab melts

Trondhjemites from the Sierra del Convento share geochemical similarities with the Californian Catalina Schist partial melts, commonly considered to be slab melts, but also with Cenozoic adakites in general (Table 2). Adakites form suites of intermediate to felsic rocks whose compositions range from andesite to dacite and rhyolite (e.g. Martin, 1986; Defant and Drummond, 1990; Maury et al., 1996; Martin, 1999). Adakitic geochemical features were recently examined (Martin et al., 2005) and are summarized in Table 2 together with the geochemistry of the Sierra del Convento trondhjemites. Both Champion and Smithies (2003) and Martin and Moyen (2003) defined two main compositional groups, high-SiO_2 adakites (HSA) and low-SiO_2 adakites (LSA) (Table 2). These groups differ in mineralogical and geochemical features, and in their petrogenesis. HSA are interpreted to be slab melts produced by partial melting of subducted hydrated basalt and latter modified by assimilation of peridotite, while it is suggested that LSA are generated by melting of a peridotite source which was metasomatized by slab melts (completely consumed during melt–peridotite interaction; Martin et al., 2005). In either case, it appears that adakites do not represent pristine slab melts. Indeed, the chemistry of slab-derived melts has been identified as affected by incorporation of metasomatic mantle wedge (Yogodzinski et al., 1995; 2001) and/or crustal material (Sen and Dunn, 1994; Stern and Kilian, 1996; Sajona and Maury, 1998).

Basalt melting experiments performed by Prouteau et al. (2001) indicate that trondhjemitic melts are generated when free water is available, whereas dehydration melting produces less sodic compositions. As for Na_2O contents of adakites, Xiong et al., (2006) have recently demonstrated that adakites usually exhibits lower Na_2O contents than experimental melts, which has been also interpreted as a consequence of melt/rock reaction within the sub-arc mantle. The geochemical features of the Sierra del Convento trondhjemites, which did not interact with the mantle wedge, support the conclusions of Xiong et al. (2006). We suggest that these rocks formed by wet melting of amphibolites, notably their Na_2O contents are similar to experimental melts of basalts and higher than those of adakites. Other significant differences between the trondhjemites from the Sierra del Convento and adakites include higher K_2O/Na_2O and Fe_2O_3+MgO+MnO+TiO_2 contents, and a peraluminous, rather than metaluminous, character. Clearly, the geochemical features of adakites may also be considered non-primary but gained during slab melt + peridotite + crust interaction.

In this respect, it is worth looking in detail at the $(La/Yb)_n$ vs. Yb_n (Martin, 1986) and Sr/Y vs. Y (Defant and Drummond, 1990) relationships widely used to characterize adakites and slab melts. Trondhjemites from Sierra del Convento plot within the adakite field in the Sr/Y vs. Y diagram (Fig. 10a)

but towards the high Sr/Y and low-Y end of the range, with common outliers with very high Sr/Y. This is a clear indication of a major participation of plagioclase and a minor participation of garnet during melting of the amphibolites. On the other hand, and in spite of the low Yb content of the Sierra del Convento trondhjemites indicating garnet fractionation as in adakites, they do not plot within the adakite field in the $(La/Yb)_n$ vs. Yb_n diagram (Fig. 10b). The reason for this is the low La contents of the trondhjemites and the corresponding weakly fractionated REE patterns. Again this feature can be explained by the lack of retention of the HREE in garnet either because it was not present or because it did not contribute significantly to the melting reaction, in addition LREE-bearing phases such as epidote and titanite were retained in the residual amphibolite. These minerals are not expected at sub-arc depths (100-200 km) in a normal, mature, subduction scenario, where eclogitic assemblages essentially made of omphacitic clinopyroxene and garnet plus rutile are expected, and plagioclase, amphibole, epidote, and titanite are not stable. These minerals are instead expected to be stable at intermediate pressure (ca. 40-60 km), which is largely far from normal sub-arc depths. Thus, differences in the extent of melting, P-T conditions of melting, and availability of fluid (which control mineral assemblages and modes of the residues) strongly control the geochemical features of resulting melts subsequently affected by interaction with the sub-arc mantle wedge. So, those REE and trace element patterns of pristine slab melts formed at sub-arc depths may differ significantly from the shallower hotter pristine slab melts of the Sierra del Convento (and Catalina Schist complex). This, in combination with their unmodified compositions, makes the Sierra del Convento trondhjemites particularly important for gaining insights into slab melt processes.

CONCLUSIONS

The geochemical characteristics of the trondhjemites of Sierra del Convento indicate that they constitute pristine slab melts generated under water-saturated partial melting of subducted N-MOR basaltic crust in response to a very hot subduction scenario likely caused by initiation of subduction involving a young hot slab. The depth of melting was shallower than typical sub-arc depths, where slab melts are segregated from garnet+clinopyroxene-rich residues.

Models of partial melting of normal-MORB indicate low degree of melting and generation of an amphibolitic residue bearing amphibole, epidote and garnet in varying amounts and containing neither plagioclase nor clinopyroxene. This model is in agreement with the mineral assemblages observed in the associated blocks of amphibolite. Based on the positive Eu anomaly of the trondhjemites and the corresponding negative anomaly of the amphibolites, plagioclase is inferred to have been present in the amphibolitic protoliths at the onset of melting. Thus, plagioclase in the amphibolites was totally consumed upon melting. The lack of plagioclase and scarcity of clinopyroxene in the amphibolites support fluid-present melting at near-solidus conditions. Plagioclase and fluid availability were the key controlling factors in the extent of melting. The external supply of water for the melting and metasomatic processes was not derived from a sedimentary source. The variable mineral mode of the amphibole-epidote±garnet residues was the result of variable protolith composition and extent of melting.

The hornblendites, locally associated with amphibolite-trondhjemite, do not represent melt residues but rocks formed after metasomatic modification of residual amphibolites.

The trondhjemitic melts produced by melting of the amphibolites have similar geochemical features to adakites, and thus we consider them to be one of the end-member sources (pristine slab melt) of this type of rock.

ACKNOWLEDGEMENTS

The authors thank K. Núñez Cambra and A. Rodríguez Vega for their field assistance. We also thank J. Scarrow, C. Marchesi, and A. Acosta for their kindly comments on an early version of this manuscript. This paper has received financial support from the Spanish MEC projects BTE2002-01011 and CGL2006-08527/BTE.

REFERENCES

Aguillón-Robles, A., Calmus, T., Benoit, M., Bellon, H., Maury, R.O., Cotten, J., Bourgois, J., Michaud, F., 2001. Late Miocene adakites and Nb-enriched basalts from Vizcaino Peninsula, Mexico: Indicators of East Pacific Rise subduction below Southern Baja California? Geology 29(6), 531-534.

Barker, F., 1979. Trondhjemite: Definition, environment and hypotheses of origin. In: F. Barker (Editor), Trondhjemites, dacites and related rocks. Elsevier, Amsterdam, pp. 1-12.

Barker, F., Arth, J.G., 1976. Generation of Trondhjemitic-Tonalitic Liquids and Archaean Bimodal Trondhjemite-Basalt Suites. Geology 4(10), 596-600.

Beard, J.S., Abitz, R.J., Lofgren, G.E., 1993. Experimental Melting of Crustal Xenoliths from Kilbourne Hole, New-Mexico and Implications for the Contamination and Genesis of Magmas. Contributions to Mineralogy and Petrology 115(1), 88-102.

Beate, B., Monzier, M., Spikings, R., Cotten, J., Silva, J., Bourdon, E., Eissen, J.P., 2001. Mio-Pliocene adakite generation related to flat subduction in southern

Ecuador: the Quimsacocha volcanic center. Earth and Planetary Science Letters 192(4), 561-570.

Bebout, G.E., Barton, M.D., 1993. Metasomatism During Subduction - Products and Possible Paths in the Catalina Schist, California. Chemical Geology 108(1-4), 61-92.

Benoit, M., Aguillón-Robles, A., Calmus, T., Maury, R.C., Bellon, H., Cotten, J., Bourgois, J., Michaud, F., 2002. Geochemical diversity of Late Miocene volcanism in southern Baja California, Mexico: Implication of mantle and crustal sources during the opening of an asthenospheric window. Journal of Geology 110(6), 627-648.

Blanco Quintero, I.F., 2003. Nuevos datos petroquímicos y petrográficos de las magmatitas y metamorfitas de algunos sectores del bloque oriental cubano (sectores Moa-Baracoa y Sierra del Convento). Master´s Thesis, University of Moa, Moa (Cuba), 77 pp.

Boiteau, A., Saliot, P., Michard, A., 1972. High-Pressure Metamorphism in Ophiolite Complex of Purial (Oriente, Cuba). Comptes Rendus Hebdomadaires Des Seances De L Academie Des Sciences Serie D 274(15), 2137-&.

Bourdon, E., Eissen, J.P., Gutscher, M.A., Monzier, M., Hall, M.L., Cotten, J., 2003. Magmatic response to early aseismic ridge subduction: the Ecuadorian margin case (South America). Earth and Planetary Science Letters 205(3-4), 123-138.

Bourdon, E., Eissen, J.P., Gutscher, M.A., Monzier, M., Samaniego, P., Robin, C., Bollinger, C., Cotten, J., 2002. Slab melting and slab melt metasomatism in the Northern Andean Volcanic Zone: adakites and high-Mg andesites from Pichincha volcano (Ecuador). Bulletin De La Societe Geologique De France 173(3), 195-206.

Champion, D.C., Smithies, R.H., 2003. Slab melts and related processes-Archaean versus Recent. In: M. Arima, Nakajima, T., Ishihara, S. (Editor), Hutton Symposium V, The Origin of Granites and Related Rocks. Geological Survey of Japan, pp. 19.

Coutinho, J. M. V., Kräutner, H. G., Sassi, F., Schmid, R. & Sen, S. 2007. A systematic nomenclature for metamorphic rocks: 8. Amphibolite and granulite. Recommendations by the IUGS Subcommission on the Systematics of Metamorphic Rocks. Web version of 01.02.2007 (http://www.bgs.ac.uk/SCMR/docs/papers/paper_8.pdf).

De Paolo, D.J., 1988. Neodymium Isotope Geochemistry: An Introduction. Springer-Verlag, Heidelberg, 187 pp.

Defant, M.J., Drummond, M.S., 1990. Derivation of Some Modern Arc Magmas by Melting of Young Subducted Lithosphere. Nature 347(6294), 662-665.

Defant, M.J., Jackson, T.E., Drummond, M.S., Deboer, J.Z., Bellon, H., Feigenson, M.D., Maury, R.C., Stewart, R.H., 1992. The Geochemistry of Young Volcanism Throughout Western Panama and Southeastern Costa-Rica - an Overview. Journal of the Geological Society 149, 569-579.

Donnelly, T.W., Beets, D., Carr, M.J., Jackson, T., Klaver, G., Lewis, J., Maury, R., Schellekens, H., Smith, A.L., Wadge, G., Westercamp, D., 1990. History and tectonic setting of Caribbean magmatism. In: G. Dengo, Case, J.E. (Editor), The Geology of North America: The Caribbean Region. Geological Society of America, pp. 339-374.

Foley, S.F., Barth, M.G., Jenner, G.A., 2000. Rutile/melt partition coefficients for trace elements and an assessment of the influence of rutile on the trace element characteristics of subduction zone magmas. Geochimica Et Cosmochimica Acta 64(5), 933-938.

Frei, D., Liebscher, A., Wittenberg, A., Shaw, C.S.J., 2003. Crystal chemical controls on rare earth element partitioning between epidote-group minerals and melts: an experimental and theoretical study. Contributions to Mineralogy and Petrology 146(2), 192-204.

García-Casco, A., 2005. Partial melting and counter-clockwise P-T path of subducted oceanic crust: a case study of hot subduction in the northern Caribbean (E Cuba), Metamorphic Studies Group Annual General Meeting, Geological Society of London, Burlington House, London.

García-Casco, A., Torres-Roldán, R.L., Iturralde-Vinent, M.A., Millán, G., Núñez Cambra, K., Lázaro, C., Rodríguez Vega, A., 2006. High pressure metamorphism of ophiolites in Cuba. Geologica Acta 4, 63-88.

García-Casco, A., Lázaro, C., Torres-Roldán, R.L., Núñez Cambra, K., Rojas Agramonte, Y., Kröner, A., Neubauer, F., Millán, G., Blanco Quintero, I., submitted manuscript to Journal of Petrology, 2007. Partial melting and counterclockwise P-T path of subducted oceanic crust (Sierra del Convento mélange, Cuba). A case of very hot subduction.

García-Casco, A., Pérez de Arce, C., Millán, G., Iturralde-Vinent, M.A., Fonseca, E., Torres-Roldán, R.L., Núñez, K., Morata, D., 2003. Metabasites from the northern serpentinite belt (Cuba) and a metamorphic perspective of the plate tectonic models for the Caribbean region. In: M.G. 2003 (Editor), IV Congreso de Geología y Minería. Centro Nacional de Información Geológica, La Habana, pp. 10.

García-Casco, A., Torres-Roldán, R.L., Millán, G., Monie, P., Haissen, F., 2001. High-grade metamorphism and hydrous melting of metapelites in the Pinos terrane (W Cuba): Evidence for crustal thickening and extension in the northern Caribbean collisional belt. Journal of Metamorphic Geology 19(6), 699-715.

Gill, J.B., 1981. Orogenic Andesites and Plate Tectonics. Springer-Verlag, Berlin, 390 pp.

Govindaraju, K., 1994. Compilation of working values and sample description for 383 geostandards. Geostandards Newsletter 18, 1-158.

Grove, M., Bebout, G.E., 1995. Cretaceous tectonic evolution of coastal southern California: Insights from the Catalina Schist. Tectonics 14(6), 1290-1308.

Gutscher, M.A., Maury, R., Eissen, J.P., Bourdon, E., 2000. Can slab melting be caused by flat subduction? Geology 28(6), 535-538.

Hart, S.R., Blusztajn, J., Dick, H.J.B., Meyer, P.S., Muehlenbachs, K., 1999. The fingerprint of seawater circulation in a 500-meter section of ocean crust gabbros. Geochimica Et Cosmochimica Acta 63(23-24), 4059-4080.

Hernández, M., Canedo, Z., 1995. Geoquímica de las ofiolitas meridionales de Cuba oriental. University of Moa, Moa (Cuba).

Hilyard, M., Nielsen, R.L., Beard, J.S., Patiño-Douce, A., Blencoe, J., 2000. Experimental determination of the partitioning behaviour of rare earth and high field strength elements between pargasitic amphibole and natural silicate melts. Geochimica Et Cosmochimica Acta 64(6), 1103-1120.

Hoernle, K., Hauff, F., and van den Bogaard, P., 2004, 70 m.y. history (139-69 Ma) for the Caribbean large igneous province. Geology 32, 697-700.

Hofmann, A.W., 1988. Chemical Differentiation of the Earth - the Relationship between Mantle, Continental-Crust, and Oceanic-Crust. Earth and Planetary Science Letters 90(3), 297-314.

Iturralde-Vinent, M.A., 1998. Sinopsis de la Constitución Geológica de Cuba. Acta Geológica Hispánica 33, 9-56.

Iturralde-Vinent, M.A., Millán, G., Korkas, L., Nagy, E., Pajón, J., 1996. Geological interpretation of the Cuban K-Ar data base. In: M.A. Iturralde-Vinent (Editor), Ofiolitas Y Arcos Volcánicos de Cuba. IGCP Project 364, Miami (USA), pp. 48-69.

Jahn, B.M., Bernardgriffiths, J., Charlot, R., Cornichet, J., Vidal, F., 1980. Nd and Sr Isotopic Compositions and REE Abundances of Cretaceous MORB (Holes 417d and 418a, Legs 51, 52 and 53). Earth and Planetary Science Letters 48(1), 171-184.

Jolly, W.T., Lidiak, E.G., Dickin, A.P., 2006. Cretaceous to Mid-Eocene pelagic sediment budget in Puerto Rico and the Virgin Islands (northeast Antilles Island arc). Geologica Acta 4(1-2), 35-62.

Kay, R.W., 1978. Aleutian Magnesian Andesites - Melts from Subducted Pacific Ocean Crust. Journal of Volcanology and Geothermal Research 4(1-2), 117-132.

Kay, S.M., Ramos, V.A., Marquez, M., 1993. Evidence in Cerro-Pampa Volcanic-Rocks for Slab-Melting Prior to Ridge-Trench Collision in Southern South-America. Journal of Geology 101(6), 703-714.

Kelemen, P.B., Hanghøj, K., Green, A.R., 2003. One view of the geochemistry of subduction-related magmatic arcs, with an emphasis on primitive andesite and lower crust. In: R. Rudnick (Editor), Geochemistry of the Crust: Treatise of Geochemistry. Elsevier, Amsterdam, pp. 593-659.

Kelemen, P.B., Kikawa, E., Miller, J., 2004. Igneous crystallization and localized deformation > 15 km beneath the Mid-Atlantic Ridge, 14-16 N. Geochimica Et Cosmochimica Acta 68(11), A690-A690.

Kerr, A.C., Iturralde-Vinent, M.A., Saunders, A.D., Babbs, T.L., Tarney, J., 1999. A new plate tectonic model of the Caribbean: Implications from a geochemical reconnaissance of Cuban Mesozoic volcanic rocks. Geological Society of America Bulletin 111, 1581-1599.

Kerr, A.C., Tarney, J., 2005. Tectonic evolution of the Caribbean and northwestern South America: The case for accretion of two Late Cretaceous oceanic plateaus. Geology 33, 269-272.

Kerr, A.C., Tarney, J., Nivia, A., Marriner, G.F., Saunders, A.D., 1998. The internal structure of oceanic plateaus: Inferences from obducted Cretaceous terranes in western Colombia and the Caribbean. Tectonophysics 292, 173-188.

Kilian, R., Stern, C.R., 2002. Constraints on the interaction between slab melts and the mantle wedge from adakitic glass in peridotite xenoliths. European Journal of Mineralogy 14(1), 25-36.

Klein, M., Stosch, H.G., Seck, H.A., 1997. Partitioning of high field-strength and rare-earth elements between amphibole and quartz-dioritic to tonalitic melts: An experimental study. Chemical Geology 138(3-4), 257-271.

Klemme, S., Prowatke, S., Hametner, K., Gunther, D., 2005. Partitioning of trace elements between rutile and silicate melts: Implications for subduction zones. Geochimica Et Cosmochimica Acta 69(9), 2361-2371.

Kretz, R., 1983. Symbols for Rock-Forming Minerals. American Mineralogist 68(1-2), 277-279.

Kulachkov, L.V., Leyva, R.C., 1990. Informe sobre los resultados de los trabajos de reconocimiento geológico para cuarzo filoniano en la parte oriental de Cuba., Instituto Superior Minero-Metalúrgico., Moa (Cuba).

Kushiro, I., 1990. Partial Melting of Mantle Wedge and Evolution of Island-Arc Crust. Journal of Geophysical Research-Solid Earth and Planets 95(B10), 15929-15939.

Le Maitre, R.W., Bateman, P., Dudek, A., Keller, J., Lameyre Le Bas, M.J., Sabine, P.A., Schmid, R., Sorensen, H., Streckeisen, A., Woolley, A.R., Zanettin, B., 1989. A classification of igneous rocks and glossary of terms. Blackwell, Oxford, 196 pp.

Lebron, M.C., Perfit, M.R., 1993. Stratigraphic and petrochemical data support subduction polarity reversal of the Cretaceous Caribbean island arc. Journal of Geology 101, 389-396.

Lewis, J.F., Escuder Viruete,J., Hernaiz Huerta P.P., Gutierrez, G., Draper, G., Pérez-Estaún, A., 2002. Geochemical subdivision of the Circum-Caribbean Island Arc, Dominican Cordillera Central: implications for crustal formation, accretion and growth within an intra-oceanic setting. Acta Geológica Hispánica, 37(2-3), 81-122.

Leyva, R.C., 1996. Características geológicas, regularidades de distribución y perspectivas de utilización del cuarzo filoniano de la region oriental de Cuba. Master´s Thesis, University of Moa, Moa (Cuba), 90 pp.

Marchesi, C., Garrido, C.J., Godard, M., Proenza, J.A., Gervilla, F., Blanco-Moreno, J., 2006. Petrogenesis of highly depleted peridotites and gabbroic rocks from the Mayarí-Baracoa Ophiolitic Belt (eastern Cuba). Contributions to Mineralogy and Petrology 151(6), 717-736.

Martin, H., 1999. The adakitic magmas: modern analogues of Archaean granitoids. Lithos 46(3), 411- 429.

Martin, H., 1986. Effect of steeper Archaean geothermal gradient on geochemistry of subduction-zone magmas. Geology 14, 753-756.

Martin, H., Moyen, J.-F., 2003. Secular changes in TTG composition: comparison with modern adakites, EGS-AGU-EUG joint meeting, Nice.

Martin, H., Smithies, R.H., Rapp, R., Moyen, J.F., Champion, D., 2005. An overview of adakite, tonalite-trondhjemite-granodiorite (TTG), and sanukitoid: relationships and some implications for crustal evolution. Lithos 79, 1-24.

Maury, R.C., Sajona, F.G., Pubellier, M., Bellon, H., Defant, M.J., 1996. Melting of oceanic crust in young subduction/collision zones: The case of Mindanao (Philippines). Bulletin De La Societe Geologique De France 167(5), 579-595.

McCulloch, M.T., Gregory, R.T., Wasserburg, G.J., Taylor, H.P., 1981. Sm-Nd, Rb-Sr, and O-18-O-16 Isotopic Systematics in an Oceanic Crustal Section - Evidence from the Samail Ophiolite. Journal of Geophysical Research 86(NB4), 2721-2735.

McDonough, W.F., Sun, S.S., 1995. The Composition of the Earth. Chemical Geology 120(3-4), 223-253.

Millán, G., 1996. Metamorfitas de la asociación ofiolítica de Cuba. In: M.A. Iturralde-Vinent (Editor), Ofiolitas y Arcos Volcanicos de Cuba. IGCP Project 364, Miami (USA), pp. 147-153.

Millán, G., Somin, M., 1985. Nuevos aspectos sobre de la estratigrafía del macizo metamórfico de Escambray. Contribución al conocimiento geológico de las metamorfitas del Escambray y Purial, Instituto de Gelogía y Paleontología, La Habana.

Morris, P.A., 1995. Slab Melting as an Explanation of Quaternary Volcanism and Aseismicity in Southwest Japan. Geology 23(5), 395-398.

O´Connor, J.T., 1965. A classification of quartz-rich igneous rocks based on feldspar ratios., 525B. U. S. Geological Survey Professional Paper, B79-B84 pp.

Pearce, J.A., 1982. Trace element characteristics of lavas from destructive plate boundaries. In: R.S. Thorpe (Editor), Andesites. Wiley, Chichester, pp. 525-548.

Pearce, J.A., Harris, N.B.W., Tindle, A.G., 1984. Trace-Element Discrimination Diagrams for the Tectonic Interpretation of Granitic-Rocks. Journal of Petrology 25(4), 956-983.

Peccerillo, A., Taylor, S.R., 1976. Geochemistry of Eocene Calc-Alkaline Volcanic-Rocks from Kastamonu Area, Northern Turkey. Contributions to Mineralogy and Petrology 58(1), 63-81.

Piepgras, D.J., Wasserburg, G.J., 1980. Neodymium Isotopic Variations in Seawater. Earth and Planetary Science Letters 50(1), 128-138.

Pindell, J.L., Kennan, L., 2001. Kinematic Evolution of the Gulf of Mexico and Caribbean. In: R. Fillon, Rosen, N., Weimer, P., Lowrie, A., Pettingill, H., Phair, R., Roberts, H., van Hoorn, B. (Editor), Transactions of the Gulf Coast Section Society of Economic Paleontologists and Mineralogists (GCSSEPM). 21st Annual Bob F. Perkins Research Conference, Petroleum Systems of Deep-Water Basins, Houston, Texas, pp. 193-220.

Pindell, J.L., Kennan, L., Maresch, W.V., Stanek, K.P., Draper, G., Higgs, R., 2005. Plate-kinematics and crustal dynamics of circum-Caribbean arc-continent interactions: Tectonic controls on basin development in Proto-Caribbean margins. In: H.G. Avé Lallemant, Sisson, V.B (Editor), Caribbean-South American plate interactions, Venezuela. Geological Society of America, Special Paper 394, pp. 7-52.

Pindell, J.L., Kennan, L., Stanek, K.P., Maresch, W.V., Draper, G., 2006. Foundations of Gulf of Mexico and Caribbean evolution: eight controversies resolved. Geologica Acta 4, 303-341.

Proenza, J., Gervilla, F., Melgarejo, J.C., Bodinier, J.L., 1999. Al- and Cr-rich chromitites from the Mayarí-Baracoa ophiolitic belt (eastern Cuba): consequence of interaction between volatile-rich melts and peridotites in supra-subduction mantle. Economic Geology 94, 547-566.

Proenza, J., Melgarejo, J.C., Gervilla, F., Lavaut, W., Revé, D., Rodríguez, G., 1998. Cromititas podiformes en la Faja ofiolitica Mayarí-Baracoa (Cuba). Acta Geologica Hispanica 33, 153-177.

Prouteau, G., Scaillet, B., Pichavant, M., Maury, R., 2001. Evidence for mantle metasomatism by hydrous silicic melts derived from subducted oceanic crust. Nature 410(6825), 197-200.

Prouteau, G., Scaillet, B., Pichavant, M., Maury, R.C., 1999. Fluid-present melting of ocean crust in subduction zones. Geology 27(12), 1111-1114.

Rapp, R.P., Shimizu, N., Norman, M.D., Applegate, G.S., 1999. Reaction between slab-derived melts and peridotite in the mantle wedge: experimental constraints at 3.8 GPa. Chemical Geology 160(4), 335-356.

Sajona, F.G., Maury, R.C., 1998. Association of adakites with gold and copper mineralization in the Philippines. Comptes Rendus De L Academie Des Sciences Serie Ii Fascicule a-Sciences De La Terre Et Des Planetes 326(1), 27-34.

Sajona, F.G., Maury, R.C., Bellon, H., Cotten, J., Defant, M., 1996. High field strength element enrichment of Pliocene-Pleistocene Island arc basalts, Zamboanga Peninsula, western Mindanao (Philippines). Journal of Petrology 37(3), 693-726.

Sajona, F.G., Maury, R.C., Pubellier, M., Leterrier, J., Bellon, H., Cotten, J., 2000. Magmatic source enrichment by slab-derived melts in a young post-collision setting, central Mindanao (Philippines). Lithos 54(3-4), 173-206.

Samaniego, P., Martin, H., Monzier, M., Robin, C., Fornari, M., Eissen, J.P., Cotten, J., 2005. Temporal evolution of magmatism in the Northern Volcanic Zone of the Andes: The geology and petrology of Cayambe Volcanic Complex (Ecuador). Journal of Petrology 46(11), 2225-2252.

Sen, C., Dunn, T., 1994. Dehydration Melting of a Basaltic Composition Amphibolite at 1.5 and 2.0 GPa - Implications for the Origin of Adakites. Contributions to Mineralogy and Petrology 117(4), 394-409.

Shervais, J.W., 1982. Ti-V Plots and the Petrogenesis of Modern and Ophiolitic Lavas. Earth and Planetary Science Letters 59(1), 101-118.

Sisson, T.W., Bacon, C.R., 1992. Garnet High-Silica Rhyolite Trace-Element Partition-Coefficients Measured by Ion Microprobe. Geochimica Et Cosmochimica Acta 56(5), 2133-2136.

Smith, D.R., Leeman, W.P., 1987. Petrogenesis of Mount St-Helens Dacitic Magmas. Journal of Geophysical Research-Solid Earth and Planets 92(B10), 10313-10334.

Smithies, R.H., 2000. The Archaean tonalite-trondhjemite-granodiorite (TTG) series is not an analogue of Cenozoic adakite. Earth and Planetary Science Letters 182(1), 115-125.

Somin, M., Millán, G., 1981. Geology of the Metamorphic Complexes of Cuba (in russian). Nauka, Moscow, 219 pp.

Sorensen, S.S., 1988. Petrology of Amphibolite-Facies Mafic and Ultramafic Rocks from the Catalina Schist, Southern-California - Metasomatism and Migmatization in a Subduction Zone Metamorphic Setting. Journal of Metamorphic Geology 6(4), 405-435.

Sorensen, S.S., Grossman, J.N., 1989. Enrichment of Trace-Elements in Garnet Amphibolites from a Paleo-Subduction Zone - Catalina Schist, Southern-California. Geochimica Et Cosmochimica Acta 53(12), 3155-3177.

Staudigel, H., Plank, T., White, W.M., Schmincke, H., 1996. Geochemical fluxes during seafloor alteration of the basaltic upper oceanic crust: DSDP Sites 417 and 418. In: G.E. Bebout, Scholl, S.W.,Kirby, S.H., Platt, J.P. (Editor), Subduction from Top to Bottom. American Geophysical Union, Washington, DC, pp. 19-38.

Stern, C.R., Kilian, R., 1996. Role of the subducted slab, mantle wedge and continental crust in the generation of adakites from the Andean Austral volcanic zone. Contributions to Mineralogy and Petrology 123(3), 263-281.

Stevenson, J.A., Daczko, N.R., Clarke, G.L., Pearson, N., Klepeis, K.A., 2005. Direct observation of adakite melts generated in the lower continental crust, Fiordland, New Zealand. Terra Nova 17(1), 73-79.

Tatsumi, Y., Kogiso, T., 1997. Trace element transport during dehydration processes in the subducted oceanic crust .2. Origin of chemical and physical characteristics in arc magmatism. Earth and Planetary Science Letters 148(1-2), 207-221.

Tiepolo, M., Oberti, R., Vannucci, R., 2002. Trace-element incorporation in titanite: constraints from experimentally determined solid/liquid partition coefficients. Chemical Geology 191(1-3), 105-119.

Wasserburg, G.J., Jacobsen, S.B., DePaolo, D.J., McCulloch, M.T., Wen, T., 1981. Precise determination of Sm/Nd ratios, Sm and Nd isotopic abundances in standard solutions. Geochimica Et Cosmochimica Acta 45, 2311-2323.

Wood, D.A., Joron, J.L., Treuil, M., 1979. Re-Appraisal of the Use of Trace-Elements to Classify and Discriminate between Magma Series Erupted in Different Tectonic Settings. Earth and Planetary Science Letters 45(2), 326-336.

Workman, R.K., Hart, S.R., 2005. Major and trace element composition of the depleted MORB mantle (DMM). Earth and Planetary Science Letters 231(1-2), 53-72.

Xiong, X.L., Adam, J., Green, T.H., 2005. Rutile stability and rutile/melt HFSE partitioning during partial melting of hydrous basalt: Implications for TTG genesis. Chemical Geology 218(3-4), 339-359.

Xiong, X.L., Xia, B., Xu, J.F., Niu, H.C., Xiao, W.S., 2006. Na depletion in modern adakites via melt/rock reaction within the sub-arc mantle. Chemical Geology 229(4), 273-292.

Yogodzinski, G.M., Kay, R.W., Volynets, O.N., Koloskov, A.V., Kay, S.M., 1995. Magnesian Andesite in the Western Aleutian Komandorsky Region - Implications for Slab Melting and Processes in the Mantle Wedge. Geological Society of America Bulletin 107(5), 505-519.

Yogodzinski, G.M., Lees, J.M., Churikova, T.G., Dorendorf, F., Woerner, G., Volynets, O.N., 2001. Geochemical evidence for the melting of subducting oceanic lithosphere at plate edges. Nature 409(6819), 500-504.

Table 1. Major (wt%) and trace (ppm) element composition of epidote-amphibolites from the Sierra del Convento mélange.

Rock type	Ep-amphibolite										
Sample	CV53b	CV237n	CV53-I	CV53x-I	CV54a	CV61a	CV62	CV62a	CV62b-I	CV237h	CV237m-I
SiO2	45.84	47.91	47.93	41.82	41.41	44.44	46.12	47.26	46.78	48.99	49.32
TiO2	1.72	0.7	0.95	1.82	1.34	1.93	1.33	1.11	1.26	1.13	0.76
Al2O3	16.4	17.16	17.05	18.76	18.19	13.87	17.9	18.11	16.98	14.96	13.21
Fe2O3	11.9	8.43	9.51	11.52	11.72	13.96	11.17	9.4	10.36	9.09	9.45
MnO	0.18	0.15	0.16	0.17	0.17	0.20	0.18	0.15	0.17	0.12	0.16
MgO	7.36	8.34	8.18	8.01	8.93	10.11	7.72	7.36	7.78	7.89	9.6
CaO	12.33	12.64	13.16	13.4	14.73	10.6	12.3	12.1	12.99	12.55	12.66
Na2O	1.58	2.38	1.2	1.47	1.14	2.06	1.89	2.13	1.58	2.85	2.00
K2O	0.27	0.13	0.13	0.23	0.25	0.32	0.21	0.16	0.2	0.15	0.07
P2O5	0.15	0.05	0.09	0.13	0.13	0.22	0.11	0.10	0.11	0.16	0.04
LOI	1.57	2.24	2.62	2.36	1.97	1.8	1.46	1.64	1.8	1.5	2.08
Zr XRF	102	29	56	104	63	49	85	70	77	198	26
Li	6.9	6.8	5.0	5.3	5.0	6.6	4.8	4.0	3.1	8.7	6.1
Rb	1.7	2.2	1.1	1.3	1.3	1.7	1.6	1.6	1.4	1.9	0.7
Cs	0.08	1.00	0.06	0.12	n. d.	0.19	0.27	0.29	0.03	0.04	0.02
Be	0.43	0.57	0.34	0.51	0.30	0.87	0.69	0.67	0.38	0.41	0.43
Sr	193	169	345	272	169	82	139	130	169	180	298
Ba	32	54	29	33	49	145	17	363	12	57	26
Sc	43	43	30	39	42	53	39	29	32	37	44
V	323	227	199	258	269	358	279	222	231	257	243
Cr	318	275	335	329	374	463	328	293	278	264	306
Co	55	44	43	46	52	54	56	56	51	58	46
Ni	111	98	154	121	133	136	133	168	106	114	126
Cu	62	26	37	15	42	36	42	28	56	8	9
Zn	106	51	70	106	90	143	105	82	81	51	51
Ga	18.0	14.9	15.2	19.6	19.1	16.9	16.6	15.1	14.8	18.3	17.5
Y	40.9	19.4	21.7	39.6	44.1	42.7	32.6	26.0	28.8	37.4	17.9
Nb	1.06	0.77	0.71	1.51	1.12	1.97	0.78	0.51	0.83	2.04	0.70
Ta	0.221	0.137	0.168	0.231	0.249	0.237	0.144	0.156	0.219	0.299	0.165
Hf	0.91	0.40	0.68	1.11	1.65	1.02	0.83	0.79	0.94	0.92	0.52
Mo	2.23	0.97	1.95	1.51	1.78	0.97	1.41	2.07	2.54	2.96	1.08
Sn	1.53	0.63	0.83	1.77	1.80	1.42	0.64	0.62	1.03	1.27	0.54
Tl	0.025	n. d.	0.017	0.019	0.027	n. d.	n. d.	n. d.	0.017	0.015	n. d.
Pb	1.07	1.61	2.17	1.46	0.82	0.90	0.48	0.52	0.76	0.99	2.83
U	0.076	0.006	0.033	0.513	1.613	0.140	0.064	0.029	0.082	0.056	0.009
Th	0.174	0.036	0.055	0.197	0.147	0.267	0.102	0.061	0.112	0.142	0.027
La	3.87	1.76	2.09	6.32	2.80	4.94	3.33	2.18	2.99	3.68	0.78
Ce	11.9	3.4	5.5	16.1	8.6	11.7	8.5	6.5	8.7	11.7	3.0
Pr	2.26	0.68	1.15	3.11	1.63	2.40	1.68	1.30	1.66	2.12	0.58
Nd	12.6	3.9	6.6	16.2	9.4	12.8	9.2	7.1	9.1	11.6	3.4
Sm	4.10	1.50	2.33	5.43	3.50	4.10	3.24	2.66	3.30	4.32	1.43
Eu	1.53	0.66	0.92	2.26	1.62	1.60	1.09	0.94	1.24	1.28	0.80
Gd	5.6	2.3	3.3	7.1	5.6	5.7	4.3	3.4	4.4	5.7	2.3
Tb	1.03	0.44	0.61	1.23	1.10	1.06	0.77	0.62	0.80	1.04	0.43
Dy	7.0	3.0	4.2	8.0	7.5	7.4	5.3	4.2	5.3	6.6	3.1
Ho	1.57	0.68	0.95	1.75	1.71	1.54	1.17	0.91	1.18	1.41	0.71
Er	4.34	1.93	2.54	4.63	4.66	4.30	3.27	2.54	3.39	4.04	2.01
Tm	0.67	0.29	0.38	0.68	0.70	0.62	0.49	0.38	0.51	0.63	0.30
Yb	4.07	1.77	2.39	3.96	4.14	3.80	3.05	2.40	3.18	4.09	1.89
Lu	0.60	0.26	0.35	0.57	0.59	0.57	0.46	0.36	0.47	0.60	0.29

Table 1. (continued). Major (wt%) and trace (ppm) element composition of epidote- and garnet+epidote-amphibolites from the Sierra del Convento mélange.

Rock type	Ep-amphibolite					Grt-amphibolite				
Sample	CV237p-I	CV53o-I	CV53o-2	CV227a	CV237r	CV139f	CV228e	CV230b	CV237j	CV279a
SiO2	42.43	47.31	46.17	42.14	49.21	48.32	48.02	43.25	43.94	40.52
TiO2	2.8	2.08	2.15	1.06	0.59	1.66	2.16	1.94	2.57	3.33
Al2O3	12.09	15.22	15.16	19.83	14.39	15.44	14.99	16.7	13.33	13.34
Fe2O3	18.23	12.5	12.31	9.9	8.94	11.26	12.95	12.69	16.64	20.37
MnO	0.25	0.18	0.17	0.15	0.16	0.19	0.18	0.39	0.20	0.26
MgO	8.89	7.48	7.78	8.04	8.99	6.82	6.57	7.72	7.56	7.51
CaO	10.37	10.8	12.07	14.8	11.49	10.65	11.51	13.99	12.97	10.82
Na2O	2.09	1.62	1.72	1.38	3.02	2.83	1.53	1.29	1.85	1.59
K2O	0.16	0.17	0.22	0.18	0.17	0.47	0.21	0.31	0.05	0.2
P2O5	0.25	0.13	0.20	0.10	0.05	0.16	0.21	0.18	0.24	0.32
LOI	1.59	1.88	1.78	1.87	2.36	1.98	1.14	1.18	0.73	1.01
Zr XRF	126	129	132	65	26	98	127	112	139	180
Li	4.2	5.5	4.0	3.7	7.9	16.5	4.0	4.8	3.8	9.5
Rb	1.18	1.10	0.68	1.49	2.32	6.80	1.98	2.24	1.07	1.54
Cs	0.050	0.024	n. d.	0.125	0.094	0.379	0.996	0.973	0.288	0.369
Be	0.64	0.56	0.36	0.41	0.22	0.96	0.78	0.74	0.69	0.94
Sr	69	202	174	305	89	271	165	426	78	84
Ba	41	16	11	16	67	243	12	57	61	85
Sc	57	45	31	36	48	43	43	43	51	63
V	556	370	327	244	239	304	365	358	499	628
Cr	145	203	206	472	392	292	223	303	158	107
Co	57	61	38	38	47	47	59	52	58	71
Ni	72	110	96	134	112	79	98	117	66	66
Cu	34	60	55	77	16	50	49	25	45	75
Zn	108	102	89	90	54	95	113	127	59	194
Ga	21	19	17	21	15	17	19	20	21	22
Y	62	47	33	25	16	27	50	48	61	72
Nb	3.1	1.4	1.1	1.0	0.8	7.2	1.1	2.4	2.3	3.2
Ta	0.30	0.29	0.092	0.13	0.16	0.60	0.22	0.28	0.31	0.39
Hf	1.54	0.98	0.74	0.83	0.36	0.87	0.88	1.01	1.56	1.35
Mo	1.44	2.15	0.20	1.02	1.27	1.71	2.39	1.73	1.81	2.18
Sn	1.81	1.41	1.83	1.19	0.60	0.81	1.25	1.23	2.41	1.71
Tl	0.008	0.013	n. d.	0.016	0.037	n. d.	n. d.	n. d.	n. d.	n. d.
Pb	0.579	0.950	0.913	1.32	0.77	3.54	0.737	7.54	0.056	1.58
U	0.116	0.081	0.069	0.159	0.024	0.188	0.072	0.205	0.080	0.129
Th	0.527	0.171	0.100	0.115	0.059	0.548	0.128	0.173	0.074	0.184
La	7.0	5.5	3.1	2.5	1.1	6.9	5.3	4.6	3.9	5.3
Ce	20.7	17.4	10.6	7.9	3.2	16.7	14.3	11.6	14.0	17.9
Pr	3.5	3.1	1.9	1.5	0.6	2.6	2.6	2.2	2.8	3.5
Nd	18.5	15.9	10.5	7.8	3.5	12.1	14.5	12.7	15.5	19.5
Sm	6.7	5.4	3.4	2.6	1.3	3.8	5.1	4.4	5.6	7.2
Eu	2.2	2.1	1.4	1.0	0.6	1.3	1.7	1.5	1.9	2.3
Gd	9.2	6.8	4.7	3.5	2.1	4.5	6.8	6.0	7.7	9.7
Tb	1.66	1.22	0.85	0.64	0.38	0.73	1.20	1.10	1.40	1.72
Dy	10.7	8.0	5.5	4.3	2.6	4.6	7.9	7.2	9.6	11.4
Ho	2.4	1.8	1.2	0.9	0.6	1.0	1.7	1.6	2.1	2.5
Er	6.7	4.9	3.4	2.6	1.6	2.7	4.8	4.8	6.1	7.1
Tm	1.02	0.75	0.52	0.39	0.26	0.40	0.70	0.70	0.93	1.08
Yb	6.5	4.8	3.3	2.4	1.6	2.4	4.5	4.5	5.8	6.9
Lu	0.95	0.69	0.47	0.36	0.24	0.37	0.68	0.67	0.91	1.02

Table 1. (continued) Major (wt%) and trace (ppm) element composition of garnet+epidote-amphibolites and hornblendites from the Sierra del Convento mélange.

Rock type	Grt-amphibolite				hornblendite					
Sample	CV54e	CV237c	CV237e	CV228d	CV139b	CV139f-1	CV61	CV61b	CV53o-1	CV139d
SiO2	50.21	43.65	45.98	46.26	45.58	47.6	43.73	44.15	51.47	48.41
TiO2	1.69	2.66	2.03	2.26	1.35	1.91	1.26	1.2	0.19	0.95
Al2O3	16.04	13.18	13.53	14.68	14.75	11.07	13.97	14.28	9.25	9.75
Fe2O3	10.37	17.99	14.61	14.46	11.32	12.78	13.95	13.95	7.25	11.55
MnO	0.17	0.25	0.21	0.20	0.17	0.17	0.20	0.21	0.18	0.19
MgO	7.27	7.98	7.71	6.98	10.62	9.61	11.35	10.9	16.55	14.44
CaO	10.67	10.41	11.68	11.4	11.02	11.52	10.36	10.79	10.6	10.29
Na2O	1.92	2.49	2.53	1.61	2.05	2.43	2.21	2.18	1.88	1.87
K2O	0.26	0.09	0.06	0.26	0.62	0.45	0.39	0.33	0.28	0.34
P2O5	0.13	0.26	0.19	0.22	0.17	0.27	0.22	0.14	0.06	0.06
LOI	1.16	1.44	0.99	0.95	1.81	1.86	1.95	1.94	2.04	1.45
Zr XRF	99	125	111	133	86	110	33	39	13	65
Li	4.6	6.1	4.5	4.9	10.6	7.0	6.8	6.7	3.4	3.0
Rb	1.68	1.77	0.94	2.6	9.7	3.1	3.0	2.5	0.92	2.2
Cs	0.28	0.12	0.069	0.0428	0.091	0.076	0.30	0.24	0.022	0.25
Be	0.70	0.50	0.197	0.62	0.46	0.67	1.01	1.02	0.155	0.91
Sr	125	98	88	133	202	158	74	121	17	42
Ba	42	15	40	13	357	94	71	57	22	56
Sc	38	53	40	47	31	51	58	60	5	27
V	266	537	366	382	225	325	391	409	68	213
Cr	252	130	216	294	608	188	345	238	805	612
Co	56	53	53	46	58	45	53	47	39	72
Ni	108	62	77	90	209	110	242	210	622	420
Cu	73	43	44	16.8	49	16.9	45	34	1.6	13.7
Zn	95	149	45	139	77	93	134	131	95	104
Ga	17.3	21	18.0	19.7	14.5	16.2	16.5	16.6	9.8	12.2
Y	34	58	48	52	22	22	18.9	20	3.5	16.4
Nb	0.95	3.1	2.1	0.9	6.1	6.4	0.88	0.76	0.149	3.5
Ta	0.22	0.30	0.26	0.10	0.54	0.42	0.34	0.08	0.04	0.32
Hf	0.80	1.16	1.36	1.04	0.77	0.88	1.06	1.03	0.25	0.85
Mo	2.53	1.33	1.72	0.85	1.33	0.38	0.84	0.76	0.03	1.77
Sn	0.81	1.55	1.77	1.57	1.16	1.42	0.95	1.16	0.35	0.76
Tl	n. d.	0.001	0.005	0.032	0.092	0.030	n. d.	n. d.	0.003	n. d.
Pb	0.90	0.44	0.28	0.61	2.75	1.59	0.77	1.05	0.11	0.78
U	0.081	0.039	0.057	0.076	0.144	0.192	0.038	0.028	n. d.	0.096
Th	0.185	0.076	0.062	0.153	0.499	0.575	0.185	0.018	0.026	0.136
La	3.5	3.3	3.6	5.7	5.9	4.2	1.5	1.4	0.093	4.7
Ce	11.1	12.4	12.6	17.6	14.7	11.7	3.7	3.7	0.30	11.7
Pr	1.90	2.55	2.42	3.23	2.24	1.81	0.82	0.81	0.06	1.82
Nd	10.3	15.2	13.6	17.1	11.1	9.3	4.4	4.2	0.4	8.9
Sm	3.6	6.0	5.2	6.0	3.4	2.9	1.6	1.7	0.2	2.5
Eu	1.21	2.15	1.80	2.13	1.20	1.06	0.63	0.65	0.09	0.93
Gd	4.7	8.3	7.3	7.3	3.9	3.5	2.3	2.3	0.37	3.0
Tb	0.83	1.46	1.31	1.29	0.68	0.61	0.41	0.44	0.08	0.46
Dy	5.4	9.7	8.7	8.7	4.3	3.8	3.0	3.2	0.55	2.9
Ho	1.20	2.17	1.96	1.85	0.92	0.82	0.65	0.72	0.12	0.60
Er	3.36	6.19	5.59	5.30	2.53	2.24	1.93	2.09	0.37	1.70
Tm	0.50	0.95	0.87	0.77	0.38	0.33	0.30	0.32	0.06	0.25
Yb	3.13	6.02	5.57	4.73	2.33	1.91	1.91	2.00	0.38	1.63
Lu	0.45	0.91	0.83	0.72	0.34	0.28	0.29	0.29	0.06	0.23

Table 1. (continued). Major (wt%) and trace (ppm) element composition of hornblendite, epidote-trondhjemites, and amphibole+epidote-trondhjemites from the Sierra del Convento mélange.

Rock type	hornblendite	Ep-trondhjemite		Ep-trondhjemite				Amp-Ep trondhjemite		
Sample	CV237i	SC-22	CV60a	CV60b	CV62b-II	CV228b	CV53c	CV53a	SC-21	SC-23
SiO2	49.59	58.802	67.83	66.86	66.32	61.82	57.89	60.63	60.456	62.452
TiO2	1.01	0.25	0.22	0.18	0.06	0.1	0.19	0.22	0.223	0.165
Al2O3	7.83	23.102	18.24	19.61	21.13	22.97	22.97	23.62	22.295	21.225
Fe2O3	8.35	1.77	0.93	0.79	0.55	0.82	1.47	0.8	1.86	1.51
MnO	0.14	0.03	0.02	0.02	0.01	0.01	0.03	0.02	0.03	0.02
MgO	17.45	0.657	0.93	0.66	0.17	0.47	1.17	0.73	1.182	0.005
CaO	11.35	6.157	3.54	3.46	3.71	5.41	6.16	5.89	6.007	5.452
Na2O	1.41	6.226	5.58	7.21	7.55	7.02	7.06	7.11	6.447	6.282
K2O	0.15	0.51	0.26	0.12	0.15	0.1	0.2	0.12	0.17	0.1158
P2O5	0.04	0.11	0.08	0.04	0.04	0.04	0.06	0.06	0.05	0.05
LOI	2.02	1.77	1.65	0.91	0.61	1.13	1.9	1.04	1.23	2.36
Zr XRF	24	110	95	90	28	62	115	96	140	90
Li	1.58	n. d.	3.49	1.93	1.43	3.53	1.99	2.31	n. d.	n. d.
Rb	1.26	7.6	4.2	2.2	0.71	0.49	2.3	0.56	1.3	5.8
Cs	0.013	0.096	0.12	0.18	0.03	0.028	0.16	0.07	0.002	0.027
Be	0.11	0.26	0.25	0.38	0.29	0.41	0.47	0.48	0.42	0.35
Sr	52	708	570	671	305	721	733	694	648	571
Ba	27	181	130	92	55	55	104	73	81	62
Sc	56	3.1	1.6	1.5	0.5	0.6	3.3	1.4	2.7	2.4
V	329	17.3	11.0	12.9	7.5	12.1	21	10.7	18.1	17.4
Cr	414	261	37	38	29	111	32	31	113	142
Co	71	3.8	27	28	39	2.2	20	23	5.0	3.0
Ni	374	7.3	31	43	10.5	6.6	12.4	10.6	7.7	8.7
Cu	32	8.7	4.4	9.1	20	4.1	2.4	2.5	33	8.8
Zn	56	18.6	11.2	6.5	n. d.	9.9	15.6	8.3	26	21
Ga	10.4	12.5	8.2	8.8	7.6	9.9	11.8	9.8	11.5	10.8
Y	15.2	4.7	0.9	1.3	1.5	0.7	4.5	0.7	3.4	2.2
Nb	1.38	1.37	1.10	0.86	0.30	0.36	0.99	1.09	0.96	0.67
Ta	0.16	0.091	0.28	0.27	0.30	0.044	0.22	0.26	0.071	0.046
Hf	0.775	0.435	0.05	0.07	0.04	0.068	0.12	0.10	0.362	0.189
Mo	1.298	3.977	5.720	3.95	5.01	0.880	3.29	4.02	0.338	0.098
Sn	0.394	0.113	0.070	n. d.	n. d.	3.046	0.160	n. d.	n. d.	0.073
Tl	0.011	0.027	0.030	0.020	0.020	0.006	0.020	0.010	0.002	0.002
Pb	0.57	1.86	1.64	2.01	0.52	1.84	2.17	1.87	1.73	1.89
U	0.03	0.59	0.02	0.01	0.02	0.044	0.30	0.04	0.18	0.09
Th	0.04	0.32	0.04	0.01	0.06	0.063	0.58	0.04	0.43	0.29
La	1.38	1.62	0.67	0.53	0.09	0.81	5.43	0.33	2.82	1.75
Ce	4.7	2.8	1.0	0.2	0.1	1.1	11.6	0.6	6.1	2.8
Pr	0.95	0.37	0.15	0.20	0.03	0.18	1.71	0.10	0.83	0.31
Nd	5.63	1.62	0.60	0.83	0.13	0.58	7.17	0.40	3.75	1.18
Sm	2.21	0.43	0.19	0.21	0.04	0.10	1.37	0.07	0.82	0.25
Eu	0.72	0.23	0.10	0.090	0.018	0.048	0.57	0.050	0.32	0.097
Gd	2.68	0.58	0.19	0.23	0.06	0.10	1.24	0.09	0.60	0.27
Tb	0.438	0.051	0.027	0.036	0.012	0.017	0.186	0.014	0.058	0.046
Dy	2.74	0.35	0.16	0.23	0.08	0.11	0.94	0.10	0.27	0.26
Ho	0.60	0.077	0.030	0.050	0.020	0.024	0.17	0.020	0.053	0.056
Er	1.62	0.15	0.080	0.18	0.070	0.074	0.41	0.064	0.14	0.16
Tm	0.23	0.024	0.013	0.030	0.010	0.013	0.050	0.010	0.018	0.024
Yb	1.41	0.12	0.081	0.22	0.070	0.090	0.30	0.064	0.11	0.14
Lu	0.19	0.039	0.011	0.040	0.010	0.015	0.040	0.010	0.016	0.021

Table 1. (continued). Major (wt%) and trace (ppm) element composition of amphibole+epidote-trondhjemites, leuco-vein from the Sierra del Convento mélange, and standars.

Rock type	Amp-Ep trondhjemite						leuco-vein	PM-S	PM-S	WS-E	WS-E
Sample	CV237p-II	CV53o-II	CV53-III	CV228a	CV227b	CV228c	CV139f-2	(CIC)	(G., 1994)	(CIC)	(G., 1994)
SiO2	60.75	58.72	59.46	56.69	58.47	60.08					
TiO2	0.6	0.33	0.15	0.28	0.28	0.19					
Al2O3	17.89	21.62	22.16	23.3	22.67	23.65					
Fe2O3	4.31	2.4	1.1	2.24	1.78	1.18					
MnO	0.08	0.05	0.02	0.04	0.03	0.02					
MgO	2.94	1.92	0.73	1.69	1.35	0.68					
CaO	6.27	5.88	7.09	6.88	5.88	5.58					
Na2O	4.23	6.57	5.62	6.9	7.33	7.29					
K2O	0.47	0.29	0.08	0.18	0.1	0.08					
P2O5	0.15	0.07	0.03	0.09	0.15	0.05					
LOI	1.71	1.52	3.33	1.45	1.17	1.15					
Zr XRF	159	62	69	149	150	94					
Li	2.66	3.05	1.63	3.18	2.13	3.37	1.24	7.48	7.3	13.5	13.6
Rb	4.5	1.5	1.0	1.1	0.8	0.45	3.9	0.91	1	25	25
Cs	0.65	0.086	0.080	0.029	0.034	0.12	n. d.	0.52	0.35	0.6	0.5
Be	0.26	0.28	0.38	0.40	0.42	0.38	0.093	0.23	0.5	0.95	1.14
Sr	271	545	406	619	605	648	1778	271	280	405	410
Ba	176	104	49	53	65	55	178	142	148	330	338
Sc	7.5	3.8	2.7	4.1	2.8	1.5	3.9	34	34	27	28
V	70	40	26	28	27	20	53	192	192	335	340
Cr	56	53	33	97	89	94	12	320	314	108	99
Co	35	29	22	8.9	7.0	6.1	5	49	49	44	44
Ni	43	37	24	18.2	14.8	12.3	14	122	115	56	55
Cu	3.5	2.7	4.0	11.3	15.5	6.1	4.8	61	59	69	65
Zn	39	18	11	23	31	17	16	69	60	129	117
Ga	18	11	10	12	11	10	21	16	16	22	23
Y	11	2.5	1.9	3.1	1.9	1.3	4.6	11	11	30.8	30.4
Nb	1.32	0.64	0.49	0.79	0.71	0.44	0.28	2.1	2.6	16	18
Ta	0.23	0.22	0.18	0.098	0.070	0.069	0.063	0.25	0.18	1.31	1.16
Hf	0.156	0.172	0.100	0.223	0.194	0.106	0.064	1.07	1.12	5.2	5.3
Mo	3.5	3.3	3.6	0.77	0.56	0.65	0.19	1.9	1.9	3.7	3.7
Sn	0.91	0.55	n. d.	0.43	0.346	0.233	0.094	3	3	18	18
Tl	0.042	0.014	0.010	0.006	0.006	0.003	0.011	0.04	0.04	0.13	0.16
Pb	0.5	1.4	0.96	1.4	1.6	1.3	8.6	2.1	2.5	13.5	13.8
U	0.054	0.030	0.080	0.175	0.079	0.065	0.017	0.01	0.03	0.63	0.65
Th	0.141	0.043	0.050	0.38	0.155	0.072	0.077	0.04	0.05	3	3
La	8.43	0.78	0.62	1.83	1.06	0.59	1.35	2.7	2.8	26	27
Ce	19	1.27	0.96	3.40	1.82	0.85	1.88	6.7	6.8	59	61
Pr	2.65	0.28	0.16	0.52	0.28	0.16	0.33	1.03	1.08	7.7	7.8
Nd	11.2	1.37	0.64	2.18	1.31	0.66	1.43	5.3	5.5	32	33
Sm	2.72	0.34	0.16	0.54	0.26	0.15	0.36	1.75	1.75	8.5	8.8
Eu	0.96	0.15	0.08	0.21	0.11	0.07	0.36	1.02	1.07	2.11	2.25
Gd	2.70	0.43	0.21	0.47	0.26	0.19	0.53	2	2	7.1	7.2
Tb	0.40	0.074	0.04	0.084	0.046	0.032	0.087	0.34	0.36	1.1	1.1
Dy	2.35	0.48	0.26	0.52	0.29	0.22	0.57	2	2	6	6
Ho	0.44	0.103	0.06	0.109	0.062	0.048	0.12	0.41	0.42	1.2	1.2
Er	1.19	0.31	0.19	0.30	0.18	0.15	0.35	1.1	1.1	2.9	3
Tm	0.17	0.045	0.03	0.047	0.028	0.022	0.049	0.17	0.17	0.41	0.43
Yb	1.03	0.28	0.21	0.29	0.19	0.14	0.30	1	1	2.4	2.5
Lu	0.15	0.044	0.032	0.041	0.026	0.021	0.043	0.15	0.15	0.36	0.37

Table 2. Geochemical comparison between trondhjemites from Sierra del Convento and acid rocks from Catalina Schist mélange (Sorensen and Grossman, 1989) and adakites (Defant and Drummond, 1990; Martin, 1999; Smithies, 2000). Both LSA (low-SiO2 adakites) as HSA (high-SiO2 adakites) are from Martin et al. (2005) and references therein.

	Trondhjemites (S. Convento)	Catalina acid rocks	Adakites	LSA	HSA
SiO_2 (wt.%)	57.8 - 69.55	68 - 75.4	>56	50.1 - 65.3	55.4 - 75.3
Na_2O (wt.%)	4.35 - 7.58	4.9 - 6.8	3.5 - 7.5	2.8 - 4.97	3.1 - 5.1
(K_2O/Na_2O)	0.01 - 0.11	0.03 - 0.24	low (~ 0.42)	0.09 - 2	0.16 - 0.98
(Fe_2O_3+MgO+ MnO+TiO_2) (wt.%)	0.79 - 8.1	0.3 - 2.7	~7	2.8 - 20.9	2.4 - 13.1
Mg#	38 - 66.5	31 - 89	~ 0.51	33 - 71.6	14,.9 - 56.53
Ni (ppm)	6.55 - 43.4	6. - 29	~ 24	0.8 - 240	2. - 88
Cr (ppm)	11.8 - 260.5	0.96 - 30.1	~ 36	2 - 426	2. - 71
Sr (ppm)	271.5 - 1778.35	680 - 1580	>400	8. - 8529	3 - 1400
$(La/Yb)_n$	0.87 - 16.82	2.9 - 15	>10	1.38 - 42.54	0.4 - 34.5
Yb (ppm)	0.064 - 1.034	0.02 - 0.4	≤1.8	0.41 - 3.42	0.37 - 2.85
Y (ppm)	0.67 - 10.84	-	≤18	0.5 - 52	2.6-31

Table 3. Rb/Sr and Sm/Nd isotope data of amphibolites, hornblendite, and trondhjemites from Sierra del Convento mélange.

	Sample	Rb*	Sr*	$^{87}Rb/^{86}Sr$*	$^{87}Sr/^{86}Sr$	±2σ	Sm*	Nd*	$^{147}Sm/^{144}Nd$*	$^{143}Nd/^{144}Nd$	±2σ
amphibolites	CV53X-I	1.35	272.4	0.014253	0.703277	28	5.434	16.175	0.202355	0.513091	10
	CV62B-I	1.43	169.2	0.026213	0.703317	14	3.301	9.077	0.213353	0.513105	10
	CV228E	1.98	165.4	0.031616	0.703171	21	5.142	14.515	0.212564	0.513109	15
	CV62a	1.63	129.7	0.047631	0.703155	56	2.658	7.066	0.216282	0.51317	10
hornblendite	CV61	2.98	74.2	0.103115	0.703871	49	1.626	4.354	0.223440	0.513046	10
trondhjemites	CV62b-II	0.71	304.6	0.006966	0.703234	14	0.044	0.13			
	SC21	1.3	647.6	0.004188	0.703088	14	0.822	3.752	0.152922	0.513022	20
	CV228a	1.12	618.6	0.004258	0.703096	21	0.54	2.182	0.147034	0.51292	10

Note: $^{87}Rb/^{86}Sr$ and $^{147}Sm/^{143}Nd$ were calculated from Rb, Sr, Sm and Nd abundances determined by ICP-MS.

Chapter IV. Geochronology and P-T-t paths

This Chapter is to be submitted to the ***Journal of Metamorphic Geology***

55 Ma history of oceanic subduction and exhumation in the northern branch of the Caribbean plate (Sierra del Convento mélange, Cuba)

C. LÁZARO[(1)] A. GARCÍA-CASCO[(1)] Y. ROJAS-AGRAMONTE[(2)] A. KRÖNER[(2)] F. NEUBAUER[(3)]

(1) Departamento de Mineralogía y Petrología, Universidad de Granada
Fuentenueva s/n, 18002-Granada, Spain Lázaro E-mail: clazaro@ugr.es García-Casco E-mail: agcasco@ugr.es

(2) Institut für Geowissenschaften, Universität Mainz
55099 Mainz, Germany. Rojas-Agramonte E-mail: rojas@uni-mainz.de Kröner E-mail: kroener@mail.uni-mainz.de

(3) Fachbereich Geographie, Geologie und Mineralogie, Universität Salzburg
Hellbrunner Strasse 34, A-5020 Salzburg, Austria E-mail: Franz.Neubauer@sbg.ac.at

ABSTRACT

Exotic blocks of amphibolite and associated tonalite-trondhjemite rocks included in the serpentinitic matrix mélange of the Sierra del Convento (eastern Cuba) elucidate several aspects concerning the dynamics of subduction in the Caribbean realm. Petrological and geochronological data of six representative samples that remained deep in the subduction environment for a significant period of time are presented in this study. The samples followed counterclockwise P-T paths, typical of young subduction zones. Peak conditions attained were ca. 750 ºC and 15 kbar, appropriate for partial melting of amphibolite. An altered boulder of tonalite provides a U-Pb zircon crystallization age of 112.8 ± 1.1 Ma. Ar-Ar amphibole dating yielded two groups of cooling ages of 106-97 Ma (interpreted as cooling of metamorphic/magmatic pargasite) and 87-83 Ma (interpreted as growth/cooling of retrograde overprints). These geochronological data, and other data published in the literature, allow establishing the following history of subduction and exhumation in the region: a) a stage of hot subduction during 120-115 Ma, developed shortly after onset of subduction in the region, b) relatively fast near-isobaric cooling during 115-107 Ma, after accretion of the blocks to the upper plate mantle, c) slow syn-subduction cooling and exhumation in the subduction channel during 107-70 Ma, and d) fast syn-collision cooling and exhumation during 70-60 Ma, when subduction terminated in the region.

KEYWORDS: Ar-Ar dating, SHRIMP dating, cooling rates, exhumation rates, Caribbean subduction.

INTRODUCTION

The dynamics of the subduction zones and the speed at which the rocks accreted to the overriding plate and/or the subduction channel return to the surface are controversial topics. Studies of heating/cooling and burial/exhumation rates of high pressures rocks provide first-hand insights into deep seated processes and the mechanism of subduction and return, and can be incorporated into Plate Tectonic models. Numerous studies have shown that a continuum exists between two distinct end-member types of exhumation of subducted rock complexes. Fast exhumation rates corresponding to the rates of plate motion (>1-10 km/Ma) have been determined for example in the Alps (Duchêne *et al*., 1997; Rubatto & Hermann, 2001), Aegean (Ring & Reischmann, 2002), and Papua New Guinea (Baldwin *et al*., 2004). However, low exhumation rates of <0.1-1 km/Ma have been reported in Pakistan (Whittington, 1996), the Franciscan complex (Anczkiewicz *et al*., 2004; Tsujimori *et al*., 2006), the Washington Cascade Range (Reiners *et al*., 2002), the Sanbagawa belt (Wallis *et al*., 2004), and the Caribbean (Krebs *et al*., 2007). The cases of fast exhumation are generally related to the collision of thick and/or buoyant oceanic or continental lithosphere with the trench-fore arc-arc system, which is normally associated with the end of subduction. The cases of slow exhumation rates, on the other hand, appear to be typical of near-steady state subduction. In this latter scenario, fragments of the subducted slab are incorporated into the overlying subduction channel, a long lived geologic element where the blocks are generally slowly exhumed (Gerya *et al*., 2002), as opposed to the former scenario of where discrete tectonic events of collision and extension/collapse make deep seated rocks to rapidly ascend to the surface.

Observations of natural rocks have also established a variety of P-T paths of subducted rocks (Ernst, 1988), in agreement with geophysical calculations and simulations (Gerya *et al*., 2002). These observations indicate that oceanic rocks exhumed in syn-subduction scenarios normally show cold exhumation paths, either clockwise or counterclockwise. Whereas the corner flow model provides an explanation for the existence of counterclockwise P-T paths (Closs, 1982), it appears that this type of path is not as general as the clockwise type. Counterclockwise P-T paths are considered to be characteristic of rocks subducted in juvenile subduction scenarios and, consequently, to document a transient thermal state during onset of subduction (e.g, Perchuk *et al*., 1999; Gerya *et al*., 2002; Wakabayashi, 2004; Willner *et al*., 2004; Krebs *et al*., 2007; García-Casco *et al*., 2007).

In this study, we proportionate P-T-t data for exotic blocks of epidote ± garnet amphibolite and associated trondhjemite from the Sierra del Convento mélange (eastern Cuba) that followed counterclockwise P-T paths during syn-subduction exhumation within a subduction channel. Petrologic studies indicate that the blocks represent the partial melting products of mafic oceanic crust subducted during the earliest stage of subduction in the region (García-Casco *et al*., 2007). These oceanic crust fragments were then accreted to the overriding plate and subsequently incorporated into the subduction channel, where they resided for a long period of time until they were finally exhumed in the latest Cretaceous, when subduction arrested in the region (García-Casco *et al*., 2006). This scenario allows determinations of cooling and exhumation rates of a subduction channel from birth to demise of the associated subduction zone, and to constrain the geotectonic evolution of the Caribbean plate.

GEOLOGICAL SETTING

The Caribbean orogenic belt fringes the Caribbean plate, from Guatemala through the Antilles and northern South America. In the Greater Antilles, the belt documents the collision of a Mesozoic-Tertiary volcanic arc with the North American plate during the late Mesozoic and Tertiary (Fig. 1). In this northern branch of the margin of the Caribbean plate, the orogenic belt is mainly formed by oceanic material, including ophiolites and intra-oceanic volcanic arcs, and fragments of the southern borderlands of North American (Bahamas platform) and the Maya (Yucatan) block. All these terrains are well exposed in Cuba (Fig. 2a). The oceanic material includes the northern and eastern ophiolite belts and the Cretaceous and Paleogene volcanic arcs (Iturralde-Vinent, 1998 and references therein). In the Cretaceous volcanic arc, the magmatic activity began in the early Cretaceous (Aptian-Albian) and lasted until the mid-late Campanian. Serpentinite mélanges associated with the ophiolite bodies all along the island document subduction during the Cretaceous (120–70 Ma, García-Casco *et al*., 2006 and references therein). The arrest of volcanic arc activity coincide with late Cretaceous isotopic ages of metamorphosed continental terrains (mostly interpreted as cooling ages; Iturralde-Vinent *et al*., 1996; García-Casco *et al*., 2001; Stanek *et al*., 2006), suggesting that the onset of arc-continent collision was in the late Cretaceous.

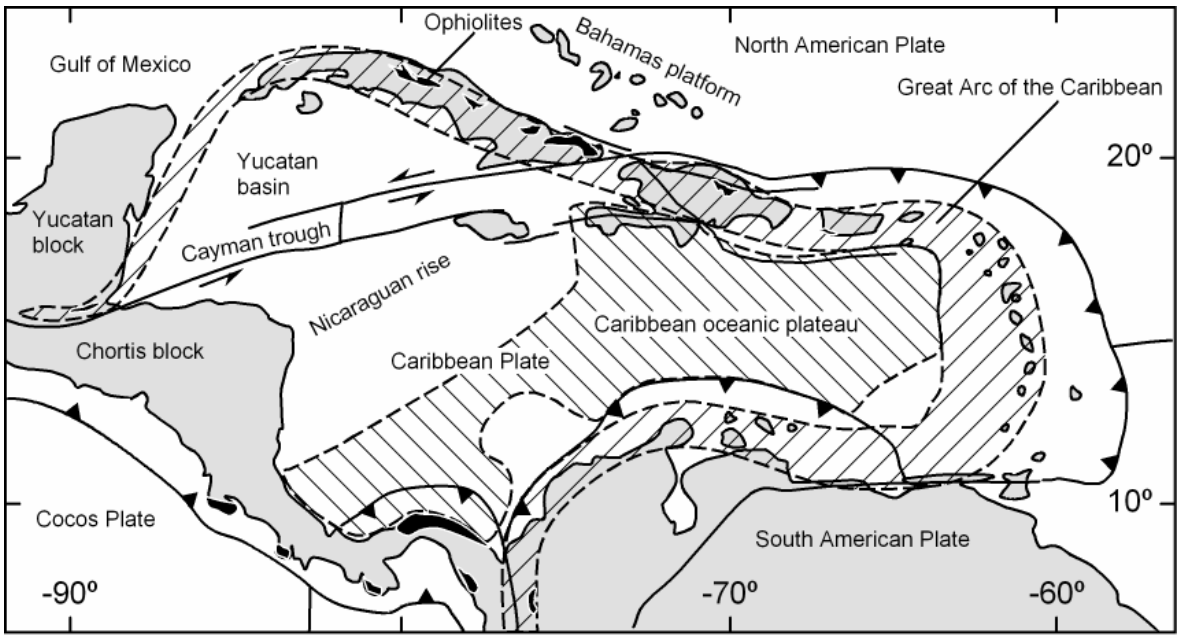

Fig. 1. Plate tectonic configuration of the Caribbean region, with important geological features including ophiolitic bodies and Cretaceous-Tertiary volcanic arc.

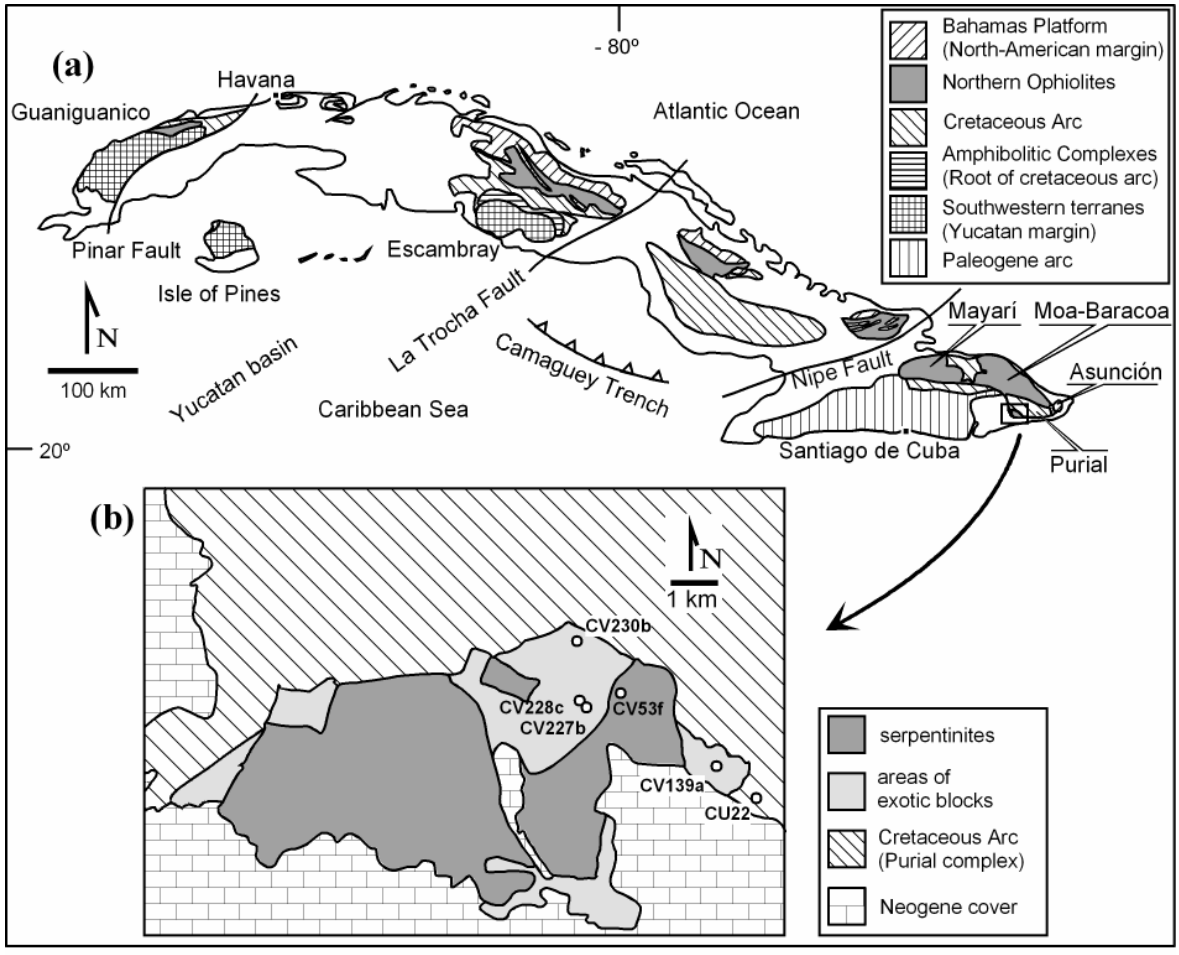

Fig. 2. (a) General geological map of Cuba (after Iturralde-Vinent, 1998) showing the main geological units. (b) Geological map of Sierra del Convento (after Kulachkov & Leyva, 1990) with location of sample sites.

In eastern Cuba, between the Nipe and Oriente faults, the ophiolitic belt comprises two large massifs: the Mayarí and Moa-Baracoa (Fig. 2a). These massifs have been recently characterized as "eastern ophiolites" by Iturralde-Vinent *et al*. (2006) to emphasize their geological singularities as compared to those of west-central Cuba. The eastern ophiolites formed in a supra-subduction environment (Proenza *et al*., 2006; Marchesi *et al*., 2007). The Cretaceous volcanic arc formations have distinct geochemical signatures including tholeiitic, boninitic and calc-alkaline (Proenza *et al*., 2006). The volcanic arc Purial complex, located to the south of the ophiolitic massifs, has island arc tholeiitic and calc-alkaline signatures and has been classically considered as the eastern prolongation of the western and central Cuba Cretaceous arc (Fig. 2a; Iturralde-Vinent *et al*., 1996, 2006). The complex is strongly deformed and metamorphosed in the greenschist and blueschist facies (Boiteau *et al*., 1972; Somin & Millán, 1981; Cobiella *et al*., 1984; Millán, 1996). This appears to be the only occurrence of a subducted volcanic arc complex in Cuba. Regionally, the ophiolitic bodies override the Purial volcanic arc complex; as opposed to central and western Cuba where the ophiolites tectonically underlie the volcanic arc formations. The latest Campanian-Danian Mícara and La Picota formations constitute syn-orogenic deposits dating the final obduction of the ophiolitic massifs in eastern Cuba. These lithostratigraphic units are composed of fragments and blocks from the ophiolitic bodies and the Cretaceous volcanic arc formations (Cobiella *et al*., 1984).

At the base of the ophiolitic units in eastern Cuba there occur serpentinite mélanges containing medium- to high-pressure metamorphic blocks. The most significant complexes are the Sierra del Convento and La Corea mélanges, both sharing similar lithological assemblages (Millán, 1996). The La Corea mélange is located in Sierra de Cristal, associated with the Mayarí ophiolitic body (Fig. 2b), and overrides the volcanic arc Santo Domingo Formation, considered as the non-metamorphosed counterpart of the Purial complex. The Sierra del Convento mélange, located southward, overrides the Purial complex (Fig. 2b). These mélanges have been interpreted as fragments of the subduction channel associated with south-westward directed subduction on the leading edge of the Caribbean plate during the Cretaceous (García-Casco *et al*., 2006; 2007).

THE SIERRA DEL CONVENTO MÉLANGE

Metamorphic blocks from Sierra del Convento mélange are variable in composition. The most significant lithologies include amphibolite, blueschist, greenschist, quartzite, impure quartz-feldspathic rocks, metagreywacke, and metapelite, whereas eclogite is rare (Somin & Millán, 1981; Kulachkov & Leyva, 1990; Hernández & Canedo, 1995; Leyva, 1996; Millán, 1996). However, the dominant rock type is a MORB-derived high-temperature epidote ± garnet amphibolite. The amphibolites commonly contain cm- to m- size layers, pockets, and veins of leucocratic melt material of trondhjemitic to tonalitic composition (henceforth termed trondhjemites), locally with pegmatoid texture. García-Casco *et al*. (2007) demonstrated that the trondhjemitic segregations formed upon fluid-assisted partial melting of the amphibolites at 675-700 ºC and 14-16 kbar. Major and trace element and isotopic data also support this view (Lázaro & García-Casco, submitted 2007). The process took place during subduction of oceanic crust in a hot-subduction scenario and, importantly, subsequent exhumation occurred in a syn-subduction setting, allowing the blocks in the mélange to follow counterclockwise P-T paths (García-Casco *et al*., 2006; 2007). These authors also showed that these high grade blocks of amphibolite and associated trondhjemite represent the first subducted material. Thus, these blocks should have been accreted to the overriding plate soon after initiation of subduction, and their P-T-t evolution, addressed in this study, may shed light on the early history of the subduction of the region.

Published geochronological data for the Sierra del Convento mélange are scarce and imprecise, precluding the development of a precise metamorphic and geodynamic model for the history of subduction in the region. Available K-Ar ages of metamorphic blocks from the Sierra del Convento range from 116 to 82 Ma (Somin & Millán, 1981; Hatten *et al*., 1989; Somin *et al*., 1992; Iturralde-Vinent *et al*., 1996). U-Pb zircon ages of 120-126 Ma and 103-105 Ma have been interpreted as the ages of the subducting crust and its metamorphism respectively (Hatten *et al*., 1989). A similar wide range of K-Ar ages (125 to 66 Ma) is available for metamorphic blocks from the La Corea mélange (Adamovich & Chejovich, 1964, and references above). Metamorphism in the underlying volcanic arc Purial complex took place in the latest Cretaceous. Somin *et al*., (1992) provided a K-Ar whole-rock age of 75 ± 5 Ma for a low-grade schist from this complex, and Iturralde-Vinent *et al*., (2006) have suggested 75-72 Ma for the timing of metamorphism based on stratigraphic-paleontological arguments. A Maastrichtian-Danian (70-60 Ma) depositional age for the syn-orogenic Mícara and La Picota formations (Cobiella *et al*., 1984) establish an upper limit for regional metamorphism in the region. In short, all these data suggest subduction since the late early Cretaceous until the late Cretaceous, whereas the Purial complex appears to have impinged into the subduction zone in the late Cretaceous, when collision began in the

region. By Danian time, the ophiolites, the mélanges, and the Cretaceous volcanic arc complexes of eastern Cuba were already structured and closed to the Earth's surface.

In this study, Ar-Ar amphibole dating, from amphibolites and trondhjemites, and SHRIMP dating of single zircon from a tonalitic rock have been performed towards clarifying the history of oceanic subduction and associated exhumation.

ANALYTICAL TECHNIQUES

Mineral compositions were obtained with a CAMECA SX-50 microprobe (University of Granada) operated at 20 kV and 20 nA, and synthetic SiO_2, Al_2O_3, $MnTiO_3$, Fe_2O_3, MgO and natural diopside, albite and sanidine were used as calibration standards. In addition, a ZEISS DSM 950 scanning microscope equipped with a LINK ISIS series 300 analytical Pentafet system operated at 20 kV and 1-2 nA beam current, with counting times of 50-100 s, and the same calibration standards as above. Amphibole compositions were normalized to 23 oxygens and Fe^{3+} was estimated according to the scheme of Leake *et al*. (1997). Garnet was normalized to 8 cations and 12 oxygens and Fe^{3+} was estimated by stoichiometry. Epidote, feldspar, lawsonite, and kyanite were normalized to 12.5, 8, 8, and 5 oxygens, respectively, and $Fe_{total} = Fe^{3+}$. Mica, chlorite, and pumpellyite were normalized to 22, 28, and 24.5 oxygens, respectively, and $Fe_{total} = Fe^{2+}$. Mineral and end-member abbreviations are after Kretz (1983) except for amphibole (Amp). The atomic concentration of elements per formula units is abbreviated apfu. Representative chemical analyses are given in Table 1 (the reader is referred to García-Casco *et al*., 2007, for analyses of minerals from samples not given in Table 1).

Elemental XR images were obtained with the same CAMECA SX-50 microprobe operated at 20 kV, 249-291 nA beam current, with step (pixel) size of 7-9 μm and counting time of 25-100 ms. The images were processes with the software *Imager* (Torres-Roldán & García-Casco, unpublished) and consist of the XR signals of Kα lines of the elements or element ratios indicated (colour-coded; expressed in counts/nA/s) corrected for 3.5 μs deadtime and with voids, polish defects, and all other mineral phases masked out, overlain onto a grey scale base-layer calculated with the expression $\Sigma[(\text{counts/nA/s})_i \cdot (A_i)]$, (A = atomic number, i= Si, Ti, Al, Fe, Mn, Mg, Mg, Ca, Na, and K) that contains the basic textural information of the scanned areas.

Cathodoluminescence (CL) images of the dated zircons (sample CU22) were obtained prior to SHRIMP analysis, to distinguish between different zircon domains. CL imaging was undertaken in the Centre for Microscopy and Microanalysis at the University of Western Australia, Perth, on a JEOL 6400 scanning electron microscope, operated at 15 kV accelerating voltage and 5 nA beam current. The U–Pb ion microprobe data were obtained on the SHRIMP II (B) of the John de Laeter Centre of Mass Spectrometry at Curtin University, Australia (De Laeter & Kennedy, 1998). Clear euhedral zircons some 80 to 150 μm in length from sample CU22 were handpicked and mounted in epoxy resin together with other samples and chips of the Perth zircon standard CZ3. Details on the SHRIMP procedure, age calculation and error assessment can be found in Compston *et al*. (1992), Stern (1997), Nelson (1997), and Williams (1998).

Precise dating of young zircons by ion-microprobe is best achieved by using $^{206}Pb/^{238}U$-ages (see Black *et al*., 2003, for explanation), and the reduced $^{206}Pb/^{238}U$ ratios were normalized to CZ3 ($^{206}Pb/^{238}U = 0.09432$, age: 564 Ma). Sensitivity was about 26 cps/ppm/nA Pb on the standard CZ3. Analyses of samples and standards were alternated to allow assessment of Pb^+/U^+ discrimination. Raw data reduction followed the method of Nelson (1997). Common-Pb corrections have been applied using the ^{204}Pb-correction method. The zircons of CU22 had very low counts on ^{204}Pb, and in these cases it was assumed that common lead is surface-related (Kinny, 1986) and the isotopic composition of Broken Hill lead was used for correction. The analytical data are presented in Table 2. Errors on individual analyses are given at the 1-sigma level and are based on counting statistics and include the uncertainty in the standard U/Pb age (Nelson 1997). The error for pooled analyses is at the 2-sigma or 95% confidence interval. The data are given in Table 2.

Preparation of mineral samples before and after irradiation for the $^{40}Ar/^{39}Ar$ analyses were carried out at the ARGONAUT Laboratory in the Institute of General Geology and Geodynamics at the University of Salzburg (Austria). Hornblende concentrates were prepared by crushing, sieving, flotation, and hand-picking of the grains with sizes of 200–250 and 250–355 μm. For isotopic measurements 10–20 grains per sample were used. The mineral concentrates were packed in aluminium-foil and loaded in quartz vials. For calculation of the J-values, flux-monitors were placed between each 4–5 unknown samples, which yielded a distance of ca. 5 mm between adjacent flux-monitors. The sealed quartz vials were irradiated in the MTA KFKI reactor (Debrecen, Hungary) for 16 hours. Correction factors for interfering isotopes were calculated from 10 analyses of two Ca-glass samples and 22 analyses of two pure K-glass samples, and are: $^{36}Ar/^{37}Ar_{(Ca)} = 0.00026025$, $^{39}Ar/^{37}Ar_{(Ca)} = 0.00065014$, and $^{40}Ar/^{39}Ar_{(K)} = 0.015466$. Variations in the flux of neutrons were monitored with a DRA1 sanidine standard for which a $^{40}Ar/^{39}Ar$ plateau age of 25.03 ± 0.05 Ma has been

reported by Wijbrans *et al*. (1995). After irradiation, the minerals were unpacked from the quartz vials and the aluminium-foil packets, and handpicked into 1 mm diameter holes within one-way Al-sample holders.

$^{40}Ar/^{39}Ar$ analyses were carried out using a UHV Ar-extraction line equipped with a combined MERCHANTEK^{TM} UV/IR laser ablation facility, and a VG-ISOTECH^{TM} NG3600 Mass Spectrometer and follow methods described in Handler *et al*. (2004). Stepwise heating analyses of samples were performed using a defocused (~1.5 mm diameter) 25 W CO_2-IR laser operating in Tem00 mode at wavelengths between 10.57 and 10.63 μm. The laser is controlled from a PC, and the position of the laser within the sample is monitored through a double-vacuum window on the sample chamber via a video camera in the optical axis of the laser beam on the computer screen. Gas clean-up was performed using one hot and one cold Zr-Al SAES getter. Gas admittance and pumping of the mass spectrometer and the Ar-extraction line are computer controlled using pneumatic valves. The NG3600 is an 18 cm radius 60° extended geometry instrument, equipped with a bright Nier-type source operated at 4.5 kV.

Measurements were performed on an axial electron multiplier in static mode. Peak-jumping and stability of the magnet are controlled by a Hall-probe. For each increment the intensities of ^{36}Ar, ^{37}Ar, ^{38}Ar, ^{39}Ar, and ^{40}Ar were measured, the baseline readings on mass 35.5 are automatically subtracted. Intensities of the peaks were back-extrapolated over 16 measured intensities to the time of gas admittance either by a straight line or a curved fit. Intensities were corrected for system blanks, background, post-irradiation decay of ^{37}Ar, and interfering isotopes. Isotopic ratios, ages, and errors for individual steps were calculated following suggestions by McDougall & Harrison (1999), using decay constants recommended by Steiger & Jäger (1977). Definition and calculation of plateau ages was carried out using the ISOPLOT/EX 3.00 software (Ludwig, 2001). The time scale calibration follows Gradstein & Ogg (2005). The analyses are presented in Table 3.

SAMPLE DESCRIPTION

Two representative epidote-garnet amphibolites (samples CV230b and CV139a) and four trondhjemite-tonalitic rocks (samples CV227b, CV228c, CV53f, and CU22) were selected for microprobe, Ar-Ar, and SHRIMP analysis (for location see Fig. 2b). Detailed petrological and geochemical data are provided by García-Casco *et al*. (2006, 2007) and Lázaro & García-Casco (submitted 2007).

Unfortunately, the samples studied petrologically from the mélange did not yield zircons even if several kg in weight of rock were sampled. This is in agreement with the low Zr concentration in these rock types from the complex. This feature is a consequence of the MORB nature of the protoliths of the amphibolites and the compatible behaviour of Zr during partial melting of amphibolites (Lázaro & García-Casco, submitted 2007). A few zircons grains, however, were recovered from a detrital boulder of tonalitic composition (CU22) collected in the bed of the Yacabo River.

In all samples, calcic amphibole shows a heterogeneous composition with peak Ti-rich pargasite compositions overprinted by Ti-poor edenite-magnesiohornblende-actinolite compositions that also form separated grains in the matrix formed throughout the retrograde path (Figs. 3b and d, and see below). These compositions translate into the brown and green colours of amphiboles respectively. Brownish and greenish amphiboles were carefully separated for dating in amphibolite sample CV139a in an effort to test the chemical composition effects of amphibole on the Ar-Ar systematics and to better constrain the timing of amphibole growth during retrogression. In all samples, the grain size fractions of Ar-Ar dated amphibole grains are 250-125 μm, except in CV53f (250-200 μm).

Petrography

Amphibolites

Sample CV230b contains a peak metamorphic assemblage consisting of pargasitic amphibole, epidote, garnet, titanite, rutile, and apatite. Pargasitic amphibole comprises most of the matrix and is oriented parallel to a weak foliation (Figs. 3a and b). Garnet forms large porphyroblasts (up to >1.5 cm in diameter) that include pargasitic amphibole, epidote, rutile, and titanite. Retrograde overprints are faint and consist of edenite-magnesiohornblende-actinolite, glaucophane, albite, chlorite, and pumpellyite. The rims of pargasitic amphibole are replaced by actinolite, glaucophane, chlorite, and albite. Garnet is slightly replaced at the rims and along fractures by edenite-magnesiohornblende-actinolite, chlorite, pumpellyite, and albite.

Sample CV139a is weakly foliated and comprises a peak metamorphic assemblage consisting of pargasitic amphibole, epidote, garnet, rutile, titanite, quartz, and phengite. Pargasitic amphibole includes epidote and titanite. Garnet porphyroblasts show inclusions of amphibole and titanite. Blocky epidote appears in the matrix and is intergrown with quartz. Faintly oriented phengite is distributed in the matrix.

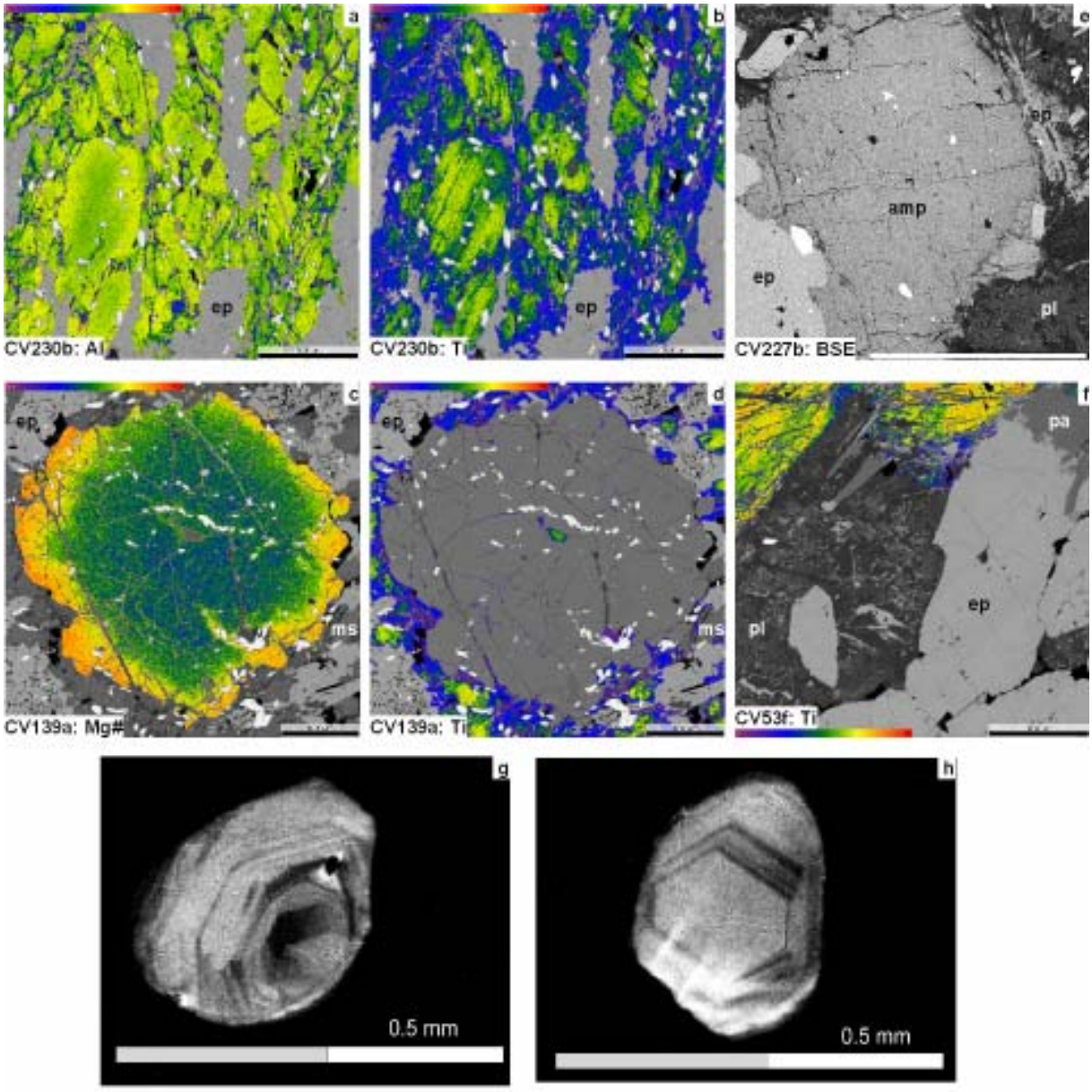

Fig. 3. XR, BSE, and CL images showing key textural and compositional data of studied samples. (a) Al-Kα XR image of amphibolite sample CV230b showing heterogeneous composition of calcic amphibole. Note that retrograde grains/compositions (dark-green too purple) of edenite-magnesiohornblende-actinolite overprinting matrix edenite(cores)-pargasite grains/compositions. (b) Ti-Kα XR image of the same amphiboles as in (a). The cores of primary Ti-richer compositions (green) and the Ti-poorer rims and fine grained overprints (blue-purple) stand out clearly. (c) Mg-Kα/(Mg-Kα+Fe-Kα) XR image of garnet from amphibolite CV139a showing prograde growth zoning. (d) Ti-Kα XR image of calcic amphiboles in the same area as in (c). The cores of primary Ti-richer compositions of matrix grains and inclusions (green) are overgrown/re-equilibrated by Ti-poorer (blue-purple) compositions located preferentially close to the garnet rims and along fractures. (e) BSE image of magmatic amphibole, epidote, and plagioclase from trondhjemite sample CV227b. Retrograde clinozoisite overprints plagioclase. (f) Ti-Kα XR image of calcic amphibole from sample CV53f showing overprints along fractures and rims by Ti-poorer magnesiohornblende-tremolite. Also shown are magmatic epidote, plagioclase, and paragonite, and the retrograde overprints (mostly clinozoisite and paragonite) in plagioclase. Scale bar: 1 mm. Colour scale bar in the XR images (counts/nA/s) indicates high (red) and low (purple) concentrations. (g) and (h) CL images of zircon from trondhjemite sample CU22 showing oscillatory bands typical of magmatic zircon.

The retrograde overprints consist of edenite-magnesiohornblende-actinolite, glaucophane, phengite, quartz, chlorite, albite, and pumpellyite. Pargasite is replaced by edenite-magnesiohornblende-actinolite and glaucophane. Garnet is slightly replaced by actinolite, glaucophane, phengite, chlorite, albite, and pumpellyite at the rims and along fractures (Figs. 3c and d).

Trondhjemites

Samples CV227b and CV228c are very similar in chemical and mineralogical compositions and microfabrics. They are not foliated and have a primary (magmatic) mineral paragenesis composed of plagioclase, quartz, paragonite, epidote, pargasitic amphibole, rutile, and titanite (Fig. 3e). Lawsonite (in sample CV228c), clinozoisite, albite, phengite, and a second generation of fine-grained paragonite formed as retrograde alteration products of magmatic plagioclase and paragonite. Retrograde tremolite, chlorite, and pumpellyite overprint pargasitic amphibole.

Sample CV53f is a trondhjemitic rock that bears somewhat higher grain size. It has a primary mineral association composed of plagioclase, epidote, pargasitic amphibole, paragonite (all of which may reach centimetric grain size), and rutile (Fig. 3f). Relict crystals of kyanite (likely magmatic) are present as inclusions within primary epidote. Fine-grained paragonite, phengite, and clinozoisite are alteration products of primary plagioclase and paragonite, whereas pargasitic amphibole is replaced by chlorite and pumpellyite.

Detrital boulder CU22 is a foliated tonalitic rock. It is made of a primary (magmatic) plagioclase, quartz, epidote, rutile, and apatite. Zircons of sample CU22 are clear to pinkish, mostly stubby or fragmented, rarely prismatic, and display well developed magmatic oscillatory zoning (Figs. 3g and h). No core-rim relationships were observed in CL images. The magmatic assemblage is strongly overprinted by albite, clinozoisite-epidote, white micas (paragonite and phengite), chlorite, and titanite. Primary plagioclase is largely transformed to albite, clinozoisite, paragonite-phengite, and cryptocrystalline material (saussurite). Epidote and white mica forms aggregates that follow the foliation. Patches of retrograde chlorite appear also following the foliation. These primary and overprinting assemblages are consistent with those of other tonalitic-trondhjemitic rocks from the Sierra del Convento mélange.

Mineral compositions

Amphibole

Amphibole from the studied samples covers a wide range of compositions (Fig. 4). The prograde grains of amphibole from the amphibolites display a faint concentric zoning with cores of edenite and outer shells of pargasite bearing higher Na-in-A, total Al, and Ti, and lower Si, Na-in-B, and Mg# than the cores. This trend correlates with the composition of amphibole inclusions within garnet that ranges from edenite to pargasite. As a whole, this indicates prograde growth and peak compositions of pargasite. Retrograde overprinting developed patches of Ti-poor edenite and magnesiohornblende compositions within the primary pargasitic grains. These patches have tiny inclusions of rutile/titanite likely formed after "exsolution" from Ti-rich primary pargasitic compositions. Post-peak overprints at the rims of the prograde grains are made of edenite, magnesiohornblende, and actinolite. The trend involves decreasing in Na-in-A, total A, and Ti, and increasing in Si and Mg#, though the latest actinolitic products show a back decrease in Mg# as Si increases (Fig. 4). Retrograde glaucophane shows a more restricted range of compositional variations (Fig. 4).

Magmatic amphibole from the trondhjemites is pargasitic and similar to that of metamorphic peak amphibole from the amphibolites, except for being richer Mg# as a consequence of a bulk-rock composition effect (García-Casco *et al*., 2007). It shows no discernible growth zoning though the grains are overprinted by retrograde edenite, magnesiohornblende, and tremolite developed as patches and along fractures, exfoliation planes, and the crystal rims. As in the amphibolites, the retrograde trend involves decreasing in Na-in-A, total Al, and Ti, and increasing in Si and Mg#, though no decrease in Mg# was detected in the latest tremolitic compositions (Fig. 4a). Glaucophane is not present as retrograde product in the trondhjemites.

Garnet

Garnet is relatively rich in almandine, intermediate in grossular and pyrope, and poor in spessartine (Fig. 5). Growth zoning is faint, with cores richer in spessartine and rims richer in Mg# denoting prograde growth (Figs. 3c and 5). Faint prograde zoning and the lack of low-temperature phases included within garnet suggest growth close to peak conditions during prograde metamorphism (García-Casco *et al*., 2006; 2007). Retrograde readjustments are noted by an increase in Mn and decrease in Mg# at the rims and along fractures traversing the grains where retrograde magnesiohornblende-actinolite, glaucophane, chlorite, pumpellyite, phengite, and/or albite may have grown.

Epidote

Epidote has low Fe^{3+} contents in the amphibolite samples, with pistacite contents (X_{Ps} = Fe^{3+}/[(Al-2)+Fe^{3+}]) ranging from 0.04 to 0.17. No distinctive zoning was detected in the studied amphibolite samples. Epidote from the trondhjemite samples

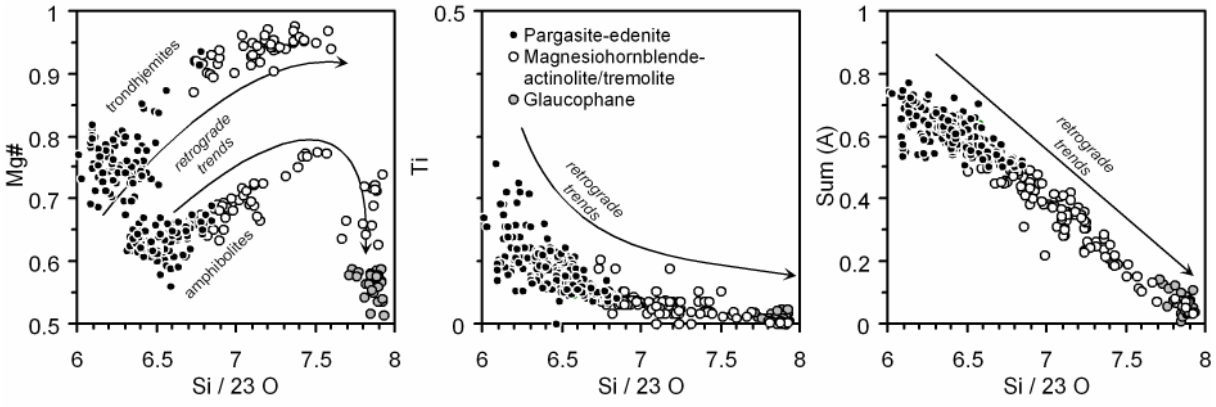

Fig. 4. Composition of studied calcic and sodic amphiboles, with indication of retrograde trends for calcic amphiboles.

shows larger compositional variations. The Fe^{3+} contents are higher in the medium-grained idiomorphic (magmatic) crystals while near-clinozoisite composition characterize the retrograde grains formed after plagioclase breakdown (X_{Ps} up to 0.56 and down to 0.04 respectively). Magmatic crystals show patchy zoning, with irregular distribution of Fe^{3+}.

Plagioclase

Plagioclase in the amphibolites is retrograde and almost pure albite in composition (X_{Ab} = 0.92-1.0). The composition of plagioclase in the trondhjemites is more varied (X_{Ab} = 0.71-1.0) as a result of magmatic crystallization and late overprinting and growth. The magmatic compositions are richer in Ca, whereas retrograde overprints trend towards albite. The maximum X_{An} recorded in the studied samples are 0.29 (CV228c), 0.19 (CV53f), and 0.11 (CV227b). Even if these relict compositions were identified with the aid of XR and BSE images, they do not necessarily represent the original magmatic composition of plagioclase. It is inferred that the maximum X_{An} recorded (in CV228c) is closer to the original composition of magmatic plagioclase of all the samples.

Paragonite

Paragonite covers a wide range of composition as a result of magmatic crystallization and late overprinting and growth (Fig. 6; see also García-Casco, 2007). Magmatic crystals have high K- and moderate to high Ca-contents. The maximum K- and Ca- contents are recorded in sample CV53f (0.41 and 0.28 apfu respectively), though in this and other samples the highest Ca-contents do not correspond with the highest K-contents (García-Casco, 2007; García-Casco *et al.*, 2007). Retrograde grains replacing magmatic plagioclase approach the paragonite end-member.

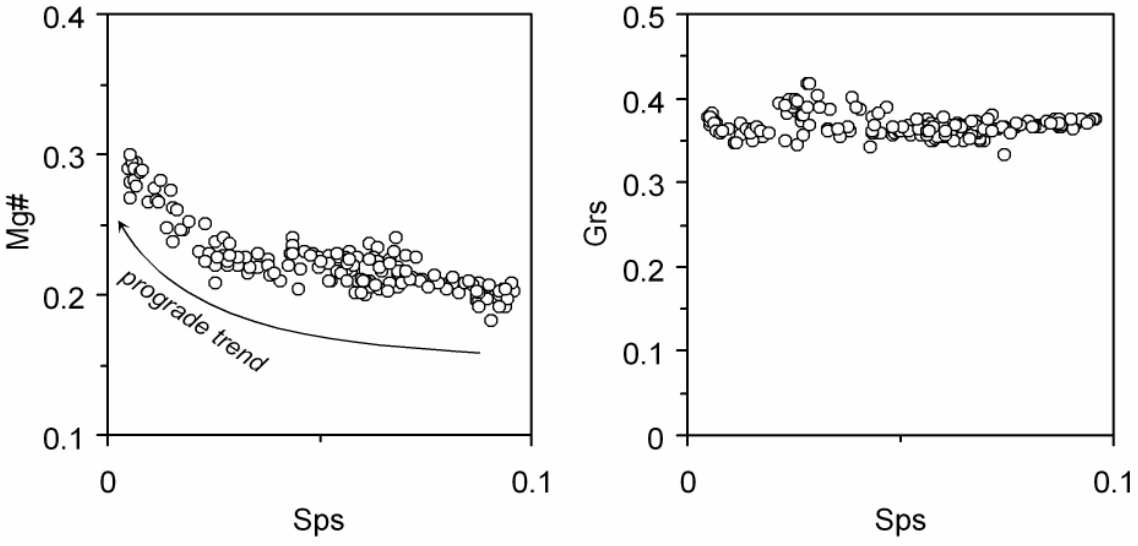

Fig. 5. Composition of the studied garnets, with indication of the prograde trend.

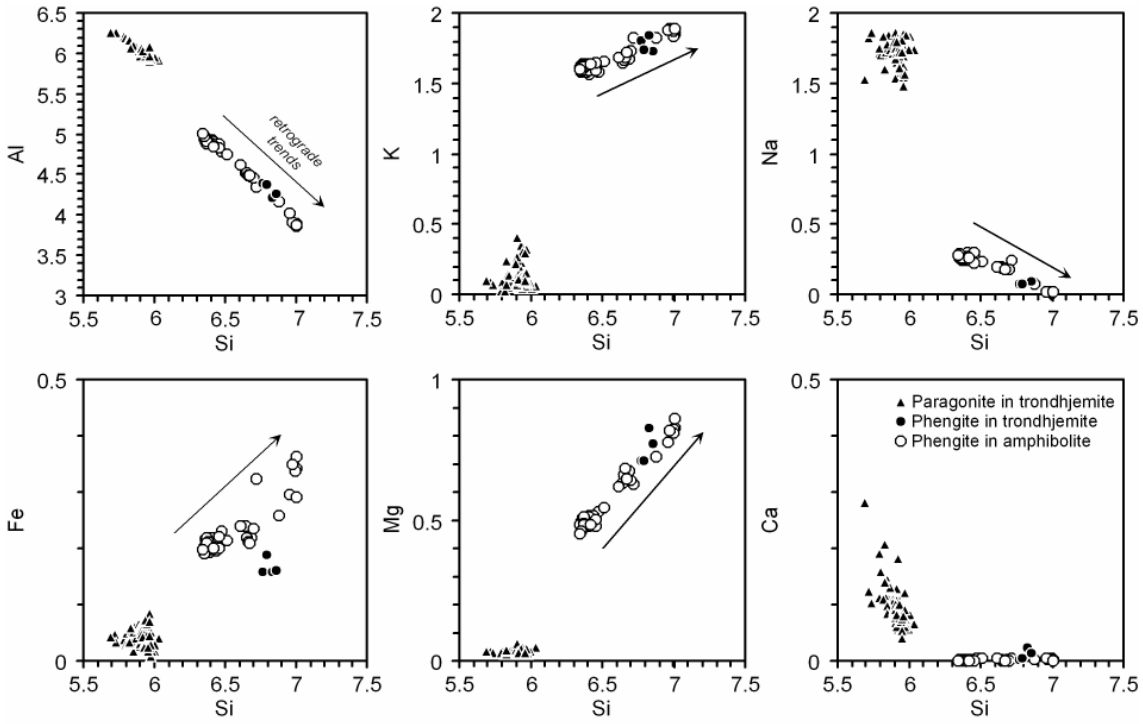

Fig. 6. Composition of paragonite and phengite, with indication of the retrograde trend of phengite.

Phengite

Phengitic mica from amphibolite CV139a shows a wide spectrum of composition (Fig. 6). Si and Ti contents range from 6.34 to 7.01 and 0.00 to 0.08 apfu respectively. Medium grained crystals show complex irregular zoning, but the areas with lower Si and higher Ti, considered to have formed at higher temperature, are preferentially distributed in cores. These less silicic compositions are rich in Ba, amounting up to 0.13 apfu. The latest retrograde grains of phengite, commonly associated with retrograde actinolite, glaucophane, chlorite, and pumpellyite in fractures and replacing other minerals, show the largest Si, Fe, and Mg, and the lowest Ba contents (down to 0.02 apfu).

The composition of retrograde phengite from the trondhjemites is similar to that of retrograde phengite from the amphibolite sample CV139a (Fig. 6). Si contents are up to 6.9 atoms pfu and Ti and Ba contents are low (up to 0.02 atoms pfu in both cases).

Other minerals

Retrograde chlorite in the amphibolites has Al = 4.75-4.99 apfu, Mn = 0.03–0.12 apfu, and Mg# (Fe^{2+} = Fe_{total}) = 0.42-0.63. Retrograde chlorite in the trondhjemites is similar to that of amphibolites, except for being more magnesian (Mg# = 0.68–0.80).

Retrograde pumpellyite in the amphibolites has Mg# (Fe^{2+}=Fe_{total}) = 0.56–0.71, whereas it is more magnesian in trondhjemites and has Mg# (Fe^{2+}=Fe_{total}) = 0.70–0.83. Titanite has Al up to 0.06 apfu. Relict magmatic kyanite (in CV53f) and retrograde lawsonite (in CV228c) are almost pure in composition.

P-T CONDITIONS AND PATHS

P-T conditions

P-T conditions were calculated using the software THERMOCALC version 3.25 and dataset 5.5 (Holland & Powell, 1998; Powell & Holland, 1994). Individual P-T conditions were calculated with different combinations of the phases grown during pre-peak, peak, and retrograde conditions. The results are presented in Fig. 7.

Amphibolites

The calculated pre-peak and peak P-T conditions are based on the inclusion and matrix assemblage Grt+Amp+Ep+H_2O, whereas the retrograde conditions were calculated using actinolitic Amp+Gl+Chl+Ep+Grt(retrograded rims)+Ab+H_2O. For sample CV230b, calculated peak and retrograde conditions were 708 ± 69 ºC 13.8 ± 2.2 kbar (corr 0.455, sigfit 0.81) and 472 ± 21 ºC 10 ± 1 kbar (0.473, 1.48) respectively (García-Casco *et al.*, 2007). For sample CV139a the calculated peak and retrograde conditions are 719 ± 37 ºC 16.2 ± 1.8 kbar (0.353, 0.83) and 383 ± 57 ºC 8.9 ± 1.8 kbar (0.921, 1.46) respectively.

Trondhjemites

Because of the generalized retrograde overprinting of magmatic plagioclase that is transformed to albitic compositions (+paragonite+clinozoisite), the conditions of magmatic crystallization of samples are uncertain. For each sample, the analyses which more closely approach to the composition of the original magmatic plagioclase are those with the highest Ca-contents. Nevertheless, there is no warranty that these analyses effectively corresponds to the original composition of magmatic plagioclase.

The magmatic P-T conditions calculated for sample CV228c and based on the assemblage Amp+Ep+high-K Pa+Qtz+high-Ca Pl (+H_2O) are 747 ± 88 ºC 14.7 ± 3.2 kbar (0.988, 0.95) (García-Casco *et al*., 2007), that overlap with the peak P-T conditions calculated for the amphibolites. Retrograde conditions of 356 ± 18 ºC, 4.7 ± 1 kbar (0.963, 0.31) were calculated in this sample using tremolitic Amp + Chl + Ep + low-K Pa + Lws + Qtz + Ab + H_2O.

The magmatic conditions for all other trondhjemite samples could not be calculated with confidence. Even if we used the spot analyses of relictic plagioclase with the highest Ca-content from individual samples, the calculations (based on the same magmatic assemblage as CV228c) yield discordant high pressures of ca. 20 kbar and large associated errors, as a consequence of using non-equilibrium plagioclase composition (cf. García-Casco *et al*., 2007). Using the composition of plagioclase with the highest-Ca content from the sample CV228c, the calculated peak conditions for sample CV227b are 721 ± 84 ºC 14.3 ± 3.1 kbar (0.987, 0.59), consistent with the peak conditions of the amphibolites. For this sample, the calculated retrograde conditions (assemblage tremolitic Amp+Chl+Ep+low-K Pa+Qtz+Ab+H_2O) are 472 ± 38 ºC 9.8 ± 2.1 kbar (0.643, 1.93).

P-T paths

The calculated P-T conditions indicate that amphibolites experienced peak metamorphic conditions corresponding to the epidote-amphibolite facies at 14-16 kbar and 700 ± 50 ºC. The prograde P-T paths of the amphibolites reached conditions above the wet-solidus of (MORB-like) basaltic composition (Fig. 7), appropriate for the generation of trondhjemitic liquids at high pressure. The P-T conditions of crystallization for these magmas occurred at ca. 14-15 kbar. The retrograded mineral assemblages in all rock types indicate blueschist facies overprints at variable P-T (8-10 kbar, 380-470ºC). This indicates cooling at relatively high pressure and counterclockwise P-T paths.

GEOCHRONOLOGY

SHRIMP zircon dating

Eight single zircons from trondhjemite boulder (CU22) produced a well defined cluster of concordant results (Table 2) with a mean $^{206}Pb/^{238}U$ age of 112.8 ± 1.1 Ma (Fig. 8). Grain 7 (Table 2) is low in U (68 ppm) and therefore has a relatively large error in the U-Pb ratios and age. The data are graphically presented in the conventional Concordia plot in Fig. 8. We consider the above pooled age to reflect the time of zircon crystallization upon cooling of the tonalitic melt.

$^{40}Ar/^{39}Ar$ amphibole dating

Ar/Ar isotopic data are given in Table 3 and are graphically shown in Figures 9 and 10.

Amphibolites

In sample CV139a the brown amphibole concentrate (i.e. peak pargasite) showed a slightly disturbed staircase-type pattern. Steps 4–8 together constitute 93.3 percent of the ^{39}Ar released and yielded an integrated age of 96.5 ± 0.8 Ma (Fig. 9a). The isochron correlation age (i.c.a.) of all steps of hornblende, equally weighted according to model 2 in the software ISOPLOT/EX (Ludwig, 2001), is 93.9 ± 2.4 Ma, with a $^{40}Ar/^{36}Ar$ intercept at 283 ± 3.5 (Fig. 9b). The green amphibole concentrate (i.e. retrograde calcic amphibole), on the other hand, shows a pattern with some slight variation and excess of Ar in the first two steps. Steps 4–7 define a plateau age of 82.67 ± 0.84 Ma, comprising 69.9 percent of the ^{39}Ar (Fig. 9c). The isotopic correlation age of this amphibole concentrate, all steps included, gives an age of 81.2 ± 5.6 with a $^{40}Ar/^{36}Ar$ intercept at 291.8 ± 8.1 (Fig. 9d). For steps 3-7, the calculated isochron age yields 82.4 ± 3.1 Ma ($^{40}Ar/^{36}Ar$ intercept at 288.5 ± 5.8).

We consider the integrated age of 96.5 ± 0.8 Ma of the brown amphibole concentrate and the plateau age of 82.67 ± 0.84 Ma of the green amphibole concentrate as geologically significant ages and to date cooling events after peak metamorphism in this rock. The older age is interpreted to represent cooling of peak amphibole through the appropriate argon retention temperature of amphibole, whereas the younger age is considered to reflect retrograde overprinting of peak amphibole.

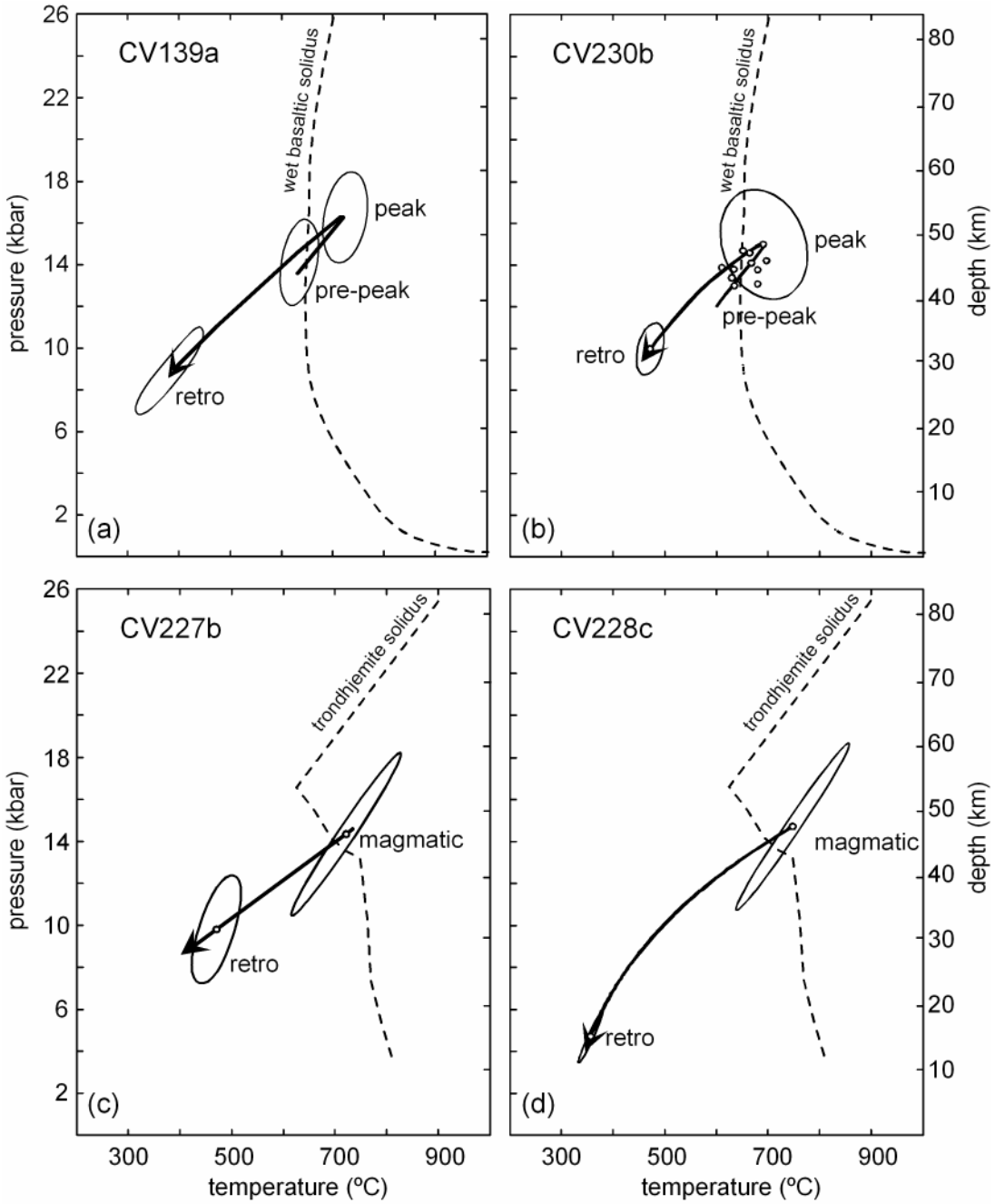

Fig. 7. P-T paths of the studied samples calculated with TERMOCALC (error ellipses: ±1σ) combined with cooling rates to estimate exhumation rates. The reference temperatures for age determinations at 700 ºC (zircon crystallization), 525ºC (pargasite cooling), and 465ºC (retrograde amphibole overprints) are indicated. The wet-basaltic solidus of Vielzeuf & Schmidt (2001) is included in (a) and (b); and the trondhjemite solidus for a representative sample from the Sierra del Convento mélange (García-Casco, 2007) is included in (c) and (d).

Amphibole from sample CV230b yielded a disturbed pattern with excess of Ar in the first step. The isochron age for all steps of hornblende is 80.5 ± 8.4 Ma with a $^{40}Ar/^{36}Ar$ intercept at 296 ± 15 (Fig. 9f). The calculation of an integrated age of steps 3–8, comprising 97.5 percent of the ^{39}Ar released, is 90.6 ± 1.1 Ma. This age can be interpreted as a mixing age of two age components. On the one side, steps 3, 4, and 8, comprising 71.4 percent of the ^{39}Ar released, yield an integrated age of 86.9 ± 0.9 Ma, whereas steps 5–7, comprising 26.1 percent of the ^{39}Ar released, yield an integrated age of 100.6 ± 1.8 Ma (Fig. 9e). Following the results of sample CV139a, we consider the integrated ages of 100.6 ± 1.8 Ma and 86.9 ± 0.9 Ma significant and to date the maximum age of cooling of peak pargasitic amphibole and the age of growth/cooling of retrograde calcic amphibole contained in the

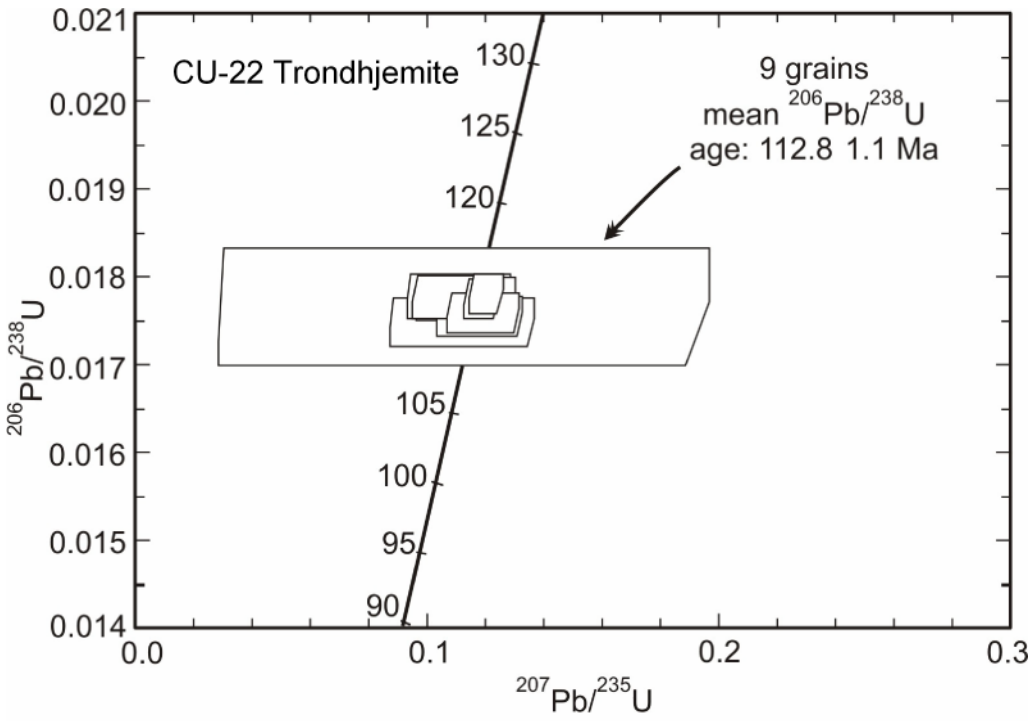

Fig. 8. Concordia diagrams showing SHRIMP analyses of zircons from a tonalitic boulder in the Yacabo River. Data boxes for each analysis are defined by standard errors in $^{207}Pb/^{235}U$ and $^{206}Pb/^{238}U$.

concentrate, respectively

Trondhjemites

Amphibole from sample CV227b yielded a slightly disturbed pattern with excess of Ar in the first three steps. The integrated age is 94.7 ± 1.1 Ma and covers 97.7 percent of the ^{39}Ar released. The age of the last step (step 9) is 97.7 ± 0.9 Ma and comprises the highest percent of the ^{39}Ar released (41.6%) (Fig. 10a). We consider the disturbed pattern as indication of the effects of retrograde overprinting of magmatic pargasite by retrograde calcic amphibole. The integrated age of 94.7 ± 1.1 Ma is thus considered as an average of cooling age of magmatic crystals and growth of retrograde amphibole. Whereas the age of cooling of pargasite is taken as 97.7 ± 0.9 Ma, the patter of this sample does not allow deciphering the ages of retrograde growth of calcic amphibole.

A similar picture arises from samples CV228c and CV53f. Amphibole from sample CV228c yielded a disturbed argon release pattern with excess argon in the first three steps. The age of the last step, which comprises 29 percent of the ^{39}Ar released, is 105.5 ± 1.9 Ma. Steps 4–7 comprise 67.9 percent of the ^{39}Ar released, yielded an integrated age of 85.7 ± 1.5 Ma (Fig. 10c). We consider these two ages as geologically significant and to represent the maximum age of cooling of magmatic pargasitic amphibole and the age of growth/cooling of retrograde amphibole, respectively.

The amphibole concentrate of sample CV53f also yielded a disturbed argon release pattern with excess of Ar in the first five steps which comprise 2.6 percent of the ^{39}Ar released. Steps 6–10, comprising 97.4 of the ^{39}Ar released were used for calculation of an integrated age of 94.8 ± 2.3 Ma (Fig. 10e). We consider this age as an average of the ages of cooling of magmatic pargasite and of overprinting by retrograde amphibole. Steps 9–10, comprising 42.2 percent of ^{39}Ar released, yield an integrated age of 103.6 ± 2.6 Ma (Fig. 10e). The higher ^{39}Ar percent released during step 7 (42.8%) yielded an age of 87.1 ± 0.9 Ma (Fig. 10e). These two latter ages are considered to represent the maximum age of cooling of magmatic pargasitic amphibole and the age of the overprinting by retrograde amphibole, respectively.

Thus, Ar/Ar results from all samples indicate two distinct groups of geologically significant ages dating cooling events in the studied rocks. The first group of ages, 106-97 Ma (average = 100.8 Ma), is considered to date cooling of peak/magmatic amphibole through the appropriate argon retention temperature of amphibole. The second group of ages, 87-83 Ma (average = 85.6 Ma), is considered to date the growth/cooling of retrograde calcic amphibole overprinting peak/magmatic pargasitic amphibole.

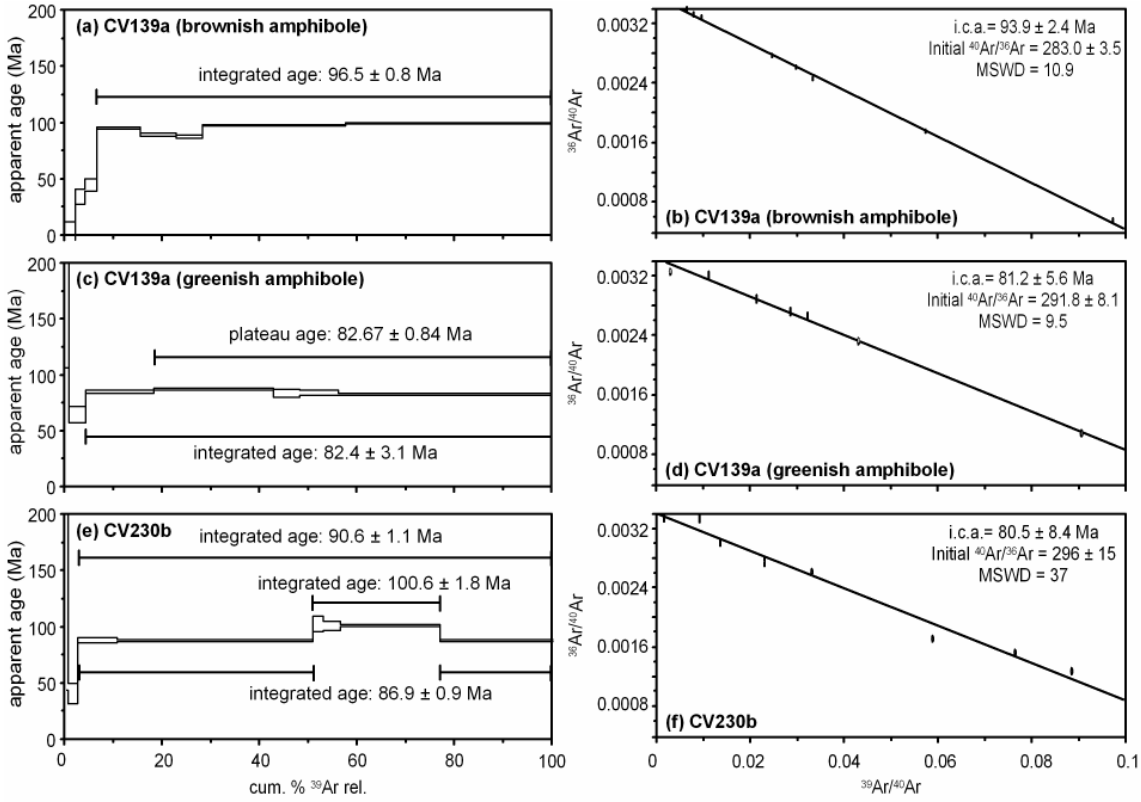

Fig. 9. Incremental step-heating analyses of amphibole from amphibolite samples CV139a (brownish and greenish amphibole) and CV230b. Rectangle heights and all errors are ±1σ.

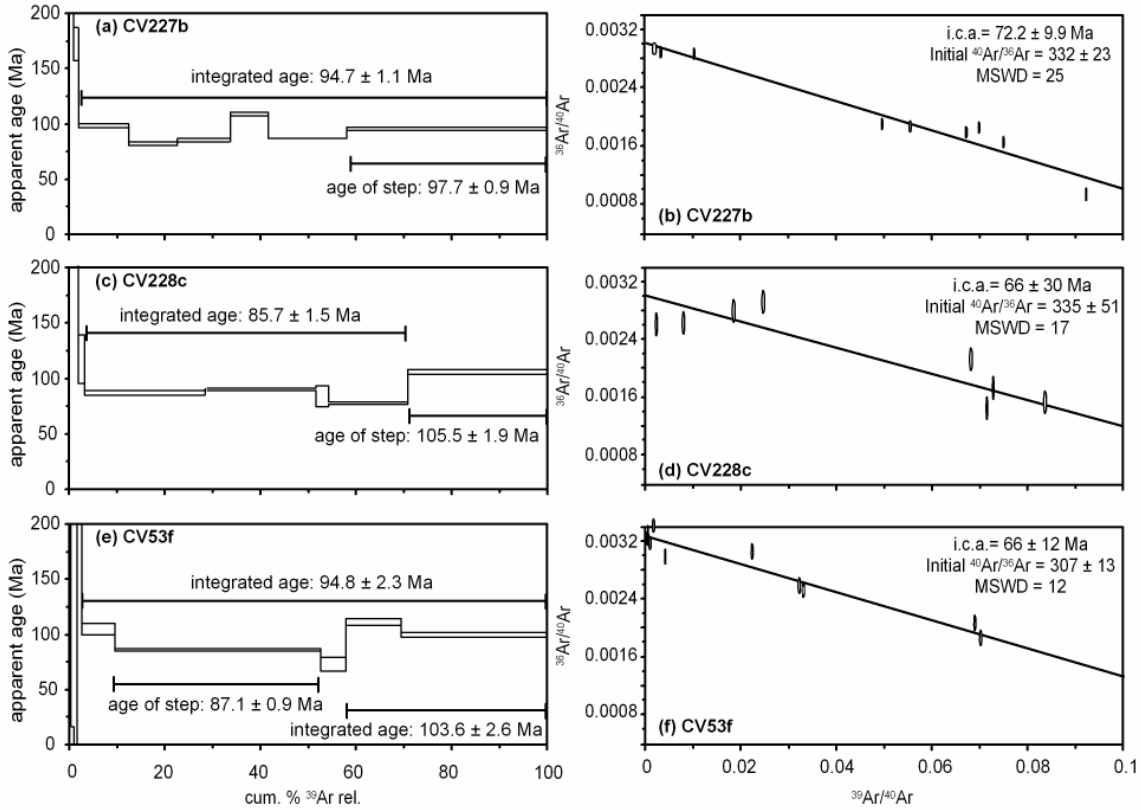

Fig. 10. Incremental step-heating analyses of amphibole from the trondhjemite samples CV227b, CV228c, and CV53f. Rectangle heights and all errors are ±1σ.

DISCUSSION

To evaluate the age data in the context of the thermal history of the studied rocks, the shape of the P-T paths must be known. These shapes are, however, uncertain because only two calculated P-T points constrain their retrograde paths. Near linear fits, as those presented in Fig. 7, would indicate cooling and decompression since the start of incorporation of the blocks to the overriding plate. However, a number of arguments indicate that retrograde P-T paths were not near linear.

García-Casco (2007) and García-Casco *et al.* (2006, 2007) have argued that the onset of retrogression was characterized by near-isobaric cooling, followed by cooling and decompression. Furthermore, as discussed by these authors and below, these blocks formed in a nascent subduction environment. Geophysical (Gerya *et al*., 2002) and geochemical (Perchuck *et al*., 1999) modelling indicate that retrograde P-T paths of rocks formed in this environment are characterized by a first stage of near isobaric cooling at high pressure, followed by a second stage of exhumation characterized by decreasing pressure and temperature. Following the results of these models, the first stage is developed once the blocks are accreted to the (essentially anhydrous) upper plate mantle, while the second stage is developed once a serpentinitic subduction channel is formed upon hydration of the upper plate mantle, allowing upward flow of the blocks. A similar multistage P-T path has been recently deduced by Krebs *et al*. (2007) in contemporaneous (ca. 103 Ma) eclogite blocks from the Rio San Juan complex (Dominican Republic), formed in the same subduction environment as that of the Sierra del Convento amphibolites and trondhjemites (García-Casco *et al*., 2007).

Consequently, we assume here similar multistage P-T paths. Also, because all studied samples attained similar P-T during peak/magmatic conditions and retrogression, the following discussion is developed considering a single retrograde multistage P-T path for all the studied rocks (Fig. 11). In addition, a previous subduction stage will be considered for the amphibolites.

Temperature-time path

The calculated peak/magmatic conditions in the amphibolites and trondhjemites suggest that the onset of the isobaric cooling section of the retrograde P-T paths took place at ca. 15 kbar, 750 ºC. However, the age of this P-T point is not known. Similarly, the temperature and age of the low-T end of the isobaric path are not known. Both must be estimated indirectly. This can be done extrapolating the T-t data of the two distinct groups of geologically significant Ar/Ar ages in the studied rocks (Fig. 11a).

The closure temperature (Tc) for the Ar-Ar system in hornblende depends on a number of factors including the cooling rate, effective diffusion, grain size, and chemical compositions (e.g. Harrison, 1981; Dahl, 1996). In general 480-580ºC is agreed as the appropriate Tc for cooling rates of 5-1000 ºC/Ma (Harrison, 1981). Baldwin *et al*. (1990) calculated lower Tc for metamorphic hornblende than for Ti-richer igneous hornblende assuming the same cooling rate. Also Dahl (1996) indicated that the closure temperature for Mg-rich clinoamphiboles is 60 ± 10ºC higher than for their Fe analogous, and 40 ± 15ºC higher for amphiboles with full A-site relative to those with empty A-sites. Following these results, we consider that the closure temperature of our Ti- and A-site-richer pargasitic amphibole should be relatively high. For simplicity, we have selected an average Tc of 525 ºC for this type of amphibole. Consequently, it will be assumed that this temperature was achieved by the studied rocks in the range 106-97 Ma. The youngest group of Ar-Ar amphibole ages (87-83 Ma) must be interpreted in terms of the retrograde overprinting. These ages may correspond either to the age of formation of retrograde amphibole, to the age of cooling of these overprints through their appropriate argon retention temperature, or both. For simplicity, we have considered a single temperature of 465 ºC for this event, although a range would probably be more appropriate in light of the heterogeneous edenite-magnesiohornblende-actinolite/tremolite composition (and hence timing crystallization) of the overprints. To further constrain the T-t dataset, the timing of blueschist metamorphism in the underlying Purial complex has been also taken into account. The available data indicate 75 ± 5 Ma (K-Ar whole-rock Somin *et al*., 1992) and average 73.5 Ma (based on stratigraphic-paleontological arguments, Iturralde-Vinent *et al*., 2006). Because no P-T data are available for these rocks, a single value of 400 ºC and 8 kbar has been assumed (Fig. 11a).

Using a lineal regression on the aforementioned T-t data (Fig. 11a), the extrapolation to temperatures higher than 525 ºC (first group of Ar-Ar ages) indicates that the low-T end of the isobaric cooling stage cannot be greater than 575 ºC. If they were, the extrapolated ages would be older than 113 Ma, conflicting with the 112.8 Ma crystallization age of zircon at 700 ºC. Consequently, we have arbitrarily chosen 550 ºC for the low-T end of the isobaric cooling stage. This temperature is fully consistent

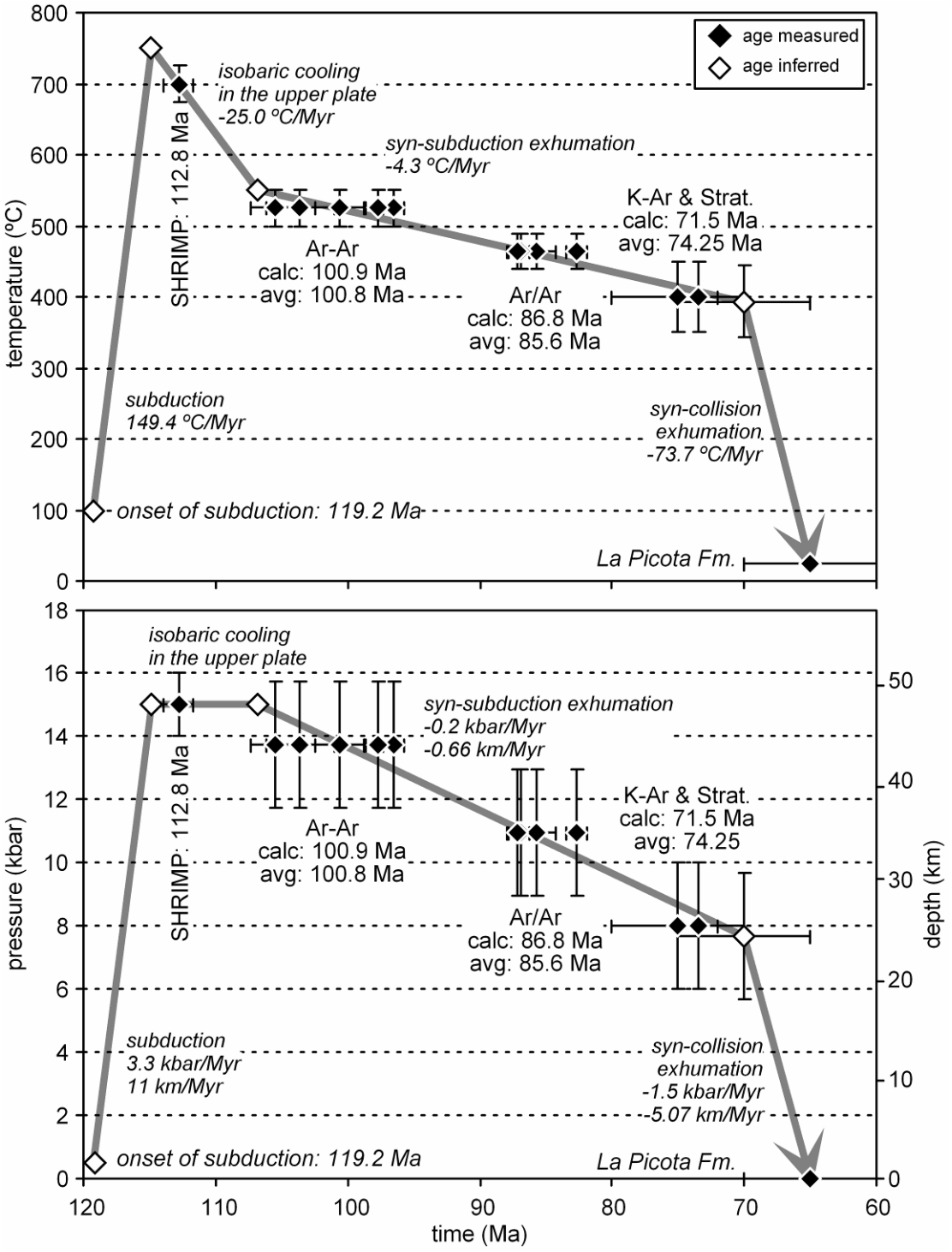

Fig. 11. T-t and P-t paths derived from geochronological and petrological data from the Sierra del Convento mélange and neighbouring geologic bodies. See text for construction of the model paths.

with calculations of Perchuck *et al*. (1999), Gerya *et al*. (2002), and Krebs *et al*. (2007). The calculated age for this temperature is 106.8 Ma using the linear regression on the Ar-Ar and K-Ar T-t data (Fig. 11a). The same technique is used to calculate the age of the high-T end of the isobaric cooling stage (i.e., the age of peak-T). A linear T-t regression was calculated using the low-T end of the isobaric cooling stage and the conditions of zircon crystallization at 112.8 Ma, 700 ºC. The calculated equation gives 114.8 Ma for 750 ºC, the assumed peak T and, consequently, the high-T end of the isobaric cooling stage. The two stages thus calculated are denoted as cooling in the upper plate

and in the syn-subduction exhumation stage, respectively (Fig. 11a).

Lineal extrapolation of the syn-subduction exhumation T-t path to ages younger than the metamorphic ages of the Purial complex indicates that an inflexion must occur in the T-t path to accommodate the age of exposure of the ophiolites and volcanic arc complexes of the region to the Earth's surface, as indicated by the age of the syn-tectonic flyschoid La Picota Fm. (65 ± 5 Ma). The inflexion is taken to have occurred at 70 Ma, for which a temperature of 394 ºC is calculated by linear extrapolation of the syn-subduction exhumation T-t path. With these data, and 65 Ma for the timing of 25 ºC (La Picota Fm.), a T-t section is calculated for the final cooling stage, denoted here the syn-collision stage (Fig. 11a).

Finally, the subduction stage of the amphibolites has been calculated following the calculations of Krebs *et al*. (2007) for the initial stages of subduction in the region. These authors suggested a convergence rate of 30 km/Ma and a burial rate of 11 km/Ma. Assuming the pre-subduction conditions of 0.5 kbar and 100 ºC for the oceanic crust represented in the Sierra del Convento and lineal burial and heating to 750 ºC, 15 kbar, the calculated age of onset of subduction of the amphibolite blocks is 119.2 Ma (Fig. 11a). Different burial rates would, of course, result in varying onset of subduction ages. For 22 and 5.5 km/Ma, the resulting ages are 117.0 and 123.5 Ma, respectively.

Pressure-time and Pressure-Temperature paths

The data and calculations presented above can be extended to calculate P-t and P-T paths (Figs. 11b and 12). However, before this is done the pressure of the two groups of Ar/Ar ages must be deduced. As was done for temperature, it has been assumed that each group of ages corresponds to a distinct pressure. These two pressures were calculated using a linear P-T regression calculated with the points representing the lower-T limit of the isobaric cooling path (i.e., 15 kbar, 550 ºC), an average estimate of 450 ºC, 10.3 kbar for the calculated retrograde conditions, and the P-T data of the Purial complex. Using this equation, the pressures calculated for cooling of pargasite (at 525 ºC) and growth/cooling of retrograde calcic amphibole (at 465 ºC) are 13.75 kbar and 10.95 kbar, respectively.

With these data and those given in the Temperature-time section, the complete P-t and P-T paths were constructed, including a) the subduction, b) cooling in the upper plate, c) syn-subduction, and c) syn-collision stages (Figs. 11b and 12).

Heating/cooling and burial/exhumation rates

Though the P-T-time paths of subducted rocks that return to the surface are highly variable (Gerya *et al*., 2002), our model P-T-t path compares well with predicted and observed paths of oceanic material subducted in a very initial stage and accreted to the hanging wall at great depth. For this type of material subducted under constant moderate convergence rate of 30 km/Ma (Gerya *et al*., 2002) calculated maximum burial and heating rates are 15-20 km/Ma and 150-250 ºC, respectively, which compare well with our model average burial and heating rates or 11 km/Ma and 149.4 ºC/Ma, respectively. In calculations developed by Gerya *et al*. (2002), accretion to the upper plate mantle takes place in a few Ma after onset of subduction (ca. 6.5 vs. 4.3 Ma in our model P-T-t path), the residence time in this environment is ca. 9 Ma (vs. our 8 Ma), and the near-isobaric cooling rates are 0-30 ºC/Ma (vs. our average 25 ºC/Ma). Onset of return flow takes place 15.5 Ma after the onset of subduction (vs. our 12.36 Ma). This time marks the formation of the subduction channel (i.e., melange) by hydration of the upper plate mantle (at ca. 550 ºC). As calculated by Gerya *et al*. (2002), the exhumation and cooling rates during the return flow in the subduction channel are much lower than the burial and heating rates. This observation is in agreement with our linear model calculations for the syn-subduction stage of 0.66 km/Ma and 4.3 ºC/Ma, respectively, which compare well to the rates calculated in blocks from other mélanges considered to have formed part of subduction channels (Reiners *et al*., 2002; Wallis *et al*., 2004; Anczkiewicz *et al*., 2004; Krebs *et al*., 2007).

Our model P-T-t path includes a last section related to collision in the region, a circumstance not modelled by Gerya *et al*. (2002). The linear model calculations for this collision stage indicate exhumation and cooling rates of 5.1 km/Ma and 73.7 ºC/Ma, respectively. These rates are 8 and 17 times higher, respectively, than those calculated for the syn-subduction exhumation stage. This result is in agreement with estimations of fast exhumation rates greater than 1 km/Ma caused by buoyancy and/or normal faulting and/or extrusion wedge processes in collision environments (e.g., Monié et al., 1994; Duchêne *et al*., 1997; Rubatto & Hermann, 2001; Ring & Reischmann, 2002; Baldwin *et al*., 2004).

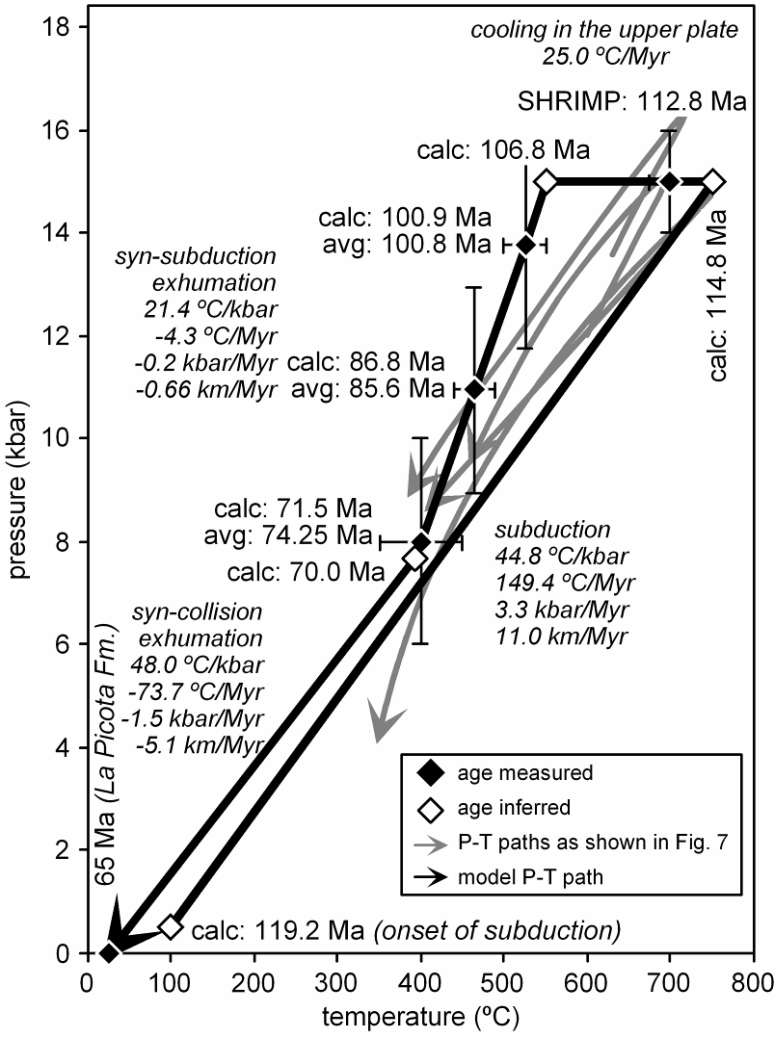

Fig. 12. Model multistage P-T-t path for the studied rocks including the subduction, cooling in the upper plate, syn-subduction exhumation, and syn-collision exhumation stages, measured and inferred P-T-t conditions and rates.

Interpretation of previous geochronology

Our model P-T-t path for the Sierra del Convento amphibolites and trondhjemites allow assessing the significance of previously published age data. These data are generally cited in the literature without appropriate interpretation of the P-T path followed by the rocks.

Somin & Millán (1981), Hatten *et al*. (1989) and Somin *et al*. (1992) have provided K-Ar (whole rock, hornblende, and paragonite) ages from garnet-amphibolite and trondhjemite ranging from 116±9 to 82.2±2.5 Ma. Somin *et al*. (1992) noted that the quoted ages are probably exaggerated due to excess argon. In light of our Ar-Ar results, however, these data must be considered as indications of the timing of cooling and retrograde overprinting rather than of peak metamorphism. The oldest K-Ar age of 116 ± 9 Ma provided by Hatten *et al*. (1989) and Somin *et al*. (1992) correspond to an amphibole separate from garnet amphibolite. This age must be interpreted as an imprecise indication of cooling of high grade pargasite ("carintine", as described by Somin *et al*., 1992).

Hatten *et al*. (1989) also provided imprecise zircon U-Pb ages in a banded zoisitite yielding 120-126 Ma and 103-105 Ma interpreted as the ages of the protolith and its metamorphism respectively (see Somin *et al*., 1992, Millán, 1996). Lázaro & García-Casco (submitted 2007) give evidence for high-temperature fluid-rock processes that formed, at near peak conditions and among other rock types, trondhjemites by partial melting and hornblendites by metasomatic alteration of amphibolites. Our observations indicate that banded zoisitites are similar metasomatic products formed at high temperature. Consequently, in light of our data and interpretations, the 103-105 Ma ages must be considered as an indication of the age of fluid-rock processes taking place at near-metamorphic peak temperature, either during subduction or the near-

isobaric cooling stage in the upper plate previous to formation of the subduction channel. On the other hand, taking into account our calculated onset of subduction at ca. 120 Ma (Figs. 11 and 12), the 120-126 Ma interpreted by Hatten *et al*. (1989) as the age of the oceanic protolith of the zoisitite would indicate a very young subducting oceanic crust (ca. 5 Ma).

Tectonic implications

Our data suggest that the magmatic mafic precursors of the amphibolites started to subduct at ca. 120 Ma (Figs. 11 and 12). The amphibolites followed a counterclockwise P-T path, fully consistent with an onset of subduction scenario (Perchuk *et al*., 1999; Gerya *et al*., 2002; Wakabayashi, 2004; Willner *et al*., 2004; Vignaroli et al., 2005; Krebs *et al*., 2007). Thus, the studied rocks document the early history of subduction in the region, which should have started by 120 Ma. This is in agreement with regional geological arguments indicating onset of subduction of the Protocaribbean (Atlantic) lithosphere during the Aptian (ca. 120 Ma; Pindell *et al.*, 2005, 2006), and with independent estimates by Krebs *et al*. (2007) in the Rio San Juan complex (Dominican Republic).

The amphibolites of the Sierra del Convento were metamorphosed to relatively high temperature (700-750 ºC) and moderate pressure (ca. 15 kbar), and underwent partial melting processes which formed trondhjemitic liquids (García-Casco *et al*., 2007). The relatively shallow (ca. 50 km) conditions of melting of oceanic crust in the Sierra del Convento points to an abnormally high geothermal environment during subduction. The age of the subducting slab critically influences the geothermal gradient in the subduction environment (Gerya *et al*., 2002), making the slab-mantle interface to attain melting conditions at shallow depths upon subduction of young lithosphere (e.g., Okudaira & Yoshitake, 2004; Uehara & Aoya, 2005). Pindell *et al.* (2005, 2006) have indicated that onset of subduction during the Aptian consumed young oceanic lithosphere of the Protocaribbean basin, which was opening at that time, while Krebs *et al*., (2007) have given geochronological evidence for ca. 20 Ma as the age of the initially subducted lithosphere during the Aptian. The fact that the metamorphic gradient for the initial subducted lithosphere is higher in the Sierra del Convento than in the Río San Juan mélange suggests that the age of the subducting lithosphere was younger than 20 Ma in the former, suggesting that the Protocaribbean ridge was closer to eastern Cuba by the Aptian (García-Casco *et al*., 2007). This is in agreement with the ca. 5 Ma age of the subducting curst inferred from the 120-126 Ma age of the subducted protolith in the Sierra del Convento (Hatten *et al*., 1989). Thus, the rocks from the Sierra del Convento mélange represent a direct evidence of Aptian onset of subduction of very young Protocaribbean lithosphere in the Caribbean region.

CONCLUSIONS

SHRIMP U-Pb (zircon) and Ar-Ar (amphiboles) data for exotic blocks of amphibolite and associated trondhjemite (formed after partial melting of the amphibolites) from the Sierra del Convento mélange provide a zircon crystallization age of ca. 113 Ma and two groups of Ar-Ar cooling ages of 106-97 Ma (cooling of metamorphic/magmatic pargasite) and of 87-83 Ma (growth/cooling of retrograde overprints). The blocks followed counterclockwise P-T paths consisting of several stages, including: a) hot subduction (only amphibolites) during 120-115 Ma, b) relatively fast near-isobaric cooling in the upper plate at 15 kbar from peak metamorphic/magmatic conditions at ca. 750 ºC to 550 ºC during 115-107 Ma, c) slow syn-subduction cooling and exhumation in the subduction channel during 107-70 Ma, and d) fast syn-collision cooling and exhumation during 70-60 Ma. The model P-T-t of the studied rocks indicates that the age of onset of subduction in the region is ca. 120 Ma, in agreement with independent estimations. The average cooling and exhumation rates within the subduction channel during the syn-subduction stage were ca. 4 ºC/Ma and 0.7 km/Ma, respectively, comparable to rates determined in intra-oceanic subduction environments. Collision in the region triggered much faster rates of cooling and exhumation of ca. 80 ºC/Ma and 5 km/Ma.

ACKNOWLEDGEMENTS

We thank K. Núñez Cambra and A. Rodríguez Vega for field assistance. We also thank the ARGONAUT laboratory team (Salzburg, Austria) for technical assistance during Ar-dating. This paper has received financial support from the Spanish MEC project CGL2006-08527/BTE.

REFERENCES

Adamovich, A. & Chejovich, V., 1964. Principales características de la geología y de los minerales útiles de la región nordeste de la Provincia de Oriente. Revista Tecnológica, 14-20.

Anczkiewicz, R., Platt, J. P., Thirlwall, M. F. & Wakabayashi, J., 2004. Franciscan subduction off to a slow start: evidence from high-precision Lu–Hf garnet ages on high grade-blocks. Earth and Planetary Science Letters, 225, 147-161.

Baldwin, S. L., Harrison, T. M. & Fitz Gerald, J. D., 1990. Diffusion of ^{40}Ar in metamorphic hornblende. Contributions to Mineralogy and Petrology, 105(6), 691-703.

Baldwin, S. L., Monteleone, B. D., Webb, L. E., Fitzgerald, P. G., Grove, M. & June Hill, E., 2004. Pliocene eclogite exhumation at plate tectonic rates in

eastern Papua New Guinea. Nature, 431(7006), 263-267.

Black, L. P., Kamo, S. L., Allen, C. M., Aleinikoff, J. N., Davis, D. W., Korsch, R. J. & Foudoulis, C., 2003. TEMORA 1: A quality zircon standard for Phanerozoic U-Pb geochronology. Chemical Geology, 200, 155-170.

Boiteau, A., Saliot, P. & Michard, A., 1972. High-Pressure Metamorphism in Ophiolite Complex of Purial (Oriente, Cuba). Comptes Rendus Hebdomadaires Des Seances De L Academie Des Sciences Serie D, 274(15), 2137-&.

Cloos, M., 1982. Flow melanges: Numerical modelling and geologic constraints on their origin in the Franciscan subduction complex, California. Geological Society of America Bulletin, 93, 330-345.

Cobiella, J., Quintas, F., Campos M. & Hernández, M. (1984). Geología de la Región Central y Suroriental de la Provincia de Guantánamo. Santiago de Cuba: Editorial Oriente, Santiago de Cuba, 125 pp.

Compston, W., Williams, I. S., Kirschvink, J. L., Zhang, Z. & Ma, G., 1992. Zircon U-Pb ages for the Early Cambrian time scale. Journal Geological Society London, 149, 171-184.

Dahl, P. S., 1996. The effects of composition on retentivity of argon and oxygen in hornblende and related amphiboles: A field-tested empirical model. Geochimica et Cosmochimica Acta, 60, 3687–3700.

De Laeter, J. R. & Kennedy, A. K., 1998. A double focusing mass spectrometer for geochronology. International Journal of Mass Spectrometry, 178, 43-50.

Duchêne, S., Blichert-Toft, J., Luais, B., Télouk, P., Lardeaux, J.-M. & Albarède, F., 1997. The Lu-Hf dating of garnets and the ages of the Alpine high-pressure metamorphism. Nature, 387(6633), 586-589.

Ernst, W. G., 1988. Tectonic history of subduction blueschists P-T paths. Geology, 16, 1081-1084.

García-Casco, A., 2007. Magmatic paragonite in trondhjemites from Sierra del Convento mélange, Cuba. American Mineralogist, 92, 1232-1237.

García-Casco, A., Torres-Roldán, R. L., Millán, G., Moniè, P. & Haissen, F., 2001. High-grade metamorphism and hydrous melting of metapelites in the Pinos terrane (W Cuba): Evidence for crustal thickening and extension in the northern Caribbean collisional belt. Journal of Metamorphic Geology, 19(6), 699-715.

García-Casco, A., Torres-Roldán, R. L., Iturralde-Vinent, M. A., Millán, G., Núñez Cambra, K., Lázaro, C. & Rodríguez Vega, A., 2006. High pressure metamorphism of ophiolites in Cuba. Geologica Acta, 4, 63-88.

García-Casco, A., Lázaro, C., Torres-Roldán, R. L., Núñez Cambra, K., Rojas Agramonte, Y., Kröner, A., Neubauer, F., Millán, G. & Blanco Quintero, I., 2007. Partial melting and counterclockwise P-T path of subducted oceanic crust (Sierra del Convento mélange, Cuba). Journal of Petrology (in press).

Gerya, T. V., Stoeckhert, B. & Perchuk, A. L., 2002. Exhumation of high-pressure metamorphic rocks in a subduction channel - a numerical simulation. Tectonics, 21(6), 6-1 - 6-19.

Gradstein, F. M. & Ogg, J. G., 2005. Time scale Encyclopedia of geology. 5. Oxford United Kingdom Elsevier Academic Press.

Handler, R., Neubauer, F., Velichkova, S. H. & Ivanov, Z., 2004. 40Ar/39Ar age constraints on the timing of magmatism and post-magmatic cooling in the Panagyurishte region, Bulgaria. Schweizerische Mineralogische und Petrographische Mitteilungen, 84(1), 119-132.

Harrison, T. M., 1981. Diffusion of ^{40}Ar in hornblende. Contributions to Mineralogy and Petrology, 78, 324-331.

Hatten, C. W., Mattison, J. M., Renne, P. R., Somin, M. L., Millán, G., Araqueliants, M. M., Kolesnikov, E. M. & Sumin, L. V., 1989. Rocas metamórficas de alta presión: nuevos datos acerca de sus edades. In: Primer Congreso Cubano de Geología, pp. 118-119, La Habana (Cuba).

Hernández, M. & Canedo, Z., 1995. Geoquímica de las ofiolitas meridionales de Cuba oriental. In: Revista de Minería y Geología (3), pp. 3-9, University of Moa, Moa (Cuba).

Holland, T. J. B. & Powell, R., 1998. An internally consistent thermodynamic data set for phases of petrological interest. Journal of Metamorphic Geology, 16, 309-343.

Iturralde-Vinent, M. A., 1998. Sinopsis de la Constitución Geológica de Cuba. Acta Geológica Hispánica, 33, 9-56.

Iturralde-Vinent, M. A., Millán, G., Korkas, L., Nagy, E. & Pajón, J., 1996. Geological interpretation of the Cuban K-Ar data base. In: Ofiolitas Y Arcos Volcánicos de Cuba (ed Iturralde-Vinent, M. A.), pp. 48-69, IGCP Project 364, Miami (USA).

Iturralde-Vinent, M. A., Díaz Otero, C., Rodríguez Vega, A. & Díaz Martínez , R., 2006. Tectonic implications of paleontologic dating of Cretaceous-Danian sections of Eastern Cuba. Geologica Acta, 4, 89-102.

Kinny, P. D., 1986. 3820 Ma zircons from a tonalitic Amitsoq gneiss in the Godthab district of southern West Greenland. Earth and Planetary Science Letter, 79, 337-347.

Krebs, M., Maresch, W. V., Schertl, H.-P., Baumann, A., Draper, G., Idleman, B., Münker, C. & Trapp, E., 2007. The dynamics of intra-oceanic subduction zones: A direct comparison between fossil petrological evidence (Rio San Juan Complex, Dominican Republican) and numerical simulation. Lithos (in press).

Kretz, R., 1983. Symbols for rock-forming minerals. American Mineralogist, 68, 277-279.

Kulachkov, L. V. & Leyva, R. C., 1990. Informe sobre los resultados de los trabajos de reconocimiento geológico para cuarzo filoniano en la parte oriental de Cuba. In: Instituto Superior Minero-Metalúrgico., Moa (Cuba).

Lázaro, C. & García-Casco, A., 2007. Geochemical and Sr-Nd isotope signatures of pristine slab melts and their residues (Sierra del Convento mélange, eastern Cuba). Chemical Geology (submitted).

Leake, B. E., Woolley, A. R., Arps, C. E. S., Birch, W. D., Gilbert, M. C., Grice, J. D., Hawthorne, F. C., Kato, A., Kisch, H. J., Krivovichev, V. G., Linthout, K.,

Laird, J., Mandarino, J. A., Maresch, W. V., Nickel, E. H., Rock, N. M. S., Schumacher, J. C., Smith, D. C., Stephenson, N. C. N., Ungaretti, L., Whittaker, E. J. W. & Touzhi, G., 1997. Nomenclature of amphiboles: Report of the Subcommittee on Amphiboles of the International Mineralogical Association, Commission on New Minerals and Mineral Names. American Mineralogist, 82, 1019-1037.

Leyva, R. C., 1996. Características geológicas, regularidades de distribución y perspectivas de utilización del cuarzo filoniano de la región oriental de Cuba. Unpub. Master´s Thesis, University of Moa, Moa (Cuba).

Ludwig, K. R., 2001. Isoplot/Ex - A Geochronological Toolkit for Microsoft Excel, Berkeley Geochronological Center, Special Publication No 1a.

Marchesi, C., Garrido, C. J., Bosch, D., Proenza, J. A., Gervilla, F., Monié, P. & Rodríguez-Vega, A., 2007. Geochemistry of Cretaceous Magmatism in Eastern Cuba: Recycling of North American Continental Sediments and Implications for Subduction Polarity in the Greater Antilles Paleo-arc. Journal of Petrology (in press).

McDougall, I. & Harrison, T. M., 1999. Geochronology and thermochronology by the $^{40}Ar/^{39}Ar$ method. Oxford University Press, Oxford.

Millán, G., 1996. Metamorfitas de la asociación ofiolítica de Cuba. In: Ofiolitas y Arcos Volcanicos de Cuba (ed Iturralde-Vinent, M. A.), pp. 147-153, IGCP Project 364, Miami (USA).

Monié, P., Torres-Roldán, R.L. & García-Casco, A., 1994. Cooling and exhumation of the Western Betic Cordilleras, $^{40}Ar/^{39}Ar$ thermochronological constraints on a collapsed terrane. Tectonophysics, 238, 353-379.

Nelson, D. R., 1997. Compilation of SHRIMP U-Pb zircon geochronology data, 1996. In: Geological Survey Western Australia, pp. 189.

Okudaira, T. & Yoshitake. Y. (2004). Thermal consequences of the formation of a slab window beneath the Mid-Cretaceous southwest Japan arc: A 2-D numerical analysis. The Island Arc, 13, 520-532.

Pindell, J. L., Kennan, L., Maresch, W. V., Stanek, K. P., Draper, G. & Higgs, R., 2005. Plate-kinematics and crustal dynamics of circum-Caribbean arc-continent interactions: Tectonic controls on basin development in Proto-Caribbean margins. In: Caribbean-South American plate interactions, Venezuela (ed Avé Lallemant, H. G., & Sisson, V.B), pp. 7-52, Geological Society of America, Special Paper 394.

Pindell, J. L, Kennan, L., Stanek, K. P., Maresch,W. V. & Draper, G. (2006). Foundations of Gulf of Mexico and Caribbean evolution: eight controversies resolved. Geologica Acta, 4, 303-341.

Perchuk, A. L., Philippot, P., Erdmer, P. & Fialin, M., 1999. Rates of thermal equilibration at the onset of subduction deduced from diffusion modeling of eclogitic garnets, Yukon-Tanana terrain. Geology, 27, 531-534.

Powell, R. & Holland, T. J. B., 1994. Optimal geothermometry and geobarometry. American Mineralogist, 79, 120-133.

Proenza, J. A., Díaz-Martínez, R., Iriondo, A., Marchesi, C., Melgarejo, J. C., Gervilla, F., Garrido, C. J., Rodríguez-Vega, A., Lozano-Santacruz, R. & Blanco-Moreno, J. A., 2006. Primitive Cretaceous island-arc volcanic rocks in eastern Cuba: the Téneme Formation. Geologica Acta, 4, 103-121.

Reiners, P. W., Ehlers, T. A., Garver, J. I., Mitchell, S. G., Montgomery, D. R., Vance, J. A. & Nicolescu, S., 2002. Late Miocene exhumation and uplift of the Washington Cascade Range. Geology, 30(9), 767-770.

Ring, U. & Reischmann, T., 2002. The weak and superfast Cretan detachment, Greece: exhumation at subduction rates in extruding wedges. Journal of the Geological Society of London, 159(3), 225-228.

Rubatto, D. & Hermann, J., 2001. Exhumation as fast as subduction?. Geology, 29(1), 3-6.

Somin, M. & Millán, G., 1981. Geology of the Metamorphic Complexes of Cuba (in russian). Nauka, Moscow.

Somin, M. L., Arakelyants, M. M. & Kolesnikov, E. M., 1992. Age and tectonic significance of high-pressure metamorphic rocks in Cuba. International Geology Review, 34, 105-118.

Stanek, K. P., Maresch, W. V., Grafe, F., Grevel, CH. Baumann, A., 2006. Structure, tectonics and metamorphic development of the Sancti Spiritus Dome (eastern Escambray massif, Central Cuba). Geologica Acta, 4, 151-170.

Steiger, R. H. & Jäger, E., 1977. Subcommission on geochronology: Convention on the use of decay constants in geo-and cosmochronology. Earth and Planetary Science Letters, 36, 359-362.

Stern, R. A., 1997. The GSC sensitive high resolution ion microprobe (SHRIMP): Analytical techniques of zircon U-Th-Pb age determinations and performance evaluation. In: Radiogenic age and isotope studies, pp. F1-31, Geological Survey Canada.

Tsujimori, T., Matsumoto, K., Wakabayashi, J. & Liou, J. G., 2006. Franciscan eclogite revisited: Reevaluation of the P–T evolution of tectonic blocks from Tiburon Peninsula, California, U.S.A. Mineralogy and Petrology, 88(1-2), 243-267.

Uehara, S. & Aoya, M., 2005. Thermal model for approach of a spreading ridge to subduction zones and its implications for high P/high T metamorphism: Importance of subduction vs ridge-approach ratio. Tectonics, 24, TC4007. doi: 10.1029/2004TC001715.

Vielzeuf, D. & Schmidt, M. W., 2001. Melting reactions in hydrous systems revisited: applications to metapelites, metagreywackes and metabasalts. Contributions to Mineralogy and Petrology, 141, 251-267.

Vignaroli, G. Rossetti, F., Bouybaouene, M, Massonne, H.-J., Theye, T., Faccenna, C., & Funiciello, R. 2005. A counter-clockwise P-T path for the Voltri Massif eclogites (Ligurian Alps, Italy). Journal of Metamorphic Geology, 23, 533-555.

Wakabayashi, J. (2004). Tectonic mechanisms associated with P–T paths of regional metamorphism: Alternatives to single-cycle thrusting and heating. Tectonophysics, 392, 193-218.

Wallis, S., Moriyama, Y. & Tagami, T., 2004. Exhumation rates and age of metamorphism in the Sanbagawa belt:

new constraints from zircon fission track analysis. Journal of Metamorphic Geology, 22(1), 17–24.

Whittington, A. G., 1996. Exhumation overrated at Nanga Parbat, northern Pakistan. Tectonophysics, 206, 215–226.

Wijbrans, J. R., Pringle, M. S., Koppers, A. A. P. & Scheveers, R., 1995. Argon geochronology of small samples using the Vulkaan argon laserprobe. Proceedings of the Koninklijke Nederlandse Akademie Van Wetenschappen, 98, 185-218.

Williams, I. S., 1998. U-Th-Pb geochronology by ion microprobe. In: Applications of microanalytical techniques to understanding mineralizing processes: Society of Economic Geologists, review (ed McKibben, M. A., Shanks III, W.C., & Ridley, W.I.), pp. 1-35.

Willner, A. P., Glodny, J., Gerya, T. V., Godoy, E. & Massonne, H.-J. (2004). A counterclockwise PTt path of high-pressure/low-temperature rocks from the Coastal Cordillera accretionary complex of south-central Chile: constraints for the earliest stage of subduction mass flow. Lithos, 75, 283-310.

Table 1. Representative analyses of calcic (Amp(Ca)) and sodic (Gl) amphiboles (normalized to 22 O and 2 OH), garnet (normalized to 12 O), and epidote (normalized to 12 O and 1 OH).

Sample	CV139a			CV227b		CV53f	CV139a	CV139a	CV227b		CV53f	
Type of rock	amphibolite			trondhjemite			amphibolite	amphibolite	trondhjemite			
Phase	Amp(Ca)	Amp(Ca)	Gl	Amp(Ca)	Amp(Ca)	Amp(Ca)	Grt	Ep	Ep	Ep	Ep	Ep
Type	peak	retro	retro	peak	retro	peak	peak	peak	peak	retro	peak	retro
SiO_2	43.07	55.08	56.73	44.04	55.32	41.97	38.07	38.89	39.01	39.54	38.88	38.51
TiO_2	1.10	0.03	0.02	0.60	0.08	0.78	0.07	0.05	0.16	0.07	0.11	0.26
Al_2O_3	14.09	1.13	11.58	16.39	4.31	17.09	21.95	31.69	28.58	32.84	26.50	33.03
FeO_{total}	12.00	12.38	12.09	9.12	3.89	8.55	22.07	2.63	6.73	1.05	8.54	0.58
MnO	0.07	0.08	0.07	0.13	0.09	0.11	0.35	0.05	0.13	0.00	0.06	0.04
MgO	12.33	16.22	8.67	13.09	20.94	13.51	4.65	0.02	0.16	0.02	0.26	0.12
CaO	11.35	12.01	0.80	10.19	11.89	11.05	12.80	23.79	22.91	23.99	22.85	24.83
BaO						0.02						0.00
Na_2O	2.61	0.52	7.02	3.41	1.09	3.28						
K_2O	0.62	0.05	0.03	0.29	0.07	0.14						
H_2O(*)	2.04	2.09	2.15	2.09	2.18	2.07		1.95	1.94	1.97	1.92	1.96
Total	99.29	99.60	99.15	99.37	99.86	98.57	99.95	99.06	99.63	99.46	99.13	99.32
Si	6.32	7.89	7.90	6.32	7.60	6.09	2.95	2.99	3.01	3.01	3.03	2.95
Ti	0.12	0.00	0.00	0.07	0.01	0.09	0.00	0.00	0.01	0.00	0.01	0.01
Al	2.43	0.19	1.90	2.77	0.70	2.92	2.00	2.87	2.60	2.95	2.43	2.98
Fe^{3+}	0.17	0.09	0.09	0.21	0.18	0.22	0.10	0.17	0.43	0.07	0.56	0.04
Fe^{2+}	1.30	1.39	1.32	0.88	0.27	0.81	1.33					
Mn	0.01	0.01	0.01	0.02	0.01	0.01	0.02	0.00	0.01	0.00	0.00	0.00
Mg	2.70	3.47	1.80	2.80	4.29	2.92	0.54	0.00	0.02	0.00	0.03	0.01
Ca	1.78	1.84	0.12	1.57	1.75	1.72	1.06	1.96	1.89	1.96	1.91	2.04
Ba						0.00						0.00
Na	0.74	0.14	1.90	0.95	0.29	0.92						
K	0.12	0.01	0.00	0.05	0.01	0.03						
Mg#	0.67	0.71	0.58	0.76	0.94	0.78	0.29					

(*) Calculated by stoichiometry.

Table 1 (continued). Representative analyses of plagioclase (normalized to 8 O) and micas (normalized to 20 O and 4 OH).

Phase	plagioclase					paragonite				phengite		
Type of rock	amphibolite	trondhjemite				trondhjemite				amphibolite	trondhjemite	
Sample	CV139a	CV227b		CV53f		CV227b		CV53f		CV139a		CV53f
Type	retro	peak	retro	peak	retro	peak	retro	peak	retro	peak	retro	retro
SiO_2	66.86	65.53	67.82	63.27	68.27	46.35	46.69	45.88	45.80	47.24	50.15	51.27
TiO_2						0.22	0.07	0.34	0.23	0.75	0.18	0.23
Al_2O_3	19.83	21.42	19.45	22.85	19.62	39.89	40.14	39.02	39.74	31.37	28.29	26.83
FeO_{total}	0.41	0.09	0.10	0.00	0.00	0.42	0.19	0.54	0.49	1.70	2.10	1.43
MnO	0.01	0.01	0.00	0.01	0.00	0.00	0.00	0.00	0.03	0.00	0.00	0.00
MgO						0.20	0.13	0.26	0.17	2.31	3.23	4.17
CaO	0.39	2.19	0.10	4.06	0.06	0.65	0.29	0.59	0.62	0.00	0.00	0.17
BaO				0.02	0.00			0.37	0.02	1.67	1.16	
Na_2O	11.74	10.31	11.74	9.34	12.01	6.48	7.30	6.11	7.21	1.12	0.70	0.32
K_2O	0.16	0.04	0.02	0.07	0.01	1.09	0.57	2.11	0.77	9.30	10.15	10.85
H_2O(*)						4.68	4.70	4.64	4.66	4.46	4.49	4.50
Total	99.40	99.59	99.23	99.62	99.97	99.98	100.07	99.84	99.73	99.91	100.45	99.76
Si	2.95	2.89	2.99	2.81	2.99	5.93	5.95	5.93	5.89	6.35	6.70	6.83
Ti						0.02	0.01	0.03	0.02	0.08	0.02	0.02
Al	1.03	1.11	1.01	1.19	1.01	6.02	6.03	5.95	6.02	4.97	4.45	4.21
Fe^{3+}	0.02	0.00	0.00	0.00	0.00							
Fe^{2+}						0.05	0.02	0.06	0.05	0.19	0.23	0.16
Mn	0.00	0.00	0.00	0.00	0.00	0.00	0.00	0.00	0.00	0.00	0.00	0.00
Mg						0.04	0.02	0.05	0.03	0.46	0.64	0.83
Ca	0.02	0.10	0.00	0.19	0.00	0.09	0.04	0.08	0.09	0.00	0.00	0.02
Ba				0.00	0.00			0.02	0.00	0.09	0.06	
Na	1.00	0.88	1.00	0.80	1.02	1.61	1.81	1.53	1.80	0.29	0.18	0.08
K	0.01	0.00	0.00	0.00	0.00	0.18	0.09	0.35	0.13	1.60	1.73	1.84
Mg#								0.46	0.38	0.71	0.73	0.84

(*) Calculated by stoichiometry.

Table 1 (continued). Representative analyses of chlorite (normalized to 20 O and 16 OH) and kyanite (normalized to 5 O).

Phase	Chl			Als
Type of rock	amphibolite	trondhjemite		trondhjemite
Sample	CV139a	CV227b	CV53f	CV53f
Type	retro	retro	retro	peak
SiO_2	25.68	30.38	29.18	36.06
TiO_2				0.01
Al_2O_3	19.30	19.41	19.78	62.48
FeO_{total}	29.76	12.13	13.77	0.60
MnO	0.57	0.05	0.10	0.00
MgO	12.31	25.45	24.59	
H_2O(*)	11.07	12.27	12.13	
Total	98.68	99.70	99.55	99.14
Si	5.57	5.94	5.77	0.98
Ti	0.00	0.00	0.00	0.00
Al	4.93	4.47	4.61	2.01
Fe^{3+}				0.01
Fe^{2+}	5.39	1.98	2.28	
Mn	0.10	0.01	0.02	0.00
Mg	3.98	7.42	7.25	
Mg#	0.42	0.79	0.76	

(*) Calculated by stoichiometry.

Table 2. SHRIMP II analytical data for spot analyses of single zircons from sample CU22 and ages.

Samle No.	U (ppm)	Th (ppm)	$^{206}Pb/^{204}Pb$	$^{208}Pb/^{206}Pb$ & 1σ error	$^{207}Pb/^{206}Pb$ & 1σ error	$^{206}Pb/^{238}U$ & 1σ error	$^{207}Pb/^{235}U$ & 1σ error	$^{206}Pb/^{238}U$ age & 1σ error
Cu 22-1-1	74	12	14587	0.0538±120	0.0494±50	0.0175±2	0.119±12	112± 2
Cu 22-2-1	136	62	5122	0.1348±174	0.0464±70	0.0177±2	0.113±17	113± 2
Cu 22-3-1	184	99	6248	0.1677±260	0.0467±10	0.0174±3	0.112±25	111± 2
Cu 22-3-2	127	51	3792	0.1156±150	0.0450±60	0.0177±2	0.110±15	113± 3
Cu 22-4-1	139	64	5224	0.1459±155	0.0489±62	0.0175±2	0.118±15	112± 3
Cu 22-5-1	83	30	8718	0.1167±179	0.0453±72	0.0177±3	0.111±18	113± 2
Cu 22-6-1	101	34	21988	0.1106±57	0.0492±23	0.0178±2	0.120± 6	114± 1
Cu 22-7-1	68	20	1637	0.0835±864	0.0464±35	0.0176±7	0.112±86	112± 5
Cu 22-8-1	72	24	49791	0.1102±60	0.0487±23	0.0177±2	0.119± 6	113± 1

Table 3. $^{40}Ar/^{39}Ar$ analytical results.

Step	$^{36}Ar/^{39}Ar^{a}$	$^{37}Ar/^{39}Ar^{b}$	$^{40}Ar/^{39}Ar^{a}$	$\%^{40}Ar^{c}$	$\%^{39}Ar$	Age (Ma)
Sample CV139a, brownish amphibole (125-250 μm), J = 0.00612 ± 0.0000327						
1	0.54549 ± 0.00217	1.8900 ± 0.0018	161.387 ± 0.738	0.1	2.3	3.6 ± 8.1
2	0.43199 ± 0.00171	3.7334 ± 0.0028	130.456 ± 0.621	2.1	2.0	33.7 ± 6.7
3	0.35163 ± 0.00160	4.0826 ± 0.0022	107.653 ± 0.516	3.5	2.4	44.2 ± 5.6
4	0.07358 ± 0.00036	7.4136 ± 0.0014	29.983 ± 0.108	27.5	8.9	95.0 ± 1.2
5	0.08751 ± 0.00045	6.2030 ± 0.0014	33.619 ± 0.136	23.1	7.3	88.9 ± 1.5
6	0.11208 ± 0.00046	7.3311 ± 0.0021	40.634 ± 0.144	18.5	5.5	87.3 ± 1.6
7	0.03044 ± 0.00012	8.2478 ± 0.0009	17.359 ± 0.036	48.2	29.3	97.1 ± 0.6
8	0.00568 ± 0.00012	8.2313 ± 0.0002	10.217 ± 0.037	83.6	42.3	98.9 ± 0.6
Sample CV139a, greenish amphibole (125-250 μm), J = 0.006134 ± 0.0000321						
1	1.16555 ± 0.01241	2.0136 ± 0.0101	358.915 ± 4.871	4.0	1.0	155.3 ± 49.5
2	0.28847 ± 0.00193	14.6566 ± 0.0112	89.994 ± 0.643	5.3	3.4	64.3 ± 6.9
3	0.08181 ± 0.00047	13.9025 ± 0.0037	30.859 ± 0.143	21.7	14.0	84.4 ± 1.6
4	0.05377 ± 0.00026	9.3327 ± 0.0016	23.156 ± 0.078	31.4	24.6	86.6 ± 0.9
5	0.13565 ± 0.00110	9.1524 ± 0.0042	47.036 ± 0.338	14.8	5.3	83.1 ± 3.6
6	0.09469 ± 0.00078	10.8091 ± 0.0038	34.867 ± 0.237	19.7	8.0	83.8 ± 2.5
7	0.01196 ± 0.00021	1.2220 ± 0.0004	11.083 ± 0.062	68.1	43.6	82.5 ± 0.8
Sample CV230b, amphibole (125-250 μm), J = 0.006177 ± 0.0000306						
1	2.27100 ± 0.02458	14.3747 ± 0.0333	683.498 ± 10.041	1.8	0.6	145.9 ± 103.2
2	0.36406 ± 0.00261	13.4384 ± 0.0114	110.140 ± 0.866	2.3	2.0	39.8 ± 9.4
3	0.07772 ± 0.00057	11.9882 ± 0.0031	30.021 ± 0.172	23.5	8.1	87.3 ± 1.9
4	0.01966 ± 0.00012	10.2710 ± 0.0010	12.976 ± 0.035	55.2	40.3	86.9 ± 0.6
5	0.21883 ± 0.00203	11.6813 ± 0.0094	73.093 ± 0.650	11.5	2.0	101.7 ± 6.9
6	0.11783 ± 0.00127	11.2745 ± 0.0049.	43.129 ± 0.384	19.3	3.5	100.0 ± 4.1
7	0.02871 ± 0.00023	11.3065 ± 0.0017	16.852 ± 0.070	49.6	20.5	100.7 ± 0.9
8	0.01437 ± 0.00032	12.3936 ± 0.0005	11.212 ± 0.094	62.1	23.1	86.7 ± 1.1
Sample CV227b, amphibole (125-250 μm), J = 0.006192 ± 0.0000304						
1	1.64532 ± 0.02761	6.3305 ± 0.0242	563.922 ± 12.288	13.8	0.7	714.9 ± 92.4
2	0.92187 ± 0.01638	11.1445 ± 0.0382	319.737 ± 6.728	14.8	0.5	473.9 ± 57.8
3	0.28281 ± 0.00474	7.0329 ± 0.0111	99.209 ± 1.534	15.8	1.1	172.9 ± 15.6
4	0.03337 ± 0.00042	12.6501 ± 0.0035	17.895 ± 0.126	44.9	10.5	98.5 ± 1.4
5	0.02615 ± 0.00039	14.8121 ± 0.0043	14.173 ± 0.118	45.5	10.1	83.4 ± 1.3
6	0.02189 ± 0.00035	14.6433 ± 0.0036	13.218 ± 0.105	51.1	11.2	86.6 ± 1.2
7	0.03802 ± 0.00053	15.7151 ± 0.0056	20.015 ± 0.161	43.9	7.8	109.2 ± 1.8
8	0.02629 ± 0.00029	16.0111 ± 0.0032	14.747 ± 0.087	47.3	16.6	90.2 ± 1.0
9	0.01019 ± 0.00024	15.7268 ± 0.0004	10.717 ± 0.070	71.9	41.6	97.7 ± 0.9
Sample CV228c, amphibole (125-250 μm), J = 0.006221 ± 0.0000305						
1	1.24131 ± 0.02753	9.3940 ± 0.0440	481.765 ± 12.487	23.9	0.5	982.6 ± 81.4
2	0.33707 ± 0.00599	12.6461 ± 0.0255	129.488 ± 2.093	23.1	1.4	319.1 ± 19.7
3	0.15038 ± 0.00631	16.1081 ± 0.0404	53.843 ± 1.956	17.5	1.2	116.7 ± 20.6
4	0.01792 ± 0.00030	17.6270 ± 0.0042	11.843 ± 0.090	55.3	25.4	87.4 ± 1.0
5	0.02346 ± 0.00034	19.6069 ± 0.0039	13.573 ± 0.102	48.9	23.1	90.2 ± 1.2
6	0.11662 ± 0.00283	22.7785 ± 0.0214	40.195 ± 0.853	14.3	2.8	83.2 ± 9.2
7	0.03068 ± 0.00047	19.2998 ± 0.0062	14.537 ± 0.140	37.6	16.6	77.2 ± 1.5
8	0.01987 ± 0.00059	20.7465 ± 0.0009	13.841 ± 0.176	57.6	29.0	105.5 ± 1.9
Sample CV53f, amphibole (200-250 μm), J = 0.006333 ± 0.0000341						
1	9.07365 ± 1.21369	69.7959 ± 2.2906	2827.290 ± 519.703	5.2	0.1	1254.3 ± 2962.6
2	4.90865 ± 0.14901	3.4822 ± 0.0425	1550.171 ± 63.735	6.4	0.4	886.1 ± 445.6
3	7.28908 ± 0.16446	5.5300 ± 0.0374	2214.258 ± 69.368	2.7	0.6	589.0 ± 571.8
4	2.43602 ± 0.05798	10.1098 ± 0.0600	722.972 ± 23.692	0.4	0.5	44.2 ± 264.1
5	0.76276 ± 0.01411	10.3975 ± 0.0345	256.884 ± 5.308	12.3	1.1	337.6 ± 50.3
6	0.07911 ± 0.00157	27.2675 ± 0.0196	30.666 ± 0.473	23.8	6.9	105.8 ± 5.1
7	0.02959 ± 0.00023	27.6012 ± 0.0068	14.303 ± 0.070	38.9	42.8	87.1 ± 0.9
8	0.13545 ± 0.00193	25.9481 ± 0.0248	44.529 ± 0.596	10.1	5.5	73.8 ± 6.6
9	0.07505 ± 0.00100	29.3309 ± 0.0148	29.913 ± 0.302	25.9	11.7	112.6 ± 3.3
10	0.02602 ± 0.00073	32.7285 ± 0.0016	14.015 ± 0.217	45.1	30.6	100.2 ± 2.4

Note: Errors of ratios, J-values, and ages are at 1-sigma level; a measured; b corrected for postirradiation decay of ^{37}Ar; c non atmospheric ^{40}Ar.

General Conclusions

The Sierra del Convento (eastern Cuba) is a serpentinitic matrix mélange that contains exotic high-pressure high-temperature plagioclase-lacking epidote±garnet amphibolite and associated tonalite-trondhjemite blocks. The metamorphic evolution of these subduction-related blocks is different from those found in mélanges from west-central Cuba, suggesting formation in different subduction environments. Available age data suggest that high-pressure rocks from west-central Cuba formed in a pre-Aptian mature (cold) subduction zone while high-pressure high-temperature rocks from the Sierra del Convento mélange formed in an Aptian juvenile subduction zone which consumed young oceanic lithosphere. The latter evolved to a mature subduction zone during the late Cretaceous until it finally arrested by 70-65 Ma when collision started in the region.

Detailed petrologic and geochemical analysis of the amphibolite and associated tonalite-trondhjemite rocks from the Sierra del Convento mélange indicate that tonalite-trondhjemite formed by partial melting of amphibolite and not as a result of differentiation or partial melting of MOR mafic material at oceanic ridges (i.e.,. the rocks are not subducted oceanic plagiogranites) nor as a result of intrusion of exotic volcanic arc magmas. Partial melting occurred at ca. 15 kbar, 750 ºC and was fluid assisted. The lack of peak metamorphic plagioclase and clinopyroxene in the amphibolites supports a fluid-present melting scenario. The process generated plagioclase-lacking epidote±garnet amphibolites (residues) and peraluminous tonalitic-trondhjemitic melts. The extent of melting was low, in the range 1-30 wt % though most likely ca. 10 wt %. The external flux of water was triggered by dehydration of subducting serpentinitic and not from a sedimentary source. Melt crystallization occurred at depth (> 12 kbar) and formed magmatic assemblages made of plagioclase, quartz, epidote, ±paragonite, ±pargasite.

All types of rock underwent blueschist facies overprinting and followed counterclockwise P-T paths indicating syn-subduction exhumation along the subduction channel in a colder scenario.

SHRIMP U-Pb zircon data constrain the onset of subduction at ca. 120 Ma, in agreement with independent estimations. Cooling Ar-Ar ages of amphibole combined with the determined counterclockwise P-T paths indicate a geodynamic evolution consisting of four stages: (a) initial hot subduction of a young oceanic lithosphere during 120-115 Ma, with heating and burial rates of 150 ºC/Ma and 11 km/Ma, respectively, which produced partial melting at high temperature, (b) accretion of the blocks to the upper plate at ca. 50 km depth (15 kbar) followed by fast near-isobaric cooling (25 ºC/Ma) during 115-107 Ma from peak metamorphic/magmatic conditions to ~ 550ºC, (c) slow syn-subduction cooling and exhumation (4 ºC/Ma and 0.7 km/Ma) in the subduction channel during 107-70 Ma, and (d) fast cooling and exhumation (70 ºC/Ma and 5 km/Ma) during 70-60 Ma when arc-continent collision occurred and subduction finished in the region.

Conclusiones Generales

La Sierra del Convento (Cuba oriental) es una mélange de matriz serpentinítica que contiene bloques exóticos de anfibolitas con epidota ± granate, sin plagioclasa, y trondhjemitas-tonalitas asociadas en condiciones de alta presión y alta temperatura. La evolución metamórfica de estos bloques asociados a una subducción oceánica es distinta de la de los bloques encontrados en mélanges de Cuba central y occidental, lo que sugiere que la formación de ambos grupos de mélanges tuvo lugar en ambientes de subducción diferentes. Los datos de edades disponibles sugieren que las rocas de alta presión de Cuba central y occidental se formaron en una zona de subducción madura (fría) en el pre-Aptiense, mientras que las rocas de alta presión y alta temperatura de la mélange de la Sierra del Convento se formaron en una zona de subducción incipiente en el Aptiense en la que se consumió corteza oceánica joven. Esta última evolucionó a una zona de subducción madura a lo largo del Cretácico terminal hasta finalizar coincidiendo con el comienzo de la colisión en la región.

Un detallado análisis petrológico y geoquímico de las anfibolitas y de las tonalitas-trondhjemitas asociadas de la Sierra del Convento, indica que las tonalitas-trondhjemitas se formaron por fusión parcial de las anfibolitas y no como resultado de la diferenciación o fusión parcial de material máfico de tipo MOR en una dorsal medioceánica (i.e. las rocas no son plagiogranitos oceánicos subducidos), ni como resultado de la intrusión de magmas de arco volcánico exóticos. La fusión parcial ocurrió a ca. 15 kbar y 750ºC en condiciones de saturación acuosa. La ausencia de plagioclasa y clinopiroxeno en la asociación mineral de pico metamórfico apoya el hecho de que la fusión tuvo lugar en condiciones de fluido-presente. Los procesos produjeron unos residuos de anfibolitas con epidota ± granate, sin plagioclasa, y unos líquidos peraluminosos de composición tonalítica- trondhjemítica. El grado de fusión parcial fue bajo, entre 1 y 30% en peso, aunque muy probablemente ca. 10%. El flujo externo de fluido fue desencadenado por la deshidratación de la serpentinita que subducía y no por una fuente de origen sedimentario. La cristalización del fundido se produjo en condiciones de elevada presión (>12 kbar) y se formaron asociaciones magmáticas constituidas de plagioclasa + cuarzo + epidota ± paragonita ± pargasita.

Todos los tipos de rocas sufrieron retrogresión en facies de esquistos azules y siguieron trayectorias P-T de tipo antihoraria indicando exhumación sincrónica con la subducción a lo largo del canal de subducción en un ambiente mas frío.

Datos de U-Pb SHRIMP en zircones proporcionan una edad para el comienzo de la subducción en torno a 120 Ma, de acuerdo con estimaciones independientes. Las edades de enfriamiento de Ar-Ar junto con las trayectorias P-T antihorarias indican una evolución geodinámica de la zona de subducción consistente en 4 estadios: (a) inicio de la subducción caliente de una litosfera oceánica joven durante 120-115 Ma, con tasas de calentamiento y exhumación de unos 150ºC/Ma y 11 Km./Ma respectivamente, que produjeron la fusión parcial a elevadas temperaturas, (b) acreción de los bloques a la placa superior a unos 50 km de profundidad (15 kbar), seguido de un rápido enfriamiento (25ºC/Ma) durante 115-107 Ma hasta alcanzar unos 550ºC, (c) enfriamiento y exhumación en el canal de subducción lentas, sincrónicas a la subducción (4ºC/Ma y 0.7 km/Ma respectivamente), durante 107-70 Ma, y (d) enfriamiento y exhumación rápidos (70ºC/Ma y 5 km/Ma respectivamente) durante 70-60Ma al producirse la colisión arco-continente y terminar la subducción en la región.